The Institute of Paper Chemistry

Appleton, Wisconsin

Doctor's Dissertation

The Properties, Structure, and Multilayer Deposition of Stearic Acid-Calcium Stearate Monolayers

Ronald D. Neuman

January, 1973

THE PROPERTIES, STRUCTURE, AND MULTILAYER DEPOSITION OF STEARIC ACID-CALCIUM STEARATE MONOLAYERS

A thesis submitted by

Ronald D. Neuman

B.S. in Ch.E. 1966, University of Washington

M.S. 1968, Lawrence University

in partial fulfillment of the requirements
of The Institute of Paper Chemistry
for the degree of Doctor of Philosophy
from Lawrence University,
Appleton, Wisconsin

January, 1973

TABLE OF CONTENTS

	Page
SUMMARY	1
INTRODUCTION	3
BACKGROUND OF THE THESIS PROBLEM	6
PRESENTATION OF THE THESIS PROBLEM	10
APPROACH TO THE THESIS PROBLEM	11
EXPERIMENTAL MATERIAL, APPARATUS, AND PROCEDURES	13
Preparation of Stearic Acid Spreading Solutions	13
Preparation of Subsolutions	15
Determination of Surface Pressure-Area Isotherms	17
Apparatus	17
Experimental	22
Surface Pressure	23
Number of Film Molecules	24
Film Area	24
Compression Barrier Displacement Calibration	25
Trough Scale Calibration	26
Area Corrections	26
Total Area Available to the Monolayer	26
Technique	27
Surface Potential Measurements	28
Apparatus	28
Experimental	30
Surface Viscosity Measurements	33
Apparatus	33
Experimental	34
Monolayer Stability Measurements	36

Langmuir-Blodgett Multilayer Deposition 36

Apparatus 36

Solid Substrates for Multilayer Deposition 38

Paraffin 38

Polytetrafluoroethylene 40

Solid Substrates for Monolayer Deposition 42

Transfer Ratio Determination 43

Adjustment for Contact Angle Changes 44

Correction for Concomitant Monolayer Loss 44

Corrections for Initial Retarded Deposition Effects 45

Technique 46

Radioactivity Measurements 47

Determination of the Withdrawal Contact Angle 49

Autoradiography 51

Electron Microscopy 52

Electron Probe Microanalysis 53

Contact Angle Measurements 54

EXPERIMENTAL RESULTS AND DISCUSSION 55

Monolayer Properties 55

Surface Pressure-Area Isotherms 55

Surface Viscosity 59

Surface Potential 65

ΔV-pH and $\mu_{\perp}$-pH Curves 65

Surface Potential Uniformity 67

Effect of Compression Time 73

Monolayer Stability Measurements 76

Transfer Ratio During Langmuir-Blodgett Monolayer Deposition 81

Monolayer Collapse 84

Size and Distribution of the Collapsed Regions 84

Nature of the Collapsed Regions 87

Langmuir-Blodgett Multilayer Deposition 89

Effect of Deposition Speed 91

Apparent Transfer Ratio from Film Balance Measurements 93

Uniformity of Deposition 96

Effect of Surface Roughness 99

Stability of the Immersed Monolayers 100

Calculated Transfer Ratio from Radioactivity Measurements 101

Local Transfer Ratio 104

Withdrawal Contact Angles 104

Ca-H-St Bilayers 104

Ca-H-St Multilayers 107

Stearic Acid Bilayers 109

Bilayer Deposition on Polytetrafluoroethylene 111

Contact Angles on Bilayers 112

Structure of Deposited Monolayers and Multilayers 112

Effect of Evaporant 112

Bilayers on Paraffin 116

Bilayer Stability 116

Calcium Stearate Aggregates 118

Effect of Shadow-Casting on Deposited Monolayers 120

Effect of Shadow-Casting on Deposited Multilayers 122

Carbon Replicas of Deposited Bilayers 126

Electron Probe Microanalysis of the Replicas 126

Carbon Replicas of Deposited Monolayers 129

Conclusions of Electron Microscopic Studies 132

Structural Model of Ca-H-St Monolayers 132

Existing Models 132

Analysis of the Existing Models 134

Surface Micelle Transformation Model 134

Analysis of the Surface Micelle Transformation Model 136

pH Range 2.0-8.0 136

Withdrawal Contact Angle 136

$\underline{A}_{31}$-pH Curve 137

Structure of Deposited Monolayers and Multilayers 138

Surface Viscosity 138

Surface Potential 138

pH Range 8.0-9.0 140

Surface Potential 140

Surface Viscosity 141

$\underline{A}_{31}$-pH Curve 141

Withdrawal Contact Angle 141

Molecular Reorientation at the Solid/Liquid Interface 142

Withdrawal Contact Angle Changes 142

Magnitude of the Withdrawal Contact Angle 144

Support for Molecular Reorientation 146

Molecular Orientation at the Solid/Liquid Interface 148

Transfer Ratio and Withdrawal Contact Angle Behavior in Multilayer Deposition 155

Surface Micelle Formation 160

CONCLUSIONS 165

GLOSSARY 169

SUGGESTIONS FOR FUTURE RESEARCH 172

ACKNOWLEDGMENTS 174

LITERATURE CITED 175

APPENDIX I. MATERIALS 182

Stearic Acid Purity 182

Surface-Active Impurities in Hexane 185

Paraffin 187

APPENDIX II. EXPERIMENTAL PROCEDURES 188

Subsolution Temperature Measurement 188

Surface Viscosity Calculations 189

Paraffin Surface Preparation 189

Operating Potential Selection for G-M Counter 192

Selection of Optimum Counting Distance 193

Tangentometer Error Estimate 194

Photographic Enlarger Alignment 195

Camera and Slide Assembly Alignment 195

APPENDIX III. EXPERIMENTAL DATA 197

APPENDIX IV. ELECTRON MICROSCOPY 201

SUMMARY

This study relates the molecular properties of a condensed stearic acid-calcium stearate (Ca-H-St) monolayer to the monolayer behavior during Langmuir-Blodgett multilayer deposition. Multilayer deposition is important to industrial processes such as pitch deposition in pulp and papermaking operations.

The behavior of stearic acid monolayers on 10^{-4} M $CaCl_2$ subsolutions over the pH range 2-9 was characterized by surface pressure-area isotherm, surface potential, surface viscosity, and monolayer stability measurements. The transfer ratio during multilayer deposition on paraffin substrates was determined for each of the initial four successively deposited monolayers by measuring the film area decrease per unit solid geometrical area and applying appropriate corrections. The transfer ratio was also calculated from radioactivity measurements on C^{14}-labeled bilayers. Multilayer deposition was further characterized by determining the withdrawal contact angle by a cinematographic method and the deposition uniformity by autoradiography. The structure of deposited monolayers and multilayers was extensively examined by electron microscopy.

Large characteristic changes occurred in the monolayer properties of condensed Ca-H-St monolayers at pH 6.4 and 8.0. This behavior was explained by a structural rearrangement occurring in the monolayer at about pH 6.4 as some of the calcium distearate molecules associated into two-dimensional or surface micelles when a critical degree of dissociation of the film molecules was exceeded. Electron micrographs of deposited monolayers and multilayers suggested that the average diameter of the calcium stearate surface micelles was approximately 50-60 A. The monolayer became nonuniform above pH 8.0. This nonuniformity was attributed to the aggregation of surface micelles into large clusters of micelles and the interspersion of a gaseous monolayer within the holes formed in the film. Surface micelle formation was discussed in terms of head-group and chain-chain interactions.

Multilayer deposition was observed to proceed by an adsorption mechanism at the three-phase line interface when the local transfer ratio was differentiated from an apparent transfer ratio. The local transfer ratio of the first and subsequent layers deposited during the immersion operations was unity, as were the withdrawal transfer ratios below pH 6.8. However, above pH 6.8 the withdrawal transfer ratio of the second layer decreased with increasing subsolution pH, becoming 0.86 at pH 9.0. The withdrawal transfer ratios also became increasingly smaller as the number of deposited layers increased. Aqueous or water-filled pores formed within the surface of the immersed multilayer during the immersion operations as molecules of the depositing layer migrated and partially filled voids or "holes" present in the underlying layers.

The decrease in the withdrawal transfer ratio was partly due to the incomplete transfer of calcium stearate surface micelles as a result of their intrinsic low mobility. In addition, the monolayer did not appear to deposit on aqueous pores; and consequently, the withdrawal transfer ratio decreased with increasing number of layers. The withdrawal transfer ratio was also influenced by the surface viscosity and withdrawal contact angle, but to a lesser extent, at least in the initial stages of multilayer deposition before positive ion adsorption became a dominant mechanism.

The withdrawal contact angle behavior was related to changes in the orientation of the molecules and the proportion of aqueous pores comprising the immersed monolayer. Although the polar groups of the calcium distearate molecules were oriented toward the subsolution, the orientation of the un-ionized stearic acid molecules and calcium stearate surface micelles was contrary to conventional views of molecular orientation at interfaces. The stearic acid molecules reoriented such that their hydrocarbon tails faced the subsolution. Although the surface micelles also overturned, reorientation did not appear to be complete. The driving force for reorientation is suggested to arise from changes in the vicinal water structure.

INTRODUCTION

Pitch can be described as the agglomeration of resinous materials in pulp and papermaking systems. The formation of pitch and its associated troubles have plagued most paper and board manufacturers at one time or another. Pitch troubles may appear either as pitch balls or as pitch deposits. These pitch balls which vary in size up to 1/4 inch in diameter may pass through the screens and cause pitch spots in the sheet, picking on the press rolls, sheet breaks, and poor sheet formation. The pitch also is capable of being invisible in the pulp, but it deposits upon practically all parts of the machine. These deposits not only lower the paper quality, but they may actually lower production due to sheet breaks and poor sheet quality. At times the pitch problem may be so severe that the mill may have to shutdown in order to remove the pitch deposits from the various machine parts.

While there has been voluminous literature on the subject of pitch, most of the suggested control methods have been the result of trial and error and are of a strictly empirical nature. The control methods have met with varying degrees of success because there appears to be no universally applicable solution to the problem of the sporadic, unpredictable occurrence of pitch. A recent industrial publication (1) has stated "Pitch control still remains one of the major problems facing the paper industry. No satisfactory solution has been found."

Knowing the organic chemistry of the pitch components alone does not solve the problem because the trouble arises from physicochemical phenomena. Swanson and Cordingly (2) have studied some of the surface-chemical properties of pitch. They have shown that most wood pulps suspended in aqueous media rapidly form an adsorbed film or a monolayer of pitch at the surface of the pulp suspension. This film is very heterogeneous in composition and contains resin and fatty acids, unsaponifiables, and lignin. These same substances comprise the major components of

pitch. Changes in the viscosity and mechanical properties of the pitch monolayer are believed to be important in the pitch problem. Pitch balls formed when rigid films collapsed and crumbled on the surface of pulp suspensions under the action of high surface pressures. Swanson and Cordingly demonstrated that multilayers or successive layers of pitch monolayers could be built-up by the Langmuir-Blodgett deposition technique (3, 4) onto solid slides. The multilayer deposition of these pitch films was dependent on the pH and the concentration of multivalent cations in the aqueous subsolution. These subsolution conditions and the type of deposition were very similar to that observed by Blodgett (4) for the multilayer deposition of alkaline earth salts of fatty acid monolayers. The principles of multilayer deposition appear to apply to mill conditions because during pitch troubles a thick layer of pitch often collects at the point where the surface of the pulp suspension contacts the sides of a pulper, tank, or chest.

Even though a considerable amount of work has been directed toward understanding the pitch problem, the deposition and adherence of pitch to solid surfaces are not very well understood. As such, the mechanism of multilayer deposition is uncertain even for fatty acid monolayers. A better understanding of the principles of multilayer deposition should provide a better understanding of pitch deposition.

In addition, the principles of multilayer deposition have important consequences for other applications of the Langmuir-Blodgett deposition technique. Deposited monolayer and multilayers are being used in the determination of the chemical composition of monolayers and the conformation of proteins and polypeptides at the liquid/air interface, as well as for model biological membrane studies. In addition, multilayers are employed as calibration standards for ellipsometers and crystal analyzers for soft x-rays in electron microprobe analysis. But there are serious questions regarding the molecular packing of the deposited monolayer compared to

that of the monolayer on the subsolution surface and the possibility of preferential transfer of one component in a mixed monolayer. Thus, the results of a study on the relationship between the behavior of the monolayer during multilayer deposition and the molecular properties of the monolayer would be of immediate interest.

BACKGROUND OF THE THESIS PROBLEM

The investigations of films which have been deposited on solid substrates are most interesting. These deposited monolayers and multilayers have been studied by many different methods including mechanical, electrical, optical, electron diffraction, and x-ray diffraction measurements. The early reviews of Langmuir (5) and Schulman (6) on multilayers are very complete. Multilayers have also been discussed in the books of Adam (7), Harkins (8), Bull (9), and Adamson (10). The recent monograph of Gaines (11) contains a good general discussion of monolayer and multilayer deposition. This literature review will be limited to a discussion of the transfer of monolayers to a solid substrate to form multilayers and the general structure of such built-up films.

Langmuir (3) in 1920 described a process for transferring a monolayer of oleic acid to a solid surface. A clean glass plate was immersed into a monolayer-covered subsolution, and the monolayer was quantitatively transferred to the solid upon withdrawing the plate as shown schematically in Fig. 1. This deposited monolayer lubricated the surface and tended to make it hydrophobic.

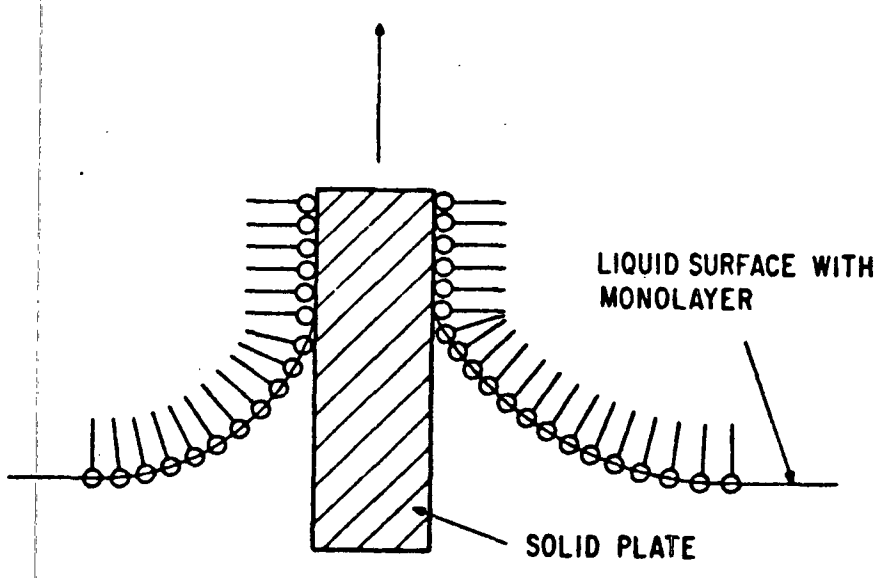

Figure 1. The Deposition of a Monolayer on a Solid Being Withdrawn from a Monolayer-Covered Subsolution

In 1934, Blodgett (4) demonstrated that multilayers or films consisting of successive monolayers of alkaline earth salts of fatty acids could be deposited on a solid substrate. This technique of multilayer deposition consists of dipping a solid into and out of a monolayer-covered subsolution and is called the Langmuir-Blodgett method. This process is schematically illustrated in Fig. 2. Multilayer deposition requires that the solid surface is initially hydrophobic. This requirement may be met by using either a monolayer-covered solid or some other hydrophobic solid. In addition, the monolayer must be maintained under constant surface pressure during the deposition process. This has classically been accomplished by the piston oil technique. The monolayer is separated from a liquid spreading oil by a long floating thread. A constant spreading pressure equal to the equilibrium spreading pressure of the piston oil is provided when excess oil is present as droplets on the subsolution surface. Recently, modern film balances are designed to automatically provide constant surface pressure operation.

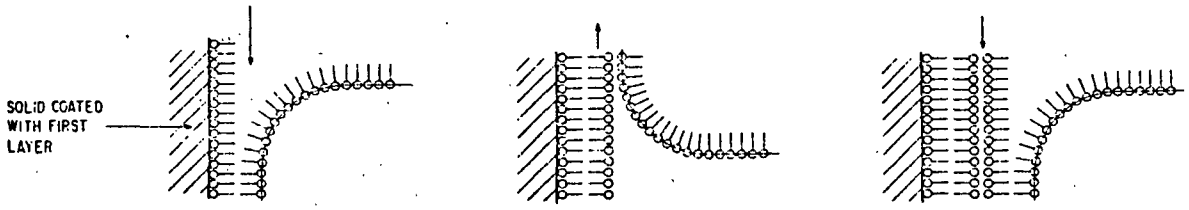

Figure 2. The Formation of Multilayers by the Successive Deposition of Monolayers

Two types of deposition were described by Blodgett. In the first, Y-deposition occurred when monolayers were deposited on the solid on both the immersion and withdrawal sequences of the dipping operation. Under certain conditions, however, the monolayer was only deposited when the solid was immersed in the subsolution and not when it was withdrawn. This type of deposition was designated X-deposition. The pH of the subsolution, the temperature, and the number of previously deposited monolayers

influence the type of deposition. Bikerman (12) has indicated that the deposition is dependent on the wettability of the surface and is related to the contact angle between the solid and the monolayer-covered subsolution surface. Y-deposition takes place if the advancing angle is obtuse and the receding angle is acute; while if the advancing and receding angles are obtuse, X-deposition only occurs. This occurs because the subsolution surface naturally conforms to the solid on immersion only if the contact angle is obtuse and on leaving only if the contact angle is acute. The withdrawal rate and the surface pressure can also influence the contact angle.

The ratio of the film area removed from the subsolution surface to the geometrical area of the solid is termed the transfer (deposition) ratio. Langmuir, et al. (13) and Stenhagen (14) found that the transfer ratio of various stearates, esters, and sterols was unity within experimental error at high surface pressures. Thus, the monolayers appear to transfer quantitatively from the water to the solid without any change in their molecular packing. The transfer ratio was 0.96 at lower surface pressures (15, 16). However, Rose and Quinn (17) have observed lower transfer ratios for stearate (0.94), cholestanol (0.63), and oleic acid (0.89) multilayers. In the initial stages of multilayer deposition, Goranson and Zisman (18) observed that the amount of film which was deposited during the withdrawal operation appeared to continually decrease until finally no monolayer was transferred. Furthermore, the transfer ratio apparently depended on the withdrawal contact angle.

The structure of Y-type multilayers is expected from the deposition process to be an alternate head-to-head, tail-to-tail structure. Optical measurements (4, 19) showed that each double layer produces an increment of thickness nearly equal to twice the length of the extended fatty acid chain. X-ray diffraction measurements (20, 21) showed that the spacing of the metal cations was also nearly twice the thickness of a single layer, confirming the head-to-head, tail-to-tail

arrangement. X-type multilayers are expected to have a different structure than Y-type multilayers. The methyl groups of one layer should be adjacent to the carboxyl groups of the next layer on the basis that deposition occurs only on the immersion sequences of the dipping operation. However, x-ray diffraction measurements (22-24) showed that the spacing of the metal cations is essentially the same in both X- and Y-type multilayers. This indicates that the orientation of the molecules in both structures is the same. Apparently, the molecules of a deposited monolayer must overturn during the building of the X-type multilayers. Goranson and Zisman (18) suggested that the molecules overturn before the solid emerges from the monolayer-covered subsolution.

It appears that the solid substrate influences the deposition of the first several monolayers. Mertens and Plumb (25) suggested that the specific interactions between the monolayer and the metal surface determine the orientation of the first layer, and subsequently the orientation of the second layer is determined by the specific interactions between the molecules of the first and second layer. Handy and Seala (26) demonstrated that the physicochemical nature of the solid surface clearly influences the withdrawal contact angle. The contact angle was observed to change with the successive deposition of monolayers.

Stephens (27) in a recent publication advanced mechanisms for both X- and Y-type multilayer deposition. The proposed mechanisms were based on the principles of ionic equilibria in solutions, and his ideas of the mechanisms evolved during the preparation of several hundred multilayers for crystal analyzers.

PRESENTATION OF THE THESIS PROBLEM

It is not generally accepted that monolayers quantitatively deposit on solid surfaces with a transfer ratio of unity during Langmuir-Blodgett multilayer deposition. Furthermore, there is some uncertainty in whether the transfer ratio is the same for both the immersion and withdrawal sequences of the dipping operation because the reported transfer ratios have usually been average values.

The behavior of the first several monolayers in multilayer deposition has not been thoroughly investigated. It appears that the transfer ratio may systematically vary as deposition proceeds. These initial monolayers are important because they will influence the type and extent of additional monolayer deposition.

Many factors such as multivalent cations, pH, temperature, surface pressure, withdrawal rate, and the solid substrate influence the transfer ratio of amphipathic molecules. Important industrial processes such as pitch deposition in pulping and papermaking systems cannot be understood until the effects of the various variables on the deposition behavior are clarified. Unequivocal interpretations of the results of investigations utilizing the Langmuir-Blodgett method are only possible if the transfer ratio is accurately known. Although a considerable amount of information has been obtained on multilayer deposition, there is a need for relating Langmuir-Blodgett multilayer deposition to the behavior of the original monolayer on the subsolution surface.

Thus, the objective of this thesis was to relate the molecular properties of a monolayer to its behavior during the initial stages of multilayer deposition on selected solid surfaces.

APPROACH TO THE THESIS PROBLEM

Stearic acid was chosen as the film-forming material because it is the classical compound of monolayer studies. Its simple structure is similar to many long-chain amphipathic compounds. The stearic acid was spread on a 10^{-4}M $CaCl_2$ subsolution whose hydrogen ion concentration was varied over the pH range 2-9. The stearic acid-calcium stearate (Ca-H-St) monolayers which are formed under these conditions were selected because of the following reasons: (1) There are striking similarities between the multilayer deposition of pitch films and the multilayer deposition of fatty acid monolayers, (2) calcium ions are commonly found in high concentrations in pulping and bleaching systems and have been shown (28) to increase the deposition of pitch above pH 6, (3) Ca-H-St multilayer deposition occurs readily and very satisfactorily between pH 6.4 and 9.0, (4) Ca-H-St monolayers have been extensively studied, and (5) the monolayer composition can be varied from un-ionized stearic acid to calcium stearate by simple adjustment of the subsolution pH.

Paraffin, a low-energy solid, was selected as the solid substrate because (1) the uncertainties that generally exist with the preparation of a high-energy solid are not present, (2) metallic impurities in the subsolution arising from the solid are avoided, (3) the surface can be made very smooth, and (4) paraffin is a model of the system in which a long-chain polar organic compound is already deposited or adsorbed as a monolayer on reactive metals such as copper and iron, a situation probably not uncommon in papermaking systems. In addition, the selection of paraffin eliminated the common procedure of rubbing a layer of ferric stearate or paraffin wax on a solid surface until a monomolecular layer remains in order to provide a good foundation on which multilayers can be built.

The behavior of stearic acid monolayers on the $CaCl_2$ subsolutions was characterized by surface pressure-area isotherm, surface potential, surface viscosity, and

monolayer stability measurements. An indication of the monolayer stability was obtained by measuring the decrease in film area as a function of time at constant surface pressure. The nature of the film area decrease was investigated further by autoradiography and electron microscopy. The monolayer properties were determined at the same surface pressure used in multilayer deposition, 31 dynes/cm. This surface pressure was selected because the transfer ratio has a greater tendency to be unity at this high pressure.

Multilayers were deposited onto paraffin substrates by the Langmuir-Blodgett method with an automatic film balance designed to maintain constant surface pressure. This system quantitatively measured the film area decrease at constant surface pressure and avoided the complications that arise from the use of piston oils. Multilayer deposition was characterized by determining the (1) withdrawal contact angle by a cinematographic method during the withdrawal operation, (2) homogeneity of deposition by autoradiography, and (3) transfer ratio by two methods.

The transfer ratio was determined by the classical method which measures the film area decrease and the geometrical area of the solid from the corresponding distances the compression barrier and the solid slide move during the deposition sequence. The transfer ratio was determined for each of the initial four successively deposited monolayers in multilayer deposition on the paraffin substrates. In addition, the transfer ratio was also determined by counting the activity of radioactive bilayers. The transfer ratios determined by the two methods were compared in order to clarify the deposition mechanism. The withdrawal contact angle was related to the behavior of the molecules of the immersed monolayer at the solid/liquid interface. The structure of the monolayers and multilayers was extensively examined by electron microscopy.

EXPERIMENTAL MATERIAL, APPARATUS, AND PROCEDURES

Zisman (29) has clearly emphasized why special research techniques and well-controlled and well-characterized materials must be used in surface-chemical research. Extreme chemical purity and care in manipulating materials are necessary to avoid obtaining incorrect, unreproducible, or confusing experimental data. Lack of awareness of these requirements is responsible for the large mass of confusing or misleading data and conclusions in the literature.

It is for this reason that the chemical purity, surface characterization, and laborious attention to details in manipulating materials and measurement of the surface-chemical properties are emphasized. With this information the reader is better able to judge the quality of the surface-chemical system and the reliability of the data which underlie the conclusions.

PREPARATION OF STEARIC ACID SPREADING SOLUTIONS

Stearic acid was obtained from Fluka A.G. and was labeled "Puriss." A sample was methylated and analyzed for its purity by gas chromatography. The sample contained 99.6% C_{18}, 0.2 C_{16}, and 0.2% C_{22} saturated acids. Its melting point was 69.2°C. The conditions of the gas chromatographic analysis are given in Appendix I.

Radioactive stearic acid, labeled with C^{14} in the carboxyl group and having a specific activity of 58 millicuries/millimole, was supplied as a benzene solution by Dhom Products, Ltd. This material was selected after evaluating the purity of several stearic-1-C^{14} acids from different suppliers in the "as-received" condition by gas chromatographic analysis. The results of a further test on the purity of these materials by a surface chemical technique, surface pressure-area (II-A) isotherms on pH 2.00 subsolutions, clearly illustrates the desirability of this supplemental evaluation for high-purity fatty acids. The results of both evaluations

are given in Appendix I. The stearic-1-C^{14} acid supplied by Dhom Products, Ltd. contained 99.5% C_{18}, 0.2% C_{20}, and 0.3% C_{22} saturated acids.

Stearic acid spreading solutions were prepared in volumetric flasks with accurately weighed samples (to the second decimal place in milligrams) with a concentration of 5×10^{-3} M in n-hexane. The flasks were calibrated by the double weighing method. The flasks were stored in clean glass bottles containing the pure solvent in order to minimize solvent evaporation from the volumetric flasks. Spreading solutions were not used for longer than 5 days in the determination of the surface pressure-area isotherms because of possible errors arising from solvent evaporation.

Reagent grade n-hexane (Matheson Coleman & Bell) was twice distilled from pyrex apparatus, and the middle cut was slowly percolated through an adsorption column of alumina and silica gel. The nonvolatile surface-active impurities in the purified hexane were estimated by the surface-chemical procedure of Robbins and LaMer (30). The maximum error in the area/molecule of stearic acid at a surface pressure of 1 dyne/cm. due to surface-active contaminants present in the hexane and subsolution is +0.03% or approximately +0.01 $A.^2$ The procedures and calculations are given in Appendix I.

The stearic-1-C^{14} acid was further purified by the method developed by Gaines (31). This procedure was employed because of the very minute amount of stearic acid, approximately 20 mg. The sample was dissolved in purified n-hexane, extracted first with 1N HCl, and then extracted with several portions of triple distilled water. The solvent was evaporated, and the stearic acid was dried over "Drierite." The radioactive stearic acid spreading solution was prepared by mixing the stearic-1-C^{14} acid with the required inactive stearic acid. The specific activity of this spreading solution was 14.3 millicuries/millimole corresponding to 23.1% C^{14}-labeled

stearic acid. The purity of the inactive and radioactive stearic acid was further attested by the essentially identical behavior of their surface pressure-area isotherms as shown in Fig. 3.

PREPARATION OF SUBSOLUTIONS

The water used for the subsolutions was triple distilled, the second distillation from alkaline permanganate. Laboratory distilled water was obtained from a commercial pyrex still using feed water deionized by passage through a mixed-bed ion-exchange resin column. Redistilled water was obtained from a two-stage pyrex still using the laboratory distilled water as feed. The first stage consisted of distillation from a solution of 0.02% potassium permanganate and 0.05% potassium hydroxide. This procedure removed residual organic matter, especially the nitrogenous material arising from the ion-exchange resins (32, 33). The second stage avoided the addition of acid in order to minimize inorganic contamination. The specific conductance was determined with a model MIC 1201 Numinco electrophoretic mass transport analyzer. Only water with a specific conductance less than 1.2×10^{-6} ohm^{-1} $cm.^{-1}$ was used for the subsolutions. The water was also free of any significant surface-active material as shown by the maximum error arising from the nonvolatile surface-active impurities in the spreading solvent and subsolution. The cleanliness of the water surface was also checked by a surface-chemical technique. No detectable surface pressure was recorded for the triple distilled water when approximately 96% of the water surface was scanned by bringing the compression barrier as close as possible to the float.

Ultra Pure calcium chloride tetrahydrate with < 10 p.p.m. foreign multivalent ions was supplied by T. J. Sas, London. A standard solution of 0.0317M calcium chloride was stored in a pyrex vessel designed for siphoning aliquots and preventing evaporation of the main solution. The calcium concentration was obtained from

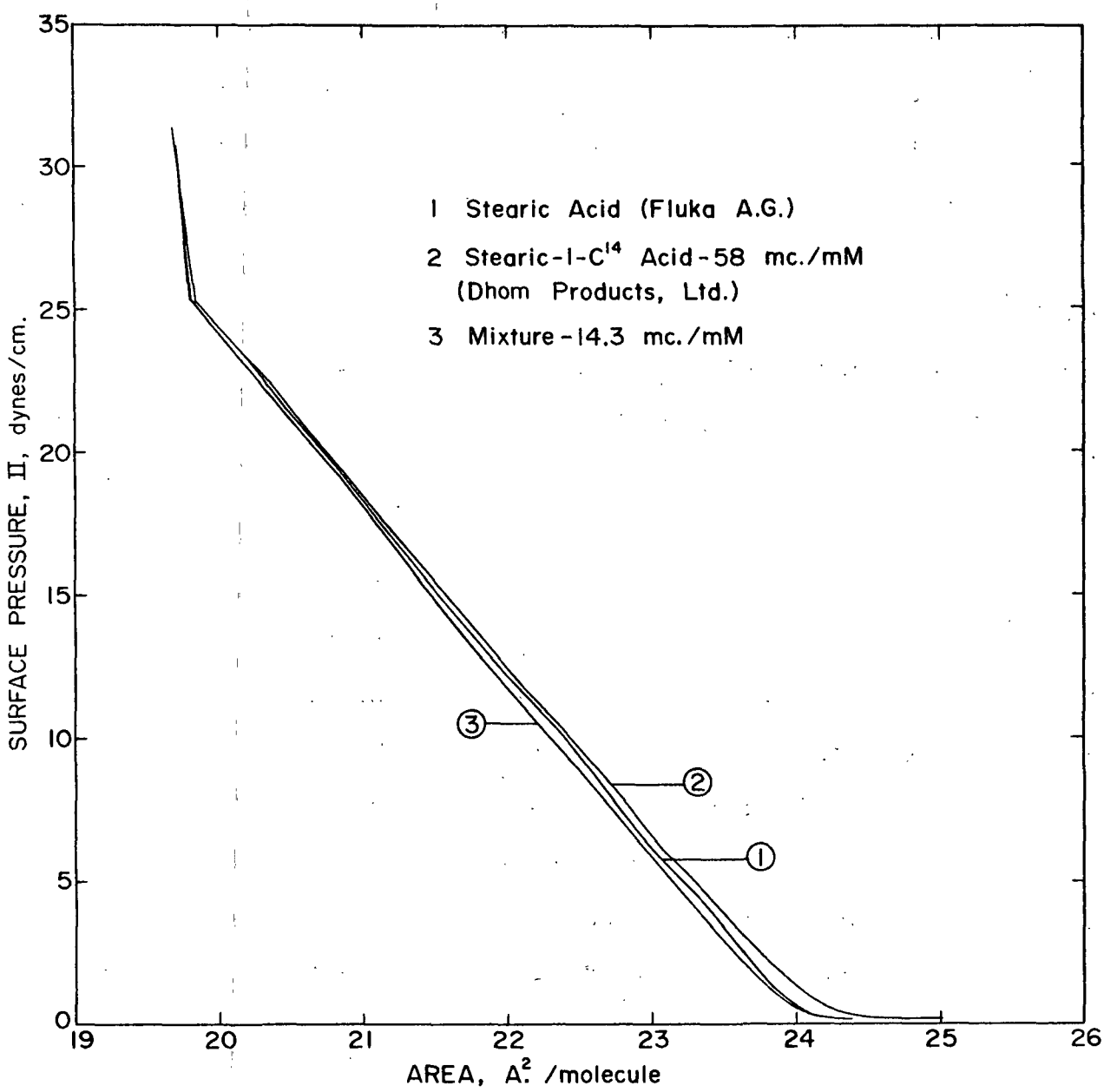

Figure 3. The Surface Pressure-Area Isotherms of Stearic Acid Monolayers on pH 2.00 Subsolutions (Corrected to Have the Same Area at $\underline{\Pi}$ = 30 Dynes/cm. as Inactive Stearic Acid). Compression Rate = 1.5 A.^{2}/Molecule/Min. $\underline{T}$ = 20.7°C.

the determination of the chloride concentration by the Volhard titration method. 10^{-4}M $CaCl_2$ subsolutions were prepared by volumetric addition of the required standard solution. The subsolution pH was varied between the pH range 2-9 by the addition of hydrochloric acid, potassium bicarbonate, and potassium hydroxide of analytical reagent quality. Potassium hydroxide was added to a subsolution containing 10^{-3}M potassium bicarbonate in order to obtain a subsolution pH greater than 8.3. The precipitation of the carbonate does not occur even at pH 9 under these conditions (34). The solutions were equilibrated with air by bubbling filtered water-saturated air through the subsolutions having a pH > 5.8 for about 30 minutes. Although the subsolutions were stable below pH 8.0, higher values of pH slowly absorbed CO_2 from the atmosphere over extended time periods. Because of this decreasing subsolution pH with time (< 0.05 pH unit/hour), the pH of all subsolutions was measured immediately after completion of the experiment. The pH of calcium-free subsolutions was adjusted and measured in an identical manner.

A Model 12 Corning Research pH meter equipped with calomel and silver-silver chloride electrodes was used for measurement of the subsolution pH. NBS potassium tetroxalate, NBS sodium tetraborate decahydrate, and commercial buffers were used to standardize the pH meter. The pH could be measured accurately to within ±0.01 pH unit with the expanded scales.

DETERMINATION OF SURFACE PRESSURE-AREA ISOTHERMS

APPARATUS

The automatic Langmuir-Adam film balance used by Major (35) was modified to include constant surface pressure operation. It was necessary to maintain a constant surface pressure for the Langmuir-Blodgett multilayer deposition studies and the surface potential, surface viscosity, and monolayer stability measurements.

The classical piston oils were not used because they provide a source of possible contamination, and the film area that is removed from the surface as a result of Langmuir-Blodgett deposition and/or lost by the processes of evaporation, dissolution, or monolayer collapse cannot be accurately measured. The design used the null-deflection balance to detect a change in the surface pressure, and the compression barrier was automatically activated to correspondingly return the balance to null position. The decrease in film area then could be accurately measured from the changes in the barrier position. The basic features of Major's apparatus were retained. A complete description of the design and the method of operation of the apparatus has been presented by Major. Views of the apparatus and automatic film balance are shown in Fig. 4 and 5. A schematic diagram of the apparatus used for insoluble monolayer and Langmuir-Blodgett multilayer deposition studies is also shown in Fig. 6.

The automatic film balance consisted of a Lucite trough (59.2 × 13.4 × 1.2 cm.) which was rigidly mounted to a brass support and contained a well (3.2-cm. long, 8.4-cm. wide, and 5.4-cm. deep) centered about 10 cm. from the mica float. The well accommodated the solid slides used for Langmuir-Blodgett multilayer deposition. The trough edges were covered with polyfluorocarbon tape, and purified white paraffin wax (melting range 63-69°C.) was applied while molten to cover the tape seams and remaining parts of the trough. The surface pressures were measured with a Cenco du Nouy torsion head equipped with a monel torsion wire (torsion constant 0.374 dynes/cm./degree), a lightly paraffined mica float, thin teflon foil end loops, and a magnetic damper. The sensitivity of the surface pressure measurements and the constant pressure operation was ±0.2 dynes/cm. The Lucite compression barrier and sweeping barriers were also covered with polyfluorocarbon tape. The compression barrier was driven by a variable speed ball/disk drive (Graham Model BD4) coupled to a reversible synchronous motor (Slo-Syn motor, Type SS150-P1). The barrier speed

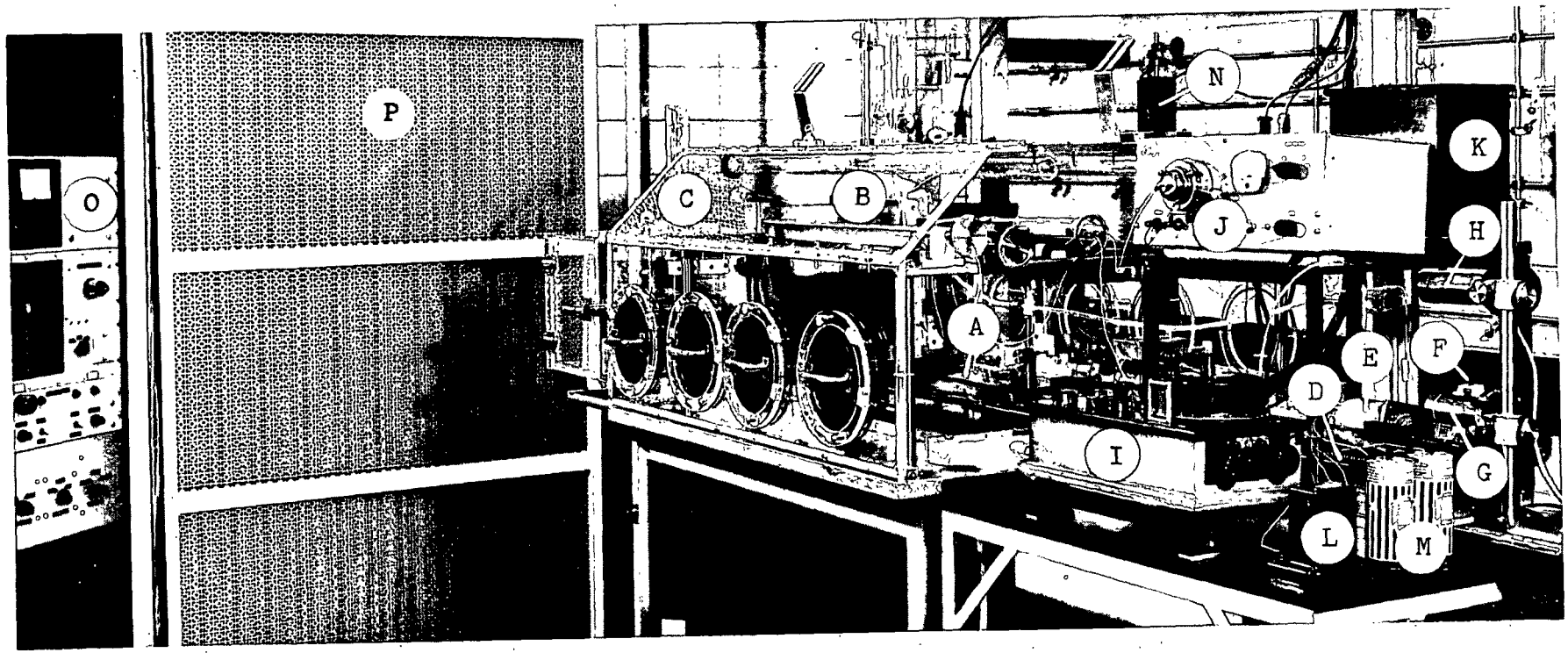

Figure 4. Apparatus for Studying Insoluble Monolayers and Langmuir-Blodgett Multilayer Deposition. A. Film Balance; B. Unislide Assemblies for Scanning the Surface with the Air Ionizing Electrode; C. Lucite Cabinet; D. Driving Screw; E. Compression Barrier Drive Motor; F. Variable Speed Drive; G. Lamp; H. Photoresistors; I. Potentiometer; J. Electrometer; K. Galvanometer; L. Standard Cell; M. Dry Cells; N. Dipping Solid Slide Drive Motor; O. Control Panel; P. Air Filter

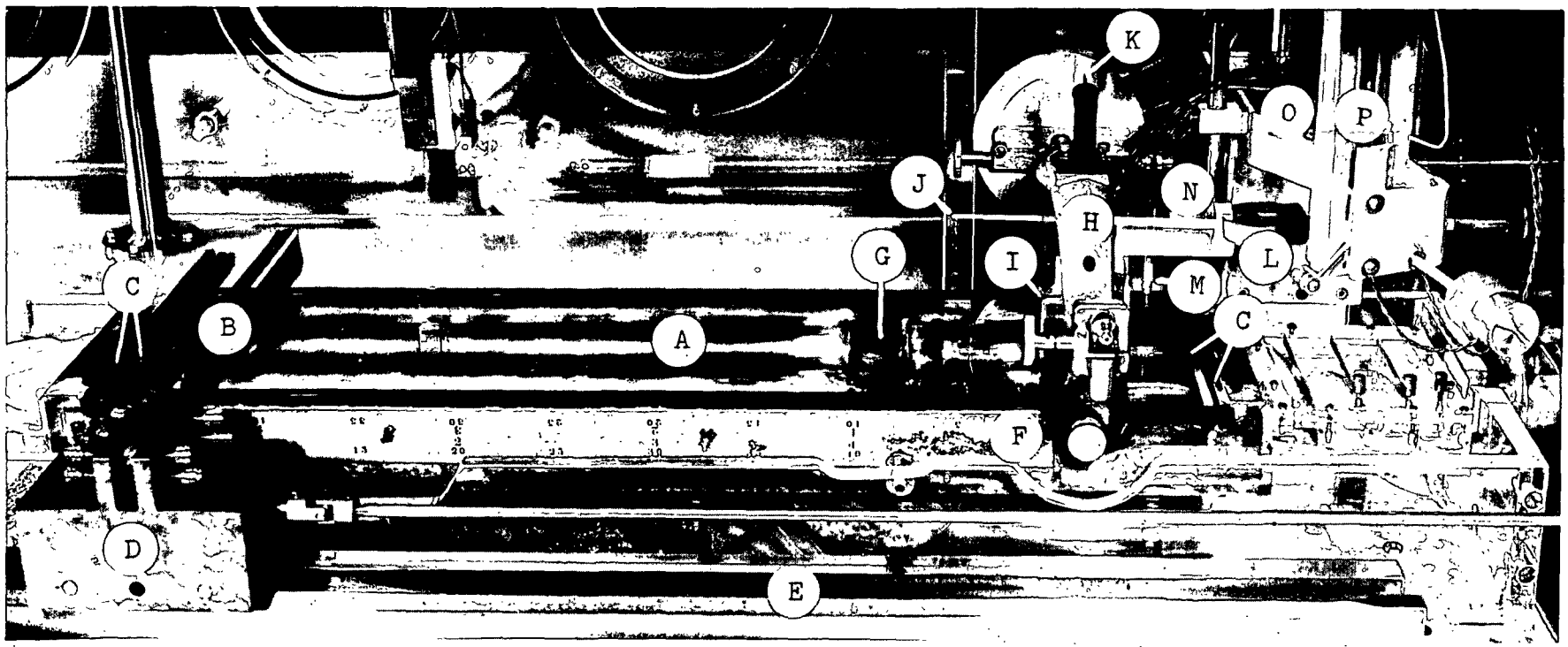

Figure 5. A View of the Automatic Langmuir Film Balance. A. Lucite Trough; B. Compression Barrier; C. Sweeping Barriers; D. Compression Barrier Carriage; E. Guide Rails; F. Trough Scale; G. Dipping Well; H. Torsion Head; I. Float Stirrup, Float, and Ribbon Assembly; J. Calibration Arm; K. Mirror; L. Magnetic Damper; M. Thermistors; N. Teflon Thermistor and Calomel Electrode Holder; O. Extension Arm; P. Rapid Advance Unislide Assembly

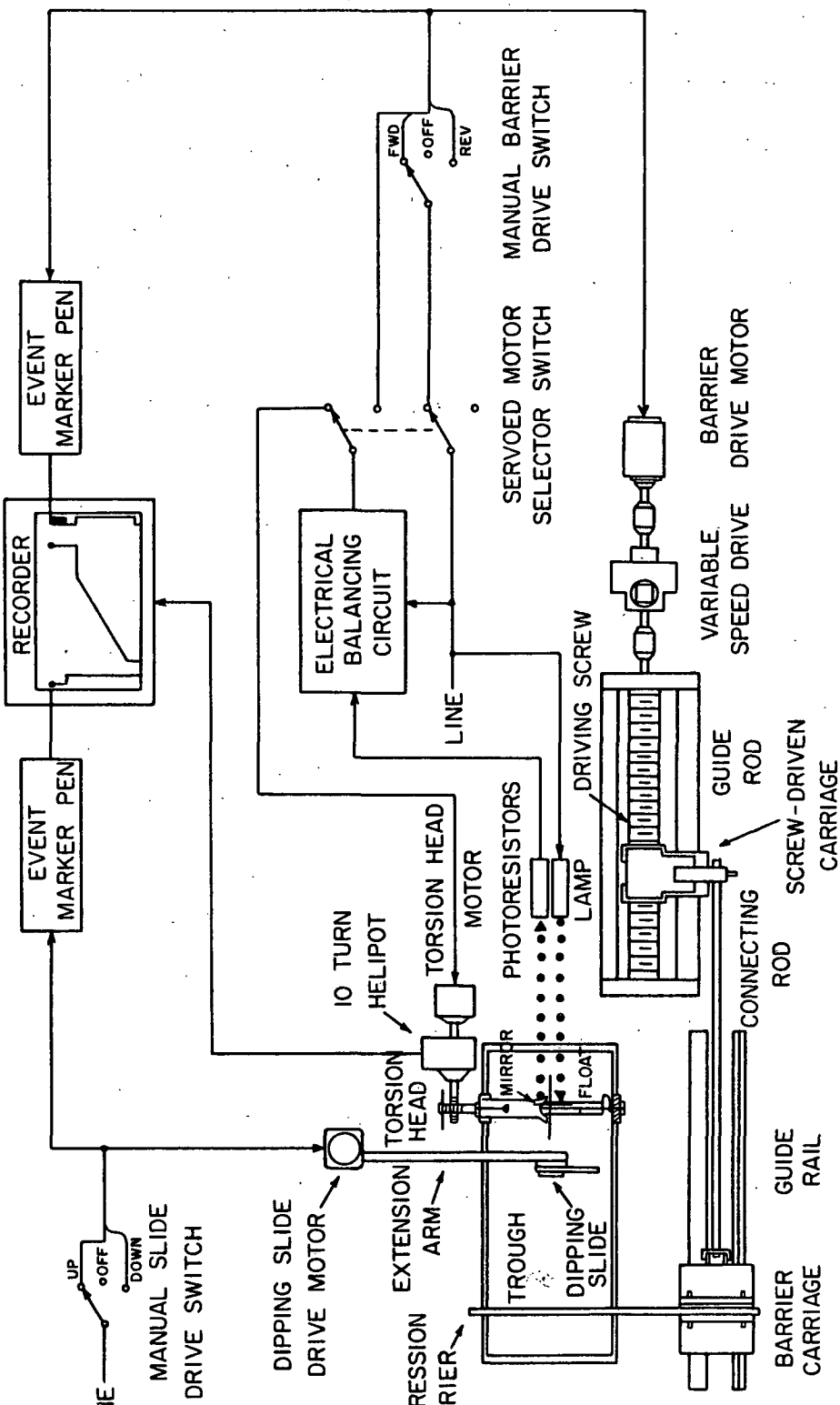

Figure 6. Schematic Diagram of the Automatic Film Balance with Constant Surface Pressure Operation Controls for Insoluble Monolayer and Langmuir-Blodgett Multilayer Deposition Studies

was 1.99 cm./min. which corresponded to an average compression rate of 1 $A.^2$/molecule/min. for the surface pressure-area isotherms. A glass probe thermistor (Fenwall GB31 P2) sensitive to ±0.01°C. was used to measure the temperature of the subsolution. (The mounting and calibration procedures of the thermistor are given in Appendix II.)

The film balance and barrier drive mechanism were mounted on separate 1-inch thick aluminum tooling plate. Unisorb pads supported the tooling plates which were located on separate tables to minimize vibration. A Lucite cabinet enclosed the film balance. The entire apparatus was placed in a dust-free atmosphere maintained at 22°C. and 50% R.H.

EXPERIMENTAL

In order to obtain surface pressure-area isotherms, it is necessary to determine, for a given surface pressure, the number of film molecules applied to the surface and the total area occupied by these molecules such that the area/molecule can be calculated. The surface pressure was determined with the automatic film balance as described by Major. The number of molecules was determined by applying a known volume of the spreading solution from an Agla micrometer syringe. The total area was obtained from the distance the compression barrier was from the mica float, trough width, and appropriate corrections.

In practice, the displacement of the recorder pen along the Y-axis of the chart on a T-Y recorder provided a measure of the surface pressure. The displacement of the chart along the time axis provided a measure of the position of the compression barrier.

Surface Pressure

The displacement of the chart recorder pen is directly proportional to the force required to maintain the film balance in null position. The torsion head is calibrated by applying known forces to the mica float by placing various weights on the calibration arm of the float stirrup. These weights were calibrated and compared to a standard NBS weight by the double weighing method. The pulley attached to the potentiometer is turned by hand until the electrical bridge is balanced as shown by the indicator lamps. The pen displacement caused by the movement of the potentiometer slider is registered on the chart recorder paper. A plot of pen displacement as a function of the surface pressure yields the calibration curve. The surface pressure is determined from the relation,

$$\Pi = (wg\ell_c)/(\ell_f L), \qquad (1)$$

where

Π = surface pressure, dynes/cm.

w = calibration weight, grams

g = gravitational constant

ℓ_c = lever arm for the calibration weights, cm.

ℓ_f = lever arm for the float, cm.

L = effective length of the float, cm.

The effective float length, L, is generally taken as the length of the float plus half the width of the gaps occupied by the Teflon end loops.

The calibration curve is essentially linear for surface pressures in excess of about 3 dynes/cm. The operational sensitivity of the film balance is 0.20 dynes/cm./mm. where the operational sensitivity is defined as the reciprocal of the slope of the calibration curve. The torsion head was calibrated daily during the Π-A isotherm

determinations. Occasional calibrations during the constant pressure operations showed that there was no appreciable change of the torsion head during the study.

Number of Film Molecules

The determination of the number of film molecules spread onto the aqueous substrate requires an accurately known concentration of stearic acid in a spreading solvent. This spreading solution, whose preparation has previously been described, must then be spread onto the subsolution surface in such a manner that the deposited volume is accurately determinable. An Agla micrometer syringe (Burroughs Wellcome Co.) fitted with a Luer glass needle was used to deposit the spreading solution onto the subsolution surface. The syringe and needle were cleaned by immersion in chromic acid cleaning solution, then copiously rinsed with distilled water, dried with a nitrogen jet, rinsed with n-hexane, and finally dried.

The Agla syringe was calibrated with distilled water. According to the manufacturer, the Agla syringe is supposed to deliver 0.0100 ml./micrometer turn; however, the calibration yielded 0.00979 ± 0.00003 ml./micrometer turn at the 95% confidence limits. Great care must be exercised in the calibration of the syringe. The estimated error for a typical delivered volume of about 0.08 ml. is ±0.5%.

Film Area

In order to obtain the occupied molecular area at a given surface pressure, it is necessary to determine the (1) displacement of the compression barrier from the corresponding displacement of the chart along the time axis of the recorder, (2) trough scale calibration, and (3) increase in available area due to the Teflon end loops and the meniscus of the subsolution.

The pointer attached to the compression barrier carriage was positioned on a reference mark (48.00 cm.) on the trough scale at the start of the II-A compression

curves. From the calibration curve of the displacement of the compression barrier, a given displacement of the chart yields a corresponding barrier displacement. However, the distance of the compression barrier from the mica float is the quantity of interest. The trough scale was independently calibrated with an accurately machined rod of known length to yield the necessary correction applicable to the scale readings given by the pointer. The total area is found by multiplying the barrier distance by the trough width and applying the necessary area corrections.

Compression Barrier Displacement Calibration

The displacement of the chart along the time axis is proportional to the total area occupied by the film molecules (assuming negligible contribution from the end loops). The displacement of the chart is directly correlated with the displacement of the compression barrier from the reference point. The recorder was equipped with an event marker pen which was activated by the compression barrier drive motor. The chart drive motor ran continuously while the barrier drive motor was turned on for various time periods. The chart displacement determined from the on-off cycle of the event marker pen and the displacement of the compression barrier determined from the initial setting and the final reading on the trough scale were recorded for each run. A plot of the chart displacement versus the displacement of the compression barrier established the calibration curve.

The linear speed of the compression barrier and the chart were 1.99 cm./min. and 60 in./hr., respectively. The regression line determined by the method of least squares was calculated over the time span from 5.0 to 15.0 minutes. The 95% confidence limits on the barrier displacement were ±0.05 cm. or a maximum error of ±0.5%.

Trough Scale Calibration

As previously mentioned, the barrier position was read indirectly via a pointer attached to the compression barrier carriage. This reading on the trough scale must be corrected to yield the true barrier distance because the zero point on the scale does not correspond to the leading edge of the mica float. The calibration of the scale was performed with a 2.500-inch long stainless steel rod mounted to a special compression barrier. The tip of the rod was positioned flush with the leading edge of the mica float, and the pointer was read on the trough scale. The difference between the two values, taking into consideration the thickness of the polyfluorocarbon tape covering the barrier, yielded the correction that was to be applied to the scale readings. This correction varies with the null position of the mica float and was rechecked occasionally.

Area Corrections

The meniscus of the subsolution and the area occupied by the Teflon end loops of the float assembly lead to increases in the area available to the film molecules. The two U-shaped ribbon areas and an end view of the meniscus were photographed. Three sets of XY coordinates were obtained from the negative of the meniscus view using a digital readout XY coordinate comparator. A computer program determined the ratio of the length of the subsolution surface to the trough width. The increase in trough width due to the meniscus effect was +0.52%. Internal calipers were used to measure the actual width of the gaps, and then a planimeter was used to determine the area occupied by the two Teflon end loops in the photographic negatives. The projected area was determined from knowledge of the camera angle. The area occupied by the two Teflon end loops was 2.25 $cm.^2$

Total Area Available to the Monolayer

The total area is equal to

$$A_t = (BW) + C \qquad (2)$$

where

$\underline{A_t}$ = total area, cm.^{2}

$\underline{B}$ = barrier distance, cm.

$\underline{W}$ = length of the subsolution surface, cm.

$\underline{C}$ = area occupied by the Teflon end loops, cm.^{2}

A propagation-of-error treatment was applied to the total area $\underline{A_t}$ at two barrier distances after the limits of error for the quantities $\underline{B}$, $\underline{W}$, and $\underline{C}$ were determined from the experimental data. A summary of the results is shown in Table I at one determination of the chart displacement.

TABLE I

CONFIDENCE LIMITS AND PERCENT ERROR OF THE TOTAL AREA

Barrier Distance, cm.	Total Area, cm.^{2}	95% Confidence Limits, cm.^{2}	Error, %
32.00	431.05	±0.72	±0.17
12.00	163.05	0.70	0.43

Failure to apply the two area corrections leads to estimated errors of -1.0 and -1.9% in the total area when the barrier distances are 32 and 12 cm., respectively.

Technique

The subsolution which was added to the trough by a graduate cylinder was allowed to condition for about one hour. The test and reference surfaces of the subsolution were cleaned by sweeping with movable barriers. The sweeping barriers were left at the ends of the trough, isolating the adsorbed insoluble impurities. The Agla syringe was used to deposit 0.07 to 0.08 ml. of the spreading solution uniformly over the subsolution surface. A minimum time of six minutes was allowed for the reaction before the monolayer was compressed at the average rate of 1 A.^{2}/molecule/min.

After each II-A isotherm determination, the compression barrier was returned to its initial position. The film material was skimmed from the trough, and then the trough was flooded with distilled water. The remaining liquid was removed from the trough by suction. The trough edges were cleaned with n-hexane. The trough was again flooded with distilled water and emptied by suction. When not in use, the trough was filled with distilled water.

The II-A isotherms were generally duplicated, and the results were superimposed. The temperature control of the subsolution was within ±0.3°C. The estimated errors were ±0.1 dyne/cm. for the surface pressure and ±0.1 $A.^2$/molecule for the area.

SURFACE POTENTIAL MEASUREMENTS

APPARATUS

The ionizing electrode method was used for the surface potential measurements. This method involves ionization of the gas phase above the liquid/air interface, so that the potential difference between two electrodes, one in the subsolution and the other in the air above the surface, can be measured directly. The arrangement of the apparatus is schematically illustrated in Fig. 7. The ionizing electrode which was fabricated by Nuclear Radiation Developments, Inc. was a 6-mm. square Ra^{226} foil with an activity of 5 μc. sandwiched between a silver base plate and a thin gold overlayer. After the edges are sealed, the square is attached to a standard brass bolt. The ionizing electrode was positioned 4 mm. above the liquid surface and was connected in series to a vibrating reed electrometer (Cary Model 32), precision potentiometer (Leeds & Northrup Co. Type K), and a miniature calomel electrode in the subsolution. The ionizing electrode was connected to the input terminal of the electrometer with ultraminiature low-noise Teflon insulated coaxial cable (Microdot 250-3808). The apparatus is shown in Fig. 4 and 8.

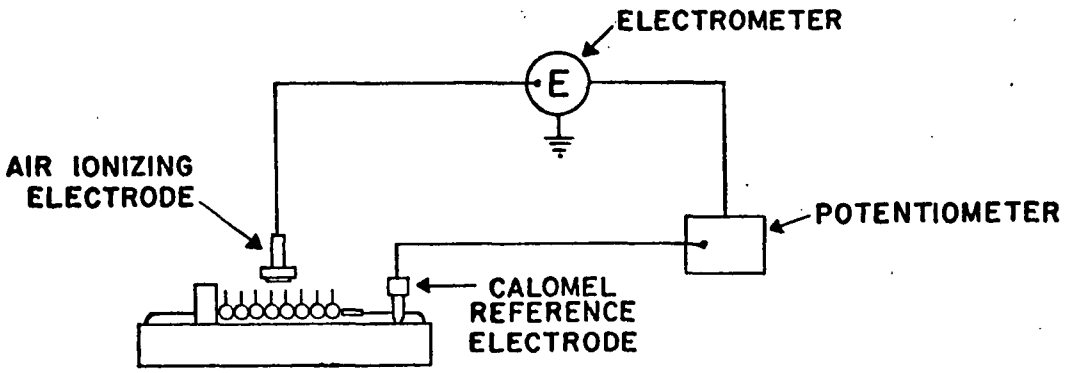

Figure 7. Schematic Diagram of Arrangement for Measuring Surface Potentials by the Ionizing Electrode Method

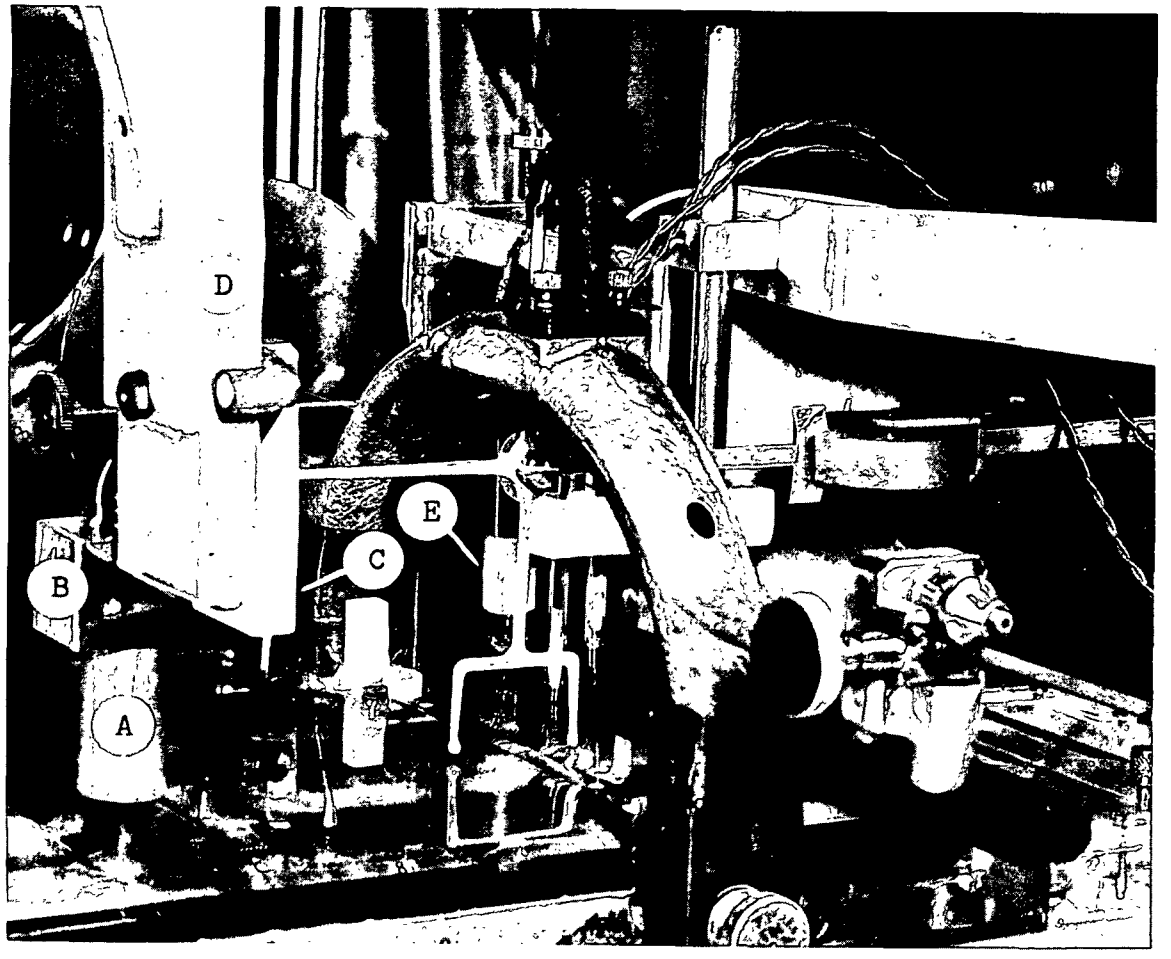

Figure 8. Apparatus for Surface Potential Measurements by the Ionizing Electrode Method. A. Brass Tube Shielding the Air Electrode; B. Additional Shielding; C. Teflon Air Electrode Holder; D. Rapid Advance Unislids Assembly; E. Calomel Reference Electrode

The ionizing electrode, carefully shielded, was mounted in a Teflon holder which was attached to a vertical Rapid Advance Unislide assembly. The assembly was mounted to two horizontal Unislide assemblies combined to provide XY motion. This entire Unislide combination having scales and verniers was mounted on a stainless steel frame above the trough. The ionizing electrode could then either be moved to scan the monolayer surface or be positioned at one specific location. The calomel electrode was mounted in the same Teflon holder containing the thermistor. This arrangement permitted quick withdrawal from the subsolution when cleaning the surface and reproducible positioning upon reimmersion.

EXPERIMENTAL

Strictly speaking, ΔV is the change in the Volta potential difference or the change in the surface potential. However, in monolayer studies the term surface potential is usually restricted to the change in the Volta potential difference which is produced when a film is introduced at an initially clean interface.

The general procedure for obtaining the surface potential, ΔV, is to measure the potential of the clean subsolution surface, V_o, and monolayer-covered surface, V. The difference between the two potentials, $V - V_o$, is then ΔV. Figure 9 shows the variation of the potential of a previously "cleaned" subsolution surface as a function of time. This decrease in the potential is probably due to the contamination of the surface by impurities. However, when the surface was swept clean, the potential of the clean surface increased with time. The stability of this reference potential was further studied. The potential of a clean water surface was measured as a function of time. The results shown in Fig. 10 indicate that the change in the reference potential is linear, to a first approximation.

Bergeron and Gaines (36) state that the reference value is the major problem in the precise measurement of ΔV. The difficulty comes from maintaining a stable

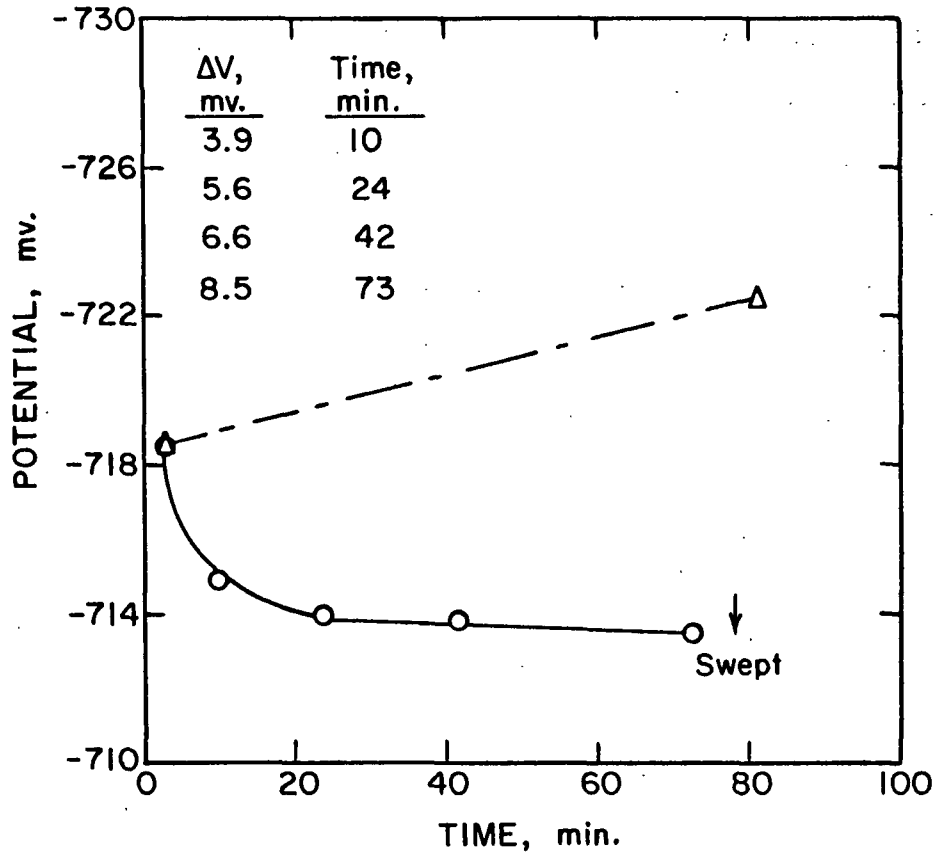

Figure 9. Typical Variation of the Potential of a Clean (Δ) and Nonmonolayer Covered (O) 10^{-4}M $CaCl_2$ Subsolution Surface with Time. pH = 5.83; T = 20.8°C.

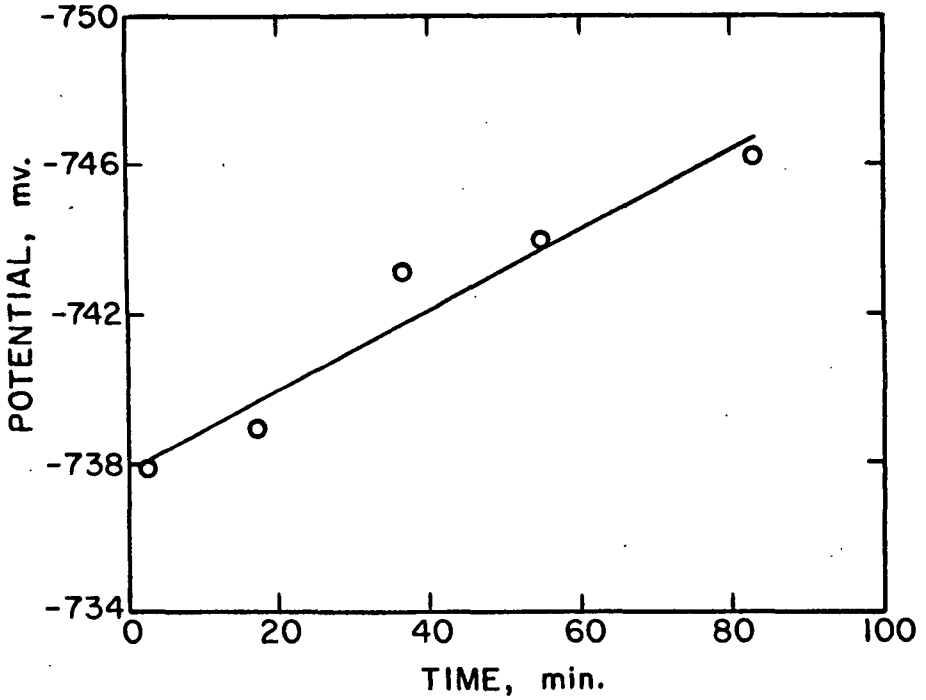

Figure 10. Variation of the Potential of a Clean 10^{-4}M $CaCl_2$ Subsolution Surface with Time (Surface Swept Before Each Determination). pH = 8.25; T = 20.8°C.

reference (ionizing) electrode in the air above the subsolution surface due to adsorption and desorption of gas phase components. This problem is very serious when the reference electrode is located over a water surface which is nearly saturated with water vapor. The common practices used to minimize reference electrode drifts include the use of a noble metal for the reference electrode, the aging of the electrode under the experimental conditions, and circulating a stream of moist air through the enclosure to stabilize the environment of the electrode.

In addition to putting trays of water on the floor of the cabinet, the reference electrode drift was corrected by measuring the reference potential, the value for a clean surface, before spreading the monolayer and after measuring the potential of the monolayer-covered surface. The reference potential at the time of the measurement of the potential of the monolayer-covered surface was calculated by assuming linear reference potential drift.

The experimental procedures were as follows: The subsolution surfaces were cleaned after the ionizing electrode was conditioned over the subsolution for about one hour. The ionizing electrode was positioned and moved over the center and along the length of the trough to determine the reference potential. The monolayer was spread, the spreading solvent was allowed to evaporate for six minutes, and then the monolayer was compressed to the desired film pressure. The ionizing electrode was then moved along the length of the trough for the measurement of the potential of the monolayer-covered surface (usually within thirty minutes after cleaning the surface). The subsolution surface behind the compression barrier was cleaned. The ionizing electrode was then moved behind the barrier, and the reference potential was once again measured.

Although the drift in the reference potential averaged 6 mv., accurate and reproducible surface potential measurements were obtained when the procedure correcting for reference electrode drift was employed. Surface potential measurements of stearic acid on hydrochloric acid subsolutions at pH 2.00 gave a value of 398 ± 2 mv. at Π = 31 dynes/cm. This value is in excellent agreement with previously reported results (37-39). The reported ΔV values were generally reproducible within ±5 mv.

SURFACE VISCOSITY MEASUREMENTS

APPARATUS

Surface viscosities were determined by the method illustrated in Fig. 11 and described by Dreher and Sears (38), Washburn and Wakeham (40), Meyers and Harkins (41), and Trurnit and Lauer (42). Interchangeable 1-inch long Teflon inserts which contained a slit were transversely mounted into a Teflon compression barrier which was substituted for the standard compression barrier. The slits were machined with a metal slitting saw on a horizontal milling machine. Because the measurements were obtained over the surface viscosity range of 10^{-4} to 10^{-1} surface poise, it was necessary to use three slit widths (0.51, 0.81, and 1.59 mm.) to determine the surface viscosity.

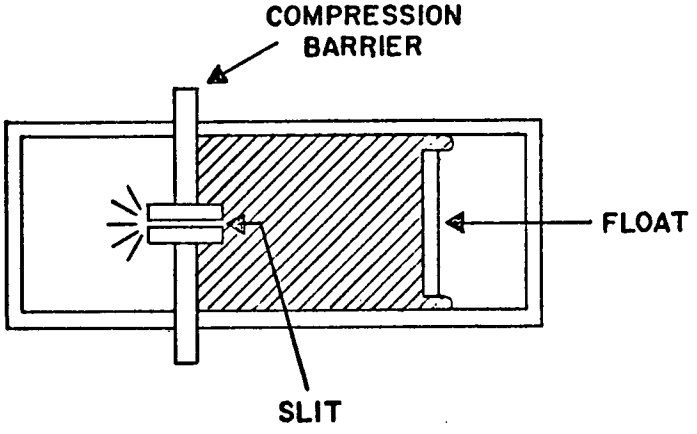

Figure 11. Schematic Diagram of Arrangement for Measuring Surface Viscosities by the Slit Viscometer. The Slit is Mounted in the Compression Barrier

EXPERIMENTAL

The back of the slit was closed with a mica gate which had been lightly paraffin-sealed to the Teflon insert. The monolayer was spread as usual; and after the film was compressed to a given surface pressure, the mica gate was removed. The monolayer began to flow through the slit onto the clean subsolution surface as a result of the pressure differential. As the surface pressure on the float began to decrease, the automatic film balance under constant pressure operation maintained the surface pressure constant by advancing the compression barrier at a corresponding rate toward the float. The flow rate of the monolayer through the slit was determined by measuring the time intervals of the barrier advancing a certain distance, usually 0.4 or 0.5 cm. After 30-60 sec., the flow rate was approximately constant for several minutes before gradually increasing or decreasing. Below pH 5 the flow rate was corrected for the barrier movement due to monolayer collapse (to be shown later) by measuring the average rate of barrier movement just before opening the slit. The contribution of the monolayer molecules to the surface pressure of the clean water surface was negligible, thus ensuring a constant pressure differential during the flow rate measurements.

The flow rate of the monolayer through the slit was used to calculate the surface viscosity by the equation given by Meyers and Harkins (41),

$$\eta_s = (\Delta\Pi a^3)/(12Q\ell) \qquad (3)$$

where

η_s = surface viscosity, g./sec. or surface poise

$\Delta\Pi$ = surface pressure differential, g./sec.^{2}

a = slit width, cm.

Q = flow rate of monolayer through slit, cm.^{2}/sec.

ℓ = slit length, cm.

This equation is valid only if the monolayer "slips" on the water surface.

However, Schulman and Teorell (43) showed that the water beneath the surface is dragged along with the flowing monolayer, and a correction must be made for this effect. Harkins and Kirkwood (44) derived a correction term for the drag of the underlying viscous liquid. The requirements that the canal be narrow and have its length much greater than its width are difficult to fulfill and limit the application to films of low viscosity.

Alternatively, Joly (45) allowed for the drag of the underlying water on the flowing film by introducing an empirical constant c. Suitable results were obtained with slits up to 5-mm. wide, and Crisp (46) demonstrated Joly's formula was applicable to slits as wide as 8 cm. Therefore, Joly's formula was also used to calculate the surface viscosity and is given by

$$Q = (\Delta\Pi/1c\eta_o)[a - 2(\eta_s/c\eta_o)^{\frac{1}{2}}\tanh\{(c\eta_o/\eta_s)^{\frac{1}{2}}a/2\}] \qquad (4)$$

where c represents the reciprocal of the thickness of the water layer influenced by the monolayer in $cm.^{-1}$, and η_o is the bulk viscosity of the subsolution. The value of $c\eta_o$ was interpolated from the table given by Joly which related $c\eta_o$ to the canal width. The interpolated values of $c\eta_o$ were 0.241, 0.216, and 0.161 $g./cm.^2/sec.$ for the slit widths of 0.51, 0.81, and 1.59 mm., respectively. The value of the surface viscosity in Joly's formula was solved with the computer program given in Appendix II.

In contrast to the results of Jarvis (47), it was more difficult to obtain reproducible measurements at the lower values of surface viscosity, apparently due to a partial closure of the narrow slit by dust particles or film material. The surface viscosity measurements were generally reproducible to within ±10% under the experimental conditions.

MONOLAYER STABILITY MEASUREMENTS

The monolayer stability at the liquid/air interface was obtained by measuring the decrease in film area as a function of time at constant surface pressure. This area decrease is due to the molecular processes of evaporation, dissolution, and/or collapse of the film molecules into a stable bulk phase. The spread monolayer was compressed to the desired surface pressure, and the automatic film balance controls were set for constant surface pressure operation. The initial barrier position was immediately recorded, and then the barrier position was measured as a function of time. The film areas were calculated from the corresponding barrier positions, and the percentage decrease in film area as a function of time was determined.

LANGMUIR-BLODGETT MULTILAYER DEPOSITION

APPARATUS

The solid slides on which monolayers and multilayers are deposited by the Langmuir-Blodgett method must be driven at reproducible, continuous, and uniform speeds. The solid substrates also must be reproducibly positioned over the dipping well. The apparatus designed to fulfill these requirements is shown in Fig. 12.

The solid slide was mounted in a Teflon holder attached to a slider which was easily inserted or removed from the base of a small Unislide assembly. This Unislide assembly was mounted on an extension arm attached to a vertical Unislide assembly equipped with a scale and vernier. An adjustable speed, reversible synchronous motor (Insco Multi-Speed Gearmotor, Model 06700-60H) was coupled to the vertical drive screw, producing six linear speeds from 0.760 to 38.0 mm./min. The second event marker pen on the recorder was connected to the slide motor.

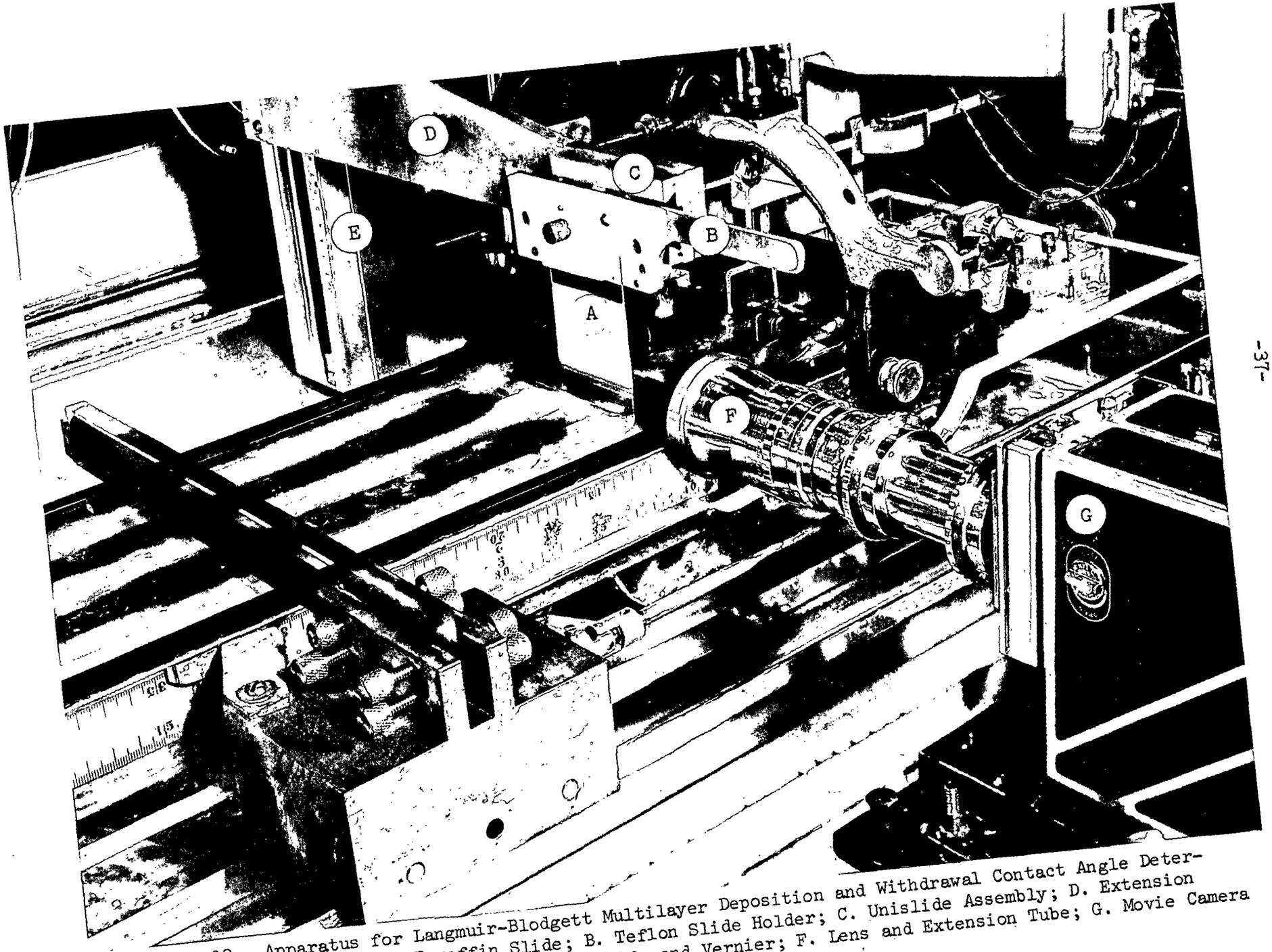

Figure 12. Apparatus for Langmuir-Blodgett Multilayer Deposition and Withdrawal Contact Angle Determination. A. Paraffin Slide; B. Teflon Slide Holder; C. Unislide Assembly; D. Extension Arm; E. Unislide Assembly with Slide and Vernier; F. Lens and Extension Tube; G. Movie Camera

The solid slide was positioned perpendicular to and centered on the trough axis 10 cm. from the mica float. The solid substrate was carefully aligned by adjusting with shims the base of the small Unislide assembly relative to the extension arm. The slides were reproducibly positioned and did not deviate more than 0.005 cm./cm. from the XYZ coordinate axes.

SOLID SUBSTRATES FOR MULTILAYER DEPOSITION

Paraffin and polytetrafluoroethylene (TFE) were selected as the low-energy surfaces onto which multilayers were deposited. In addition to the requirement that the solid have a very high chemical purity, it is necessary to prevent contamination of the solid substrate during the preparation and manipulation procedures. The procedure for preparing the solid substrate must be designed to produce a smooth surface in order to obtain reproducible deposition results. The prepared solid must also have a geometric structure whose area on which a multilayer is deposited can be accurately measured.

Paraffin

Paraffin wax (Sun Oil number 5512) with a melting range of 63-69°C. was purified to remove surface-active impurities by passing the molten paraffin through a silica gel adsorption column. Further details are given in Appendix I. The paraffin substrates on which the multilayers were deposited were paraffin-coated microscope slides (Corning 2947, 75 × 50 mm.) formed by immersing and withdrawing the slide from molten paraffin three times. The details of the procedure are presented in Appendix II. Three paraffin layers were required to ensure saturation backscattering of the paraffin substrate for the radiocounting measurements. This procedure was capable of producing very smooth, uniform, and reproducible paraffin substrates.

Figure 13 shows a typical cross section of the paraffin substrate. Photographs were obtained of the cross sections of the paraffin slide at the two extremes, about 3.0 cm., of the slide area over which a typical multilayer was deposited. A digital readout XY coordinate comparator was used to obtain the sets of XY coordinates of the paraffin perimeter and the microscope slide width. A computer program was used to determine the ratio of the perimeter length to the slide width. The paraffin perimeter was calculated after the microscope slide width was measured with a micrometer. The thickness of the paraffin on the glass slide over the corresponding length was measured with a dial indicator to determine the average thickness and taper of the paraffin. The results of the physical measurements of the paraffin slide are presented in Table II. Even though there was a small taper, a constant and reproducible perimeter (within ±0.3% at the 95% confidence limits) was obtained along the paraffin slide length. The smooth curvature of the perimeter (Fig. 13) at the sides of the slide permitted uniform deposition across the slide perimeter. Thus, accurate measurements of the slide area per unit slide length were obtained.

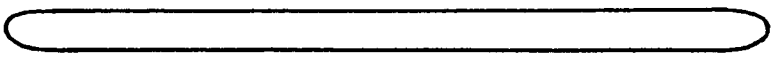

Figure 13. Typical Cross Section of the Paraffin-Covered Glass Slides

TABLE II

PHYSICAL MEASUREMENTS OF PARAFFIN SUBSTRATE

Perimeter, cm.[a]	10.45 ± 0.03[b]
Thickness, cm.[c]	0.048
Taper, cm./cm.[c]	0.003

[a] Average of four samples with two determinations per sample.
[b] 95% Confidence limits.
[c] Average of five samples.

The surface of the paraffin was examined by electron microscopy. Figure 14 shows typical electron micrographs of the paraffin surface at low and high magnifications. Although the surface was not macroscopically planar and may best be described as appearing to resemble "gentle rolling hills and valleys," the paraffin surface was extremely smooth. The procedure of molding paraffin against clean ferrotype plates is claimed to consistently produce specularly smooth paraffin surfaces (48). Typical electron micrographs of paraffin surfaces prepared by this technique are presented in Fig. 15 for comparative purposes. It is clearly evident that the paraffin surfaces used in this study were greatly superior with respect to surface smoothness.

In a further evaluation of the surface-chemical properties of the paraffin, the contact angles of water on the paraffin substrate were measured. The average contact angle is $111.7^\circ \pm 0.4^\circ$. Contact angles from 105 to 114° have been recorded by various workers for paraffin wax, the higher angles with very carefully purified specimens. According to Adam (49), 112 to 114° is probably the best value for really pure paraffin wax.

This preparation technique produced a paraffin substrate which was highly purified and very smooth. The paraffin slide area per unit slide length was very reproducible and accurately measured. The paraffin substrates were placed near an α-particle source for several minutes before use to discharge any possible static charges.

Polytetrafluoroethylene

The TFE used in this study was obtained from Chemplast, Inc. as white 3/32-in. Chemfluor TFE flattened stock. Clean, smooth TFE surfaces were prepared by the procedures developed by Fox and Zisman (50, 51). Pieces which were cut from the stock sheet and free from gross irregularities were machined into 75 × 50-mm. samples.

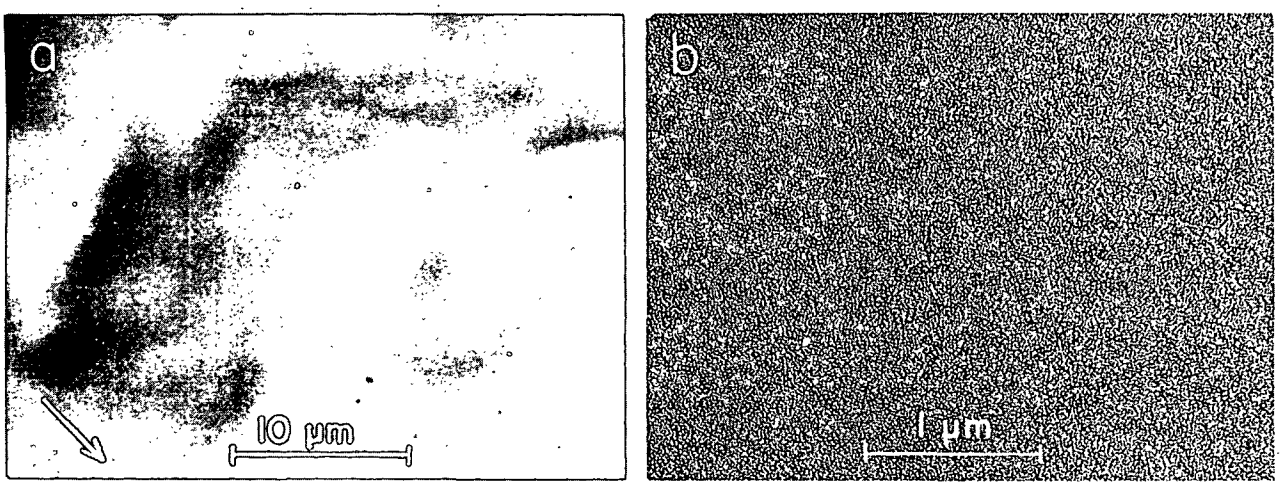

Figure 14. Electron Micrographs of (a) Paraffin Surface Prepared by Dipping a Microscope Slide Three Times Into Molten Paraffin (2260X), and (b) Same as (a) Except Greater Magnification (23,100X). Pd Preshadowed Replica at 20°. Arrow Indicates Direction of Shadow-Casting.

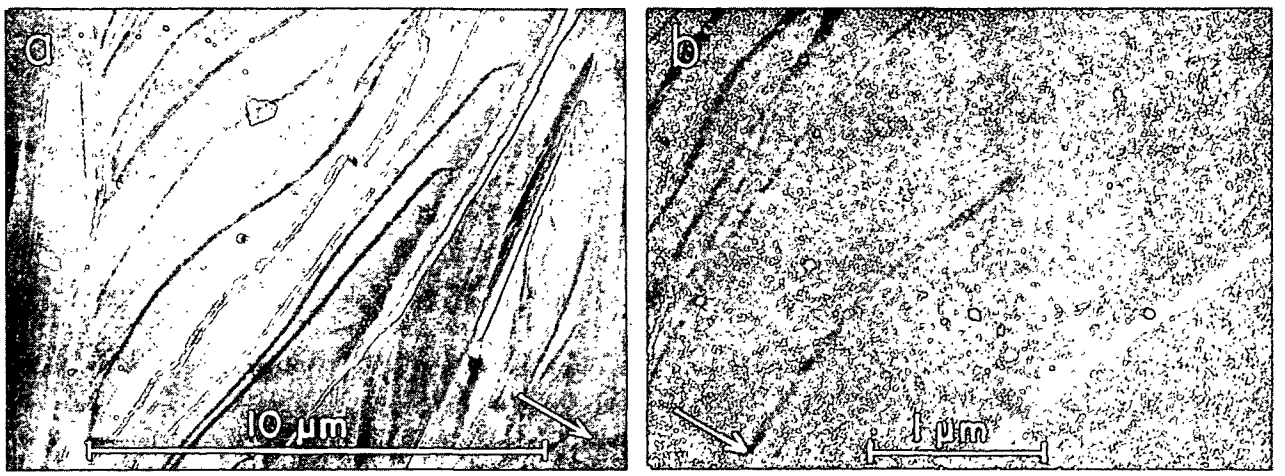

Figure 15. Electron Micrographs of (a) Paraffin Surface Prepared by Molding Against a Ferrotype Plate (6000X), and (b) Same as (a) Except Greater Magnification (23,300X). Pd Preshadowed Replica at 30°. From McIntyre (48).

A selected sample was boiled in nitric-sulfuric acid (1:2), rinsed by boiling in three successive changes of triple distilled water, and dried in a grease-free atmosphere. The clean TFE was placed between two blocks of thick scratch-free Pyrex plate glass which had been previously acid-cleaned. This system was then pressed in a Baldwin Southwark Universal Tester at 1000 p.s.i. and heated to about 160°C. Constant pressure was maintained as the system cooled to room temperature. This treatment produced flat, specularly smooth TFE surfaces; however, the sample shape had become distorted because of the plastic properties of Teflon. The sample remained in contact with the glass until used. The static charges developed by the TFE upon separation from the glass were discharged by placing the sample near an α-particle source for several minutes.

The distorted sample area of the Teflon substrates was determined by a radiometric technique. An autoradiograph of the deposited C^{14}-labeled stearic acid or Ca-H-St bilayer was obtained. The deposited area was readily measured with the aid of a planimeter. The area of the two sides was determined from their length and thickness. This technique produced fairly reliable values of the geometric area on which a multilayer was deposited.

SOLID SUBSTRATES FOR MONOLAYER DEPOSITION

Monolayers were transferred by the Langmuir-Blodgett method onto collodion (nitrocellulose), mica, and glass in order to study the behavior of monolayers at the liquid/air interface by autoradiography and electron microscopy. The deposition of monolayers on collodion and glass was also studied by radioactivity measurements. Collodion is the classical solid on which monolayers have been deposited for electron microscopic examination and, in addition, the structure of deposited monolayers on glass and mica has also been studied.

Collodion-covered microscope slides (Corning 2947, 3 × 1 in.) were prepared by the spread film technique (52) using a 2% solution of purified Parlodion in amyl acetate. Brazilian Ruby mica (United Mineral and Chemical Corp., 0.015-0.020 in.) was cut into 3 by 1-inch samples which were cleaned by freshly cleaving before used. Glass microscope slides (Corning 2947, 75 × 50 mm.) were washed with a detergent solution, cleaned in chromic-sulfuric acid solution, rinsed copiously with triple distilled water, and dried in a grease-free oven. The cleaved mica surfaces were likely to develop a static charge; therefore, all the substrates were placed near an α-particle source for several minutes before use to discharge any possible static charge.

TRANSFER RATIO DETERMINATION

The ratio, $\underline{A}_m/\underline{A}_s$, of the area of the monolayer, $\underline{A}_m$, on the subsolution surface that is deposited onto a slide of geometrical area, $\underline{A}_s$, is historically defined as the transfer (deposition) ratio. The classical technique of obtaining the transfer ratio determined $\underline{A}_m$ from the decrease in the number of film molecules on the subsolution surface by measuring the change in a "movable barrier" position. The slide area, $\underline{A}_s$, was determined from the perimeter of the solid slide and the distance the slide moved during the deposition process.

It is evident that an apparent transfer ratio is determined because the number of film molecules deposited on the solid is not measured directly, but rather it is inferred from the decrease in film area on the subsolution surface. In addition, the molecular concentration on the solid refers to that on the geometrical surface area instead of the real surface area. Thus, the local transfer ratio is not necessarily determined by the classical method.

The apparent transfer ratio in this study was accurately determined by measuring the film area decrease per solid geometrical area and applying appropriate corrections for contact angle changes between successive layers, concomitant monolayer losses, and initial retarded deposition effects. These corrections were not included in previous measurements of the transfer ratio by other investigators.

Adjustment for Contact Angle Changes

An obtuse contact angle was observed during the immersion operation, whereas an acute contact angle was formed during the withdrawal operation. As a result of the transition between the two contact angles, there is a time lag between the movement of the slide and the deposition of monolayer molecules onto the solid. The following procedure was employed to correct for this effect. There was no transfer of film molecules to the solid at the commencement of an immersion or withdrawal stroke because of this change in contact angles that had to occur. But when the film deposition finally became uniform, the slide motion was terminated. Thus, the approximate contact angle was established before measurements determining the transfer ratio were obtained. This contact angle adjustment increases the determined transfer ratio.

Correction for Concomitant Monolayer Loss

Not all the molecules which leave the monolayer on the subsolution surface during the deposition process are deposited onto the solid slide, but rather some film molecules simultaneously disappear from the water surface by evaporation, dissolution, or a monolayer collapse mechanism. This concomitant monolayer loss is time dependent and varies to some extent from one experimental run to another because it is a kinetic process which is sensitive to mechanical and thermal disturbances. Each transfer ratio was corrected for this effect by determining the rate of monolayer loss before and after each deposition operation and assuming

the average rate was constant throughout the deposition. The average rate multiplied by the time interval of the particular deposition operation gave the appropriate correction. Failure to correct for this effect leads to higher values of the transfer ratio.

Corrections for Initial Retarded Deposition Effects

These corrections are, in effect, an extension of the adjustment for contact angle changes. Even though the approximate contact angle was established, there is still a time lag between the slide motion and uniform deposition once the slide motion is started again. Figure 16 illustrates the final corrections that are necessary to determine the transfer ratio and corresponds to the deposition behavior at low withdrawal contact angles (< 50°). The lower the contact angle, the greater was the correction.

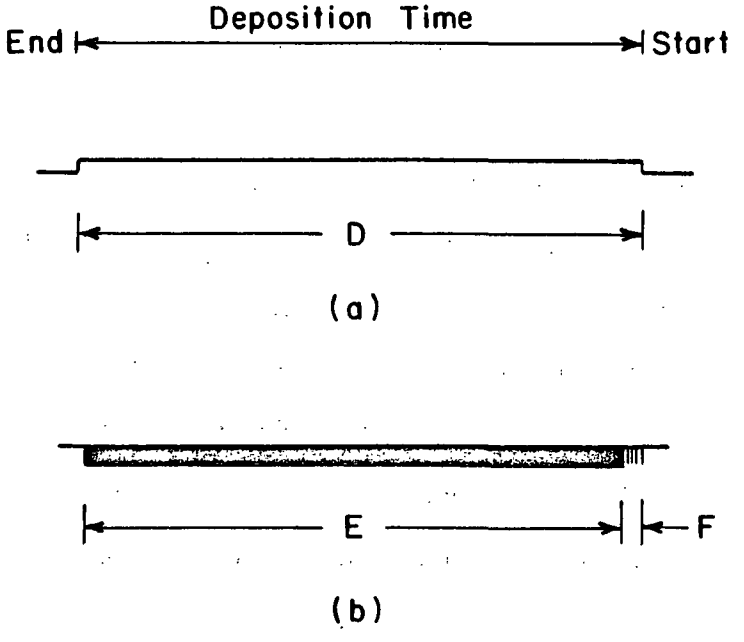

Figure 16. Event Marker Pen Traces of the (a) Slide Motor and (b) Compression Barrier Drive Motor During the Withdrawal Operation of Multilayer Deposition

Lengths D, E, and F correspond to the time intervals of the slide movement, uniform deposition, and initial deposition of some film molecules (F = D - E), respectively. All measurements of the barrier and slide positions were corrected to correspond to the time interval that uniform deposition occurred. The length of the slide motion was corrected by multiplying by the ratio, E/D, which corresponds to the fraction of the slide movement during which deposition was uniform. The change in the barrier position was corrected by subtracting the barrier distance which corresponded to the small amount of film transfer which occurred before the deposition became uniform. The former correction yields higher transfer ratios, while the latter tends to reduce the transfer ratio. However, the net effect is one of increasing the transfer ratio.

Technique

The general procedure for determining the set of transfer ratios corresponding to the first several monolayers in multilayer deposition on a low-energy surface was as follows: The paraffin substrate was lowered until its leading edge was immersed in the subsolution. The stearic acid spreading solution was applied, and the film was allowed to age for six minutes. The monolayer was compressed to a surface pressure of 31 dynes/cm., and the automatic film balance controls were set for constant pressure operation. Several minutes were allowed for possible mechanical disturbances to level out. The slide was started downward for a few seconds in order to establish the approximate immersion contact angle, and then the slide was stopped. The initial measurements of barrier and slide positions were recorded; and during this time, the rate of concomitant monolayer loss was determined. Then the first immersion operation of the deposition process was commenced. After the termination of the first stroke, the final barrier and slide positions along with the rate of monolayer loss were measured. This required one to two minutes before the second deposition (first withdrawal) operation was

commenced. This sequence was continued until the desired number of monolayers were deposited as a multilayer onto the paraffin slide.

In the region of continuous and uniform multilayer deposition (pH $\geq$ 6.8), the estimated errors in the apparent transfer ratios for the inactive and C^{14}-labeled Ca-H-St monolayers are ±0.01 and ±0.02, respectively. The reproducibility of the apparent transfer ratio is generally within ±0.01.

RADIOACTIVITY MEASUREMENTS

The radiocounting measurements on the transferred monolayers and multilayers were performed with an end-window Geiger-Muller tube (Nuclear Chicago Model 108) having a mica window with a density of 1.4-2.0 mg./cm.^{2} The counting area was restricted by fitting over the end of the tube a 0.031-inch thick brass mask having a 1/4-inch diameter aperture. The mask was a distance of 1 mm. away from the window. A Model 2000 Berkeley Decimal Scaler with timer and register was used for data registration. A minimum of 10,000 counts was obtained in order to reduce the standard deviation in the net counting rate to ±1.0% (53). Background corrections which always were in the range of 50-55 c.p.m. were applied. It was not necessary to apply corrections for coincidence losses because the maximum counting rate was less than 1800 c.p.m. Backscattering corrections were neglected because the counting rates were always determined under the identical counting geometry on paraffin substrates having a uniform thickness of 0.048 cm. which constitutes a uniform saturation backscatterer. For C^{14} β-particles of maximum energy 0.154 Mev., the empirical relationships of Yaffe and Justus (54) give 33.3 and 9.3 mg./cm.^{2} as the mass required for saturation backscattering (55). The thickness of paraffin necessary to ensure saturation backscattering on the basis of the above required masses is 0.038 and 0.011 cm., respectively. The paraffin substrates satisfy the saturation backscattering requirements.

An operating potential of 900 v. was selected from an examination of the experimentally determined characteristic curve of the G-M tube shown in Appendix II. The optimum height of the brass mask from the paraffin surface was selected as 0.4 mm. because the counting rate is essentially independent of the counting geometry for separations less than 1 mm. as shown in Appendix II.

The G-M tube was mounted to a rack and pinion which was positioned above a mechanical stage assembly capable of XY motion. The paraffin substrate was positioned on an aluminum holder machined such that the tapered paraffin surface was now horizontal and parallel with the G-M tube when the aluminum holder was positioned on the mechanical stage. The circular area of counting on the paraffin surface could be accurately located or positioned under the G-M tube by means of the XY scales and verniers. Raising or lowering the rack to accommodate substrates of different thicknesses while still maintaining the same vertical separation between the G-M tube and substrate was possible because a dial indicator was mounted to the apparatus. The G-M tube could be accurately and reproducibly set at any desired distance within ±0.05 mm. from a monolayer-covered substrate of arbitrary thickness.

The counting aperture of 1/4-inch diameter permitted the determination of the distribution and uniformity of the activity of the monolayer-covered substrate by measuring the net counting rate at fifteen different locations immediately after the deposition process. A typical counting pattern is shown in Fig. 17. Although the series of measurements required as much as four hours, negligible contamination of the window of the G-M tube occurred because the background rates before and after the counting sequence were approximately identical.

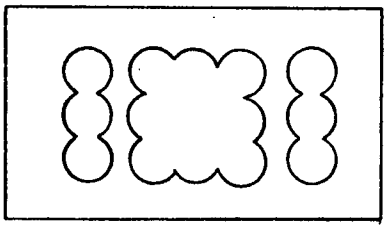

Figure 17. Location of the Radioactivity Measurements on a Typical Deposited Bilayer on a Paraffin Substrate

An autoradiograph of the deposited bilayer was obtained after the counting measurements. By superimposing the locations of the counted areas upon the autoradiograph, visual observation showed whether the counting rate of a 1/4-inch diameter area at a given location was representative of a uniform deposition process. Those counting rates which were visually associated with heterogeneous film behavior such as voids or film-free regions (low activity) and monolayer collapse (high activity) were excluded. Thus, a local net counting rate associated with continuous and uniform film deposition was obtained instead of an apparent net counting rate which includes film heterogeneities. The reproducibility of the local net counting rates is within ±0.5%.

DETERMINATION OF THE WITHDRAWAL CONTACT ANGLE

The withdrawal contact angle was photographed during the withdrawal operation with a Ciné-Kodak Special 16-mm. movie camera which was motor-driven at 1 frame/sec. Eastman Plus-X Type 7231 panchromatic negative film was used. The camera was fitted with a 3-inch lens on a 2-inch extension tube. The positioning of the camera relative to the slide is shown in Fig. 12. The contact angle was back lighted with a stereoscopic microscope illuminator. Precision alignment is required to avoid distortion of the image and obtain reproducible results. The film plane was aligned

parallel with the inside edge of the trough. The camera was also aligned so that the intersection of the liquid surface and the slide was centered in the lens. The illuminator was carefully centered and aligned parallel with the slide. Additional vibration from the motor drive was undetectable.

The camera was positioned in the Lucite cabinet after the surface was swept clean by the barriers. The paraffin slide was lowered, and then the final camera alignment was made by centering the vertical axis of the slide in the lens. The monolayer was spread, and the usual procedures for multilayer deposition were observed. When the slide was withdrawn, the camera was activated by a foot switch. The withdrawal contact angle was photographed for the entire withdrawal operation. The strip of film, six to twelve feet in length, was then removed from the camera and custom developed by hand in Kodak HC 110 developer (7 parts water/1 part developer). A minimum of eight representative frames from each film strip was selected and enlarged onto Ortho film with an Omega D2 condenser-type enlarger. A jig positioned the negative in the center of the enlarger lens. The condenser, lens plane, negative plane, and easel were carefully aligned level with one another. The movie camera lens system and enlarger produced a magnification of about 1-1/4 and 11 diameters, respectively. Measurements were then made on contact angles which had an overall magnification of about 14 diameters.

The Ortho films were placed on a light box, and the withdrawal contact angles were measured by the contact angle tangentometer described by McIntyre (48). The contact angles were directly read on the protractor when the curvature of the liquid surface at the intersection of the slide and its reflected image in a vertical mirror formed a continuous curve. The tangentometer is a very accurate instrument because an error of only $\pm 0.2^{\circ}$ is introduced in the measurement of constructed contact angles. The details and results are presented in Appendix II.

Estimates of the errors in the withdrawal contact angle due to misalignment of the camera-slide and/or enlarger system were obtained. The procedures and results are given in Appendix II. The results indicate that the photographic and enlarger systems are adequately aligned to minimize distortion. Each contact angle measurement is estimated to be accurate to ±1°. Each reported withdrawal contact angle is the average of six to sixteen measurements per film strip. The 95% confidence limits of the average values are about ±0.5°.

AUTORADIOGRAPHY

Autoradiography was used to determine the uniformity and continuity of monolayer and multilayer deposition and investigate the nature of the collapse phenomena in monolayers. Autoradiographs were made by pressing a piece of Kodak No-Screen Medical X-ray film against both sides of the radioactive monolayer-covered substrate in an aluminum exposure cassette. The cassette was designed in such a manner that fine-textured foam rubber applied even pressure. The film was exposed five hours at 5°C. in a dry atmosphere.

The films were then developed by the following procedure. The films were immersed for five minutes in Kodak Liquid X-ray Developer, then two minutes in Kodak Indicator Stop Bath, and finally ten minutes in Kodak Liquid X-ray Fixer. The films were then washed for thirty minutes in running water. Before drying the films in air, the washed films were immersed for one minute in Kodak Photo-Flo Solution to prevent water spots. All the solutions and wash water were controlled to 20°C. Throughout the procedure, the films were agitated at intervals according to a prescribed schedule.

ELECTRON MICROSCOPY

The physical structure of deposited monolayers and multilayers on solid substrates was extensively examined by transmission electron microscopy (TEM). Direct carbon replicas preshadowed with palladium (Pd) and platinum (Pt) at an angle of 20° were prepared in a vacuum evaporator (Denton Vacuum DV-502). The palladium (2.5 cm. of 0.008-in. diameter wire) was evaporated from a heated tungsten filament, and the platinum (0.5 in. of 0.005-in. diameter wire) was evaporated from a resistance-heated carbon rod. The specimen-to-source distances for the Pd and Pt evaporants were 10 and 12 cm., respectively. A heat shield with a 1/4-inch aperture was used during platinum shadowing to minimize heat effects. The specimens were rotated as the carbon was deposited at 45°.

Samples, 1/4-inch square, were cut and removed from the preshadowed carbon replicas of the multilayers on paraffin. Standard 100-mesh nickel electron microscope grids covered with a thin film of collodion and then coated with a light deposit of carbon (collodion-carbon covered) were positioned on the samples. The composite sample was inverted and placed in a xylene evaporator. The samples were copiously washed with the condensing xylene vapors, effectively dissolving the wax and producing very clean replicas draped over the grids. The grids were then removed and dried before examination by TEM.

Monolayer samples were transferred from the film balance to collodion-covered microscope slides and mica by the Langmuir-Blodgett method. The preshadowed carbon replicas of monolayers on collodion were stripped from the glass slide by gradual immersion in water with the slide inclined at an angle with the liquid surface. The stripped replicas (includes the collodion layer) floated off onto the water surface and were picked up from below on 100-mesh grids by raising a screen containing the grids through the floating replicas. The preshadowed carbon replicas

of monolayers on mica could not be stripped from the mica. Replicated specimens of monolayers on mica were prepared by a shadow-transfer technique which includes embedding the replica in polystyrene as described by Dunning (56).

Several carbon replicated specimens were examined by TEM. The unshadowed carbon replicas of multilayers on paraffin were prepared in the same manner as that of preshadowed carbon replicas. The unshadowed carbon replicas of monolayers on mica, in contrast to the preshadowed carbon replicas, were stripped from the mica surface, floated on water, and transferred to 200-mesh grids.

The replicas were examined and photographed in a RCA EMU-3F electron microscope equipped with high-voltage fine focusing. The images were recorded on Kodak 4489 electron microscope film (3-1/4 × 4 in.) and Kodak projector slide plates (medium, 3-1/4 × 4 in.) and developed with Kodak D-19 developer and VDH film developer (Brandywine Photo Chemical), respectively. Most electron micrographs were taken at a magnification of 23,000 diameters and 50 kv. The electron microscope was calibrated with a diffraction grating containing 28,800 lines/inch.

ELECTRON PROBE MICROANALYSIS

The technique of electron probe microanalysis was used to investigate whether calcium stearate was embedded or associated with the replicas prepared for TEM. A Jeol JSM-U3 scanning electron microscope (SEM) equipped with an Ortec x-ray spectrometer and Quanta/Metrix EDX 80 energy dispersive x-ray analysis system scanned sample areas of 1 $mm.^2$ for 1000 seconds at an accelerating voltage of 25 kv. The net intensity of the Ca Kα peak was obtained, and the x-ray spectrum was recorded on a X-Y plotter.

The palladium preshadowed carbon replicas of a Ca-H-St bilayer at pH 9 on paraffin were transferred to collodion-carbon covered 100-mesh nickel grids and

copiously washed in the xylene evaporator. The cleaned grids were then mounted on previously unused graphite holders with silver colloidal paint. The graphite holder was then inserted into the SEM for analysis.

The unshadowed carbon replicas of Ca-H-St monolayers at pH 6 and 9 on mica were easily stripped from the mica surface by gradual immersion in water. Graphite holders were then immersed into the water and raised through the floating replicas. The unshadowed carbon replicas which were draped over graphite holders were then air dried before analysis.

CONTACT ANGLE MEASUREMENTS ON BILAYERS

The contact angle measurements were obtained with a NRL contact angle goniometer (Ramé-Hart, Model A-100). Immediately after preparation of the Ca-H-St bilayers, the contact angles of water and glycerol were measured within thirty seconds after formation of the drops which had a volume of about 10 λ. The water and glycerol contact angles were determined on the same sample, and the reported values are the average of at least six measurements. The contact angles are reproducible to $\pm 1^{\circ}$. The measurements were performed in a room maintained at 22°C. and 50% R.H.

EXPERIMENTAL RESULTS AND DISCUSSION

MONOLAYER PROPERTIES

SURFACE PRESSURE-AREA ISOTHERMS

The II-A isotherm of a monolayer of stearic acid on a pH 2.00 subsolution is shown in Fig. 3 (page 16). The stearic acid monolayer under these conditions of pH and temperature is characteristic of a liquid condensed film. Areas which are characteristic of the molecular cross section are usually determined from the II-A isotherms. The usual procedure is to extrapolate the linear, or nearly linear, parts of the II-A curve to zero surface pressure. This extrapolated area at zero surface pressure is a measure of the molecular cross section (57). Attaching particular significance to this area has been questioned (34, 58). Extrapolation of the liquid condensed part and the steep, high pressure, linear part of the II-A isotherm back to zero surface pressure gives areas of 24.1 and 20.5 $A.^2$/molecule, respectively. These values are in excellent agreement with those reported (59, 60) as is the transition pressure of 25.5 dynes/cm.

The effect of calcium ions on the II-A isotherm of stearic acid monolayers at various hydrogen ion concentrations is shown in Fig. 18. The formation of calcium stearate results in a gradual transition from the liquid condensed film to a solid film having an area at zero surface pressure of about 20.0 $A.^2$/molecule.

This pH dependence of the II-A isotherms of stearic acid monolayers on calcium-containing subsolutions is well-documented (37, 60-68). The generally accepted explanation is that a single divalent calcium ion reacts with two stearate ions to produce a di-soap molecule of calcium stearate (61, 68-71). Examination of the results of other studies (37, 60-64) indicates that stearic acid and Ca-H-St

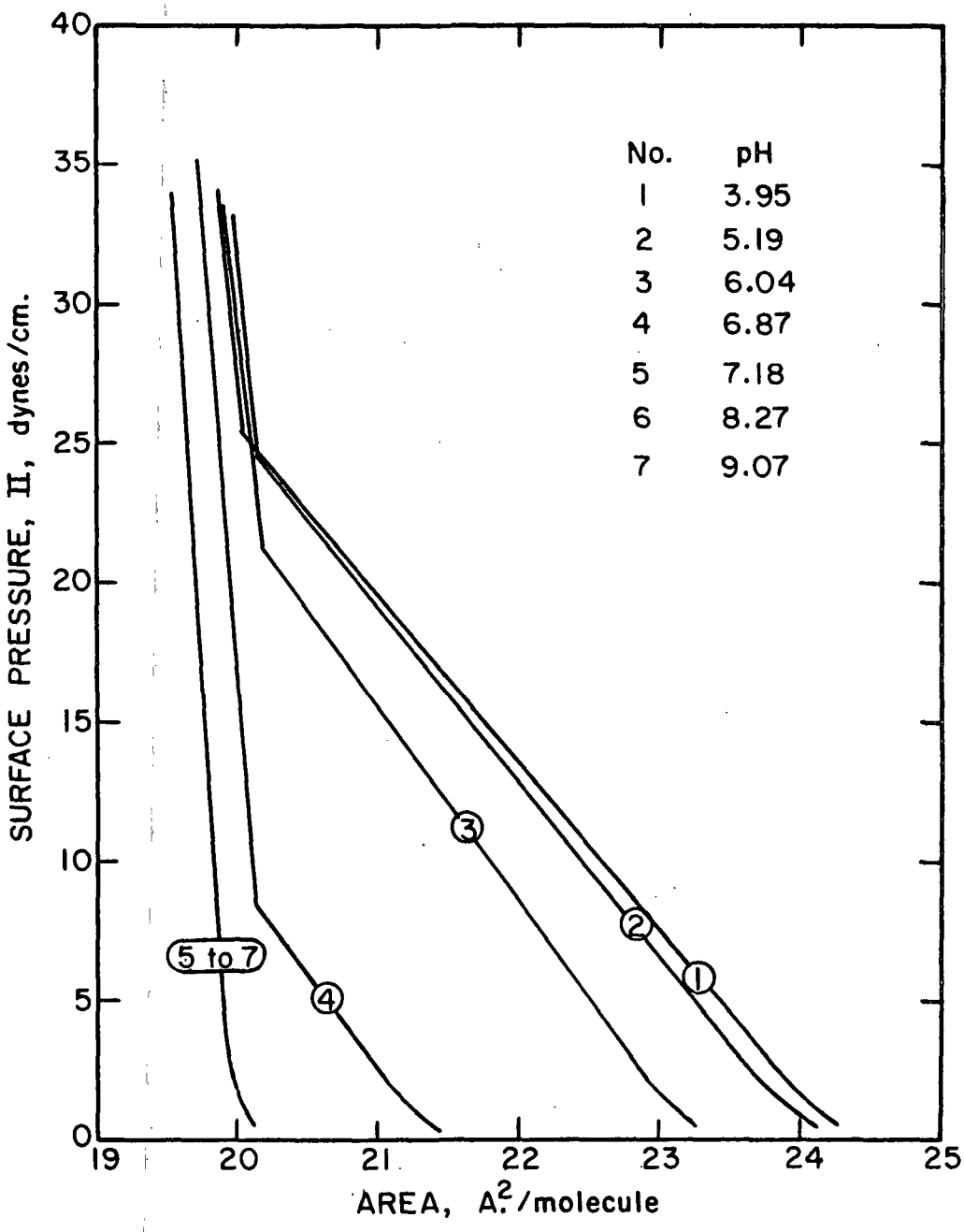

Figure 18. The Effect of pH on the Surface Pressure-Area Isotherms of Ca-H-St Monolayers. Compression Rate = 1 A.^{2}/Molecule/Min.; $\underline{T}$ = 20.6°C.

monolayers appear to have the same molecular area at corresponding surface pressures above the transition pressure of 25.5 dynes/cm. Thus, it appears there is no change in the packing of the hydrocarbon chains within the condensed monolayers.

However, Fig. 18 shows that in this study the average area/molecule at a given surface pressure above the transition pressure is not constant with increasing subsolution pH. The area at a surface pressure of 31 dynes/cm., $\underline{A}_{31}$, is plotted as a function of pH in Fig. 19. Above pH 6.4 the hydrocarbon chains appear to pack more tightly together. The area per hydrocarbon chain appears to be reduced by about 2.3% above pH 7.2.

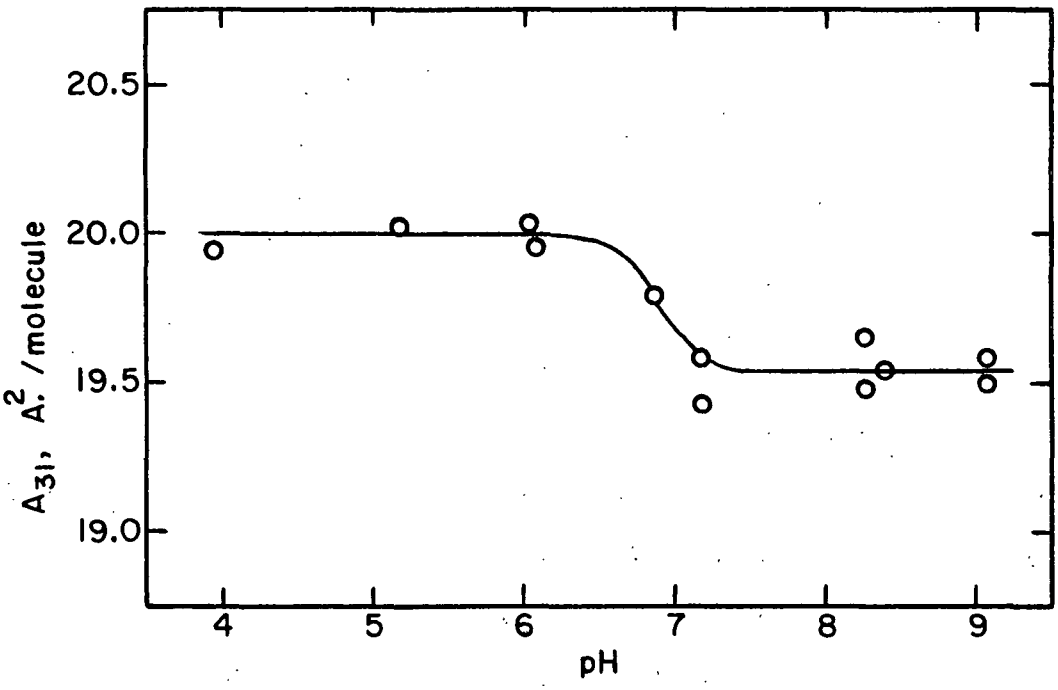

Figure 19. $\underline{A}_{31}$-pH Curve for Ca-H-St Monolayers. Compression Rate = 1 A.^{2}/Molecule/Min.; $\underline{T}$ = 20.6°C.

The conclusion that the hydrocarbon chains pack tighter together above pH 6.4 is valid only if it can be shown that the monolayer is stable at these conditions. Possible explanations for this reduction in the average molecular area are

(1) losses from the monolayer by evaporation and/or dissolution, (2) the phenomenon of monolayer collapse occurring during compression with the formation of a bulk crystalline phase, and (3) a structural rearrangement of the long-chain molecules within the monolayer.

Dissolution or evaporation at room temperature of fatty acids having chains of eighteen or more carbon atoms long is very slow. Gaines (72) obtained a loss rate of less than 0.001% per minute for a stearic acid monolayer on a 10^{-4} N H_2SO_4 subsolution held at a constant surface pressure of 10 dynes/cm. The solubility of stearic acid is enhanced when it is spread on an alkaline subsolution due to ionization of the carboxyl group. Spink (66) claimed that stearic acid was stable well above a subsolution pH of 10; however, Goddard and Ackilli (37) observed that pH 9 corresponded to the incidence of solubility in a stearic acid monolayer. In any event, a stearic acid monolayer appears to be stable at a subsolution pH $\leq$ 9.

The presence of calcium ions in the subsolution should further reduce the solubility of the stearate film. The heterogeneity of Ca-H-St monolayers at very low surface pressures ($\sim$ Π=0 dynes/cm.) increases as the concentration of calcium stearate in the film increases. Large islands are formed, and the molecules in these islands are in a close-packed state (63, 73). The monolayer stability should be increased because the Van der Waals dispersion forces of the aliphatic chains are greatly increased in the condensed state (74), and the contribution from these forces to the energy barrier for dissolution and evaporation is increased. In addition, the presence of the divalent calcium ions reduces the electrostatic potential at the interface with a consequential decrease in the desorption tendency. This stabilization of fatty acid monolayers by calcium ions has been observed (61, 62, 75).

Furthermore, if dissolution and/or evaporation are significant molecular processes, then changes in the monolayer properties should be evident when the residence time of the monolayer on the surface is increased before compression. However, an increase in the reaction time from six to fifteen minutes on an alkaline subsolution did not produce any significant change in the II-A isotherm.

Thus, the decrease in A_{31} above pH 6.0 is not due to monolayer losses by dissolution or evaporation during the reaction time. The other three possibilities of monolayer collapse, structural rearrangement, and monolayer losses by dissolution and evaporation during compression will be discussed later.

SURFACE VISCOSITY

Calcium ions, in addition to reducing the solubility and condensing ionized fatty acid monolayers, markedly increase their viscosity to give brittle solid films on alkaline subsolutions (34, 64, 65, 68, 75, 76). The surface viscosity-pH curve for Ca-H-St monolayers at a surface pressure differential to 31 dynes/cm. is presented in Fig. 20 and 21. The surface viscosities calculated from the equations proposed by Meyers and Harkins (41) and Joly (45) are plotted on a logarithmic scale in Fig. 20. The surface viscosity calculated from Joly's equation is plotted on a linear scale in Fig. 21 in order to more clearly define the incidence of the sharp increase in viscosity.

The surface viscosity appears to remain constant until about pH 4.5 and then gradually increases to about pH 6.4. Then the viscosity sharply increases up to a maximum at pH 8.0 with a twentyfold increase in the surface viscosity between pH 6.4 and 8.0. There is a 100-fold increase in the surface viscosity of the Ca-H-St monolayer from pH 2.0 to 8.0. But in the pH range 8.0-9.0, the surface viscosity decreases 10% from the maximum value at pH 8.0.

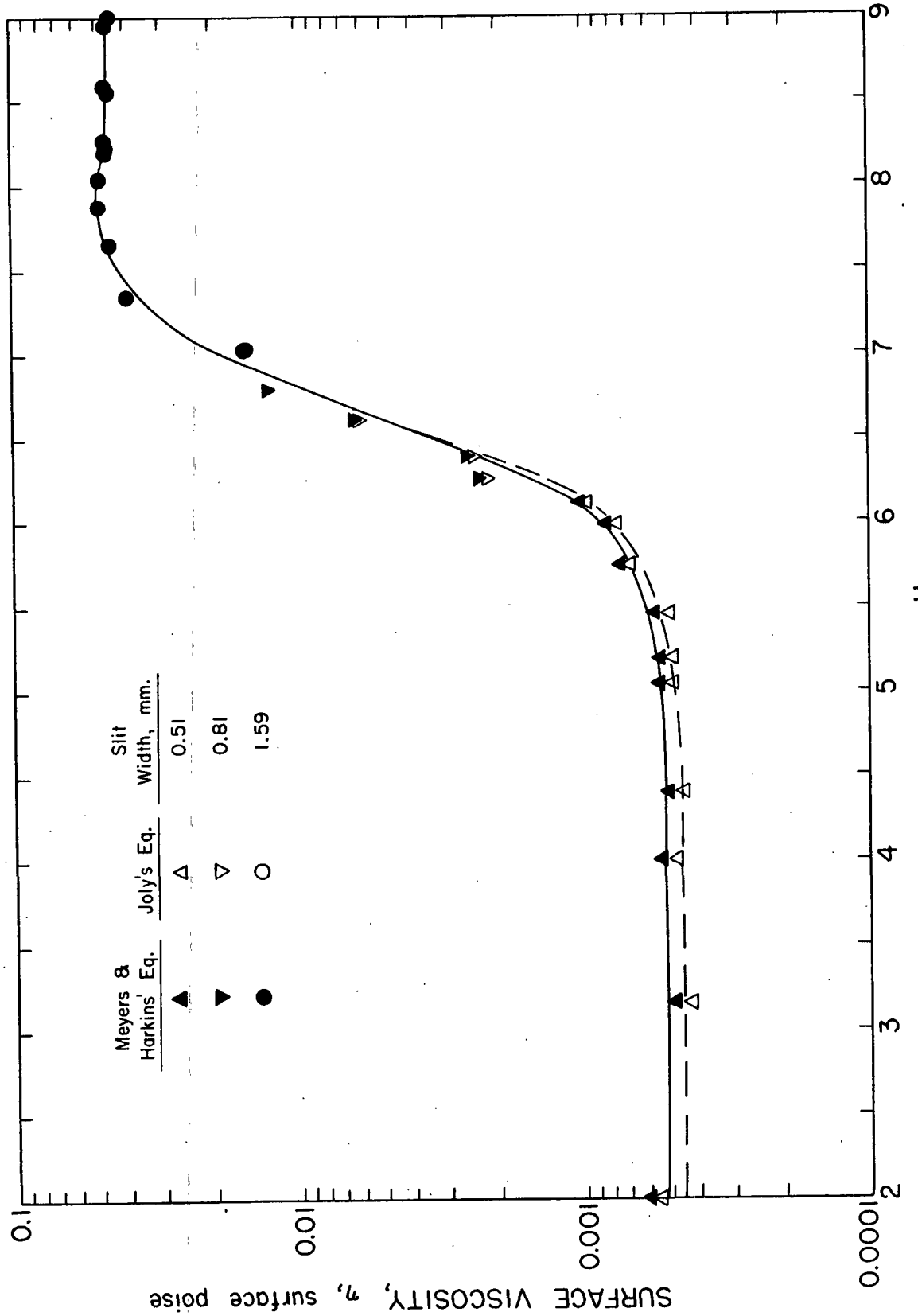

Figure 20. Surface Viscosity-pH Curve for Ca-H-St Monolayers at a Surface Pressure Differential of 31 Dynes/cm. The Uncorrected Surface Viscosity (Meyers & Harkins' Eq.) is Compared with the Surface Viscosity Corrected for Subsolution Drag (Joly's Eq.). The Surface Viscosity is Plotted on a Logarithmic Scale. $\underline{T}$ = 20.3°C.

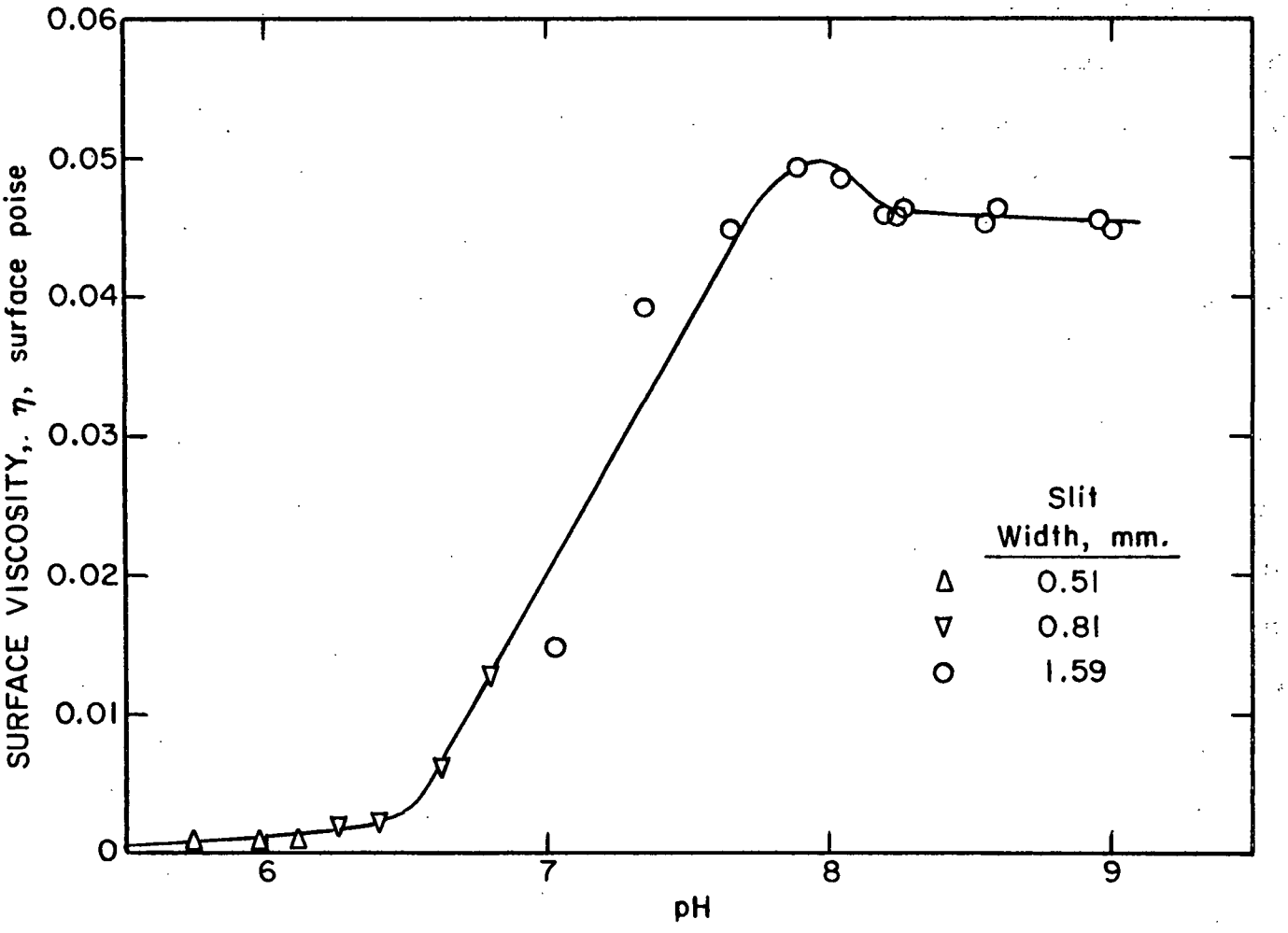

Figure 21. Surface Viscosity-pH Curve for Ca-H-St Monolayers at a Surface Pressure Differential of 31 Dynes/cm. Surface Viscosity Calculated from Joly's Equation. $\underline{T}$ = 20.3°C.

Qualitative measurements of the surface viscosity can be obtained by the talc test. If some talc is sprinkled on a water surface and the investigator blows gently across the surface, the motion of the talc particles depends on the nature of the film. The particles move around freely with a monolayer of low viscosity; but if the monolayer is very rigid, the particles do not move. Preliminary to the quantitative surface viscosity measurements an indication of the mechanical properties of the films was obtained by the talc test. The results were in qualitative agreement with the surface viscosity-pH curve.

The surface viscosity-pH curve is also in qualitative agreement with the following results that Rogeness and Abood (68) obtained by a ring torsion pendulum. At pH 3 calcium did not have any effect on the viscosity of a stearic acid monolayer. However, calcium markedly increased the viscosity of the stearic acid monolayer at pH 7.6; and at pH 8 the viscosity was even greater than that at pH 7.6. In addition, the rotation of the ring was jerky at high pH, behaving as if the film were a solid which alternately broke and reformed.

Joly's equation (page 35) which corrects for the viscosity of the subsolution gives lower surface viscosities than the equation of Meyers and Harkins. The calculated surface viscosity is lowered by about 12% in the pH range 2.0-4.5. As the subsolution pH increases, the difference decreases until the two surface viscosities are essentially the same at pH $\geq$ 7. Above pH 7 the surface viscosities calculated by Joly's equation are only 1% lower so that the contribution of the subsolution viscosity to the surface viscosity becomes negligible.

The surface viscosities of inactive and C^{14}-labeled stearic acid on pH 2.00 subsolutions are presented in Table III. The surface viscosities determined on each of two pH 2.00 subsolutions show the same trend, i.e., the surface viscosity of the C^{14}-labeled stearic acid is about 5% greater than that of the inactive stearic acid. Although the surface viscosities are higher on Subsolution B by almost 20%, the similar increases in surface viscosity for the inactive and radioactive stearic acids suggest that some systematic error arose in the determination of the surface viscosities on Subsolution B. This error may possibly be due to aging effects of the subsolution or deposited monolayer, inadvertent contamination of the subsolution, or even alteration of the slit width by foreign material. In any event, the two stearic acid monolayers on Subsolution B appear to have been subjected to the same experimental conditions. Thus, although by no means

conclusive, the results suggest the possibility that the surface viscosity of C^{14}-labeled stearic acid monolayers may be higher than that of inactive stearic acid monolayers.

TABLE III

SURFACE VISCOSITY OF STEARIC ACID MONOLAYERS ON pH 2.00 SUBSOLUTIONS

	Surface Viscosity $\times 10^4$, surface poise					
	Subsolution A		Subsolution B		Average	
	M & H[a]	Joly	M & H	Joly	M & H	Joly
Stearic acid (Fluka A.G.)	4.77	4.15	5.85	5.22	5.31	4.69
C^{14}-Labeled stearic acid	5.20, 4.92	4.58, 4.30	6.08	5.46	5.57	4.95

[a] Meyers and Harkins.

Washburn and Wakeham (40) used the same method for measuring the surface viscosity of a stearic acid monolayer at pH 3.8 and a surface pressure of 30.7 dynes/cm. Their result of 6.7×10^{-4} surface poise calculated from the equation of Meyers and Harkins is comparable to the values obtained in this study on pH 2.00 subsolutions. Dreher and Sears (38) also obtained a surface viscosity value of about 6.3×10^{-4} surface poise for a stearic acid monolayer on 0.01N HCl at a surface pressure differential of 12 dynes/cm.

It should be pointed out that the equations from which the surface viscosity is calculated are based on the conditions, strictly speaking, of steady, laminar flow of an incompressible film through a slit or canal. The assumptions and the experimental satisfaction of the requirements have been discussed by Gaines (77). The requirement of an incompressible film implies that the viscosity of the film is constant while passing through the slit. In order to satisfy this condition, the surface pressure drop across the slit or canal should be maintained as small

as possible, usually a pressure differential of the order of 2-4 dynes/cm. Surface viscometers have been designed to provide constant surface pressure on both sides of the slit or canal. The viscosity obtained then represents an average over a range of surface pressure.

The slit viscometer used in this study does not measure the surface viscosity of the film at an average surface pressure of 31 dynes/cm., but rather measures the surface viscosity of the film at a surface pressure differential of 31 dynes/cm. However, the advantage of the selected surface viscometer is its simplicity and convenience with an automatic film balance designed for constant pressure operation. In addition, the selected method was satisfactory because only surface viscosity differences were required for this study.

Jarvis (47) has measured the surface viscosity of stearic acid on a 0.01N H_2SO_4 subsolution at various surface pressures under low surface pressure differentials. The corrected surface viscosity values at surface pressures of 12 and 20 dynes/cm. were about 6×10^{-4} and 1×10^{-3} surface poise, respectively. Thus, even though the slit viscometer used in this study does not fully experimentally satisfy all the criteria on which the surface viscosity equations are based, it does give comparable surface viscosity values.

An observation noteworthy of mention is that there appears to be slow changes in the surface viscosity with time. The effect is most pronounced between pH 5 and 6 where the surface viscosity appears to increase with time (order of 20-40% in 5 min.). However, the surface viscosity appears to remain constant or slightly decreases with time between pH 6 and 9. The effect of time on the surface viscosity at pH < 5 is difficult to ascertain due to the complications of simultaneously occurring significant film collapse which will be shown later. A possible explanation of the changes in the surface viscosity with time is that the chemical

composition of the Ca-H-St monolayer under high surface pressure slowly changes with time due to a change in the equilibrium constant with surface pressure. As such, the nature and extent of these slow changes in the surface viscosity may be important to the chemical composition analyses and multilayer deposition of Ca-H-St monolayers.

SURFACE POTENTIAL

ΔV-pH and μ_i-pH Curves

The dependence of the surface potential at 31 dynes/cm. on the subsolution pH is shown in Fig. 22. The ΔV-pH relationship in the pH range 2.0-6.4 appears to be better represented by a curvature away from the pH axis. The surface potential decreases from +396 mv. at pH 2.0 to +290 mv. at pH 6.4 and then sharply falls 200 mv. to +90 mv. at pH 8.0. The rate of decrease of ΔV becomes increasingly smaller at pH > 8.0 until ΔV is +5 mv. at pH 9.0. The surface potential results of Sanders and Spink (78) are also presented in Fig. 22.

The surface potentials of inactive and C^{14}-labeled stearic acid monolayers are in agreement within the experimental error as are also the inactive and radioactive Ca-H-St monolayers on a pH 8.8 subsolution. Accordingly, there appears to be no difference as to whether ΔV of inactive or radioactive monolayers is measured.

The ΔV-pH curve of behenic acid monolayers has been shown to be highly sensitive to the choice of the buffer and presence of atmospheric CO_2 (79). However, the close agreement between the bicarbonate buffered results of this study and the unbuffered results of Sanders and Spink differs from the large ΔV lowering of stearic and behenic acid monolayers on bicarbonate buffers reported by Goddard, et al. (79). The general appearance of the ΔV-pH curve of the Ca-H-St monolayer

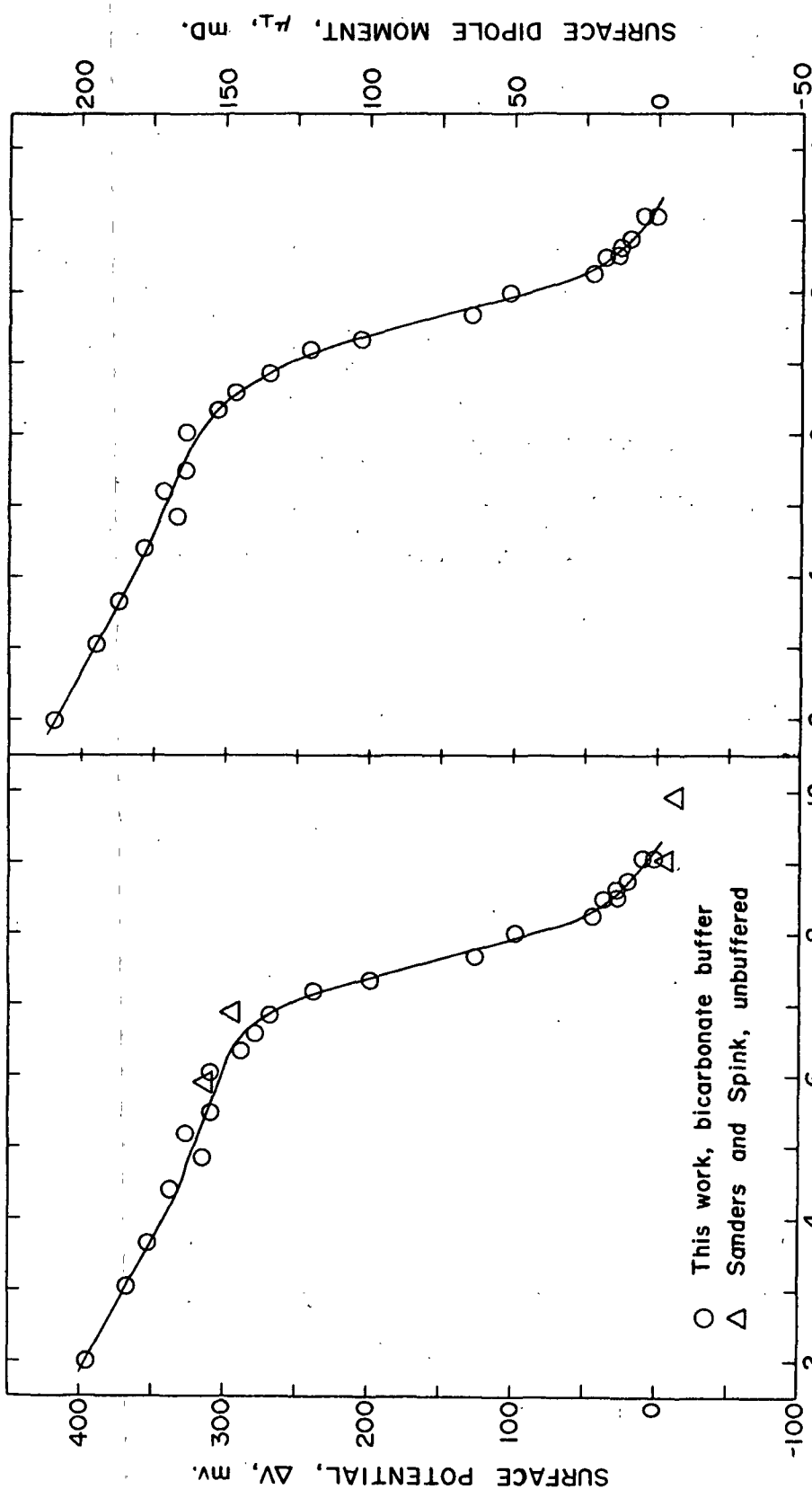

Figure 22. ΔV-pH and μ_L-pH curves for Ca-H-St monolayers at 31 Dynes/cm. T = 20.6°C.

is similar to that of the reported ΔV-pH curves (37, 79) for stearic acid monolayers on monovalent salt subsolutions.

Figure 22 also shows the relationship between the apparent surface dipole moment at 31 dynes/cm. and the subsolution pH. The apparent surface dipole moment, $\mu_\perp$, was calculated using the equation (80),

$$\mu_\perp = A\ \Delta V/12\pi, \qquad (5)$$

where

$\mu_\perp$ = component perpendicular to the water surface of the apparent dipole moment of the molecule, milliDebyes

A = area per molecule, $A.^2$

ΔV = surface potential, mv.

π = constant

The A_{31}-pH curve of Fig. 19 was used in the calculations. As expected, the $\mu_\perp$-pH curve behaves similarly as the ΔV-pH curve.

Surface Potential Uniformity

The surface potential was measured at different locations within a monolayer in order to determine whether the monolayer was uniform. The 95% confidence limits which were calculated from eight or more measurements of ΔV were employed as a measure of the uniformity.

Throughout the entire pH range 2-9, the monolayer is observed to be nonuniform at areas greater than 25 $A.^2$/molecule and corresponding to essentially zero surface pressure. The uniformity of ΔV at 31 dynes/cm. is shown in Fig. 23. It is evident that the monolayer becomes homogeneous during compression at pH < 8.0. However, the degree of nonuniformity becomes progressively larger with increasing alkalinity above pH 8.0.

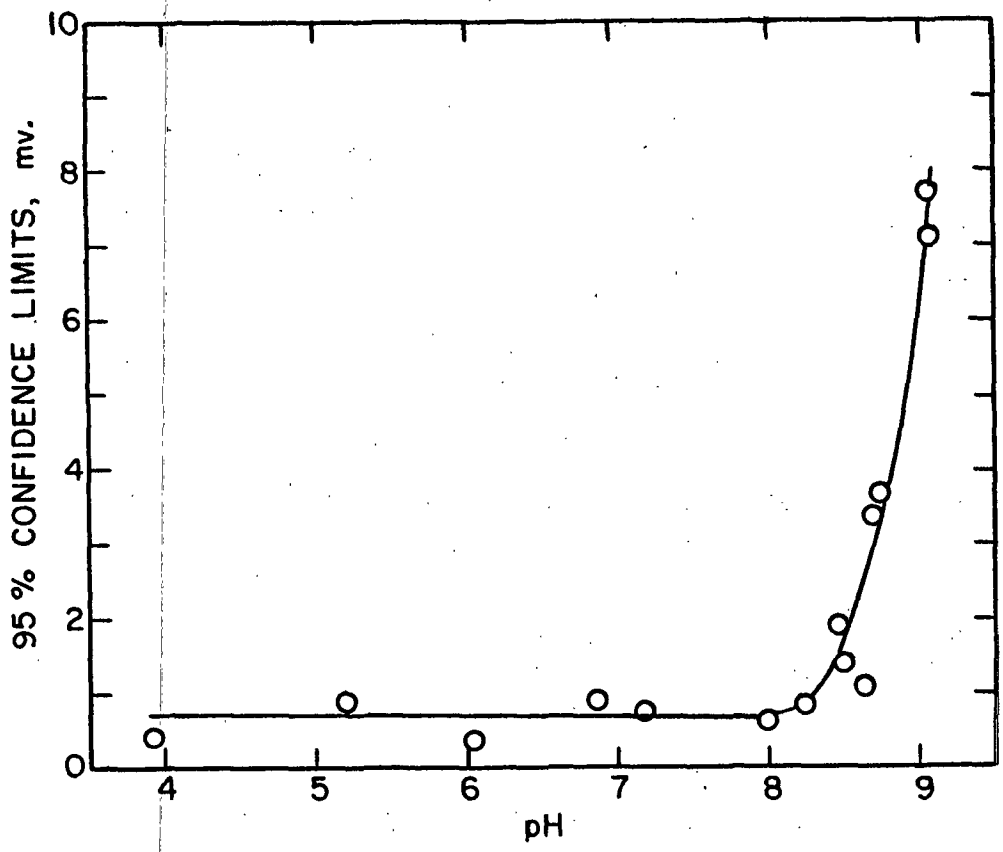

Figure 23. The Uniformity of the Surface Potential Within Ca-H-St Mono-Layers at 31 Dynes/cm. Confidence Limits Calculated from Eight or More Measurements Along 16 cm. of Trough Length During one ΔV Determination. T = 20.6°C.

The increase in the degree of nonuniformity with increasing subsolution pH above 8.0 is also demonstrated in Fig. 24 which shows the individual surface potential measurements obtained at various trough positions during the ΔV determination. Although the median value of ΔV at pH 9.07 is 2.1 mv., the monolayer is composed of large regions of negative and positive surface potentials.

Harkins and Fischer (81) showed the existence of two-phase regions in monolayers near zero surface pressure by surface potential measurements. The heterogeneous film consisted of islands of either liquid expanded, liquid condensed, or solid film (depending on the particular monolayer) in a sea of gaseous film. Ellipsometric (82) and ultramicroscopic studies (83) also indicated heterogeneous film formation

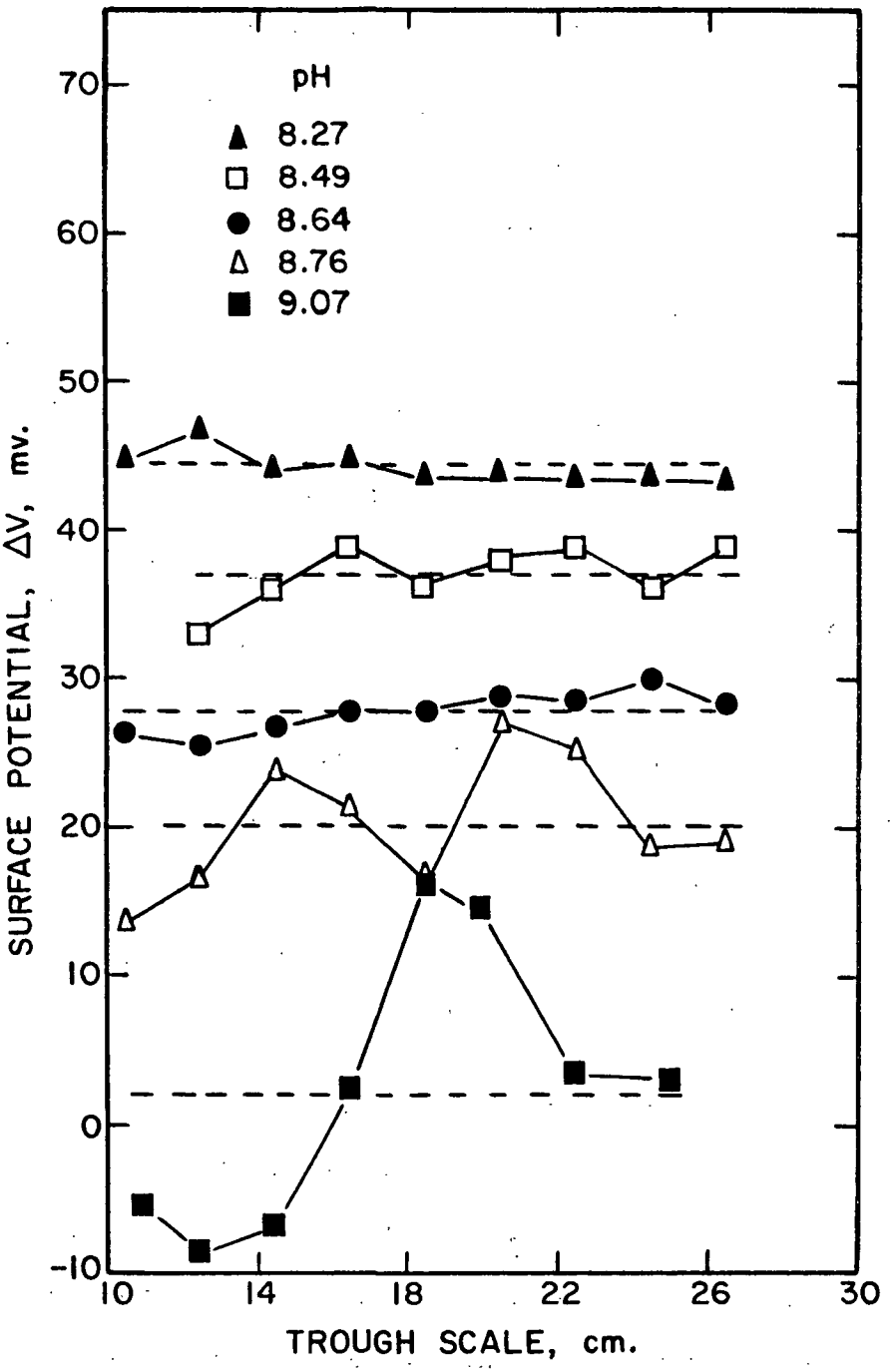

Figure 24. The Effect of pH on the Variation of the Surface Potential with the Trough Position During the $\Delta\underline{V}$ Determination of Ca-H-St Monolayers at 31 Dynes/cm. The Dashed Lines Represent the Average $\Delta\underline{V}$ Values. $\underline{T}$ = 20.6°C.

at very low surface pressures. Island structures were observed in electron micrographs (84) of monolayers near zero surface pressure. The classical electron microscopic studies of Ries and Kimball (85) also indicated the presence of island structures in fatty acid monolayers at higher surface pressures. However, more recent studies (84, 86) showed that irregular-shaped islands of film are obtained under nonideal conditions of spreading and/or transferring a monolayer. Cook and Ries (87) showed that at very low surface pressures the radioactivity-area isotherms for radioactive stearic acid indicate a nonhomogeneous distribution of the monolayer. They suggested that the uncompressed monolayers exist in large clusters of extremely small islands; and that during compression, the clusters may coalesce and the islands may deform to give the observed homogeneous condensed stearic acid films.

The Ca-H-St monolayers appear to behave similar to the stearic acid monolayers because Ryan and Shepard (73) demonstrated the presence of islands by observing heterogeneity in autoradiographs of radioactive Ca-H-St monolayers transferred at very low pressures by the Langmuir-Blodgett technique. However, autoradiographs of condensed Ca-H-St monolayers appeared to be homogeneous. Matsubara, et al. (63) observed that the Ca-H-St monolayer is heterogeneous at low surface pressures, but they concluded that the Ca-H-St monolayer becomes homogeneous and composed of close-packed molecules as it is compressed.

Based on the results of these previous studies, it is generally accepted that monolayers are heterogeneous at very low surface pressures and homogeneous at high surface pressures. However, the surface potential results of this study demonstrate that the condensed Ca-H-St monolayer at 31 dynes/cm. is uniform below pH 8.0 and nonuniform at higher values of the subsolution pH. In fact, the Ca-H-St monolayer increasingly manifests its heterogeneous character as the subsolution pH increases above 8.0.

The surface potential of a Ca-H-St monolayer at pH 9.07 was determined before and after compression to 31 dynes/cm. The surface potential measurements at various trough positions are shown in Fig. 25. The maximum positive surface potential reoccurs in the vicinity of the same trough position. In addition, there is a resemblance between the general profiles of the concentrated and dilute regions within the monolayer before and after the compression. These results suggest a general juxtaposition of large clusters in the monolayer on compression. However, redistribution of the clusters is minimal apparently due to the high viscosity and low compressibility of the Ca-H-St monolayer which is in the solid state under these conditions.

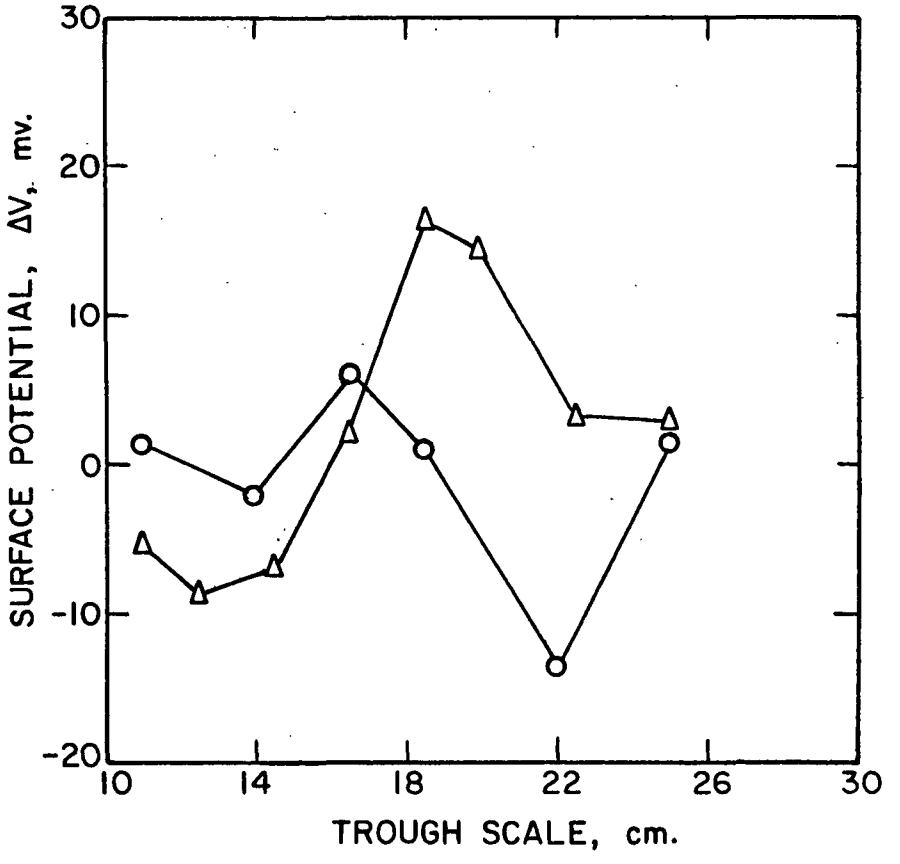

Figure 25. Comparison of the Variation of the Surface Potential with the Trough Position Before (O) and After (Δ) Compression to 31 Dynes/cm. for a Ca-H-St Monolayer at pH 9.07. $\underline{T}$ = 20.6°C.

The influence of compression time on ΔV is shown in Table IV. The degree of nonuniformity becomes less as shown by the decrease in the 95% confidence limits with compression time. The deformation of clusters consisting of close-packed molecules not only would decrease the heterogeneity of the monolayer, but it also would require a concomitant decrease in film area. Calculations based on the proposed surface micelle transformation model which is presented later indicate that up to 5% "subsolution surface" or gaseous film may be present at pH 9.0 (assuming a molecular area of 18.5 $A.^2$/molecule). The observed film area decrease is small, a little more than 1% in sixty minutes; but the contributions to the film area decrease by cluster deformation and monolayer collapse cannot be differentiated. Furthermore, this deformation would occur only with difficulty because of the solid state of the film molecules. Thus, the alternative view that the condensed Ca-H-St monolayer above pH 8 consists of large juxtaposed clusters of aggregated small islands interspersed with gaseous film is preferred. The decrease in monolayer heterogeneity with compression time is then suggested to occur from a redistribution of the extremely small islands within and between the clusters.

TABLE IV

EFFECT OF COMPRESSION TIME ON THE UNIFORMITY OF THE SURFACE POTENTIAL WITHIN A Ca-H-St MONOLAYER AT pH 8.70[a]

Compression Time, min.[b]	Surface Potential, ΔV, mv.	95% Confidence Limits, mv.
5	18.4	3.4
30	35.1	2.8
66	49.8	1.9

[a] Π = 31 dynes/cm.; T = 20.9°C.

[b] Average time after compression to 31 dynes/cm.

The ΔV-pH and $\mu_\perp$-pH curves of Fig. 22 drop very sharply between pH 6.4 and 8.0, and then the rate of decrease changes at about pH 8.0. This is the subsolution pH at which the condensed Ca-H-St monolayer commences to become nonuniform. If the monolayer were not heterogeneous, extrapolation of the linear portion between pH 6.4 and 8.0 suggests that ΔV and $\mu_\perp$ would be negative at pH 9. The large regions of negative and positive surface potential at pH 9.07 in Fig. 24 are ascribed to regions more concentrated in islands and gaseous phase, respectively. The surface potential and apparent surface dipole moment are positive for undissociated fatty acids. Consequently, there appears to be associated with the formation of the islands a change in the surface potential and apparent surface dipole moment from positive to negative values.

Effect of Compression Time

In addition to the Ca-H-St monolayer at pH 8.7 becoming less nonuniform with compression time, Table IV shows an increase in ΔV with compression time. Because the monolayers will be under compression for considerable time (up to 60 minutes) during the multilayer deposition studies, several additional experiments were conducted on this observed effect in order to shed insight into any possible slow changes that may occur in the monolayer.

Table V presents a summary of the effect of compression time on the surface potential and monolayer stability measurements at several values of the subsolution pH. The experimental results are illustrated in more detail in Appendix III. In each case a significant increase in ΔV with time occurred. This effect is opposite to the slow ΔV lowering of myristic acid monolayers observed by Addink (88) who attributed this decrease to the dissolved fatty acid molecules.

Examination of Table V indicates that there is no direct correlation between the increase in ΔV and the film area decrease arising from monolayer collapse.

The electron microscopic results of this study show that the slow monolayer collapse process is bimolecular in nature. If the collapsed film is a completely symmetrical bimolecular leaflet, then this double layer should not make any contribution to the surface potential due to a zero effective electrostatic dipole moment. It appears that monolayer collapse does not significantly affect ΔV, and collapse occurs in symmetrical bimolecular layers having a zero electrostatic dipole moment.

TABLE V

EFFECT OF COMPRESSION TIME ON THE SURFACE POTENTIAL AND MONOLAYER STABILITY OF Ca-H-St MONOLAYERS[a]

pH	Compression Time, min.[b]	Surface Potential Increase, mv.	Film Area Decrease, %
2.00[c]	24	17	43
5.88	51	11	4.3
8.25	56	15	0.5
8.70	66	31	N.D.[d]

[a] Π = 31 dynes/cm.; T = 20.6°C.

[b] Average time after compression to 31 dynes/cm.

[c] $CaCl_2$ not added to subsolution.

[d] Not determined, estimated to be 1.2%.

That the increase in ΔV is approximately the same under the different conditions of subsolution pH suggests that a common mechanism of the ΔV increase occurs for condensed stearic acid and Ca-H-St monolayers. It is assumed that there exists within the homogeneous stearic acid and Ca-H-St monolayers uniformly distributed holes or pores whose contribution to ΔV is that of the clean subsolution surface. These holes arise from the random fluctuations in monolayer density (89). These holes, dynamic in nature, are assumed to be the sites for water evaporation from the subsolution surface. The holes within the Ca-H-St monolayer above pH 8.0 are

assumed to be nonuniform and unevenly distributed; in addition, the contribution to ΔV is that of the gaseous film. It has been shown (90-92) that straight-chain fatty acid monolayers can significantly retard evaporation from the subsolution surface only when in the highly condensed or solid state. It may then be argued that molecularly dispersed water will be present only throughout monolayers which are unable to retard water evaporation. However, water is a unique liquid such that it readily permeates between the long aliphatic chains of a condensed monolayer of a fatty acid (93). Thus, there will also be dipole contributions from the molecularly dispersed water molecules which have penetrated between the aliphatic chains in the monolayer.

The orientation and polarization of these molecularly dispersed water molecules, especially those nearest the terminal CH_3 group of the aliphatic chain, is expected to decrease the vertical component of the dipole moment that is associated with the aliphatic chain. This assumes, as is usual, that only the terminal CH_3 group determines the value of the surface dipole moment in an aliphatic chain (94). A similar explanation of polarization of molecularly dispersed water near the C-F bonds of the fluorinated chain segment of fluorinated fatty acid monolayers has been advanced by Bernett and Zisman (94). Although uncertainties remain in the literature concerning the correct value of the vertical component of the dipole moment of the CH_3 group, a value of 0.3 Debye (95) with the positive end of the dipole oriented toward the carbon atom has been preferred by many investigators and is used in this study. On this basis, an increase in the molecularly dispersed water molecules associated with the monolayer will lead to a decrease in the vertical component of the moment contributed by the CH_3 group and, consequently, an increase toward more positive values of the surface potential because the negative contribution of the vertical component of the CH_3 group is opposite that of the polar group and its associated water molecules.

In the case of the uniform stearic acid and Ca-H-St monolayers, a decrease in the number of pores causes an increase in ΔV because the contribution due to the holes is zero. This assumes the monolayer behaves as an ideal two-dimensional solution in which ΔV is additive at constant surface pressure.

The situation for the Ca-H-St monolayer above pH 8.0 is far more complicated. A decrease in the amount of gaseous film is believed to cause a decrease in ΔV. Furthermore, the larger increase in ΔV at pH 8.70 is also due, in part, to the slow decrease in subsolution pH from atmospheric CO_2 absorption.

It is suggested that the increase in ΔV with compression time may be due to an increase in molecularly dispersed water molecules which have penetrated between the oriented aliphatic chains of the condensed monolayer.

MONOLAYER STABILITY MEASUREMENTS

The results of the monolayer stability measurements of stearic acid are shown in Fig. 26. The stearic acid monolayers are not very stable at a surface pressure of 31 dynes/cm. because there is a large decrease in the film area. The stearic acid monolayer is more stable at pH 6 than at pH 2. In addition, the C^{14}-labeled stearic acid appears to be more stable than the inactive stearic acid.

This observed increased stability at pH 6 is consistent with the known increased attraction of partially ionized fatty acid monolayers (66). The nature of the molecular interaction between the ionized and un-ionized molecules is controversial and has been attributed to either increased head-group or chain attractions (66, 96). In any event, this increased attraction requires a larger amount of energy to transfer a molecule from the monolayer to a bulk phase; and, consequently, the monolayer stability is increased.

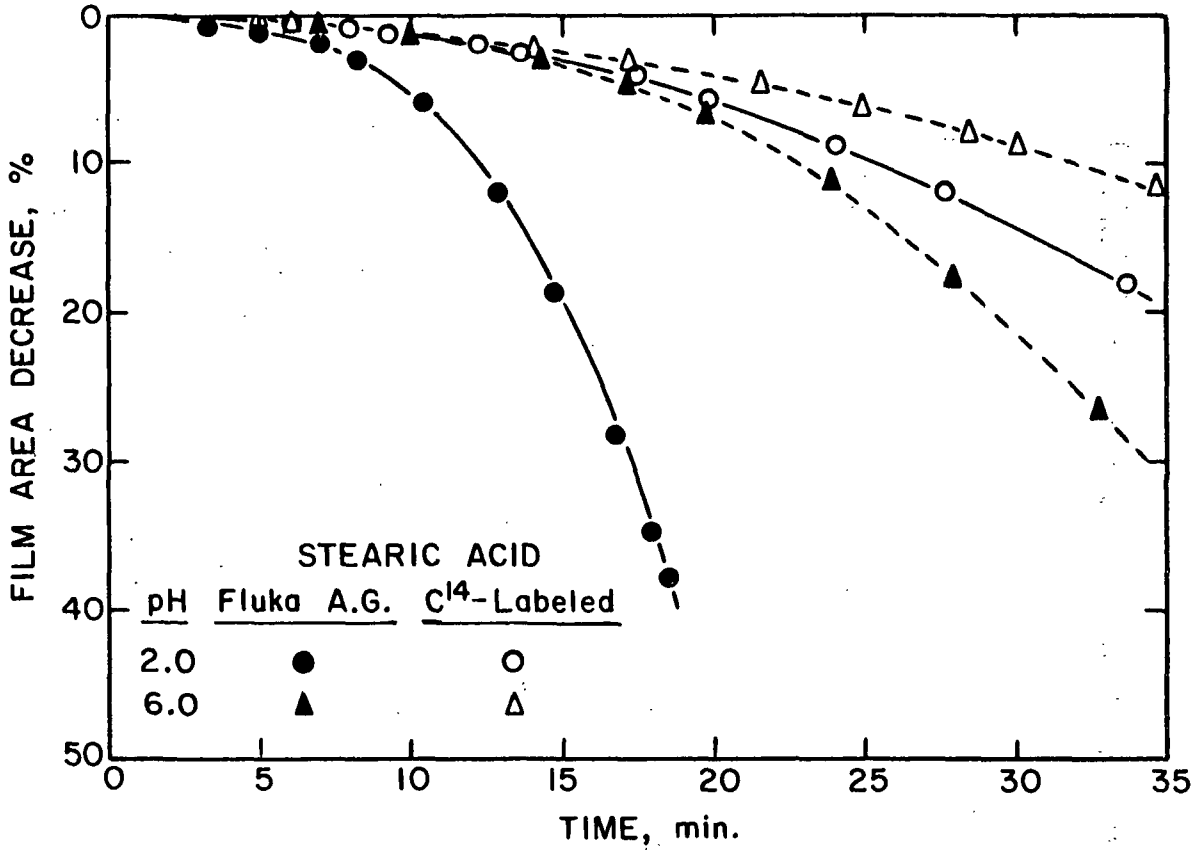

Figure 26. Stability Measurements of Stearic Acid Monolayers at 31 Dynes/cm. $\underline{T}$ = 20.5°C.

The stability measurements of the Ca-H-St monolayers shown in Fig. 27 are compared at a selected compression time of fifteen minutes in order to evaluate the relative stabilities of the Ca-H-St monolayers at various values of the subsolution pH. The results are presented in Fig. 28. Because fifteen minutes was the maximum time interval for depositing bilayers, the results represent the maximum percentage decrease in the film area which concomitantly occurs during bilayer deposition. It is readily evident that very significant errors can arise in the determination of the transfer ratio by surface balance measurements unless corrections for this concomitant decrease in film area are applied.

Figure 28 shows that below pH 6 the inactive Ca-H-St monolayer becomes increasingly less stable with decreasing subsolution pH. However, the inactive

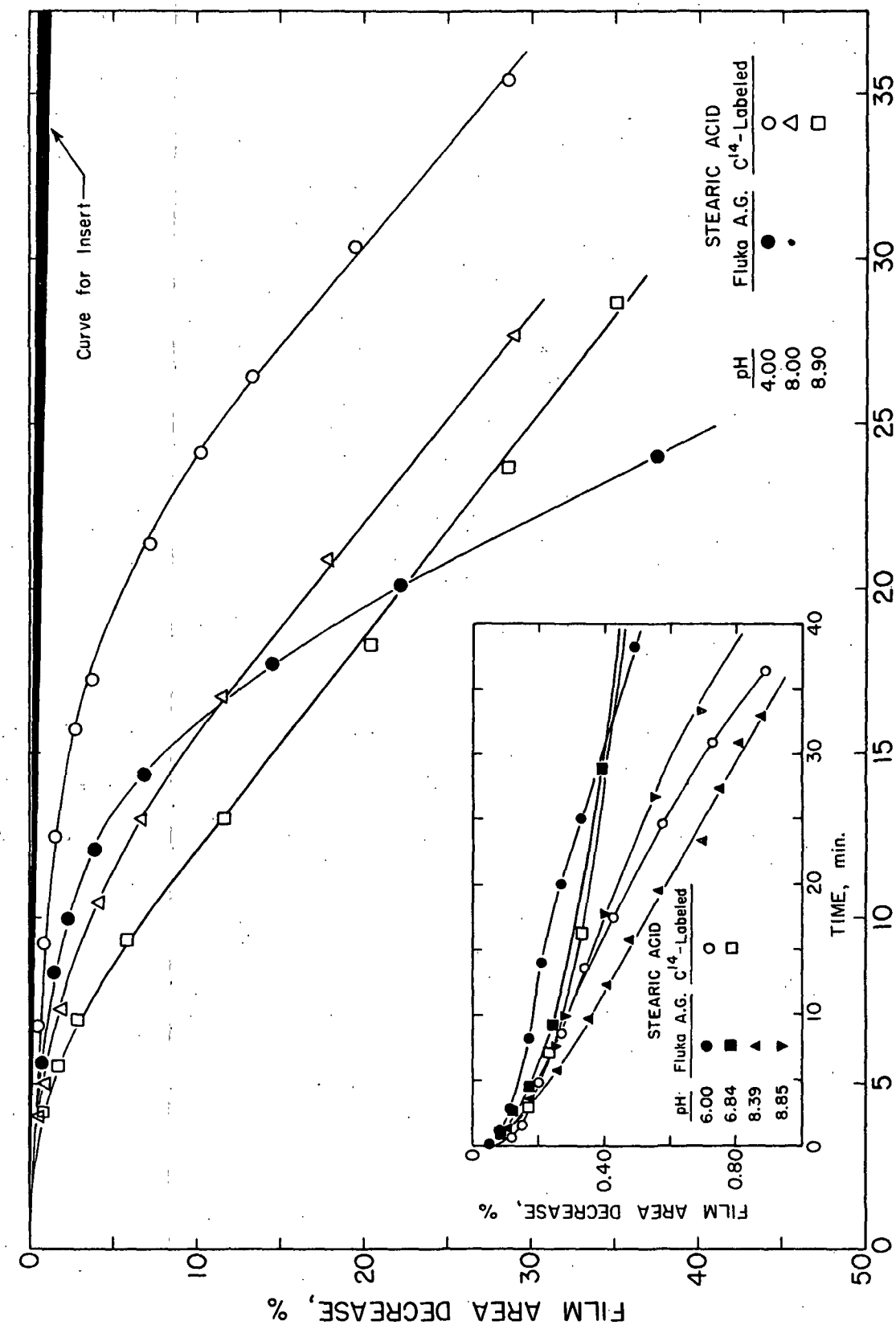

Figure 27. Stability Measurements of Ca-H-St Monolayers at 31 Dynes/cm. $\underline{T}$ = 20.5°C.

Ca-H-St monolayer is very stable above pH 6, its film area decreasing less than 0.5% in 15 minutes. On the basis of these stability measurements, it is concluded that the decrease in $\underline{A}_{31}$ above pH 6.4 in Fig. 19 is not attributable to monolayer losses by dissolution, evaporation, or collapse during the compression time. Thus, this observed decrease in $\underline{A}_{31}$ must be the result of a structural rearrangement of the molecules within the monolayer.

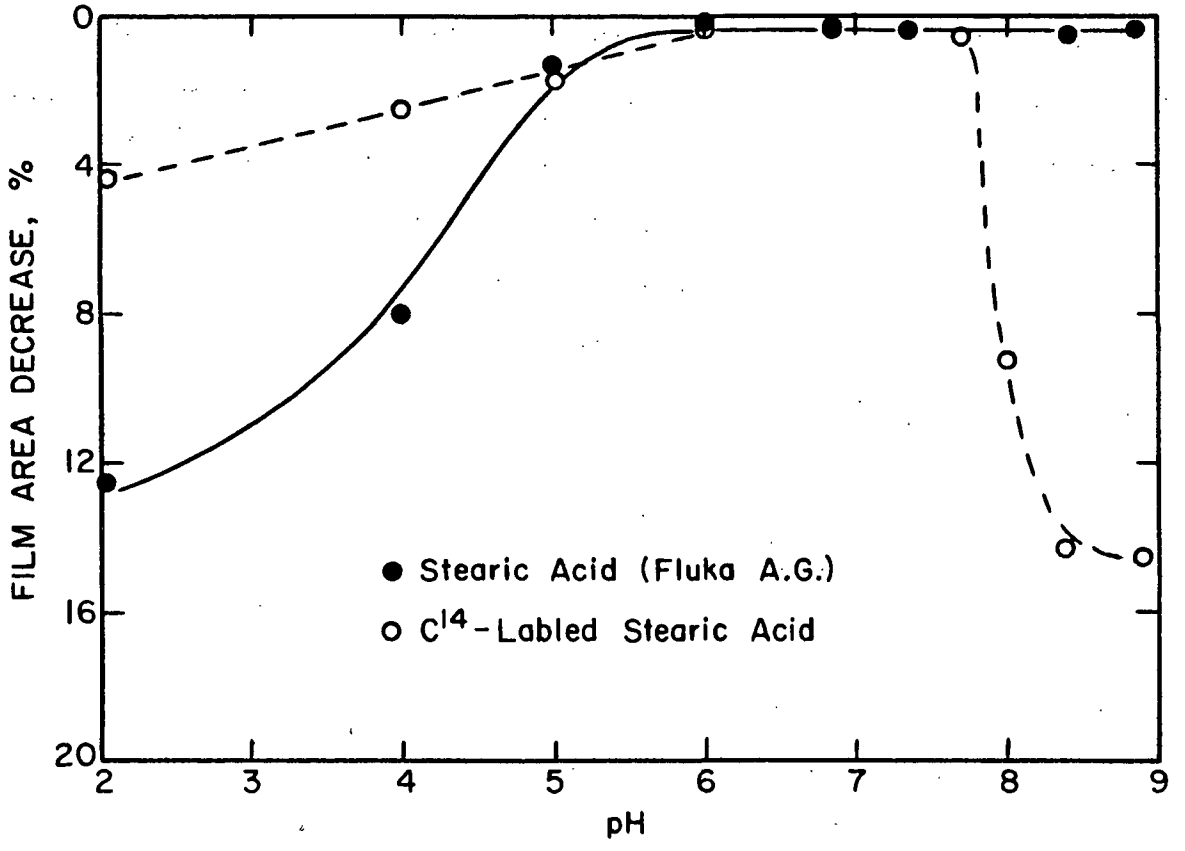

Figure 28. Comparison of the Stabilities of Ca-H-St Monolayers at 31 Dynes/cm. at a Compression Time of 15 min. $\underline{T}$ = 20.6°C.

A most surprising result is readily observed in Fig. 26 and 28. There appears to be a difference between the behavior of inactive and C^{14}-labeled stearic acid and Ca-H-St monolayers as indicated by the monolayer stability measurements. At pH < 5.0 where the molecules are predominantly un-ionized stearic acid, the radioactive monolayer is more stable; both monolayers possess the same stability in the

pH range 5.0-7.8; and then above pH 7.8 a reversal in stability occurs with the inactive monolayer now being much more stable.

Although the explanation of this difference in behavior between the inactive and radioactive monolayers is uncertain, it is worthwhile to discuss the observation in more detail because of its significance. It is generally assumed in radioisotope studies that the radioactive species behaves the same as the unlabeled form. This is only approximately correct because the masses of the C^{14} and C^{12} nuclei are different. According to kinetic theory, the velocities of atoms of different masses are not the same. The difference in the rate of movement between a C^{14} and C^{12} atom due to the difference in the masses is about 7% (97). The stearic acid was only labeled in the C-1 position which represents about 4.2% of the total mass of the molecule. Thus, the effect of the C^{14} atom on the rate of movement of the total molecule is very small.

Two considerations strongly suggest that the observed difference does not arise from impurities in the system. The high purity of both stearic acids minimizes the effect of chemical impurities. In addition, the peculiar behavior of the stability of the radioactive Ca-H-St monolayer, rising to a maximum and then decreasing again with increasing alkalinity, and the magnitude of the differences in stability appear to rule out the impurity explanation. However, this peculiar stability behavior of the C^{14}-labeled and inactive Ca-H-St monolayers is not understood at the present time and needs further clarification. It is conceivable that high specific activity compounds existing in the highly oriented arrays of the two-dimensional state may exhibit effects not commonly found or observed in bulk systems. Unexplained differences in the behavior of radioactive and inactive surface-active agents have also been observed (17, 98-100).

TRANSFER RATIO DURING LANGMUIR-BLODGETT MONOLAYER DEPOSITION

The instability or decrease in film area of the monolayers under compression was further studied by the techniques of autoradiography and electron microscopy. These two experimental techniques require the transfer of the monolayer from the subsolution surface to a solid substrate by the Langmuir-Blodgett method. The observed features in the autoradiographs and electron micrographs are more likely to be artifacts if the transfer ratio is less than unity. Therefore, it was necessary to determine whether the average area/molecule remains unchanged during the monolayer transfer, i.e., whether the transfer ratio is unity.

The transfer ratios of stearic acid monolayers for a variety of experimental conditions are given in Table VI. These results indicate that essentially no variation in the area/molecule occurs during transfer of the monolayer from a subsolution surface to the solid substrate when the withdrawal contact angle between the film-covered subsolution surface and the emerging solid is zero. A zero withdrawal contact angle is obtained with the high-energy solids, glass and mica, even at very low surface pressures. However, significantly lower transfer ratios occur with collodion substrates at low surface pressures when an acute withdrawal contact angle is formed. Autoradiographs of the monolayers deposited on collodion at low surface pressure also indicate that the transfer ratio is very low, but autoradiographs of monolayers simultaneously deposited on glass show the normal background intensity corresponding to a transfer ratio of unity.

The withdrawal contact angles were determined during monolayer deposition of stearic acid monolayers onto collodion at various surface pressures. The cosine of the withdrawal contact angle is plotted against the surface tension of the monolayer-covered subsolution in Fig. 29. These results indicate that the withdrawal contact angle during monolayer deposition on collodion is zero degrees only

when the surface tension is less than 47 dynes/cm. or the surface pressure is greater than 26 dynes/cm.

TABLE VI

TRANSFER OF STEARIC ACID MONOLAYERS TO SOLID SUBSTRATES

Substrate	Deposition Conditions[a] pH	Ca	Surface Pressure, dynes/cm.	Local Net Counting Rate,[b] c.p.m.	Transfer Ratio Measured[c]	Calc.[d]	Withdrawal Contact Angle, °
Glass	6.85	Yes	31	481 ± 3[e]	1.01	--	Zero
	4.01	Yes	31	479 ± 4	1.02	--	Zero
	2.00	No	20	458 ± 4	--	1.00	Zero
Mica	2.00	No	1.5-31	--	--	--	Zero
Collodion	8.83	Yes	31	483 ± 4	--	1.01[f]	Zero
	6.83	Yes	31	482 ± 9	--	1.00	Zero
	2.00	No	31	--	--	--	Zero
	2.00	No	20	105 ± 3	--	0.23	28
	2.00	No	10	76 ± 3	--	0.18	42

[a] $Ca = 10^{-4}$ M; T = 20.3°C.
[b] Radioactivity at each location on the sample was counted to a 1% standard deviation.
[c] Determined by film balance measurements.
[d] Calculated from radioactivity measurements relative to the radioactivity at II_{31} on glass and corrected for the average area/molecule determined from the II-A isotherms.
[e] 95% Confidence limits.
[f] Assumed 0.2 μm.-thick collodion film has negligible contribution to the back-scattering of glass.

At a surface pressure of 31 dynes/cm., a zero withdrawal contact angle occurs during Langmuir-Blodgett monolayer deposition on mica, glass, and collodion substrates. Thus, the monolayers were deposited onto mica and collodion substrates at 31 dynes/cm. for autoradiographic and electron microscopic examination. Under these conditions, the transfer ratio during Langmuir-Blodgett monolayer deposition is unity.

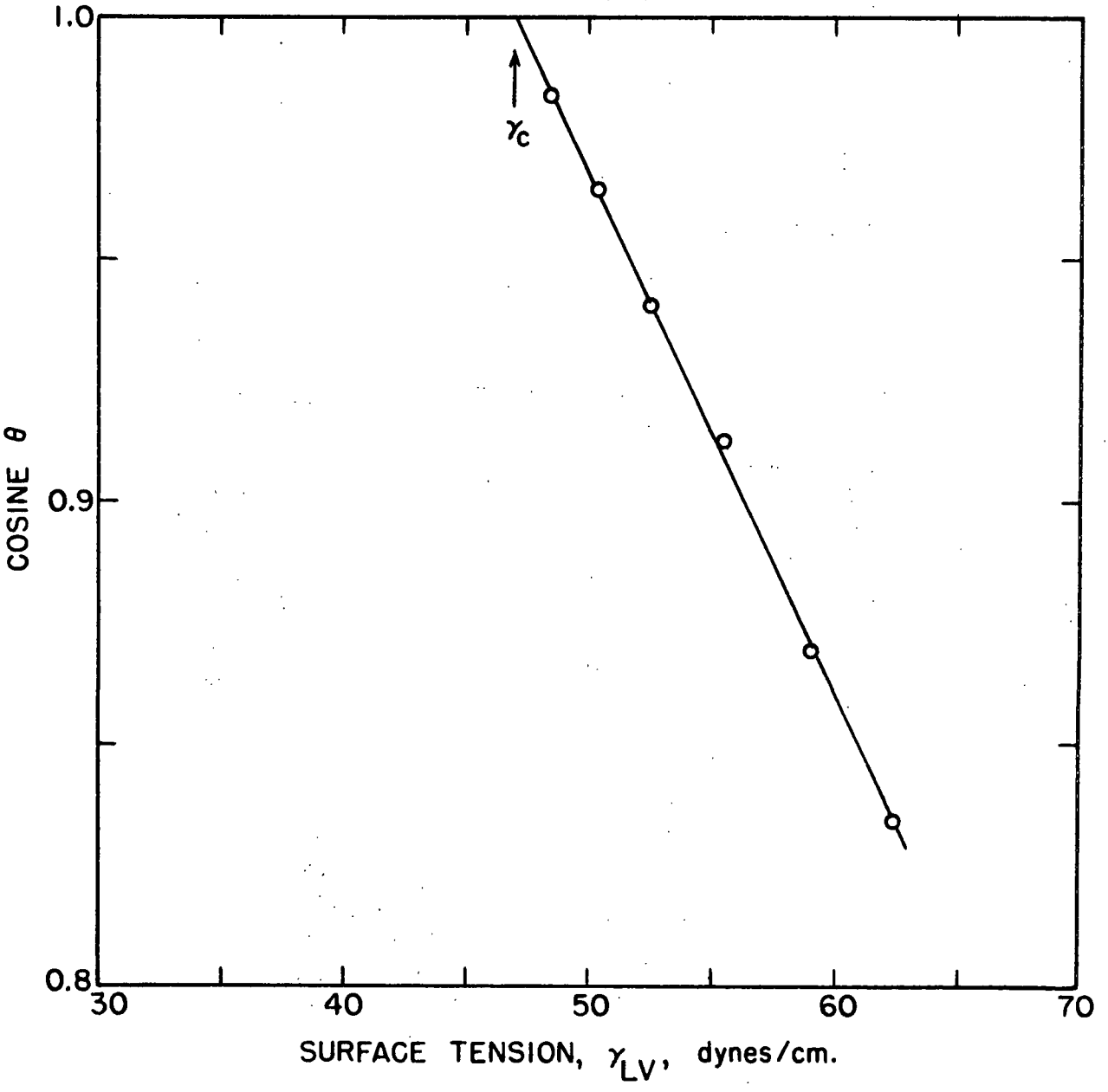

Figure 29. The Wettability of Collodion by Stearic Acid Monolayers at pH 6.0 During Langmuir-Blodgett Monolayer Deposition at Various Surface Tensions of the Monolayer-Covered Subsolution. $\underline{T}$ = 20.2°C.

MONOLAYER COLLAPSE

Size and Distribution of the Collapsed Regions

Autoradiographs of deposited Ca-H-St monolayers were obtained at values of the subsolution pH where instability was observed and at known average reductions in the film area. Typical autoradiographs are shown in Fig. 30. The dark areas are the regions of high activity. The correspondence between the growth of these regions and the decrease in film area indicates the formation and growth of a new bulk phase, i.e., a slow collapse process, with compression time. This slow collapse process is to be distinguished from catastrophic collapse which occurs when the surface pressure is so high that the monolayer fails by a folding process (85, 101).

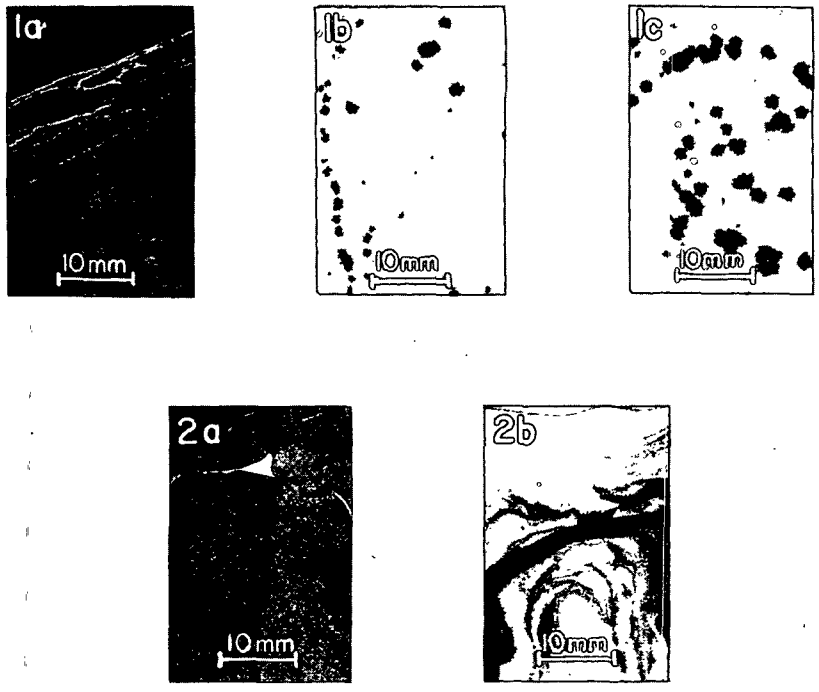

Figure 30. Typical Autoradiographs of Ca-H-St Monolayers at Various Stages of Collapse Deposited on Collodion at 31 Dynes/cm. Dark Areas are the Regions of Highest Activity

1. pH 4.0; (a) 0.5%, (b) 10%, and (c) 20%
2. pH 8.9; (a) 0.5%, and (b) 20%

The sequence of this collapse process for Ca-H-St monolayers at pH 4.0 is also observed to be representative of that for stearic acid monolayers at pH 2.0 and 6.0. It is important to realize that the similarities between the behavior of Ca-H-St monolayers at pH 4.0 and stearic acid monolayers at pH 2.0 occur because they have the same chemical composition. Bagg, et al. (102) determined by the infrared analysis of multilayers that the chemical composition of Ca-H-St monolayers at pH 4.0 was un-ionized stearic acid. Furthermore, Bagg, et al. (103) also determined that stearic acid monolayers at pH 6.0 are only slightly ionized.

Although the deposited films in Fig. 30 are fairly continuous, light areas which are regions of very low molecular concentration or of no film occur and resemble fracture lines in the deposited monolayer. Such mechanical separation is suggested by the matching contours of the film edges. This type of nonuniform deposition is believed to arise from irregularities in the mechanical manipulation of these films. But while these fissures are also present in autoradiographs of monolayers deposited on mica substrates, they are absent in monolayers deposited on glass. This raises the question to what extent does the substrate influence the fracturing of the film.

Figure 30(1a) shows that very small collapse regions with a diameter up to 0.3 mm. exist even in short compression times of less than four minutes. At 10% collapse, there is an increase in the number and size of the collapsed areas. The additional decrease in film area at 20% collapse is accounted for primarily by increased growth of the collapsed areas, not by an increase in their number. Large collapsed regions having a diameter of 2 mm. are commonly observed. When a typical collapsed region is magnified, a growth pattern which radiates from a nucleus is observed.

Figure 30(2a) shows a large triangular-shaped void in the autoradiograph of the Ca-H-St monolayer at pH 8.9. If disruption of the monolayer during deposition is the origin of the void, a region of higher activity might be expected at the void's periphery. The void in the Ca-H-St monolayer may represent a region concentrated in gaseous film because the deposited monolayer is uniform up to the peculiar shaped void.

The collapse mechanism of the Ca-H-St monolayer at pH 8.9 does not appear to resemble the slow collapse process at pH 4.0. The collapse pattern at pH 8.9 has a marbled appearance with bands of varying activity approximately perpendicular to the compressive forces, neglecting edge effects. Figure 30(2b) shows that the collapsed regions are extremely small and distributed more uniformly throughout the film in contrast to the discrete collapsed regions at pH 4.0. The intense bands appear to be composed of many coalesced collapsed regions. The growth rate of a crystal is limited by the rate at which molecules may diffuse to and be incorporated into the crystal. The high surface viscosity and brittle nature of the Ca-H-St monolayer are believed to be responsible for the collapsed regions being very small and occurring in "bands" parallel to the compression barrier.

As is well-known, the stearic acid and Ca-H-St monolayers may be considerably compressed beyond their equilibrium spreading pressures (ESP) because their stable bulk phases are crystalline solids. The ESP is defined as the pressure where the monolayer is in equilibrium with the stable bulk phase under the experimental conditions (104). The ESP of stearic acid at 25°C. is about 5 dynes/cm. (105). The slow collapse processes occur and form adjacent bulk phases because the overcompressed monolayers at 31 dynes/cm. are not in thermodynamic equilibrium with respect to the bulk crystalline phase. However, such systems can often remain in a metastable state for an extended period of time as shown by the monolayer stability measurements of Fig. 27.

Nature of the Collapsed Regions

The nature of the collapsed regions which were observed in Fig. 30 was further studied by electron microscopy. Electron micrographs were obtained of a 20% collapsed Ca-H-St monolayer deposited on collodion at pH 4.0. Inactive and radioactive monolayers give the same results. A sequence of electron micrographs beginning outside of a collapsed region and proceeding inward is shown in Fig. 31. The monolayer structure is fairly smooth and uniform as shown in Fig. 31(a). The initial stages of monolayer collapse are represented by Fig. 31(b). Then Fig. 31(c) and 31(d) show the large crystals of stearic acid up to 3 μm. in diameter and 0.2 μm. high that are capable of being formed during monolayer collapse on the subsolution surface.

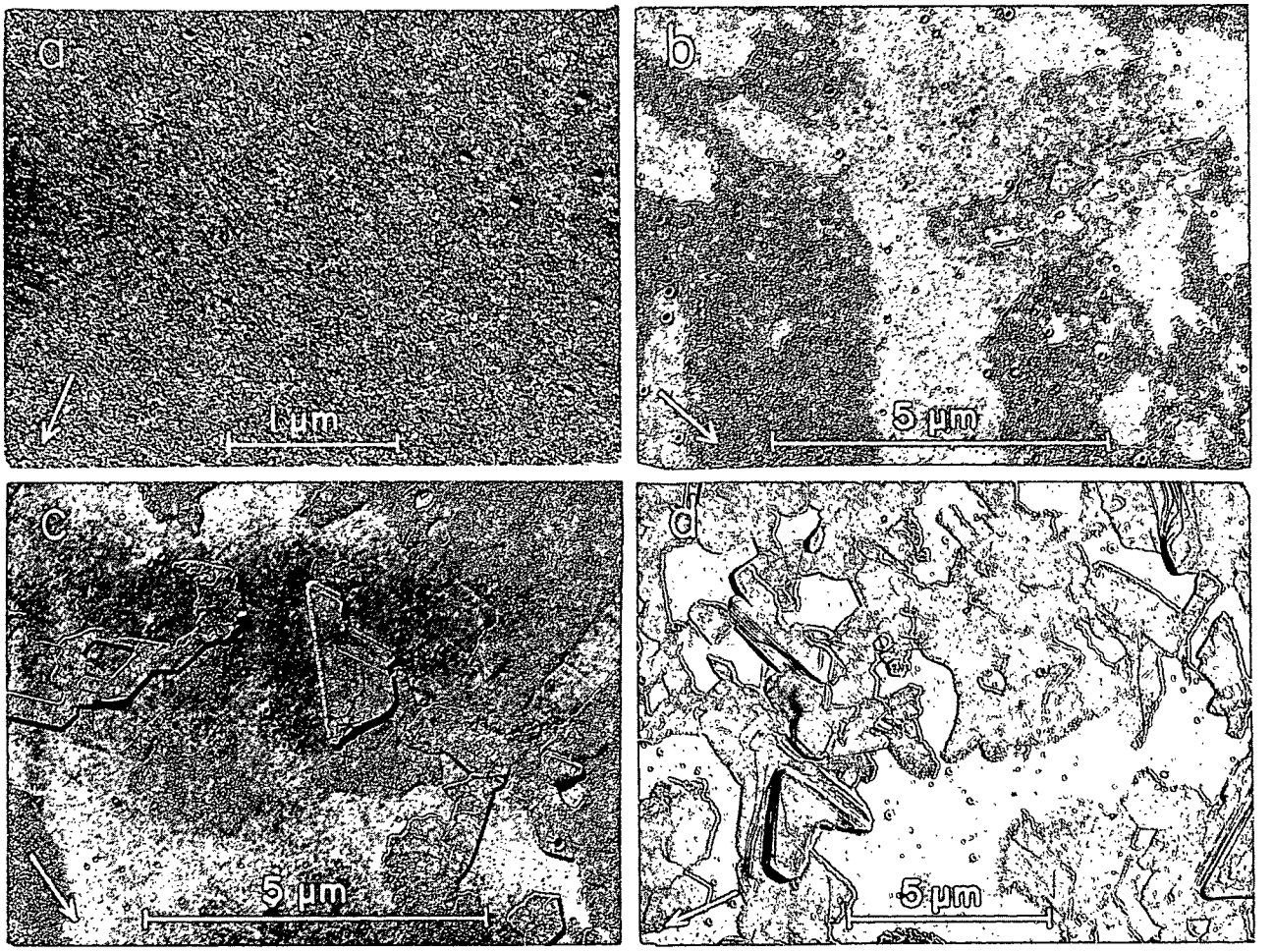

Figure 31. Sequence of Electron Micrographs of Pd Preshadowed Replicas of Collapsed Regions of a 20% Collapsed Ca-H-St Monolayer Deposited on Collodion at pH 4.0 and 31 Dynes/cm. (a) Beginning Outside the Collapsed Region (21,800X); (b) Just Inside (8900X); (c) Proceeding Inward (8900X); and (d) Near the Center (5410X)

Measurements of the shadow lengths of the crystal steps of the collapsed monolayers give heights about 50 A. These measurements were obtained from Ortho film enlargements of the electron microscope film. Blodgett (4) determined by an optical method the thicknesses per double layer of stearic acid and Y-type calcium stearate multilayers to be 45.8 and 48.8 A., respectively. The x-ray diffraction measurements of several workers (23, 106) have shown that the spacings of the metal cations in X- and Y-type calcium stearate multilayers are 49.4 and 50.1 A., respectively. Thus, the slow collapse of a stearic acid monolayer appears to be bimolecular in nature and proceeds by a stable-crystal nucleated collapse mechanism.

Monolayer collapse of Ca-H-St monolayers above pH 8.0 was examined with radioactive monolayers. Because inactive Ca-H-St monolayers are very stable above pH 8.0, very few collapsed regions are formed. It is extremely difficult to locate a collapsed region, and many electron microscope grids must be examined before a collapsed region is found. But upon using radioactive Ca-H-St monolayers, monolayer collapse readily occurs with collapsed regions being easily found for examination.

Figure 32 shows electron micrographs of the typical collapsed regions in Ca-H-St monolayers at pH > 8.0 at both low and high magnifications. The collapsed regions are seen to exist as patches having a diameter of about 10-50 μm. There are numerous platelets up to about 1 μm. in diameter laying on top of one another within the collapsed regions. The thickness of the platelets as determined by measurements of the shadow lengths is about 50 A., and so the calcium stearate platelets also appear to be bimolecular.

Additional electron micrographs of deposited monolayers are presented in Appendix IV. The Ca-H-St monolayers at pH 4.0 and pH > 8.0 were deposited on collodion and mica substrates and were shadow-cast with either Pd or Pt. The employment of various substrates and shadow-casting procedures is advantageous

in that greater insight can be gained into the structure of Langmuir-Blodgett monolayers. Minimal structural rearrangements and maximum monolayer stability are to be expected when mica substrates and Pd shadow-casting are used. However, some structural details may be lost by Pd shadow-casting.

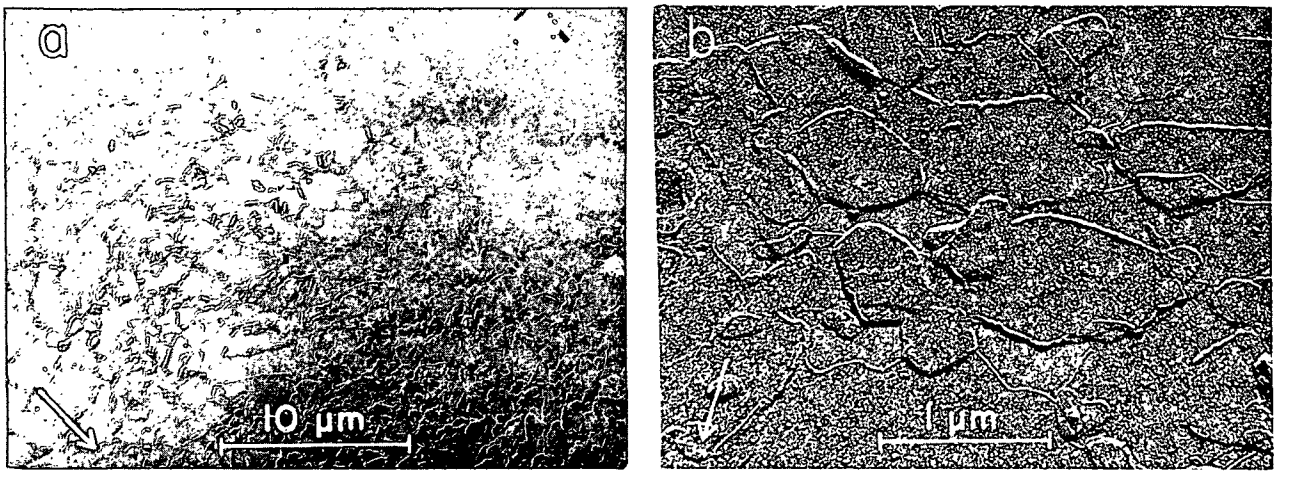

Figure 32. Electron Micrographs of Pd Preshadowed Replicas of (a) Collapsed Regions of a 10% Collapsed C^{14}-Labeled Ca-H-St Monolayer Deposited on Mica at pH 8.3 and 31 Dynes/cm. (2480X); and (b) Same as (a) Except Greater Magnification (22,000X)

LANGMUIR-BLODGETT MULTILAYER DEPOSITION

In preparing multilayers on paraffin, the first monolayer or layer is deposited only when the paraffin substrate is lowered through the compressed monolayer at the liquid/air interface as shown in Fig. 33(a). The second layer is deposited when the monolayer-covered paraffin is withdrawn from the subsolution as shown in Fig. 33(b). Additional layers may successively be deposited by repeating the immersion and withdrawal sequence. Consequently, odd-numbered monolayers are deposited during the immersion operation, and even-numbered monolayers are deposited during the withdrawal operation.

The transfer ratio, ρ, has already been defined as the ratio of the area of the monolayer removed from the subsolution surface to the area that the deposited

monolayer occupies on the solid surface. If the transfer ratio is unity, then there is no change in the molecular packing of the monolayer during the transfer from the subsolution to the paraffin surface. However, if the transfer ratio is less than unity, then the average area/molecule has increased as a result of the deposition process. The transfer ratios are designated as ρ_1, ρ_2, ..., ρ_i where i = 1, 2, ..., n refers to the individual deposited monolayers of a multilayer.

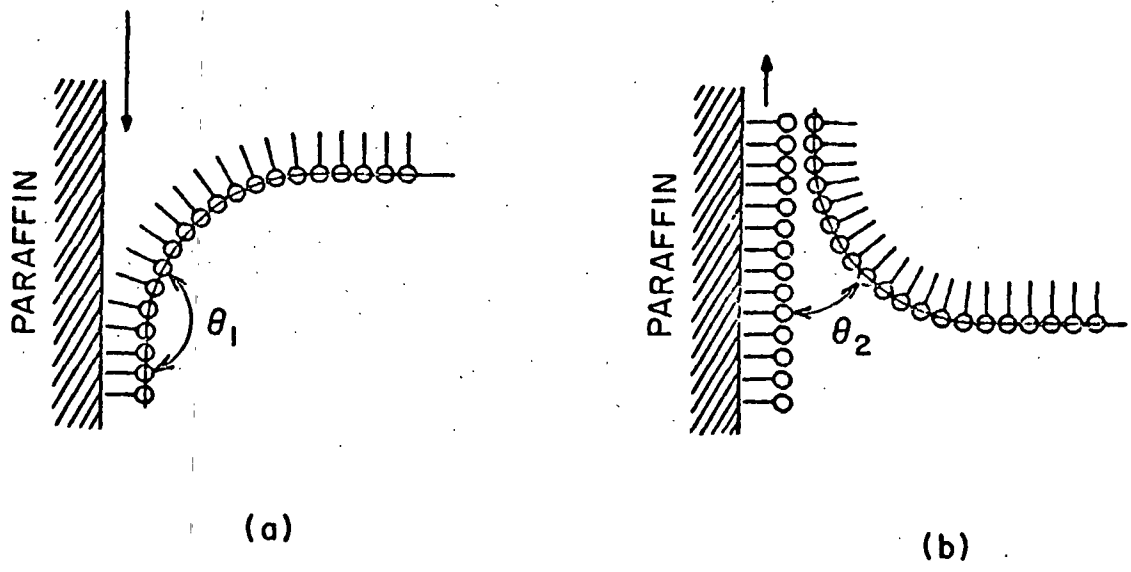

Figure 33. The (a) Immersion and (b) Withdrawal Operations of Bilayer Deposition on a Paraffin Substrate

Multilayer deposition is further characterized by the contact angle developed between the solid or multilayer and the monolayer-covered subsolution. The contact angle is always obtuse during the immersion operation. But, during the withdrawal operation, the contact angle is acute, at least during the initial stages of multilayer deposition. In a similar manner as the transfer ratios, the contact angles developed during the deposition of individual monolayers are designated as θ_1, θ_2, ..., θ_i where i = 1,2, ..., n.

EFFECT OF DEPOSITION SPEED

The immersion and withdrawal speed of the solid substrate have been shown by various investigators (4, 19, 55, 107) to have an effect on Langmuir-Blodgett monolayer and multilayer deposition. This effect of the deposition speed on multilayer deposition on paraffin was determined.

Table VII shows the effect of the deposition speed on Ca-H-St bilayer deposition on paraffin. In addition, the effect of deposition speed on the contact angle developed during the withdrawal of an immersed paraffin slide through a stearic acid monolayer is also shown in Table VII. Under these conditions, the stearic acid monolayer does not deposit on the paraffin on the basis of the film balance measurements. Autoradiographs and radioactivity measurements give confirmatory evidence that no film is deposited on the paraffin surface.

TABLE VII

THE EFFECT OF DEPOSITION SPEED[a]

Deposition Speed, mm./min.	Withdrawal Contact Angle, °		Transfer Ratio[b]	
	Bilayer, θ_2[b]	Monolayer[c]	ρ_1	ρ_2
38.0	--	70.2 ± 0.8[d]	--	--
19.0	50.0 ± 0.3[d]	72.8 ± 0.4	1.03	0.87
7.6	58.2 ± 0.3	74.3 ± 0.4	1.02	0.91
3.8	59.0 ± 0.7	73.8 ± 0.3	1.03	0.91
1.9	60.8 ± 0.4[e]	74.0 ± 0.4	0.97[e]	0.93[e]
0.76	--	74.9 ± 0.5	--	--

[a] C^{14}-labeled stearic acid. Π = 31 dynes/cm.; T = 20.4°C.
[b] pH 8.4 and 10^{-4}M $CaCl_2$ subsolution.
[c] Contact angle developed when a paraffin substrate is withdrawn through a stearic acid monolayer at pH 5.8.
[d] 95% Confidence limits.
[e] pH 8.3 and 10^{-4}M $CaCl_2$ subsolution.

The results indicate that at a speed of 7.6 mm./min. or less, the withdrawal contact angle is essentially independent of the relative motion between the solid and the subsolution. In addition, the error associated with the determination of the transfer ratios for C^{14}-labeled Ca-H-St bilayers above pH 8.0 becomes increasingly greater at deposition speeds less than 7.6 mm./min. At these longer residence times, the contribution of monolayer collapse to the decrease in film area becomes excessive. Accordingly, a deposition speed of 7.6 mm./min. was used throughout this study.

This selected speed of 7.6 mm./min. is an order of magnitude less than the deposition speeds of about 60 mm./min. used by Goranson and Zisman (18). By contrast, Blodgett (4) used speeds of 250 mm./min. and even faster to build Y-films of calcium stearate.

A noteworthy observation is that there is a small, but real, difference between the withdrawal contact angles of the two sides of the solid slide. The withdrawal contact angle on the side between the movable compression barrier and the solid is 1-2° lower than the contact angle on the side between the float and the solid. The contact angle should not be influenced by the proximity of the float because it is 10 cm. away from the solid slide. The difference occurs for both fluid and solid Ca-H-St monolayers. The effect is believed to be real because of the camera, slide assembly, and enlarger alignment verification results presented in Appendix II. In addition, this contact angle difference also appears in the withdrawal contact angle developed when an immersed paraffin slide is withdrawn through a stearic acid monolayer. This indicates that the effect is not a result of the deposition process.

This observation is not fully understood, but a possible explanation is that a surface tension gradient exists within condensed stearic acid and Ca-H-St

monolayers maintained at high constant surface pressures by the automatic film balance. A surface tension gradient would produce a contact angle difference.

This small difference in the withdrawal contact angles was neglected. Furthermore, the withdrawal contact angle values reported in this study were determined from measurements on the compression barrier side of the solid.

APPARENT TRANSFER RATIO FROM FILM BALANCE MEASUREMENTS

The apparent transfer ratio-pH curve of the initial layers in Ca-H-St multilayer deposition on paraffin is shown in Fig. 34. The transfer ratio of the first monolayer, ρ_1, is approximately constant at 1.03 throughout the pH range 4-9. However, the transfer ratios of the subsequent layers are only reproducible at about pH $\geq$ 6.8. The transfer ratio of the second layer, ρ_2, decreases with increasing subsolution pH from 1.03 at pH 6.8 to about 0.92 at pH 8.0. The rate of decrease is smaller above pH 8.0 with the transfer ratio decreasing to 0.88 at pH 9.0. However, the transfer ratio of the third layer, ρ_3, which is deposited during the second immersion operation is again constant at 1.03 in the pH range 6.8-9.0. The transfer ratio of the fourth layer, ρ_4, behaves similar to ρ_2 with increasing subsolution pH, but the value of ρ_4 is always less than that of ρ_2 at corresponding values of the subsolution pH > 6.8.

These results confirm the qualitative observations of Goranson and Zisman (18) that there are less film deposits during the withdrawal operation at pH 9.0 than at pH 6.3 during the initial stages of Ca-H-St multilayer deposition. In addition, the transfer ratio results at pH > 6.8 which are shown in Fig. 34 and Table VIII are also in agreement with the observation of Goranson and Zisman that the amount of film that is deposited during the withdrawal operations appears to decrease with increasing number of deposited layers.

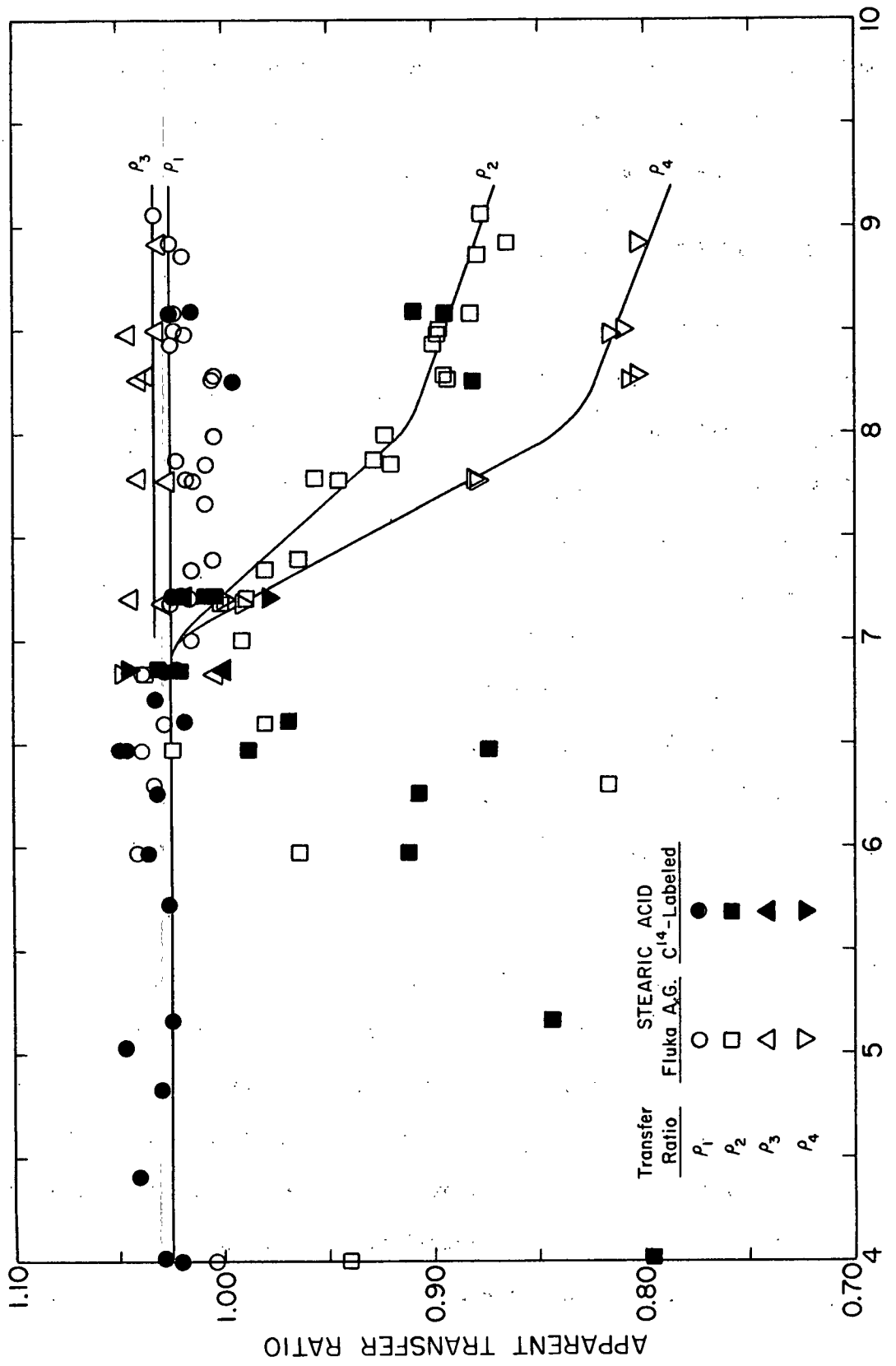

Figure 34. The Apparent Transfer Ratio-pH Curve of Ca-H-St Monolayers During the Initial Stages of Multilayer Deposition on Paraffin at 31 Dynes/cm. $\underline{T}$ = 20.4°C.

TABLE VIII

APPARENT TRANSFER RATIOS IN Ca-H-St MULTILAYER DEPOSITION ON PARAFFIN[a]

pH	Apparent Transfer Ratio					
	ρ_1	ρ_2	ρ_3	ρ_4	ρ_5	ρ_6
6.8[b]	1.03	1.02	1.00	1.03	1.00	1.02
8.3[c]	1.01	0.89	1.04	0.81	1.03	0.75
8.9[c]	1.03	0.87	1.03	0.80	1.05	0.76

[a] $\underline{\Pi}$ = 31 dynes/cm.; $\underline{T}$ = 20.3°C.

[b] C^{14}-labeled stearic acid.

[c] Stearic acid (Fluka A.G.).

It is encouraging to observe that the ρ_2 values of inactive and radioactive Ca-H-St monolayers at about pH 8.5 are in excellent agreement even though the radioactive monolayer has undergone 10-15% collapse. This affirms the validity of the technique of correcting for monolayer loss which arises from the independent molecular process of monolayer collapse. Furthermore, monolayer collapse does not influence the transfer ratio.

It is to be emphasized that the transfer ratio determined by the film balance measurements must be called an apparent transfer ratio because it has not been confirmed that the film "deposited" during multilayer deposition is, indeed, completely deposited on the solid or multilayer. But, on the contrary, a portion of the film may dissolve in the subsolution at the solid/liquid/air interface during the deposition process. Nonuniform deposition may also occur. Thirdly, the transfer ratio was calculated on the basis of the geometrical area of the solid slide, not the real area determined by the roughness ratio. If multilayer deposition is to be characterized and understood, the required quantity of interest is the real or local transfer ratio.

angle, θ_2, at the locus of spreading most likely remains obtuse. These returned molecules are available again for further deposition.

Film balance measurements and autoradiographs support the view that previously deposited molecules return to the subsolution surface at the line interface instead of dissolving at the solid/liquid interface and then adsorbing at the liquid/air interface. There is no decrease in the rate of monolayer collapse in the time interval between the immersion and withdrawal operations. Secondly, the compression barrier has occasionally been observed to retreat, instead of advancing, during deposition of the second layer; and later inspection of the autoradiographs has revealed appreciable areas where bilayer deposition has not occurred at the corresponding time when the barrier motion was reversed. In addition, a return of some of the first deposited molecules to the surface at the line interface during the withdrawal operation explains the observed decrease in ρ_2 below pH 6.8 even though the local transfer ratio may be unity.

Figure 36(a) is an electron micrograph of a Ca-H-St bilayer at pH 4.0. There are regions in the deposited film where a bilayer does not appear to be present. Shadow length measurements indicate that the thickness of the deposited film is about 50 A. This demonstrates that the first layer has been removed from the paraffin surface at these particular areas.

The return of some of the previously deposited film to the subsolution surface implies that the spreading forces are greater than the adhesive forces at only certain areas. The reason for why the spreading forces are greater than the adhesive forces at distinct regions is not understood. The roughness of the paraffin surface, even though it is minor, may have an important influence on the deposition process.

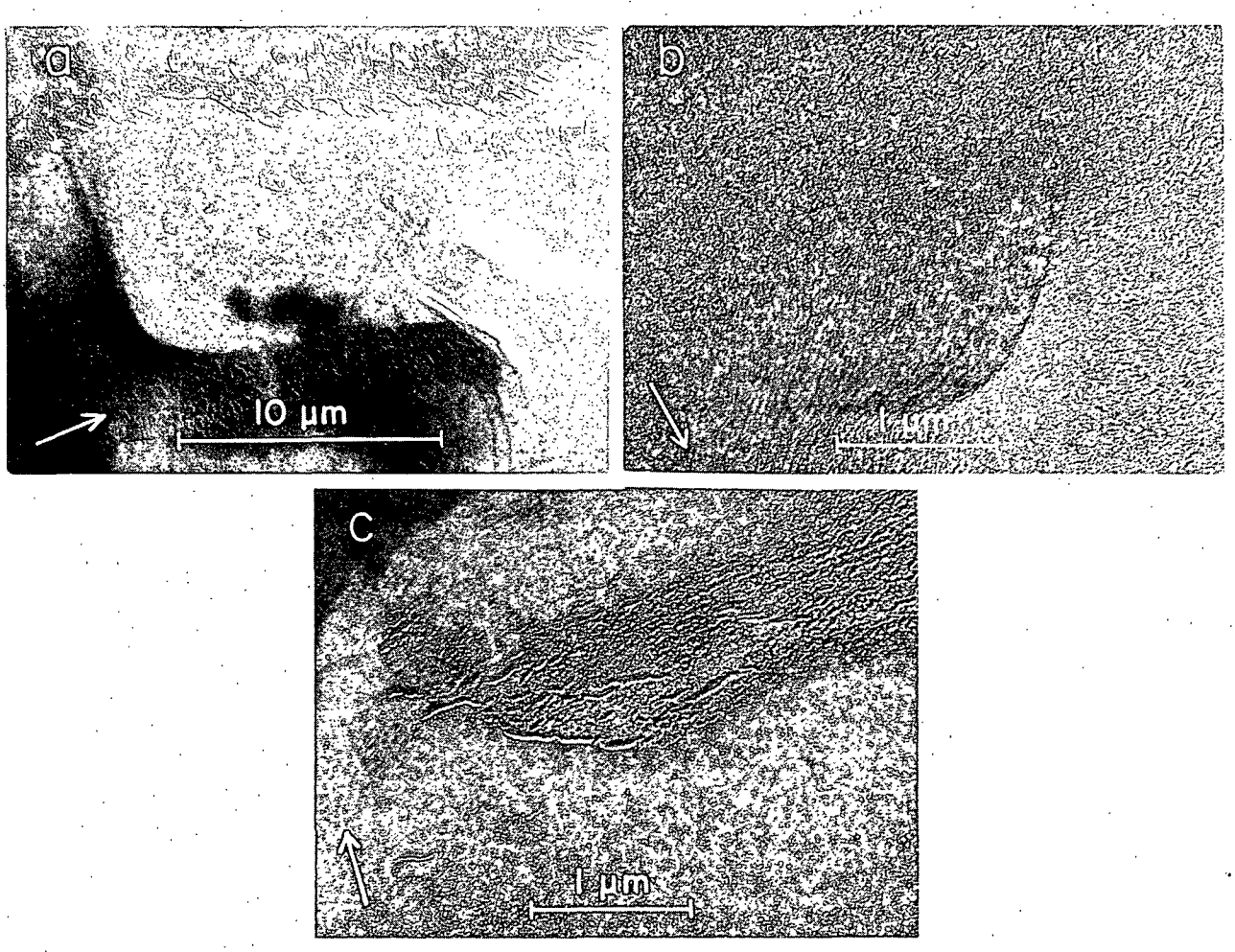

Figure 36. Electron Micrographs of Pd Preshadowed Replicas of Ca-H-St Bilayers on Rough Regions of the Paraffin at 31 Dynes/cm. at (a) pH 4.0 (3550X); (b) pH 6.0 (22,000X); and (c) pH 7.9 (21,600X)

EFFECT OF SURFACE ROUGHNESS

The electron micrographs shown in Fig. 36 demonstrate that deposition does occur on the hills and ridges of the paraffin surface. This indicates that the roughness of the paraffin surface does not significantly affect multilayer deposition.

The areas which are devoid of a deposited bilayer in Fig. 36(a) do not necessarily originate from the rough regions on the paraffin surface. Other electron micrographs show similar nondeposited areas existing on the smooth regions of the paraffin surface.

Ca-H-St monolayers containing a significant proportion of calcium stearate also deposit on the rough regions of the paraffin surface. However, occasionally there is a structural rearrangement of the type shown in Fig. 36(c).

STABILITY OF THE IMMERSED MONOLAYERS

A radiometric technique was used to determine whether the immersed molecules of the first deposited monolayer at the solid/liquid interface were stable or dissolved in the subsolution. The time that the first layer was immersed in the subsolution was varied before the second layer was deposited. The radioactivity measurements of the bilayer at different immersion times are shown in Table IX. The results of Table IX show that the local net counting rate and ρ_2 are independent of the immersion time. Consequently, this demonstrates that the deposited monolayer is stable and does not dissolve in the subsolution during its immersion.

TABLE IX

THE EFFECT OF IMMERSION TIME ON Ca-H-St BILAYER DEPOSITION[a]

pH	Immersion Time, min.[b]	Local Net Counting Rate, c.p.m.	Apparent Transfer Ratio, ρ_2
6.8	3.9	902 ± 6[c]	1.02[d]
	4.4	897 ± 6	1.02
	20.0	900 ± 4	1.02
8.5	0.1	865 ± 7	--
	3.1	864 ± 7	0.89, 0.91
	10.0	863 ± 7	--
	4.1	--	0.90[e]
	10.6	--	0.88[e]
	20.8	--	0.89[e]

[a] $\underline{\Pi}$ = 31 dynes/cm.; $\underline{T}$ = 20.5°C.
[b] Time interval between the termination of the immersion and the commencement of the withdrawal operations.
[c] 95% Confidence limits.
[d] C^{14}-labeled stearic acid.
[e] Stearic acid (Fluka A.G.).

It is to be emphasized that the values of the counting rate are local net counting rates associated with uniform film deposition. Those counting rates which corresponded to heterogeneous film behavior such as collapsed regions and voids as observed from the autoradiograph were excluded.

CALCULATED TRANSFER RATIO FROM RADIOACTIVITY MEASUREMENTS

It has been an implicit assumption in Langmuir-Blodgett multilayer deposition studies that the molecules which disappear from the subsolution surface are completely deposited on the solid during multilayer deposition. Radiometric techniques were employed to determine the validity of this assumption in order to gain insight into the mechanism of transfer. The local net counting rate-pH curve of Ca-H-St bilayers on paraffin is shown in Fig. 37. The counting rate is constant between pH 4.0 and 7.0, and then it decreases with increasing pH in a manner similar to the apparent withdrawal transfer ratios determined from the film balance measurements.

The local transfer ratio of the second layer, ρ_2, can be calculated from the local net counting rate-pH curve. The results of the film balance measurements shown in Table X suggest that the local values of ρ_1 and ρ_2 are both unity below pH 7.0 when the apparent values are corrected for the roughness ratio of the paraffin substrate. The local net counting rate is constant between pH 4.0 and 7.0; and, accordingly, it is reasonable to assume that the two layers equally contribute to the total counting rate. If half of this counting rate ($\underline{N}_1$) is subtracted from all net counting rates, the remaining counting rate ($\underline{N}_2$) is attributable to the molecules of the second layer. The ratio, $\underline{N}_2/\underline{N}_1$, is equivalent to the transfer ratio. Furthermore, this procedure tacitly assumes there is no change in the molecular packing throughout the pH range. However, the $\underline{A}_{31}$-pH curve of Fig. 19 shows there is a smaller average area/molecule above pH 6.4. The calculated local transfer ratio must be corrected for this increased molecular packing.

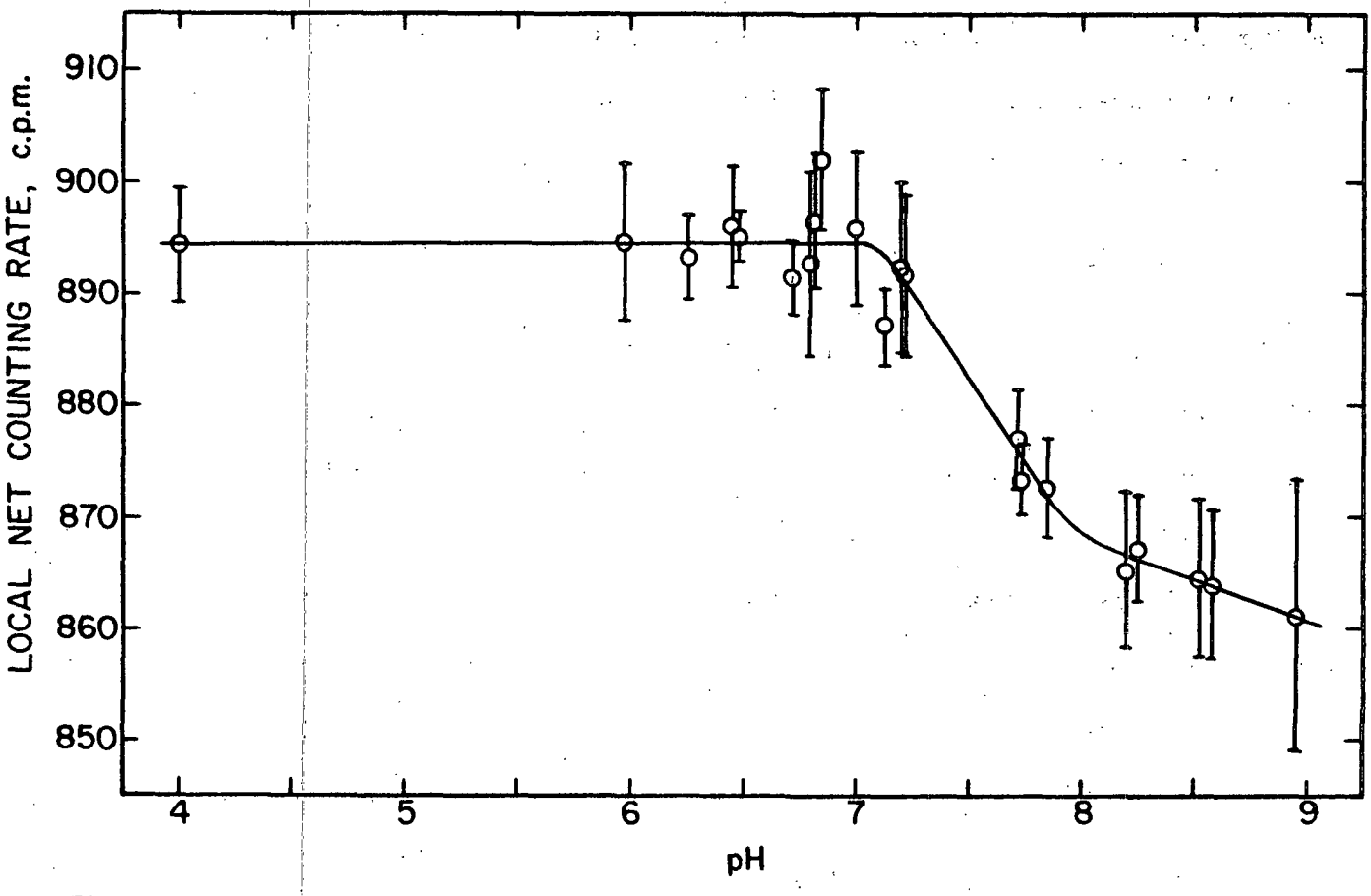

Figure 37. The Local Net Counting Rate-pH Curve of Ca-H-St Bilayers Deposited on Paraffin at 31 Dynes/cm. $\underline{T}$ = 20.4°C.

TABLE X

APPARENT TRANSFER RATIOS IN Ca-H-St MULTILAYER DEPOSITION ON PARAFFIN BELOW pH 7.0[a]

pH	Apparent Transfer Ratio ρ_1	ρ_2	ρ_3	ρ_4
3.1[b]	1.04	1.00	--	--
5.7[b]	1.03	--	0.97[c]	0.90[c]
6.5[d]	1.04	1.02	0.99	1.03
6.9[b]	1.03	1.02	1.00	1.03

[a] $\underline{II}$ = 31 dynes/cm.; $\underline{T}$ = 20.4°C.
[b] C^{14}-labeled stearic acid.
[c] The large number of voids in the autoradiograph suggest the local transfer ratio is much larger, probably unity.
[d] Stearic acid (Fluka A.G.).

Table XI compares the apparent transfer ratios determined from the film balance measurements with the calculated local transfer ratios. The roughness ratio correction was applied to the apparent transfer ratios. The calculated local transfer ratios above pH 8.0 are probably a little on the high side because it is next to impossible to eliminate all traces of monolayer collapse in the radiocounting measurements. However, there is excellent agreement between the measured apparent and calculated local transfer ratios when the molecular packing corrections are applied. This agreement is additional support that the roughness ratio of the paraffin surface is about 1.03. These results indicate that the apparent transfer ratios above pH 6.8 determined by the film balance measurements are equivalent to local values of the transfer ratio when the roughness ratio correction is employed.

TABLE XI

COMPARISON OF THE MEASURED APPARENT AND CALCULATED LOCAL TRANSFER RATIOS[a]

	Transfer Ratio, ρ_2		
		Radiometric Calculations[b]	
pH	Film Balance Measurements[c]	Constant Area/Molecule	Corrected for Area/Molecule[d]
6.8	1.00	1.00	0.99
7.2	0.98	0.99	0.95
7.7	0.92	0.96	0.92
8.2	0.88	0.94	0.89
8.6	0.87	0.93	0.89
9.0	0.86	0.93	0.88

[a] Π = 31 dynes/cm.; T = 20.4°C.
[b] Local transfer ratio calculated from the local net counting rate-pH curve.
[c] Apparent transfer ratio determined from the apparent transfer ratio-pH curve and corrected for a roughness ratio of 1.03.
[d] Area/molecule determined from the A_{3T}pH curve.

Furthermore, agreement between the measured and calculated transfer ratios indicates that the transferred film molecules are completely deposited on the solid. Thus, film molecules do not dissolve in the subsolution at the three-phase line interface during the deposition process. The withdrawal contact angles also indicate that the transfer occurs at the line interface and is not a spreading process such as that of Langmuir-Blodgett monolayer deposition when the contact angle is zero (to be shown later). But rather, the deposition mechanism during withdrawal is an adsorption process at the solid/liquid/air interface.

LOCAL TRANSFER RATIO

The measured apparent and calculated local transfer ratios collectively indicate that during the initial stages of Ca-H-St multilayer deposition on paraffin the local transfer ratio of the first and all subsequent odd-numbered layers deposited during the immersion operations is unity. The behavior of the local transfer ratio of the even-numbered layers which are deposited during the withdrawal operations is not so straightforward. Below pH 6.8, the local withdrawal transfer ratios are also unity. But above pH 6.8, ρ_2 decreases with increasing pH, becoming 0.86 at pH 9.0. With increasing number of layers, the withdrawal transfer ratios at pH > 6.8 become increasingly smaller.

WITHDRAWAL CONTACT ANGLES

Ca-H-St Bilayers

The θ_2-pH curve of Ca-H-St bilayers deposited on paraffin is shown in Fig. 38. The withdrawal contact angle, θ_2, is 78° in the pH range 2.0-4.2, decreases almost linearly to 30° at pH 6.4, then increases to 61° at pH 8.0, and finally decreases slightly to 53° at pH 9.0. Photographs of θ_2 at several characteristic values of the subsolution pH are shown in Fig. 39 as an aid in the physical interpretation of the withdrawal contact angle behavior.

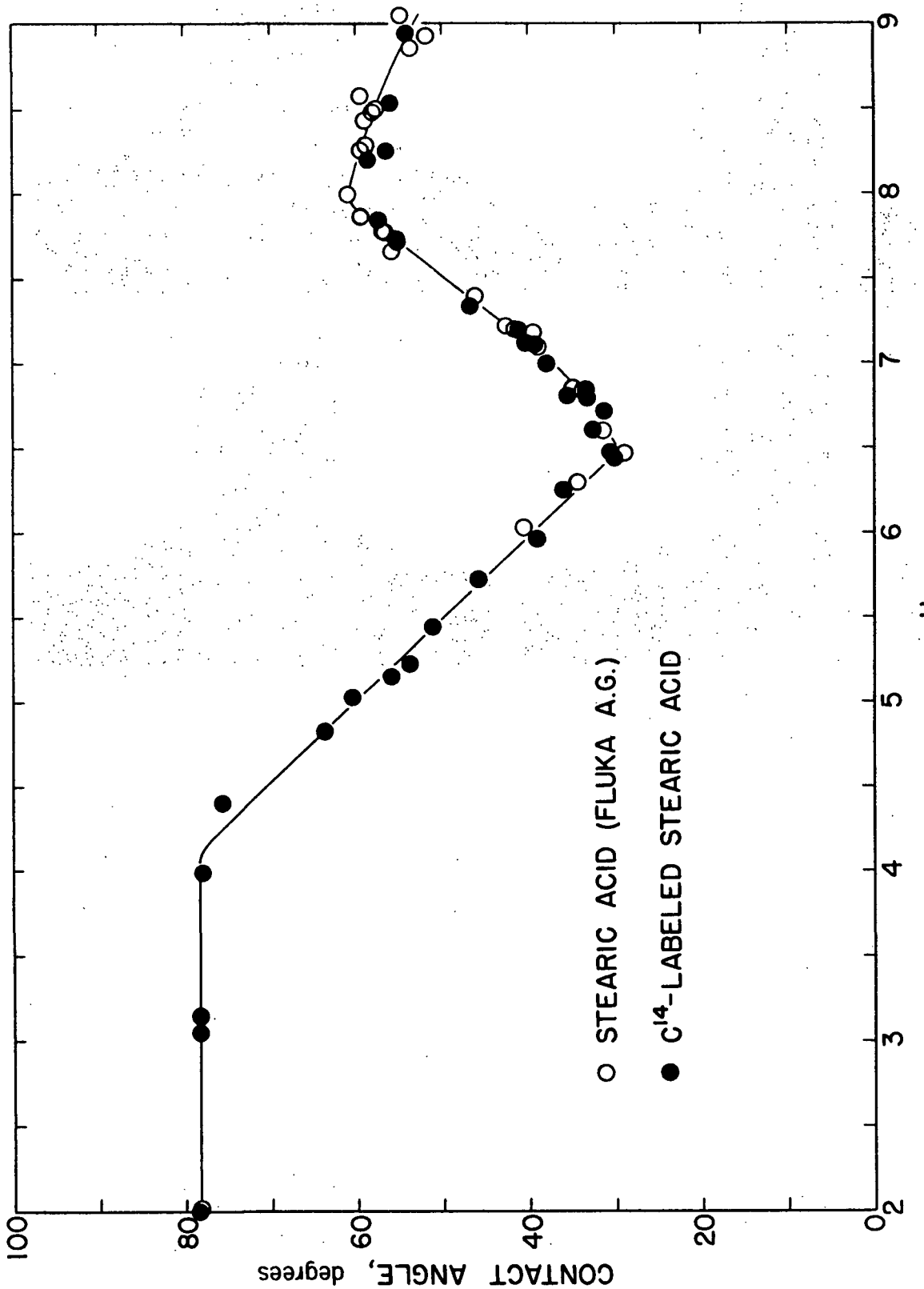

Figure 38. The θ_2-pH Curve of Ca-H-St Bilayers Deposited on Paraffin at 31 Dynes/cm. $\underline{T}$ = 20.4°C.

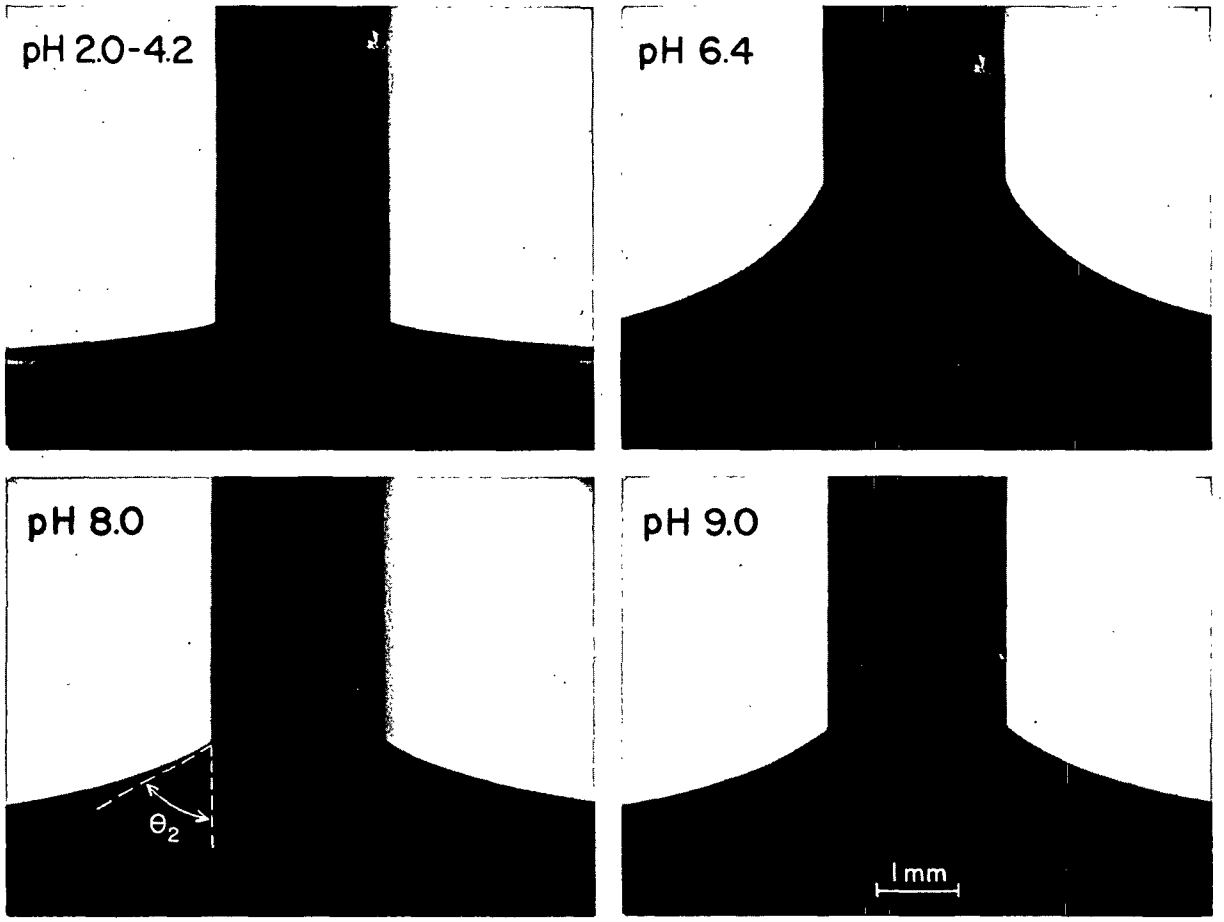

Figure 39. Photographs of θ_2 During Ca-H-St Bilayer Deposition on Paraffin at 31 Dynes/cm. $\underline{T}$ = 20.4°C.

The effect of immersion time on the withdrawal contact angle is shown in Table XII. Under the conditions that appreciable monolayer collapse does not occur, the results of Table XII show that θ_2 does not change with immersion time. Although the slide can be withdrawn "immediately," the contact angle change requires 15-30 sec. before deposition commences. Thus, any time-dependent phenomena which is capable of occurring within that short time would not be observed under the present experimental conditions.

However, Goranson and Zisman (18) observed withdrawal contact angle behavior which may be related to changes occurring in the immersed monolayer. The faster

immersion and withdrawal speeds of Goranson and Zisman were probably responsible for their detection of systematic contact angle changes along the length of the solid.

TABLE XII

THE EFFECT OF IMMERSION TIME ON THE WITHDRAWAL CONTACT ANGLE[a]

pH	Immersion Time, min.[b]	Withdrawal Contact Angle, θ_2, degrees
4.0	0.1	78.0 ± 0.7[c,d]
	3.2	78.2 ± 0.7
8.5	0.1	55.9 ± 1.1
	4.1	57.7 ± 0.2[e]
	6.3	58.1 ± 0.5[e]
	20.8	57.1 ± 0.8[e]
	21.3	58.4 ± 0.3[e]

[a] Π = 31 dynes/cm.; T = 20.4°C.
[b] Time interval between the termination of the immersion and the commencement of the withdrawal operations.
[c] 95% Confidence limits.
[d] C^{14}-labeled stearic acid.
[e] Stearic acid (Fluka A.G.).

When appreciable monolayer collapse occurs at both low and high subsolution pH, random decreases in the withdrawal contact angle are observed. Observation of the three-phase line interface during the withdrawal operation indicates that this contact angle decrease is a local phenomenon. This local and random decrease in θ_2 is ascribed to the deposition of collapsed regions of the monolayer. The reason for the contact angle decrease is not clearly understood, but it is believed to be due to the local rigidity of the collapsed region.

Ca-H-St Multilayers

The withdrawal contact angles of the first several layers in Ca-H-St multilayer deposition are given in Tables XIII and XIV. The results of Table XIII indicate that

the withdrawal contact angle of the fourth layer is the same as that of the second layer when the Ca-H-St monolayer consists of un-ionized stearic acid molecules at pH 3.2. However, Table XIII indicates that with increasing subsolution pH up to about pH 8.0 the withdrawal contact angle of the fourth layer is greater than the withdrawal contact angle of the second layer. But, above pH 8.0, the withdrawal contact angle of the fourth layer is smaller than that of the second layer. However, Table XIV shows that the withdrawal contact angles at pH > 8.0 also gradually increase with an increasing number of deposited layers, but only after the occurrence of the initial decrease in the withdrawal contact angles.

TABLE XIII

COMPARISON OF THE WITHDRAWAL CONTACT ANGLES DURING DEPOSITION OF THE SECOND AND FOURTH LAYERS[a,b]

pH	θ_2, degrees	θ_4, degrees	$\theta_4 - \theta_2$, degrees
3.2	78.3 ± 0.4[c]	77.6 ± 0.4[c]	-0.7[d]
5.7	45.9 ± 0.9	54.8 ± 0.5	+8.9[d]
6.0	40.5 ± 0.5	47.9 ± 0.5	+7.4
6.5	28.9 ± 0.4	32.5 ± 0.5	+3.6
6.9	34.8 ± 0.4	36.3 ± 0.5	+1.5
7.1	39.0 ± 0.4	42.7 ± 0.6	+3.7
7.2	42.6 ± 0.4	47.2 ± 0.6	+4.6
7.8	57.0 ± 0.2	60.5 ± 0.4	+3.5
8.3	59.3 ± 0.3	56.2 ± 0.5	-3.1
8.5	58.1 ± 0.5	53.3 ± 0.3	-4.8
8.9	51.8 ± 0.9	48.9 ± 0.5	-2.9

[a] Π = 31 dynes/cm.; T = 20.4°C.
[b] Stearic acid (Fluka A.G.).
[c] 95% Confidence limits.
[d] C^{14}-labeled stearic acid.

TABLE XIV

WITHDRAWAL CONTACT ANGLES IN Ca-H-St MULTILAYER DEPOSITION ON PARAFFIN[a]

Withdrawal Contact Angle, degrees	Subsolution pH		
	6.8[b]	8.3[c]	8.9[c]
θ_2	33.7 ± 0.4[d]	58.8 ± 0.3	51.8 ± 0.9
θ_4	34.6 ± 0.8	55.8 ± 0.6	48.9 ± 0.5
θ_6	34.6 ± 0.2	55.7 ± 0.5	50.0 ± 0.8
θ_8	--	56.8 ± 0.5	52.7 ± 0.9
θ_{10}	--	59.3 ± 1.2	52.7 ± 0.4
θ_{12}	--	--	53.8 ± 0.6

[a] $\underline{\Pi}$ = 31 dynes/cm.; $\underline{T}$ = 20.3°C.
[b] C^{14}-labeled stearic acid.
[c] Stearic acid (Fluka A.G.).
[d] 95% Confidence limits.

Stearic Acid Bilayers

The θ_2-pH curve of stearic acid bilayers deposited on paraffin is shown in Fig. 40. The withdrawal contact angle is constant at 78° in the pH range 2.0-5.5 and decreases linearly to zero degrees at pH 7.8. When the withdrawal contact angle is zero as shown in Fig. 41(a), the film emerges wetted from the subsolution; and film balance measurements indicate only a partial monolayer is deposited during the withdrawal operation. The deposition of a partial monolayer during the withdrawal operation is confirmed by the autoradiograph shown in Fig. 41(b). Consequently, it appears that multilayers cannot be built up under conditions where the withdrawal contact angle is zero degrees.

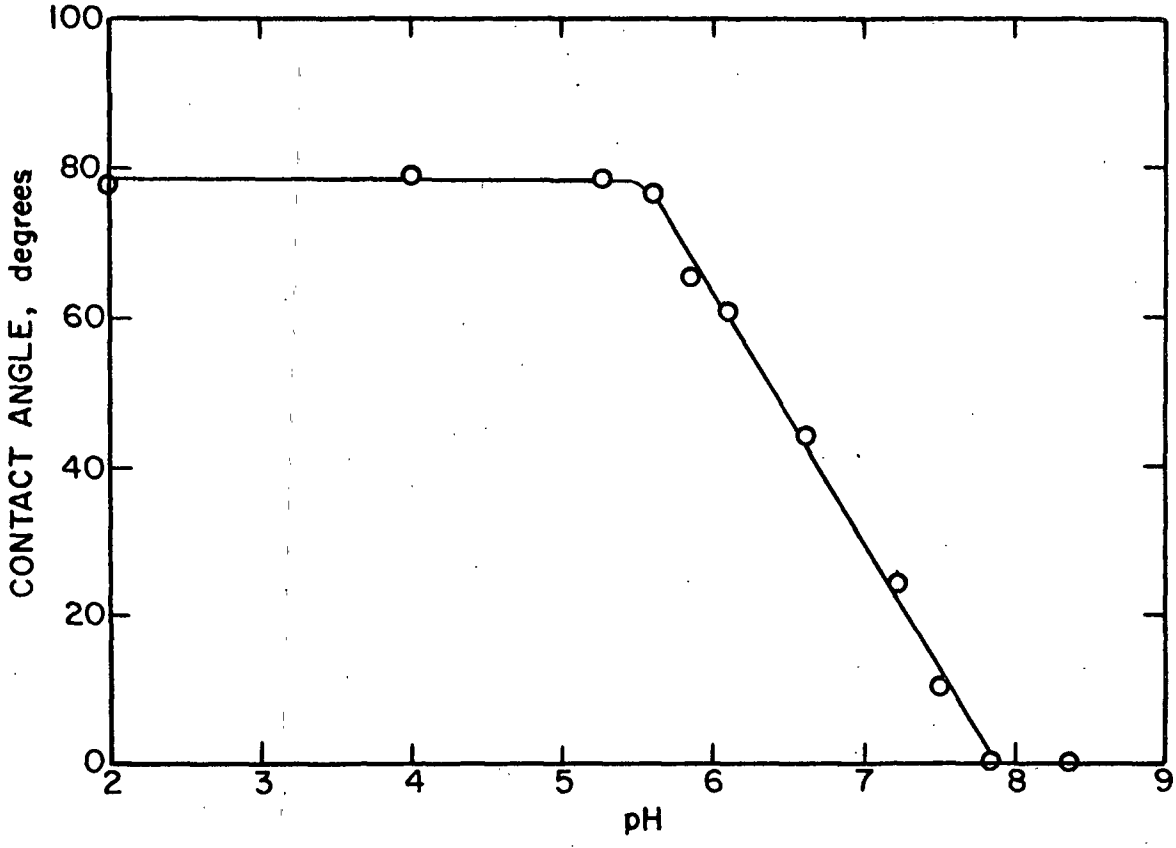

Figure 40. The θ_2-pH Curve of Stearic Acid Bilayers Deposited on Paraffin at 31 Dynes/cm. $\underline{T}$ = 20.4°C.

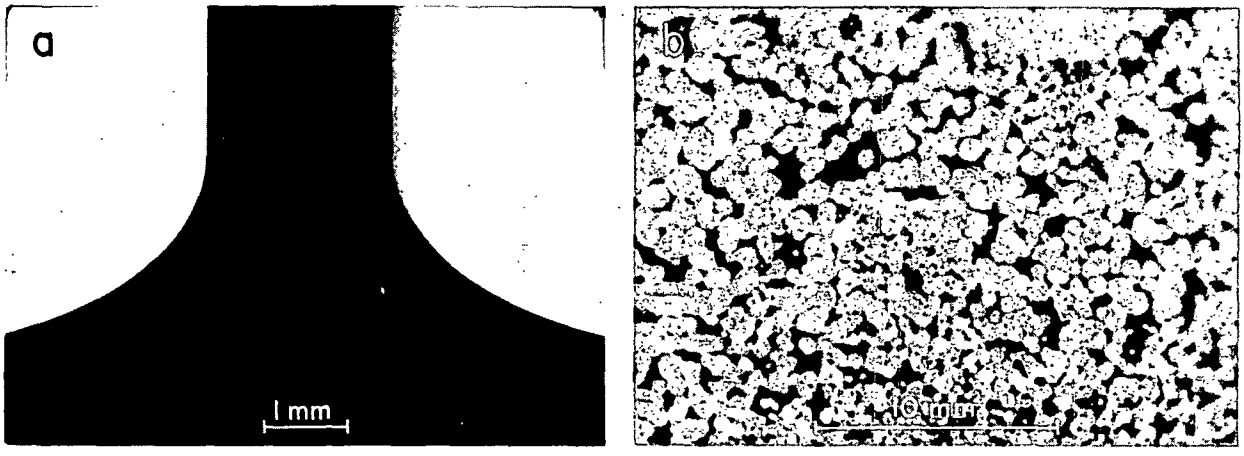

Figure 41. Stearic Acid Bilayer Deposition on Paraffin at pH > 7.8 at 31 Dynes/cm. (a) Photograph of the Zero Withdrawal Contact Angle; and (b) Autoradiograph of the Deposited Bilayer

BILAYER DEPOSITION ON POLYTETRAFLUOROETHYLENE

The withdrawal contact angles and apparent transfer ratios for Ca-H-St and stearic acid bilayer deposition on polytetrafluoroethylene substrates are given in Table XV at several values of the subsolution pH. The corresponding withdrawal contact angles on paraffin are also included in Table XV for comparison. Table XV indicates that there is a difference between the withdrawal contact angles on polytetrafluoroethylene and paraffin. The withdrawal contact angles on polytetrafluoroethylene are smaller than that on paraffin except when the Ca-H-St monolayer is predominantly calcium stearate, then the withdrawal contact angle is greater on polytetrafluoroethylene.

TABLE XV

Ca-H-St BILAYER DEPOSITION ON POLYTETRAFLUOROETHYLENE[a]

Subsolution pH	Withdrawal Contact Angle, θ_2, degrees		Apparent Transfer Ratio	
	Polytetrafluoroethylene	Paraffin[b]	ρ_1[c]	ρ_2
2.1	63.2 ± 0.7[d]	78.3	0.99	0.86
5.5	39.7 ± 0.8	49.7	1.02	0.96
8.4	74.7 ± 2.3	58.0	--	--
6.0[e]	48.2 ± 1.5	62.3	1.03	--

[a] $\underline{II}$ = 31 dynes/cm.; $\underline{T}$ = 20.5°C.

[b] Determined from the θ_2-pH curve.

[c] Preliminary measurements indicated ρ_1 is unity throughout pH range.

[d] 95% Confidence limits.

[e] $CaCl_2$ not added to subsolution.

The apparent transfer ratio of the first layer is slightly greater than unity. The roughness ratio of the polytetrafluoroethylene is presumed to be very close to unity because the surfaces were heat-cast against smooth glass plates. Thus, the

local transfer ratio of the first layer, ρ_1, appears to be unity as is the case for bilayer deposition on paraffin substrates.

CONTACT ANGLES ON BILAYERS

The contact angles of water and glycerol were measured on Ca-H-St bilayers deposited on paraffin at pH 6.7 and 8.5 immediately after deposition. The results given in Table XVI show that the contact angles on a Ca-H-St bilayer at pH 8.5 are only very slightly larger, if at all, than those on the bilayer at pH 6.7.

TABLE XVI

CONTACT ANGLES ON Ca-H-St BILAYERS DEPOSITED ON PARAFFIN[a]

Subsolution pH	Contact Angle, degrees	
	Water	Glycerol
6.7	101.0 ± 0.8[b]	91.9 ± 1.0
8.5	102.9 ± 0.9	92.6 ± 0.6

[a] $\underline{T}$ = 22°C.

[b] 95% Confidence limits.

STRUCTURE OF DEPOSITED MONOLAYERS AND MULTILAYERS

The structure of deposited Ca-H-St monolayers and multilayers was examined by electron microscopy with a variety of replication techniques in order to shed insight into the Ca-H-St monolayer structure at the liquid/air interface.

EFFECT OF EVAPORANT

It is generally acknowledged (109, 110) that during shadow-casting the thermal radiation from the source may seriously damage labile specimens. However, it appears that this consideration has not received sufficient attention in past electron microscopic studies of monolayers and multilayers because the melting

behavior of surface phases is known to deviate from that of the bulk phase. Beischer (111) has shown that the two-dimensional lattice of a stearic acid monolayer becomes unstable well below its normal melting point of 69.6°C. Therefore, temperature rise of the monolayer specimen during shadow-casting must be minimized.

The effect of palladium and platinum shadow-casting using conventional techniques on the paraffin substrates of the multilayer deposition studies was investigated. Electron micrographs of the Pd and Pt preshadowed replicas of the paraffin substrate are shown in Fig. 42(a) and 42(b), respectively. All electron micrographs are positive prints with the shadows appearing dark. The direction of shadow-casting is indicated by the arrows. The IPC plate numbers of the electron micrographs are presented in Appendix IV. The granularity observed in Fig. 42(a) is due to the Pd metal, and the paraffin surface appears uniformly smooth. However, even though a heat shield with a 1/4-inch aperture was used to minimize heat effects, the paraffin surface appears to have been disrupted during the Pt shadow-casting. Paraffin appears to have evaporated from the substrate surface as a result of the greater radiant energy emanating from the Pt source. The vaporization temperature at 1 Newton/m.^{2} (10^{-2} torr) are 1566 and 2090°C. for Pd and Pt, respectively (110).

It may be argued that Pd shadow-casting also damages the paraffin surface, but the disrupted surface is masked by the known increased granularity and thicker films of the Pd metal used in shadow-casting. The paraffin substrate was given a pretreatment simulating the vacuum and radiant heat effects of Pt shadow-casting before the specimen was shadow-cast with Pd. Experimentally, the simulation was effected by pumping down to the proper vacuum (10^{-5} torr), heating the Pt up to the point just before evaporation occurs, and finally breaking the vacuum. The results of Fig. 42(c) indicate the Pd metal does not mask the surface disruptions caused by the radiant energy associated with the Pt source. Consequently, Pd shadow-casting does not appear to significantly damage the paraffin substrate.

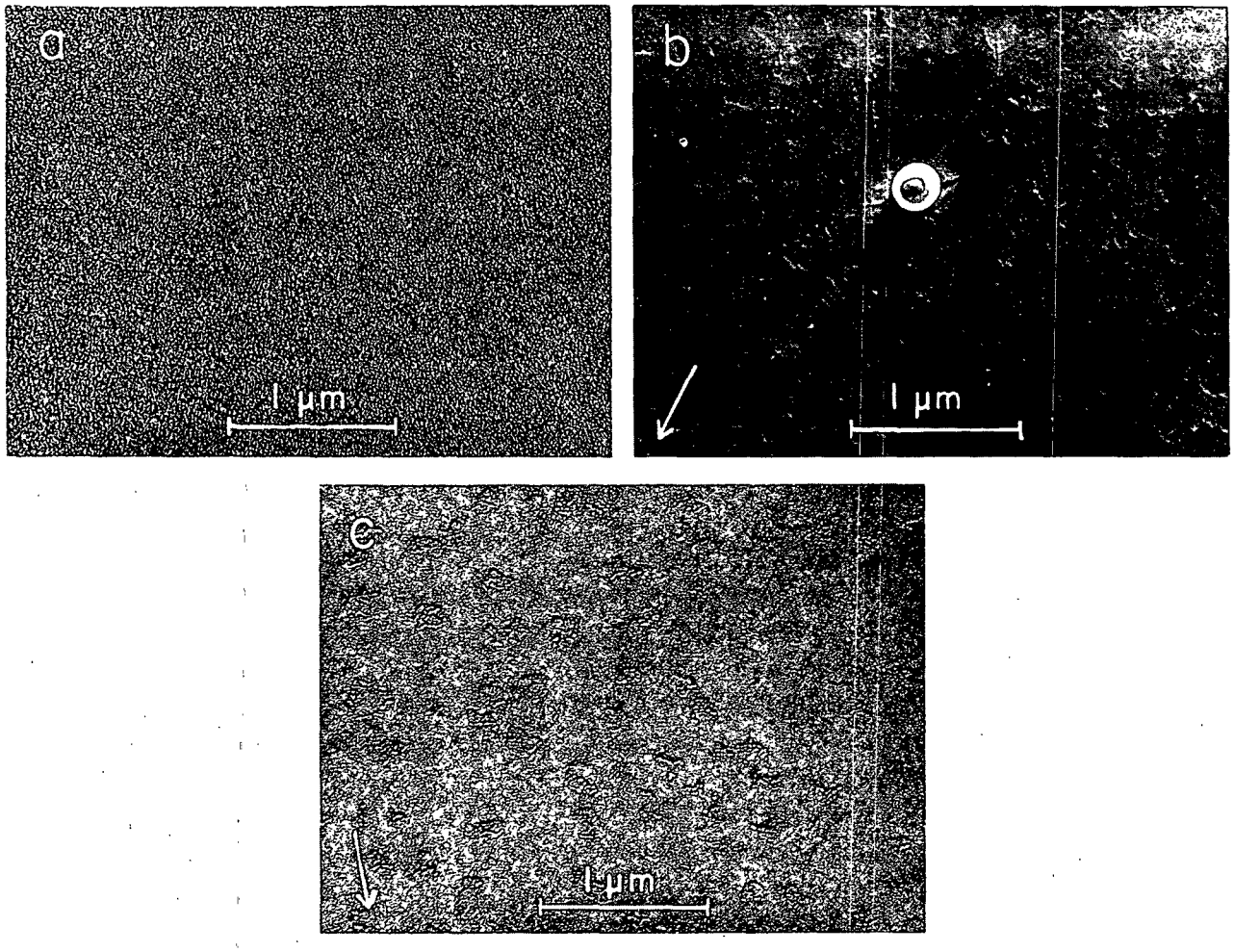

Figure 42. Electron Micrographs of the Paraffin Substrate (a) Shadow-Cast with Pd (23,100X), (b) Shadow-Cast with Pt and Showing a Polystyrene Latex Particle on Surface (21,600X), and (c) Pretreated by Simulating Pt Shadow-Casting Before the Sample was Shadow-Cast with Pd (23,100X)

The previous three shadow-casting treatments were applied to Ca-H-St bilayers deposited on paraffin at pH 6.8. The results of the shadow-casting treatments are shown in Fig. 43. The disrupting effect of Pt shadow-casting is again evident.

Some of the monolayer is lost by evaporation during the shadow-casting process because it is known (112-115) that deposited monolayers and multilayers undergo desorption in vacuum. The stabilities of the Ca-H-St bilayers at pH 6.8 to the vacuum and heat conditions simulating those of Pd and Pt shadow-casting were

determined by measuring the radioactivity of sample specimens before and after these treatments. The bilayer losses due to the simulated Pd and Pt shadow-casting processes are 7 and 8%, respectively. The increased loss in Pt shadow-casting is due to either the increased radiant energy associated with the Pt source or the longer exposure time to vacuum. Although the bilayer losses are comparable, Pt shadow-casting appears to rearrange or disrupt the bilayer structure.

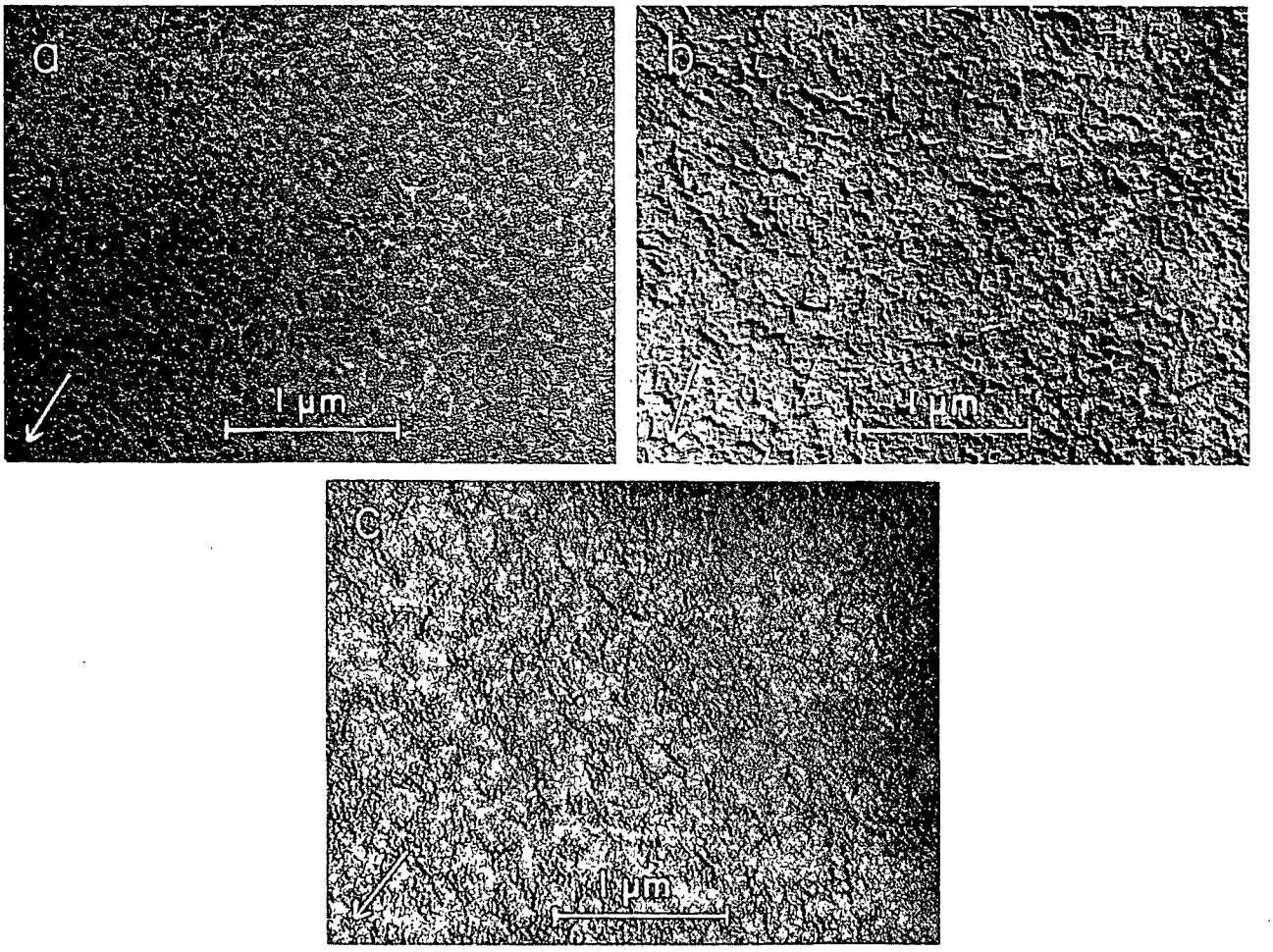

Figure 43. Electron Micrographs of a Ca-H-St Bilayer Deposited on Paraffin at pH 6.8 and 31 Dynes/cm. (a) Shadow-Cast with Pd (23,100X), (b) Shadow-Cast with Pt (23,100X), and (c) Pretreated by Simulating Pt Shadow-Casting Before the Sample was Shadow-Cast with Pd (23,100X)

Although Pt is the preferred evaporant for shadow-casting because it is highly opaque to the electron beam and provides a finer grain when evaporated than the other heavy metals, Pt shadowing is likely to disrupt or restructure monolayers and multilayers unless precautions are taken to minimize the radiant energy from the source. It is recommended that further electron microscopic studies of deposited monolayers use a shuttered aperture and low temperature techniques to minimize the radiant energy effects. Pd shadow-casting appears to do minimal damage to the basic structural features of the deposited monolayers and multilayers. However, some structural details may be lost by Pd shadow-casting.

BILAYERS ON PARAFFIN

The electron micrographs of the Ca-H-St bilayers deposited on paraffin in the pH range 2-9 are shown in Fig. 44. The same bilayer structures were observed with either inactive or C^{14}-labeled Ca-H-St monolayers. Molecular aggregates of stearic acid having a diameter in the order of 200 A. and a height of about 50 A. tapering off to the bilayer are present on the uniform background structure of the bilayers in the pH range 2.0-4.0. The background structure of the bilayer now has a general striped appearance between pH 5.5 and 6.6. There is a transition at pH 6.8 such that the background structure of the bilayers in the pH range 7.4-8.9 becomes uniform again. Molecular aggregates of calcium stearate resembling strands of beads are often superimposed upon the background of the bilayers in the pH range 8.5-9.1.

BILAYER STABILITY

Successful interpretation of the electron micrographs requires knowledge of the stability of the bilayers. The stabilities of the Ca-H-St bilayers to simulated Pd shadow-casting conditions and dry air are shown in Table XVII. The data obtained during the determination of the stability of the bilayers to dry air are presented in Appendix III. It is apparent that the bilayers are fairly stable.

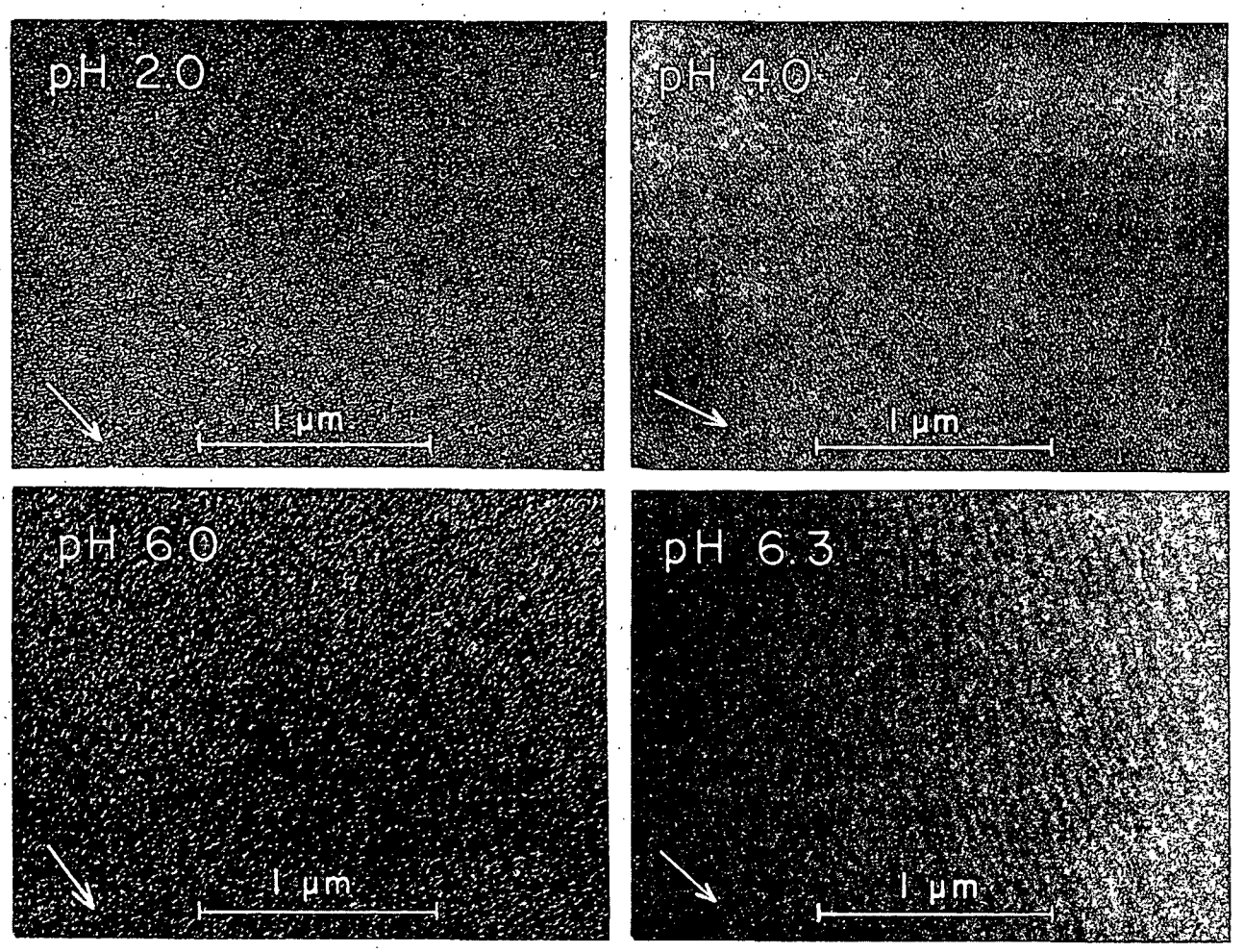

Figure 44. Electron Micrographs of Pd Preshadowed Replicas of Ca-H-St Bilayers Deposited on Paraffin at 31 Dynes/cm. (33,000X)

TABLE XVII

STABILITY OF Ca-H-St BILAYERS TO Pd SHADOW-CASTING AND DRY AIR

	Bilayer Loss, %		
		Dry Air[b]	
pH	Shadow-Casting Conditions[a]	2 Days	5 Days
4.0	3	2	10
6.1	4	4	10
8.4	2	2	4

[a] 5 Min. rough pumping down to 50×10^{-3} torr; then 4 min. to 2×10^{-5} torr with the diffusion pump; held at maximum vacuum for 1 min. while a bare tungsten filament was heated for 30 sec.; then atmospheric pressure was attained in 2 min. after the vacuum was released.

[b] Stored in grease-free pyrex desiccator over Drierite.

Careful examination of the Pd shadow-cast monolayer shown in Fig. 48(b) also reveals the presence of larger holes (encircled areas) in the monolayer. However, microholes cannot conclusively be detected because the granularity and texture of the Pd film on the monolayer-covered collodion apparently masks their presence.

The stability of a stearic acid monolayer on a collodion substrate was determined by radioactivity measurements before and after simulated Pd shadow-casting conditions. Approximately 50% of the stearic acid monolayer (range 44-59%) is lost during the simulated Pd shadow-casting procedure. Therefore, deposited monolayers on collodion are very unstable during replication in contrast to stearic acid monolayers deposited on mica. Spink (55) demonstrated that only about 5% of the stearic acid monolayer deposited on mica was lost during preparation of the replicas.

The transfer ratio is unity as shown by Table VI; and consequently, the microholes appear to occur as a result of evaporation during the shadow-casting procedure. The uniformity of the size of the microholes suggests the possibility of a fundamental structural unit in the deposited Ca-H-St monolayer. This characteristic grouping of the molecules, called a micelle, appears to be about 50 A. in diameter and 25 A. or one molecule in height. The calcium stearate aggregates which are present on the deposited bilayers above pH 8.5 are also about 50 A. in diameter, but 50 A. in height. Because the aggregates are often observed to separate into two smaller structural units each about 50 A. in diameter, the aggregates are suggested to consist of two micelles associating together. The calcium stearate aggregates will now be called paired micelles.

EFFECT OF SHADOW-CASTING ON DEPOSITED MULTILAYERS

The effects of various shadow-casting procedures on Ca-H-St bilayers deposited on paraffin at pH $\geq$ 8.3 are shown in Fig. 49. The calcium stearate paired micelles

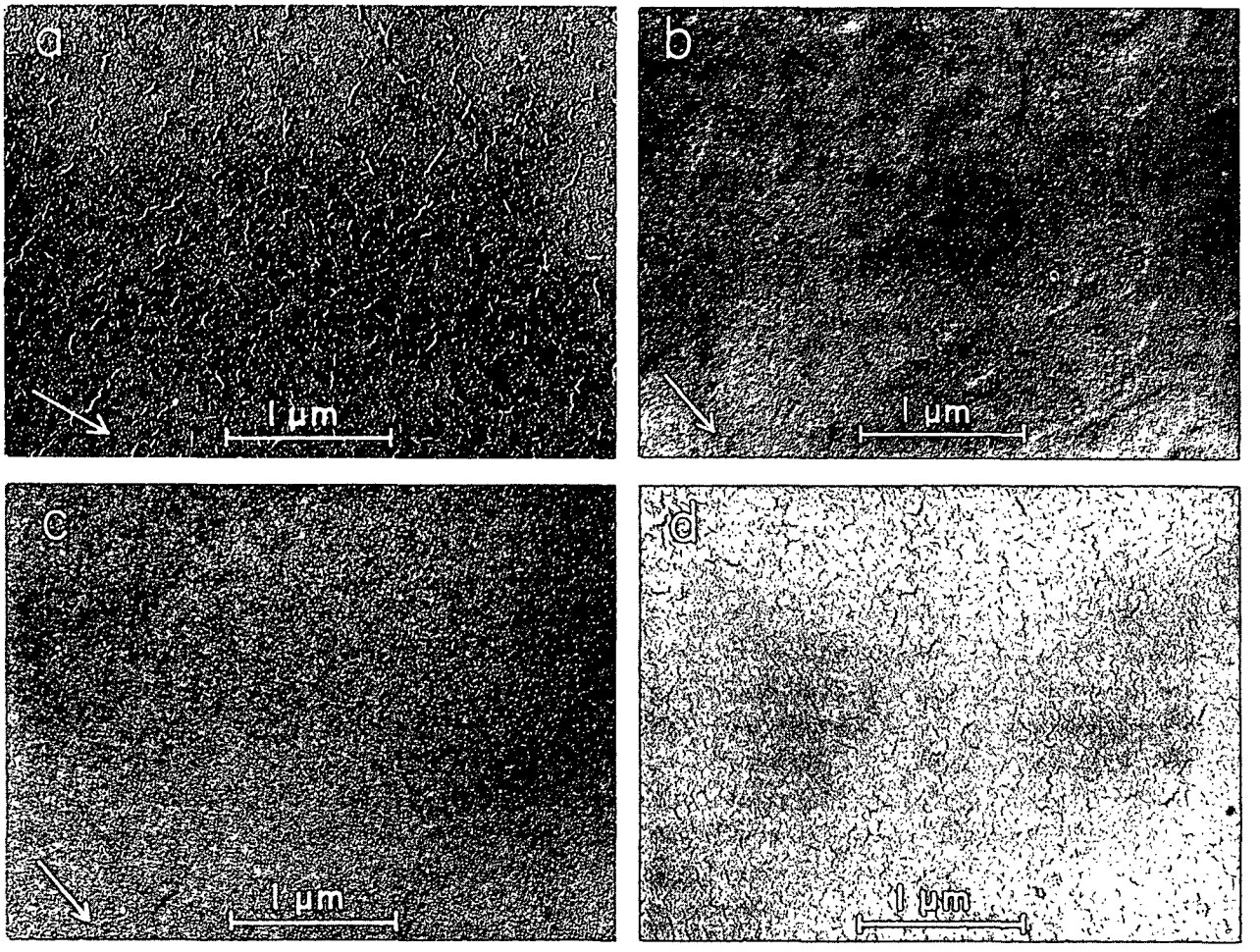

Figure 49. Electron Micrographs of Ca-H-St Bilayers Deposited on Paraffin at 31 Dynes/cm. (a) pH 8.9, Shadow-Cast with Pd (22,000X); (b) pH 8.9, Shadow-Cast with Pt (21,800X); (c) pH 8.3, Pre-treated by Simulating Pt Shadow-Casting Before the Sample was Shadow-Cast with Pd (21,800X); and (d) pH 8.6, Shadow-Cast with Chromium (21,600X)

are present in Fig. 49(a) when the Ca-H-St bilayer is shadow-cast with Pd. However, Fig. 49(b) shows that Pt shadow-casting apparently evaporates the paired micelles and some of the micelles and paired micelles within the bilayer as evidenced by the numerous microholes. In addition to the individual microholes which are about 50-60 A. in diameter, paired microholes are also present in the Ca-H-St bilayer. The microholes are also present in Fig. 49(c) whereas they do not appear to be present in the bilayers conventionally shadow-cast with Pd. If microholes are present within the

bilayer structure, Fig. 49(c) indicates that the microholes would be observed and not masked by the Pd film. Thus, the microholes appear to occur as a result of either evaporation or possibly a restructuring within the bilayer during Pt shadow-casting. But because the microholes which are present in the Pt preshadowed replicas of Ca-H-St monolayers on collodion must occur by evaporation, the microholes in the multilayers are also believed to occur primarily by evaporation of either the micelles or paired micelles during the Pt shadow-casting procedure.

The bilayer was shadow-cast with chromium (Cr) because Cr has a lower vaporization temperature than Pd. The vaporization temperatures at 1 Newton/m.^{2} of Cr and Pd are 1205 and 1566°C., respectively (110). Comparison of the chromium results shown in Fig. 49(d) with that of the Pd results suggests that paired micelles are possibly present in the Cr preshadowed replica from the appearance of the apparent shadows. It may be argued that the dark regions are not shadows, but are breaks in the Cr film, because the general appearance of the replica apparently shows no paired micelles capable of causing the shadows. However, close examination indicates that in some instances there is the suggested appearance of paired micelles in front of the apparent shadows. There appears to be insufficient contrast to show clearly the existence of the paired micelles, possibly as a result of too thin a film of Cr metal. Figure 50 shows electron micrographs comparing Ca-H-St trilayers deposited on mica at pH 8.3 and which have been Pd and Pt shadow-cast. Microholes and paired microholes are present when Pt shadow-casting is employed. Measurements of the microholes again show them to be about 50-60 A. in diameter.

Figure 51 shows a large hole in the Ca-H-St trilayer. Measurements of the shadow length give a depth of about 50 A. The appearance of the edge of the hole in Fig. 51(a) suggests it is lined with particles. The beaded appearance was further enhanced when an electron micrograph was obtained at a defocus of -2500 A.

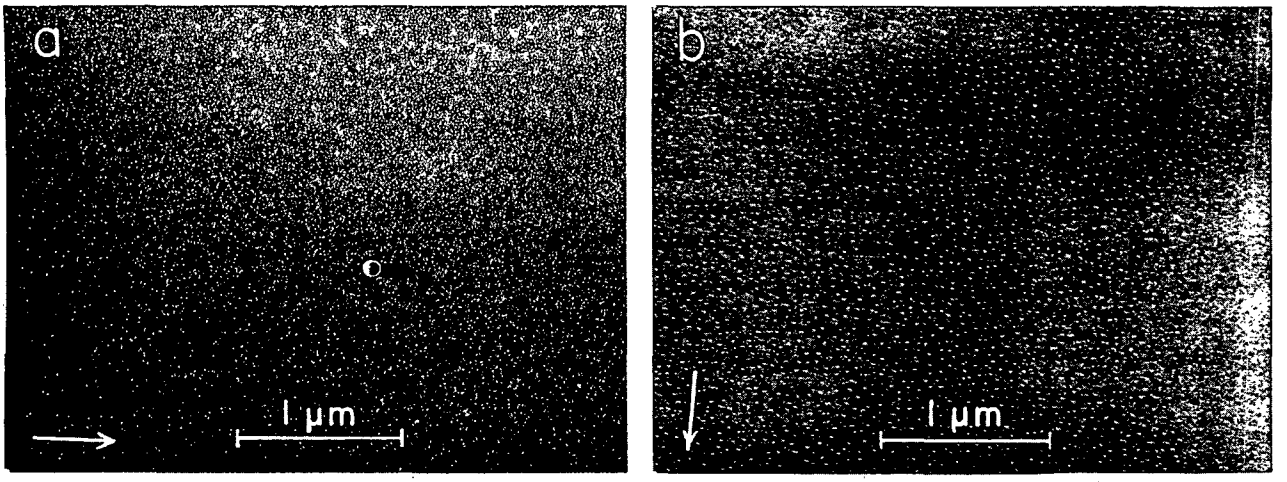

Figure 50. Electron Micrographs of Ca-H-St Trilayers Deposited on Mica at pH 8.3 and 31 Dynes/cm. (a) Shadow-Cast with Pd and Showing Polystyrene Latex Particle on Surface (21,600X); and (b) Shadow-Cast with Pt (21,600X)

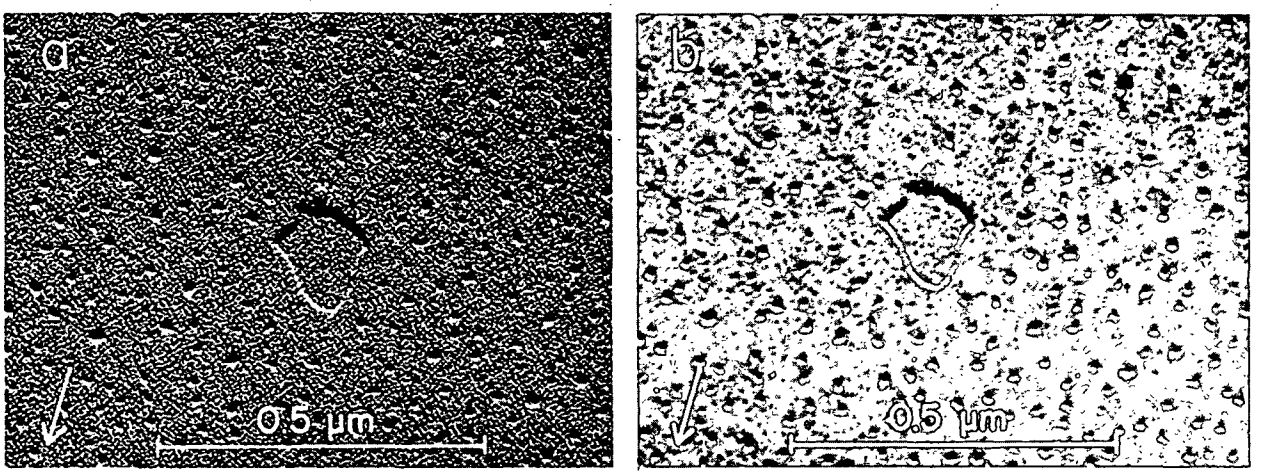

Figure 51. Electron Micrographs of a Pt Preshadowed Replica of a Large Hole in a Ca-H-St Trilayer Deposited on Mica at pH 8.3 and 31 Dynes/cm. (a) Near Focus (86,400X); and (b) 2500 A. Underfocused (86,400X)

as shown in Fig. 51(b). Similar effects due to underfocusing are known (117). Accurate measurements at the "at focus" condition are most difficult to obtain. However, it is estimated that the width of the "beads" is of the order of 60 A. Thus, it appears that calcium stearate paired micelles line the boundary of the hole.

CARBON REPLICAS OF DEPOSITED BILAYERS

Electron micrographs of unshadowed carbon replicas of Ca-H-St bilayers deposited on paraffin at pH 2.0 and 9.0 were obtained. Unshadowed carbon replicas should be transparent to the electron beam, and the electron micrographs should appear as the blank paraffin having no deposited film shown in Fig. 52(a). The Ca-H-St bilayer at pH 2.0 shown in Fig. 52(b) gives the expected result. However, the Ca-H-St bilayer at pH 9.0 shown in Fig. 52(c) consists of many electron dense (white) circular regions which have a diameter of about 50-60 A. The electron micrograph of Fig. 52(c) was enlarged to a magnification of 56,700 diameters in order to show the effect more clearly.

The diameter measurements suggest that the electron dense regions correspond to the calcium stearate paired micelles. The electron density apparently arises from the calcium ion arrangement in the paired micelle. The presence of the electron dense regions then suggests that the Ca-H-St bilayer is embedded in the carbon replica.

ELECTRON PROBE MICROANALYSIS OF THE REPLICAS

Pd preshadowed replica of a Ca-H-St bilayer deposited on paraffin at pH 9.1 was analyzed for calcium by electron probe microanalysis. The results are shown in Fig. 53. Spectrum 1 is from a blank graphite holder while Spectrum 2 is from the Pd preshadowed replica on a nickel grid mounted with silver colloidal paint

to a graphite holder. The presence of the calcium Kα peak at 3.71 keV. in the spectrum of the replica is evident; however, its intensity has been attenuated by the presence of the Pd film which strongly absorbs calcium Kα radiation.

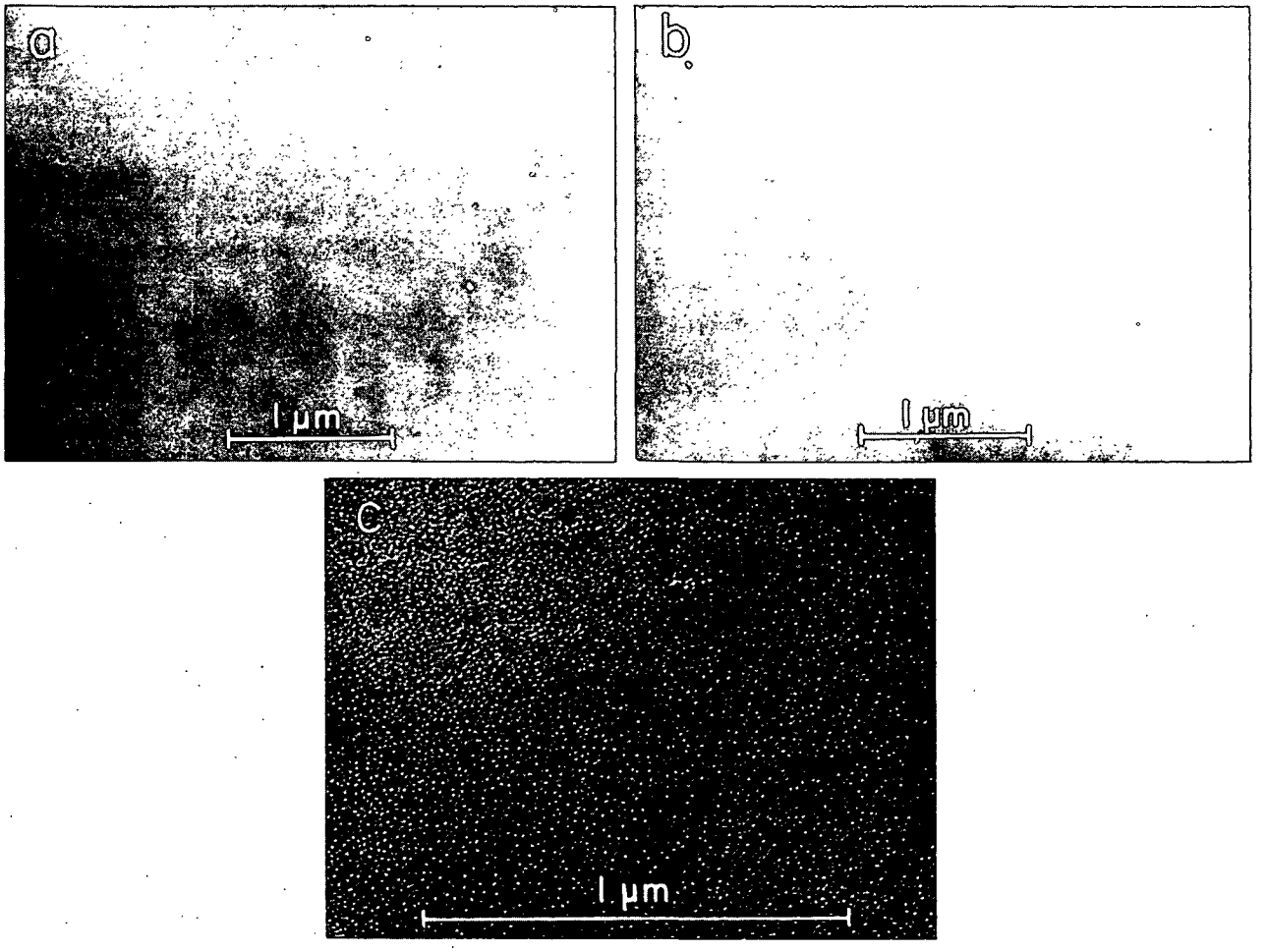

Figure 52. Electron Micrographs of Carbon Replicas of (a) Paraffin Substrate (21,800X); (b) Ca-H-St Bilayer Deposited on Paraffin at pH 2.0 and 31 Dynes/cm. (21,600X); and (c) Ca-H-St Bilayer Deposited on Paraffin at pH 9.0 and 31 Dynes/cm. (56,700X)

The maximum possible concentration of calcium in the replica was only 6×10^{-16} g./μm.^{2} Even though this calcium concentration is near the limit of detectability, the presence of calcium in the replica is established. Thus, the calcium stearate bilayer is embedded in the Pd preshadowed replica. The electron dense regions in the carbon replica then are due to the embedded calcium stearate bilayers.

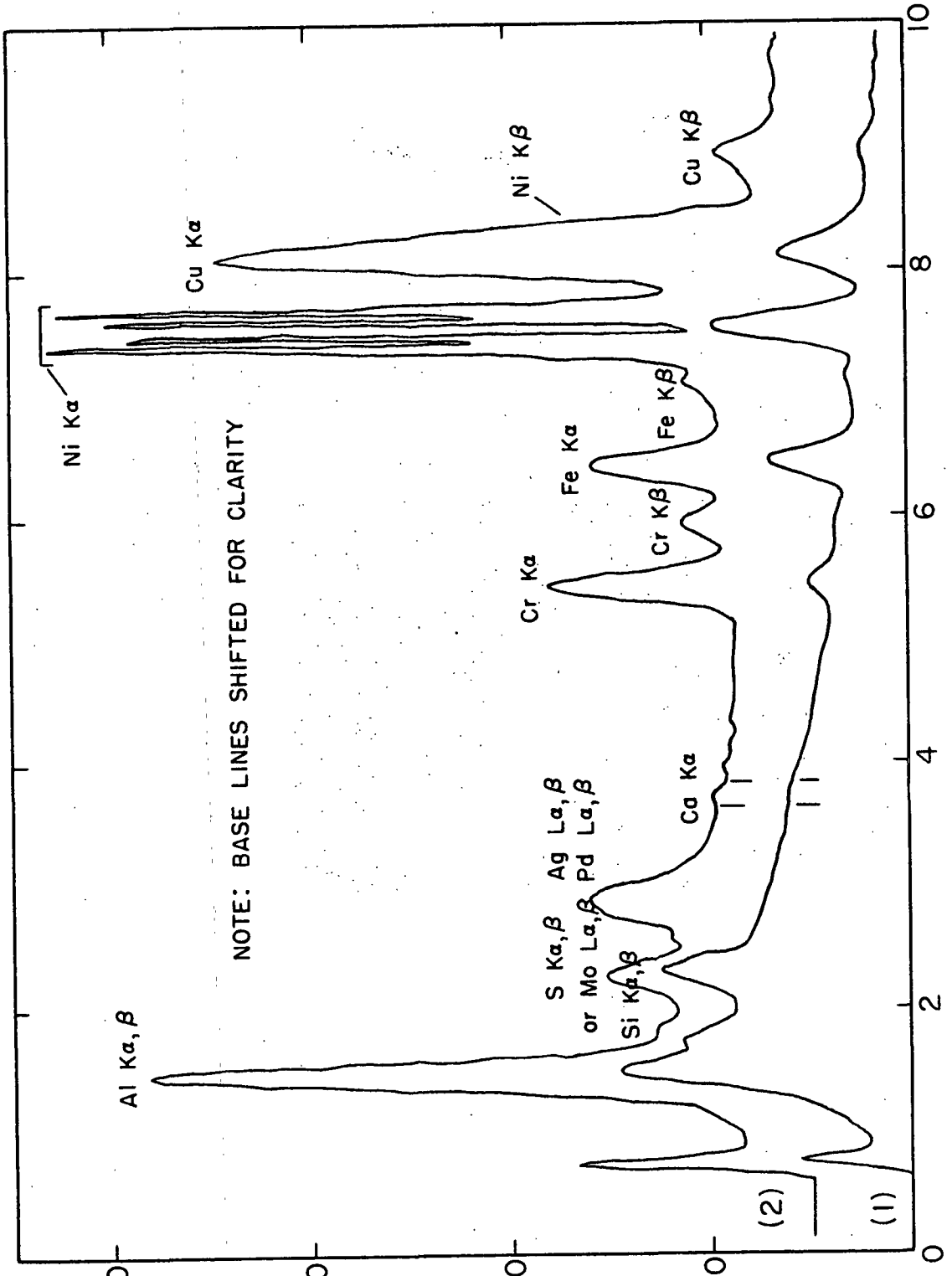

Figure 53. X-ray Spectra of a (1) Blank Graphite Holder; and (2) Pd Preshadowed Replica of a Ca-H-St Bilayer Deposited on Paraffin at pH 9.1 and 31 Dynes/cm. The Replica on a Nickel Grid was Mounted to the Graphite Holder with Silver Colloidal Paint

CARBON REPLICAS OF DEPOSITED MONOLAYERS

The electron micrographs of unshadowed carbon replicas of Ca-H-St monolayers deposited on mica are shown in Fig. 54. Figure 54(d) shows that the Ca-H-St monolayer at pH 8.6 gives electron dense regions similar to those of the Ca-H-St bilayer on paraffin at pH 9.0. However, these electron dense regions are absent at pH 2.1 and 6.2.

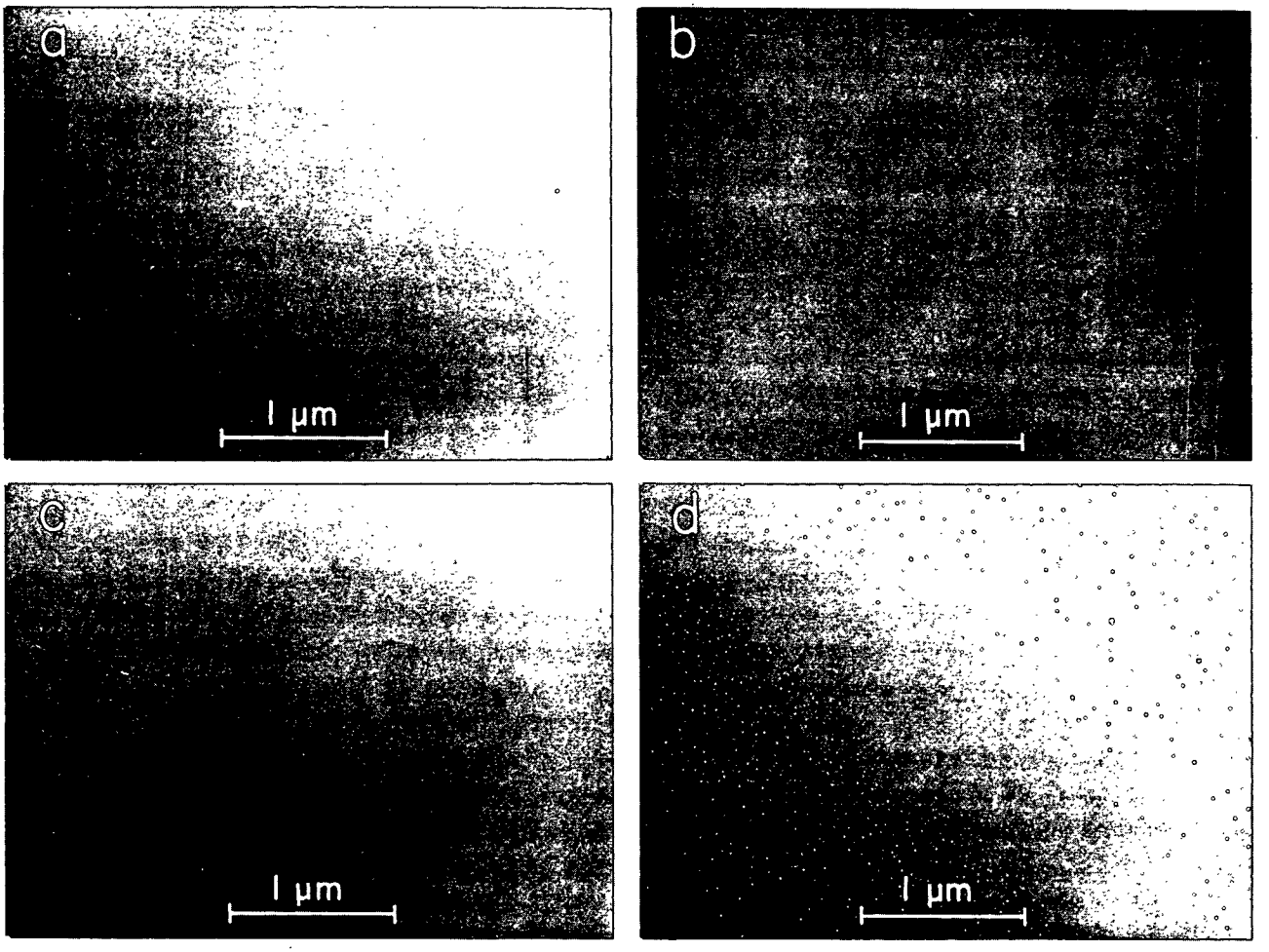

Figure 54. Electron Micrographs of Carbon Replicas of (a) Mica Substrate; and Ca-H-St Monolayers Deposited on Mica at (b) pH 2.1, (c) pH 6.2, and (d) pH 8.6 at 31 Dynes/cm. (21,600X)

Measurements show that the electron dense regions are present in two diameters of about 60 and 120 A. The regions which are about 60 A. in diameter are assumed to correspond to the calcium stearate micelles. In addition, the regions which are about 60 A. in diameter appear to have two different electron densities, the higher electron density also corresponds to that of the larger region which is about 120 A. in diameter. One interpretation of the two diameters and the two electron densities is that the high vaporization temperature during carbon replication causes part of the calcium stearate micelles to evaporate and other micelles to restructure into paired micelles and larger diameter aggregates. The vaporization temperature of carbon at 1 Newton/m.^{2} is higher than even Pt (2090°C.) and is 2681°C. (110).

If the calcium stearate molecules exist as calcium stearate micelles at pH 6.2, then electron dense regions should also appear in the carbon replica of the Ca-H-St monolayer at pH 6.2. However, electron dense regions do not appear in the carbon replica at pH 6.2. Either the calcium stearate molecules do not exist in the micelle form at pH 6.2 or the calcium stearate micelles did not embed in the carbon replica at pH 6.2.

The carbon replicas of the Ca-H-St monolayers at pH 6.2 and 8.6 were analyzed for calcium by electron probe microanalysis. The results are presented in Fig. 55. Spectrum 3 clearly indicates that calcium is present in the carbon replica of the Ca-H-St monolayer at pH 8.6 because of the existence of the calcium Kα peak at 3.68 keV. But Spectrum 2 indicates that calcium is "not present" in the carbon replica of the Ca-H-St monolayer at pH 6.2.

The reason that calcium was not present in the carbon replica is probably that the calcium concentration at pH 6.2 was below the limits of detectability. An alternative explanation is that the calcium stearate is not embedded, for some

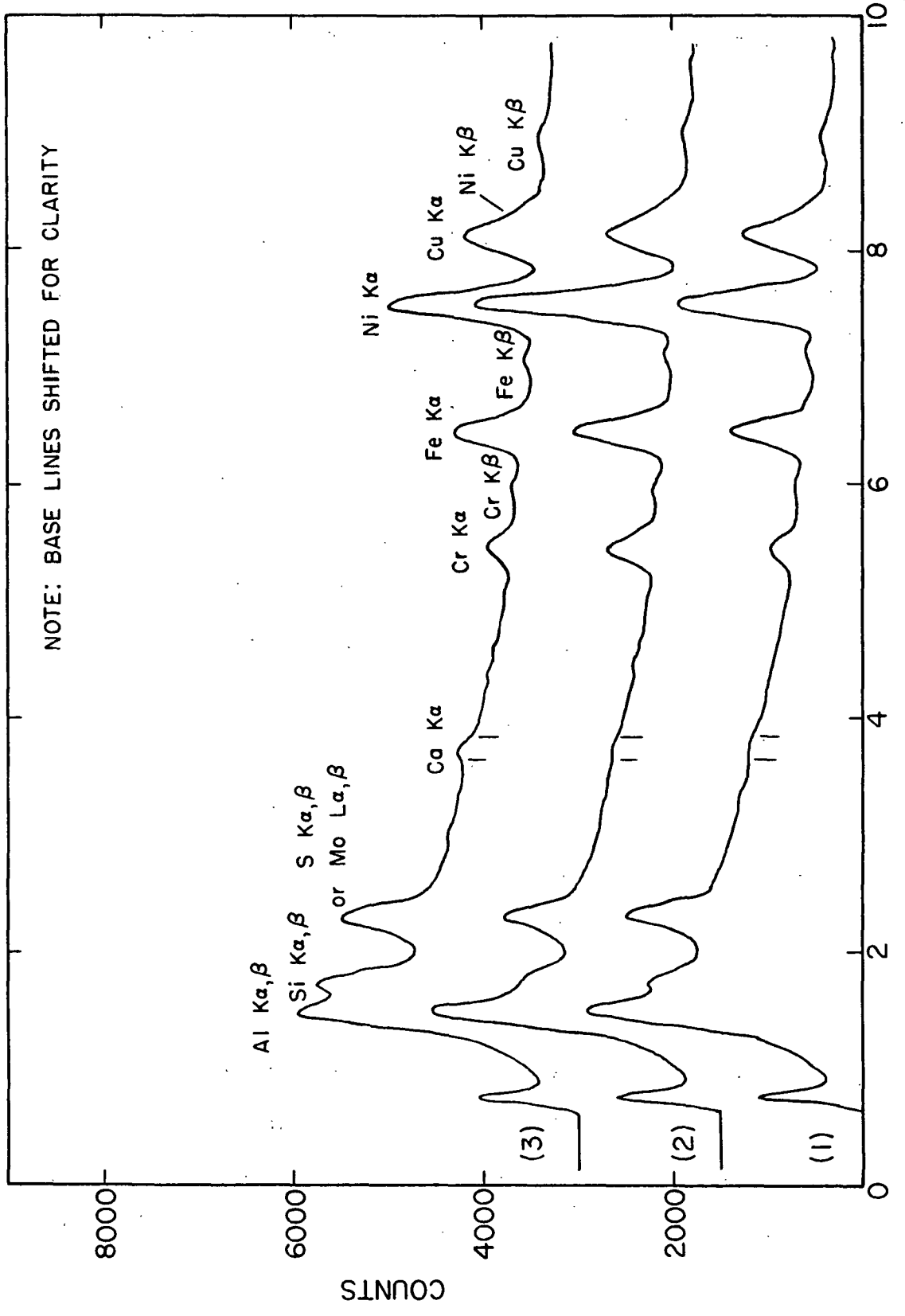

Figure 55. X-ray Spectra of a (1) Blank Graphite Holder; and Carbon Replicas of Ca-H-St Monolayers Deposited on Mica at (2) pH 6.2 and (3) pH 8.6 at 31 Dynes/cm. The Replica was Draped Over the Graphite Holder

unknown reason, in the carbon replica. The former explanation that calcium is present in the carbon replica, but at such low concentration that it is not detectable, is preferred. Thus, the possibility arises that the calcium stearate molecules at pH 6.2 do not exist in the calcium stearate micelle arrangement.

CONCLUSIONS OF ELECTRON MICROSCOPE STUDIES

A characteristic grouping of the molecules in deposited Ca-H-St monolayers and multilayers in the pH range 8.3-9.1 has been demonstrated. This structural unit has a diameter of about 50-60 A. and a height of about 25 A.

STRUCTURAL MODEL OF Ca-H-St MONOLAYERS

The interaction of calcium with fatty acid monolayers is also of great interest in the biological and medical sciences because calcium is important in many biological systems. Fatty acid monolayers have been employed as model membranes in order to study calcium interactions at anionic sites (64, 68, 118-122). However, the nature of calcium binding and its effects on surface properties are not clearly understood.

There have also been many attempts by various workers (63, 65, 102, 123-126) using a variety of techniques to determine the chemical composition of Ca-H-St monolayers. The results of these monolayer composition studies are presented in Fig. 56.

EXISTING MODELS

Two hypotheses are generally proposed for the effects of calcium on the fatty acid monolayers. The generally accepted or classical hypothesis is that a single divalent calcium ion reacts with two fatty acid anions to produce a di-soap molecule. Thus, the monolayer behaves as a mixture of un-ionized stearic acid and calcium

distearate molecules throughout the pH range. This hypothesis has been proposed by Harkins (69), Sasaki and Matuura (61), Rogeness and Abood (68), Kavanau (70), and Shah (71). However, an alternative hypothesis has been proposed by Harkins (69), Archer and LaMer (92), and Deamer and Cornwell (64) to explain the calcium effect on alkaline subsolutions. The calcium ions and fatty acid anions have been suggested to form a copolymeric lattice structure in which each calcium ion coordinates with four fatty acid anions and four water molecules.

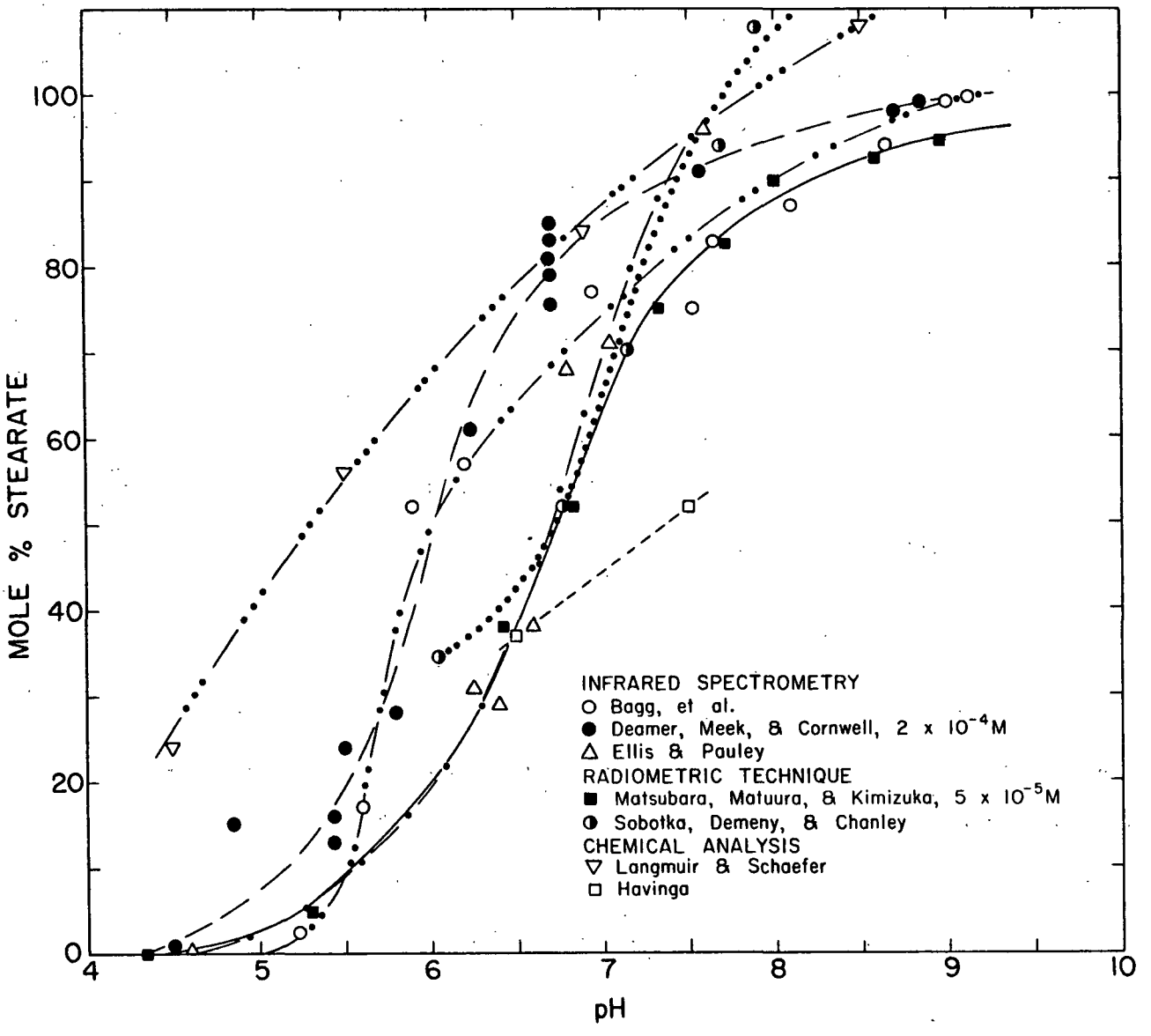

Figure 56. Composition of Stearic Acid Monolayers on 10^{-4}M Ca^{2+} Subsolutions Except Where Noted.

ANALYSIS OF THE EXISTING MODELS

This study demonstrates that large, characteristic changes occur in the monolayer properties and multilayer deposition behavior at pH 6.4 and 8.0. The decrease in $\underline{A}_{31}$ (Fig. 19), the large increase in the surface viscosity (Fig. 20 and 21), and the large decrease in the surface potential (Fig. 22) which begin at pH 6.4 cannot be explained by the classical model in which calcium distearate molecules are formed with increasing subsolution pH. In a similar manner, the occurrence and increase in the degree of nonuniformity (Fig. 23) and the decrease in the surface viscosity which occur above pH 8.0 are difficult to understand on the basis that the monolayer exists as a copolymeric lattice structure.

An alternative explanation of the calcium effect which is consistent with the $\Delta\underline{V}$-pH curve (Fig. 22) is the formation of an acid-soap complex with increasing metal ion content in the monolayer and its dissociation to calcium distearate molecules at pH 6.4. However, the large increase in the surface viscosity and the decrease in $\underline{A}_{31}$ are not compatible with the consequential increase in the calcium distearate concentration above pH 6.4.

SURFACE MICELLE TRANSFORMATION MODEL*

A new structural model of the Ca-H-St monolayer is proposed. This model offers an explanation for the behavior of condensed Ca-H-St monolayers over the pH range 2-9 and is schematically shown in Fig. 57. The central feature of this surface micelle transformation model is that a structural change occurs in the condensed Ca-H-St monolayer as the calcium distearate molecules associate into

*It should be emphasized that the proposed model is a hypothetical model which is consistent with the experimental results and observations. The same caution should be extended to the proposed molecular orientations at the solid-liquid interface.

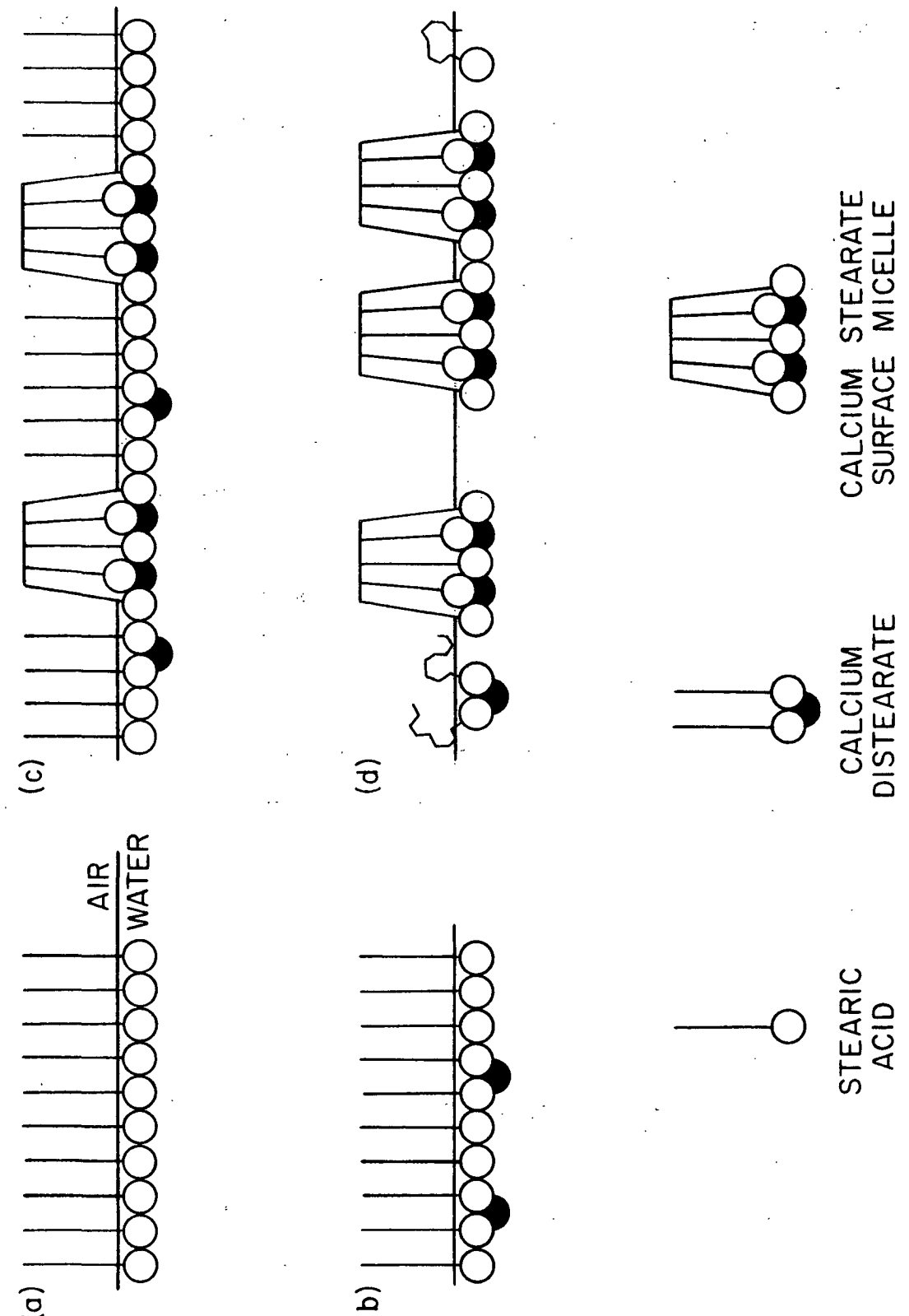

Figure 57. Schematic Representation of Condensed Stearic Acid Monolayers on 10^{-4} M $CaCl_2$ Subsolutions at (a) pH 2.0-4.2; (b) pH 4.2-6.4; (c) pH 6.4-8.0; and (d) pH 8.0-9.0

two-dimensional or surface micelles when a critical calcium ion concentration in the film is exceeded.

The condensed monolayer primarily consists of un-ionized stearic acid molecules in the pH range 2.0-4.2. The monolayer is a mixture of stearic acid and calcium distearate molecules between pH 4.2 and 6.4. With increasing subsolution pH, some of the calcium distearate molecules begin associating into calcium stearate surface micelles. The average surface micelle diameter is suggested to be about 50-60 A. The Ca-H-St monolayer becomes nonuniform at pH 8.0. The number of surface micelles becomes sufficient such that they now aggregate into large clusters of micelles. The imperfect fitting together of these clusters leads to "holes" existing within the monolayer structure. Thus, gaseous film of stearic acid and calcium distearate molecules or "free" subsolution surfaces are interspersed among the micelles and micelle clusters. The degree of nonuniformity of the Ca-H-St monolayer increases with increasing subsolution pH.

ANALYSIS OF THE SURFACE MICELLE TRANSFORMATION MODEL

This analysis of the experimental results which support the surface micelle transformation model is divided into two sections corresponding to the pH range 2.0-8.0 in which the monolayer is uniform and to the pH range 8.0-9.0 in which nonuniformity occurs.

pH Range 2.0-8.0

Withdrawal Contact Angle

The θ_2-pH curve of Ca-H-St bilayer shown in Fig. 38 indicates that θ_2 (1) is constant at 78° in the pH range 2.0-4.2, (2) decreases almost linearly to 30° at pH 6.4, and (3) then increases to 61° at pH 8.0. This behavior of θ_2 of the Ca-H-St bilayers is compared with that of the stearic acid bilayers (Fig. 40) in

which θ_2 (1) is also constant at 78°, but between pH 2.0 and 5.5, and (2) decreases linearly to zero degrees at pH 7.8. Inspection of Fig. 56 reveals that pH 4.2 corresponds to the subsolution pH at which ionization appears to become significant in the Ca-H-St monolayer. Bagg, et al. (103) found that pH 5.5 corresponds to the subsolution pH at which ionization appears to become significant in the stearic acid monolayer. Thus, the Ca-H-St monolayer appears to consist of un-ionized stearic acid molecules in the pH range 2.0-4.2.

The decrease in θ_2 with increasing subsolution pH above pH 4.2 is ascribed to the increasing content of calcium distearate molecules. If there were no change in the structural arrangement of the calcium distearate molecules within the monolayer, then θ_2 should continue to decrease at pH 6.4 until a zero contact angle occurs just as for the stearic acid bilayers. However, the increase in θ_2 at pH 6.4 suggests a structural rearrangement of the calcium distearate molecules. This change in the behavior of the withdrawal contact angle is support for the calcium stearate surface micelles.

Several remarks concerning the analysis of the chemical composition curves shown in Fig. 56 are relevant at this time. Upon considering the different methods of chemical analysis, individual techniques within the methods, and the results of the present investigation, it is concluded that the best estimate of the degree of dissociation of the Ca-H-St monolayer at pH 6.4 is given by Bagg, et al. (102) and is 62%. The degree of dissociation of the Ca-H-St monolayer at pH 8.0 is 90% from the same chemical composition curve of Bagg, et al.

A_{31}-pH Curve

The decrease in A_{31} above pH 6.4 in Fig. 19 is the result of the structural rearrangement of the calcium distearate molecules into the surface micelles.

Structure of Deposited Monolayers and Multilayers

A characteristic grouping of the molecules in deposited Ca-H-St monolayers and multilayers in the pH range 8.3-9.1 is observed in the electron micrographs. It is suggested that this structural unit which is about 50-60 A. in diameter corresponds to the surface micelles that exist at the liquid/air interface. Although the average size and the size distribution of the surface micelles may vary with the subsolution pH, the average size of the surface micelles is suggested to be approximately 50-60 A. in diameter and the size distribution is suggested to be not very large. The surface micelles then contain about 100-150 stearate anions.

Surface Viscosity

The fivefold increase in the surface viscosity (Fig. 20 and 21) from about pH 4.5 to pH 6.4 is attributed to the increasing concentration of calcium distearate molecules while the fiftyfold increase from pH 6.4 to pH 8.0 is again ascribed to surface micelle formation. Because the surface micelle lattice contains about 100-150 molecules, the large viscosity increase is due to the large increase in the size of the kinetic units in the monolayers.

Surface Potential

The ΔV-pH curve of Fig. 22 drops very sharply between pH 6.4 and 8.0, and then the rate of decrease changes at pH 8.0. The condensed Ca-H-St monolayer is uniform below pH 8.0 while the condensed Ca-H-St monolayer commences to become nonuniform at pH 8.0 as shown in Fig. 23. If the monolayer were uniform, extrapolation of the linear portion of the ΔV-pH curve between pH 6.4 and 8.0 suggests that ΔV would be negative at pH 9. The large region of negative surface potential at pH 9.07 in Fig. 24 is ascribed to the region being more concentrated in surface micelles. Consequently, there appears to be associated with surface micelle formation a change in the surface potential from positive to negative values.

The basic form of Schulman and Hughes expression (127) for the surface potential of an ionized monolayer was expanded in order to examine the reason for the sharp decrease in the ΔV-pH curve. In the pH range 2.0-8.0 where the monolayer is uniform, the surface potential may be expressed as

$$\Delta V = (12\pi/A)\,[(1 - \alpha - \beta)\,\mu_1 + \alpha\mu_2 + \beta\mu_3] + \psi_o \qquad (6)$$

where

μ_1 = surface dipole moment of the un-ionized stearic acid molecules, mD.

μ_2 = surface dipole moment of the calcium distearate molecules, mD.

μ_3 = surface dipole moment of the calcium stearate surface micelles, mD.

α = mole fraction of the molecules existing as calcium distearate molecules

β = mole fraction of the molecules existing as calcium stearate surface micelles

ψ_o = electrostatic potential in the plane of the charged head-groups of the monolayer and is given by the Gouy expression (128)

The initial decrease in the ΔV-pH curve of stearic acid monolayers has been attributed to the change in the ψ_o term due to the initial dissociation of the stearic acid molecules (37). The initial decrease in the ΔV-pH curve of Ca-H-St monolayers between pH 2.0 and about pH 4.2 can be similarly explained by the change in ψ_o. The large decrease in the surface potential of Ca-H-St monolayers has been generally ascribed to the attraction of Ca^{2+} below the negatively charged carboxylate groups resulting in vertical ionic dipoles oriented oppositely to the bond polarity in the un-ionized carboxyl groups (66, 129). However, the decrease in ΔV between pH 4.2 and 6.4 is minor although 62% of the stearic acid molecules have reacted at pH 6.4 to form calcium distearate molecules. Thus, the above-advanced hypothesis appears to be incorrect, and the surface dipole moment of calcium distearate molecules is comparable to that of the un-ionized stearic acid, 210 mD.

Therefore, it is suggested that the sharp decrease in ΔV is primarily due to the surface dipole moment of the calcium stearate surface micelles. The decrease in ΔV is suggested to be attributable to the highly oriented and tightly bound water molecules of the surface micelles. These water molecules appear to have a dipole moment with the negative end pointing away from the subsolution which in turn reduces the surface potential. Cooperative hydrogen bonding which produces an ordered vicinal water structure associated with the surface micelles also contributes to the reduction in the surface potential.

It is uncertain whether the surface dipole moment of the surface micelles is positive or negative because a sufficiently large negative ψ_o value would offset a small positive surface dipole moment and produce the negative ΔV associated with the surface micelles. Further experimental and theoretical work is required to determine the surface dipole moments associated with the calcium distearate molecules and calcium stearate surface micelles.

pH Range 8.0-9.0

The condensed Ca-H-St monolayer is nonuniform above pH 8.0, and the degree of nonuniformity increases with increasing pH. One possible explanation of this nonuniformity is that there are holes in the monolayer arising from the imperfect fitting together of the micelle clusters or aggregates of surface micelles. The following experimental results taken collectively support this hypothesis.

Surface Potential

It has previously been indicated (p. 138) that ΔV should be negative at pH 9.0. However, the rate of decrease of the ΔV-pH curve (Fig. 22) becomes smaller at pH 8.0 such that a positive average value of ΔV is obtained at pH 9.0. The presence of holes in the monolayer adds another term to Equation (6), and this term due to either a gaseous film or "free" subsolution surface makes a positive contribution

to ΔV. The presence of a gaseous film in the holes apparently causes the increase in ΔV to the small positive value at pH 9.0.

Surface Viscosity

The nine percent decrease in the surface viscosity (Fig. 20 and 21) between pH 8.0 and 9.0 is ascribed to the greater mobility of the surface micelles and micelle clusters as more gaseous film and "free" subsolution surface becomes available in the heterogeneous monolayer.

A_{31}-pH Curve

The A_{31}-pH curve of Ca-H-St monolayers (Fig. 19) decreases between pH 6.4 and 7.2, and then the average area/molecule appears to be constant at 19.5 $A.^2$ between pH 7.2 and 9.0. Because the nonuniform monolayer is assumed to consist of holes, the area/molecule in the surface micelle is suggested to be less than 19.5 $A.^2$ In fact, the area/molecule in the basal plane in crystals of calcium stearate monohydrate has been determined to be 19.4 $A.^2$ (130). If the area/molecule in the surface micelles is less than 19.5 $A.^2$, A_{31} is expected to continually decrease; however, the A_{31}-pH curve levels out on an alkaline subsolution. The increasing number of surface micelles causes the average area/molecule to decrease, but the increasing number of holes within the monolayer above pH 8.0 causes the average area/molecule to increase. The balance of these two effects is such that they offset each other, and the A_{31}-pH curve appears to be horizontal within experimental error.

Withdrawal Contact Angle

The θ_2-pH curve of Ca-H-St bilayers in Fig. 38 shows that θ_2 decreases from 61° to 53° in the pH range 8.0-9.0. If there are holes in the nonuniform monolayer, immersion of this monolayer at the solid/liquid interface would result in aqueous pores being formed, i.e., water molecules would fill the holes. Above

pH 8.0 the increasing number of aqueous pores contributes to the surface free energy of the solid/liquid interface; and as a result, the withdrawal contact angle decreases.

MOLECULAR REORIENTATION AT THE SOLID/LIQUID INTERFACE

WITHDRAWAL CONTACT ANGLE CHANGES

The contact angle of the three-phase line interface is dependent on the velocity with which the interface between a liquid and a second, immiscible fluid moves over a solid surface (131-134). In the siliconed glass/water/air system of Elliott and Riddiford (134), the advancing and receding contact angles were independent of the interfacial velocity in the range 0-1 mm./min. The withdrawal contact angle in Langmuir-Blodgett multilayer deposition is a dynamic receding contact angle. However, Table VII shows that the withdrawal contact angle is essentially independent of the deposition speed at interfacial velocities of 7.6 mm./min. or less. This indicates that the measured withdrawal contact angles are a good approximation of the static receding contact angles because a deposition speed of 7.6 mm./min. was used throughout the study.

Figure 38 shows that the withdrawal contact angles at pH 5.0 and 8.0 have the same value of 61°. In addition, photographs of the two contact angles demonstrate that the curvature of the liquid/air interface is the same even though the maximum surface viscosity of the Ca-H-St monolayer occurs at pH 8.0 and is 100 times greater than the surface viscosity at pH 5.0 as seen in Fig. 20. Furthermore, in the pH range 6.4-9.0 the dependence of the withdrawal contact angle on the subsolution pH does not correspond to the surface viscosity behavior. Thus, the withdrawal contact angle is not influenced by the surface viscosity of the Ca-H-St monolayer.

Young's equation (135) is assumed to be applicable to the withdrawal contact angle because the withdrawal contact angle appears to be independent of the deposition speed and the surface viscosity of the Ca-H-St monolayer. Young's equation is given as

$$\cos \theta = (\gamma_{SV} - \gamma_{SL})/(\gamma_{LV}) \qquad (7)$$

where

θ = contact angle between the liquid and solid, degrees

γ_{SV} = specific surface free energy of the solid/vapor interface, erg/cm.^{2}

γ_{SL} = specific surface free energy of the solid/liquid interface, erg/cm.^{2}

γ_{LV} = specific surface free energy of the liquid/vapor interface, erg/cm.^{2}

The results given in Table XVI show that the contact angles of water and glycerol on a Ca-H-St bilayer at pH 8.5 are only very slightly larger, if at all, than those on Ca-H-St bilayers at pH 6.7. As a result, it is assumed that the specific surface free energy of the Ca-H-St bilayers, γ_{SV}, is constant in the pH range 6.7-8.5. The upper surface of Ca-H-St bilayers consists of CH_3 groups having the same molecular packing if the local withdrawal transfer ratio is unity. Because the local withdrawal transfer ratios are unity below pH 6.8, it is assumed that the specific surface free energy of the Ca-H-St bilayers is constant below pH 6.8. Therefore, it is assumed that the specific surface free energy of the Ca-H-St bilayers is constant in the pH range 2-9.

Changes in the withdrawal contact angle are determined by individual or collective changes in the specific surface free energies of the interfaces, γ_{LV}, γ_{SV}, and γ_{SL}. Because multilayer deposition was studied at constant surface pressure, γ_{LV} is constant. In addition, it is demonstrated that γ_{SV} appears to be essentially constant, assuming that γ_{SV} does not change in the time of measurement. Therefore,

to a first approximation, changes in the withdrawal contact angle are determined primarily by changes in the surface free energy of the solid/liquid interface.

MAGNITUDE OF THE WITHDRAWAL CONTACT ANGLE

Bernett and Zisman (136, 137) have shown that aqueous solutions spread on a low-energy solid when the surface tension of the solution is less than the value of the critical surface tension, γ_c, of the solid. In addition to a zero contact angle during Langmuir-Blodgett monolayer deposition on high-energy surfaces such as mica, glass, silica, and certain metals, initially there is a layer of water between the transferred monolayer and the substrate. The monolayer goes on the solid as a carpet with a transfer ratio of unity. Under these conditions, monolayer deposition strongly resembles a spreading process. Thus, the hypothesis is advanced that a zero withdrawal contact angle occurs in Langmuir-Blodgett monolayer deposition when the surface tension of the monolayer-covered subsolution is less than the γ_c of the solid substrate.

The hypothesis was tested by determining the withdrawal contact angle and the calculated local net transfer ratio of Langmuir-Blodgett monolayers of C^{14}-labeled stearic acid deposited on a collodion substrate at various surface pressures. The cosine of the withdrawal contact angle is plotted against γ_{LV} of the monolayer-covered subsolution in Fig. 29. Extrapolation of the cos θ-γ_{LV} curve to cos θ = 1 gives γ_c of the solid. In general, higher γ_c values correspond to higher specific surface free energies of the solid. The γ_c of collodion (nitrocellulose) is estimated as 47 dynes/cm. This value is in good agreement with the previously reported γ_c values (42-44 dynes/cm.) of regenerated cellulose viscose films (138, 139) and the γ_c values (40-45 dynes/cm.) of nitrated hydrocarbon surfaces (140). The higher γ_c value obtained in this study is ascribed to the water-saturated nature of the nitrocellulose.

Thus, when γ_{LV} is less than 47 dynes/cm. or the surface pressure is greater than 26 dynes/cm., the monolayer-covered subsolution spreads on collodion as observed. Quantitative measurements of the transfer ratio on collodion from film balance measurements were not possible because the preparation procedure of the collodion substrate only coats one side of the glass slide. However, the film balance measurements and autoradiographs strongly suggest that the transfer ratio is unity when the surface pressure is greater than 28 dynes/cm. Table VI confirms that the transfer ratio is unity on collodion at high surface pressures. At surface pressures of 20 dynes/cm. or lower, only a fractional monolayer is deposited, apparently by an adsorption process. These results verify the hypothesis that when γ_{LV} of the monolayer-covered subsolution is less than the γ_c of the solid, a monolayer-covered subsolution spreads on the solid with a transfer ratio of unity during the withdrawal operation of Langmuir-Blodgett monolayer deposition.

The classical concept of the orientation of the molecules in the immersed monolayer during multilayer deposition is one in which the polar groups are oriented toward the aqueous phase as shown in Fig. 2 and 33. It is generally acknowledged that if the polar carboxyl groups of a paraffinic acid are oriented toward water, the contact angle should be zero (141). Thus, a zero withdrawal contact angle should be observed for Ca-H-St bilayers even when it is composed of un-ionized stearic acid molecules; however, a withdrawal contact angle of 78° is observed. The surface tension of the Ca-H-St monolayer-covered subsolution was constant at 42 dynes/cm. (Π = 31 dynes/cm.). Because the withdrawal contact angles of the Ca-H-St bilayers are acute angles, the γ_c of the Ca-H-St monolayer-covered paraffin substrate, i.e., the immersed monolayer, is less than 42 dynes/cm. This γ_c value is representative of a low-energy surface. This suggests that the molecules of the immersed monolayer have undergone a reorientation such that their nonpolar methyl groups, instead of the polar groups, are primarily oriented toward the subsolution.

SUPPORT FOR MOLECULAR REORIENTATION

It may be argued that molecular reorientation does not occur, but rather the orientation of the molecules at the liquid/air interface is maintained upon transfer to the paraffin substrate. This then implies that an appreciable fraction of the molecules at the subsolution surface have their nonpolar groups oriented toward the water. However, this is contrary to the conventional view (142) that in a monolayer at the subsolution surface the polar head-groups are immersed in the water and the hydrophobic groups are oriented away from the water. Transient localized molecular inversion (molecular overturning) occasionally occurs due to the random movements of the monolayer molecules. Blank and Britten (143) estimated the ratio of molecular overturning as one in 100,000 on the basis that the surface potential determines the distribution. Thus, the probability and rate of overturning is small. Accordingly, if molecular reorientation does not occur to an appreciable extent at the solid/liquid interface, then the polar groups of the molecules of the immersed monolayers must be oriented toward the water. However, this does not appear to be the case, and molecular reorientation does appear to occur at the solid/liquid interface.

Ca-H-St and stearic acid bilayers were deposited on clean, smooth polytetrafluoroethylene substrates. Table XV indicates that there is a difference between the withdrawal contact angles on polytetrafluoroethylene and paraffin. In addition, the apparent transfer ratio, ρ_2, is less than unity. However, the autoradiographs show that the deposition was nonuniform with voids being present in the bilayer. Thus, the local transfer ratios are certainly higher than the apparent values. Whether or not the local transfer ratio is unity, the γ_{SV} of the bilayer is assumed to be the same on both the polytetrafluoroethylene and paraffin on the grounds previously advanced that γ_{SV} is essentially independent of local values of ρ_2

greater than 0.87. As before, γ_{LV} of the monolayer-covered subsolution is the same for bilayer deposition on both substrates. These results suggest that the differences between the withdrawal contact angles on polytetrafluoroethylene and paraffin are due to changes in the surface free energy of the solid/liquid interface.

As previously discussed, Table XV also indicates that the local transfer ratio of the first deposited layer on polytetrafluoroethylene appears to be unity. This indicates there is no difference in the molecular packing on either paraffin or polytetrafluoroethylene substrates. There is no apparent reason why the chemical composition should differ in the first layer, so it is assumed that the same proportion of chemical species are present at the solid/liquid interface of both substrates as at the subsolution surface. Furthermore, the immersed molecules of the first layer on polytetrafluoroethylene are assumed to be stable and do not dissolve in the subsolution. It has been shown that contact angles are unaffected, or at most very slightly affected, by the attractive forces arising from a highly polar surface below a hydrocarbon chain monolayer five to seven carbon atoms long (144, 145). The withdrawal contact angle is not influenced then by the intermolecular forces arising from the polytetrafluoroethylene and paraffin surfaces. The observed differences in the withdrawal contact angle on polytetrafluoroethylene and paraffin cannot be accounted for except by inferring that there is a difference in the orientation of the immersed monolayers on the two substrates.

Langmuir (3) deposited oleic acid monolayers on different high-energy solids. The solid surfaces became hydrophobic upon the deposition of the monolayer, and the contact angles depended on the nature of the underlying solid. The differences in the contact angles were attributed to the differences in the strength of anchorage of the polar groups of the oleic acid to the solid surfaces. If the solid possessed a weak force field, an appreciable fraction of the monolayer overturned to bring the

polar groups to the solid/liquid interface. Thus, the solid substrate did not directly influence the contact angle, but determined the degree of orientation of the deposited monolayer which in turn determined the observed contact angle.

The decrease in the withdrawal contact angle on polytetrafluoroethylene is attributed to a greater fraction of the polar groups at the solid/liquid interface as a result of a decrease in the extent of molecular overturning. Presumably this orientation is a consequence of the dipole moment of the CF_2 groups comprising the polytetrafluoroethylene surface. These results suggest that the molecules at the solid/liquid interface undergo reorientation. Furthermore, the changes in the withdrawal contact angle appear to be determined primarily by changes in the surface free energy of the solid/liquid interface arising from changes in the orientations of the molecules comprising the immersed monolayer.

MOLECULAR ORIENTATION AT THE SOLID/LIQUID INTERFACE

The θ_2-pH curve (Fig. 38) of the Ca-H-St bilayers suggests the following orientation of the molecules in the immersed monolayer at the solid/liquid interface. In the pH range 2.0-4.2 the monolayer of un-ionized stearic acid molecules reorients with the carboxyl groups toward paraffin and the methyl groups toward the subsolution. The withdrawal contact angle decreases above pH 4.2 because the hydrophilic groups of the calcium distearate molecules remain oriented toward the water (at pH > 5.5 for sodium stearate molecules) while the un-ionized stearic acid molecules continue to reorient. At pH > 6.4 the calcium stearate surface micelles reorient such that their hydrophilic groups are oriented toward the paraffin surface and their hydrophobic groups toward the subsolution; and, consequently, the withdrawal contact angle increases. Above pH 8.0 the increasing number of aqueous pores among the surface micelles and the micelle clusters contribute to the surface

free energy of the solid/liquid interface; and as a result, the withdrawal contact angle decreases. A schematic representation of the proposed orientations is given in Fig. 58.

Cationic surfactants adsorb at the paraffin/water interface by orienting their paraffin chains against the hydrophobic solid and the polar group toward the aqueous solution (146). In a similar manner, the wettability of a paraffin surface increases by the adsorption of sodium stearate on the solid surface (147).

Thus, the proposed orientation of the calcium distearate molecules at the solid/liquid interface is in agreement with other studies on hydrophobic solids. However, the proposed orientation of the stearic acid molecules and calcium stearate surface micelles appears to be contrary to conventional views of molecular orientation at interfaces.

The major factor in the driving force for this molecular reorientation of unionized stearic acid molecules and calcium stearate surface micelles is suggested from a consideration of the enthalpy and entropy contributions to the overturning process schematically illustrated in Fig. 59. An enthalpy increase arises from the formation of the methyl/water and carboxyl/paraffin interfaces. In addition, desolvation of the carboxyl groups leads to a further increase in enthalpy. It is reasonable to assume that there is no change in the state of the hydrocarbon chains and polar groups in either orientation. Therefore, the origin of the greater enthalpy decrease or entropy increase necessary to offset these enthalpy increases arises in the water phase and is attributed to a change in the water structure.

Hydrocarbon chains in an aqueous medium are believed to be surrounded by regions of highly structured water which are often described as "Frank-Evans icebergs" (143). The dipoles of the monolayer molecules apparently orient and hinder

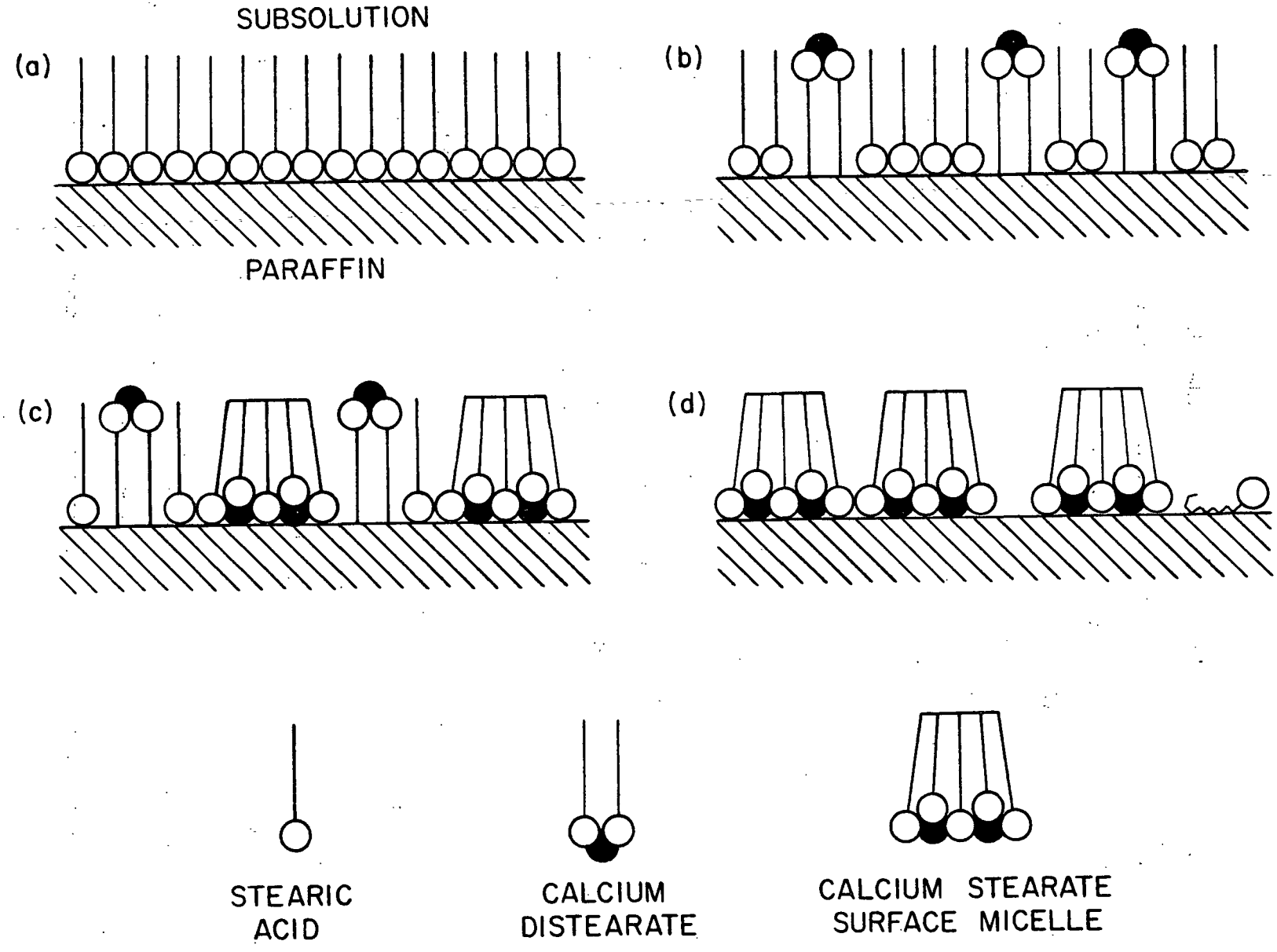

Figure 58. Schematic Representation of the Orientation of the Molecules of a Condensed Ca-H-St Monolayer at the Paraffin/Liquid Interface at (a) pH 2.0-4.2; (b) pH 4.2-6.4; (c) pH 6.4-8.0; and (d) pH 8.0-9.0

the rotation of the dipoles of several layers of water molecules below the head groups to form a rather rigid layer of "soft ice" (149). Stearic acid monolayers structure the water molecules of the subsolution, and compression of the monolayer further enhances the water structure (38). Because micelle formation for both ionic and nonionic surface-active agents involves positive enthalpy or small negative enthalpy changes, it is generally accepted that entropy rather than enthalpy is the driving force for micelle formation, at least below 25°C., and arises from the decreased ordering of the water structure (150). A large gain in entropy also occurs in the elimination of soft ice (151).

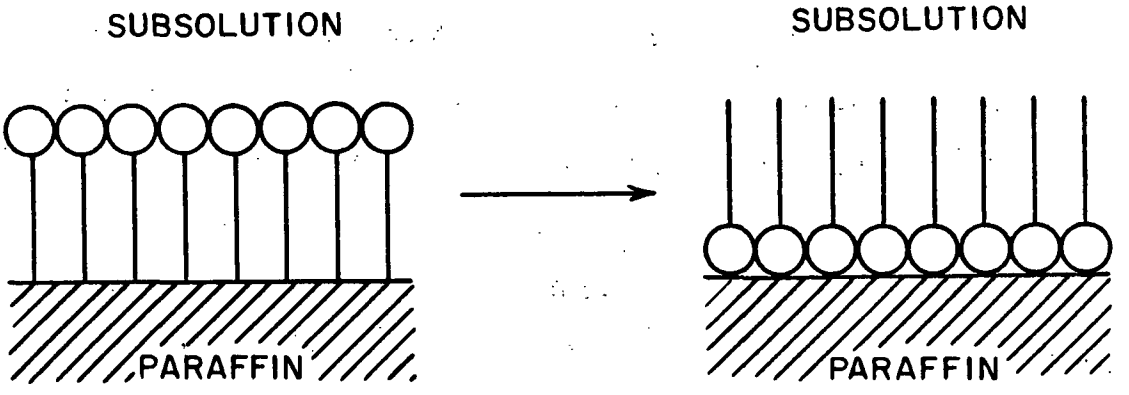

Figure 59. Molecular Reorientation of Condensed Un-ionized Stearic Acid Monolayer at the Solid/Liquid Interface During Bilayer Deposition on a Paraffin Substrate

Recently, Gershfeld and Pagano (152) evaluated the entropies of compression of the polar groups for the process of compressing a monolayer from the "ideal gas" to a condensed state and suggested that characteristic changes in water structure occur in the formation of each condensed monolayer state. The enthalpy and entropy of compression of the polar groups for a liquid-condensed stearic acid monolayer were determined to be -880 cal./mole and -15.5 e.u. ($T\Delta S$ = -4455 cal./mole), respectively. While the entropy is the major component of the polar group contribution to the free energy of compression, it is important to realize that the entropy and energy changes reflect possible changes in film hydration, hydrogen bonding, and water structure.

While it is not possible at the present time to evaluate the relative magnitude of the enthalpy and entropy changes associated with the change in the water structure, the process of overturning would appear to be most likely an entropy-directed process. Accordingly, the water structure change is attributed to a decreased ordering of the water structure and would be accompanied by a large increase in entropy. This then implies that the water structure below the head groups of condensed un-ionized stearic acid monolayers and calcium stearate surface micelles is more highly structured than the water at a hydrocarbon/water interface.

Calcium distearate molecules do not reorient because the hydrophilic-solvent affinity of the carboxylate ion is much greater than that of the carboxyl group (153). Accordingly, the work of adhesion of the carboxylate ions to water is much greater than that of the carboxyl groups. Water molecules are highly polarized, immobilized, and compressed by an ionic field with an associated large decrease in the entropy and volume (154). Any favorable enthalpy or entropy change due to the change in the water structure on reorientation of the di-soap molecule apparently is not sufficient to offset the large enthalpy increase. Consequently, the calcium distearate molecules do not overturn, and their polar groups remain oriented toward the water and decrease the surface free energy of the solid/liquid interface.

It should be emphasized that the observed orientations may be peculiar to the condensed monolayer and would not occur at other monolayer states where the associated water structure may be different.

It is worthwhile to examine the question of the extent of molecular reorientation of the un-ionized stearic acid molecules and the calcium stearate surface micelles. The work of adhesion of water to the paraffin substrate was determined from the withdrawal contact angles given in Table VII for withdrawing a paraffin

substrate through a stearic acid monolayer. Young's equation is combined with Dupre's equation (155) to give

$$W_{SLV} = \gamma_{LV} (1 + \cos \theta) \qquad (8)$$

where W_{SLV} is the "practical" work of adhesion of the liquid to the solid in equilibrium with the saturated vapor pressure of the liquid. The work of adhesion of water to paraffin was calculated as 54 ergs/cm.^{2} from the withdrawal contact angle of 74°. The work of adhesion of water to highly purified and smooth paraffin surfaces has been determined by several investigators (156, 157) to be 45-47 ergs/cm.^{2}

However, Phillips and Riddiford (158) have shown that there are grounds for assigning a value of 33 ergs/cm.^{2} to the specific surface free energy of paraffin. Combining Fowkes' expression (159) of the interfacial tension with Dupre's equation gives the dispersion force contribution to the work of adhesion of the liquid to a film-free solid, W^d_{SLO}, as

$$W^d_{SLO} = 2 \sqrt{\gamma^d_L \gamma^d_S} \qquad (9)$$

where γ^d_L and γ^d_S are the dispersion force contributions to the specific surface free energy of the liquid and solid, respectively. Assuming the paraffin solid is an ideal hydrocarbon and the film pressure of the adsorbed water vapor is negligible, W_{SLV} equals W^d_{SLO}. The work of adhesion is evaluated as 54 ergs/cm.^{2} when γ^d_S equals 33 ergs/cm.^{2}, whereas the usual γ^d_S value of 25.5 ergs/cm.^{2} for paraffin yields 47 ergs/cm.^{2} Thus, the work of adhesion of water to paraffin determined in this study by the withdrawal contact angle is in good agreement with previously determined and theoretical values.

The work of adhesion of water to the un-ionized stearic acid molecules of the immersed monolayer at the solid/liquid interface is calculated as 51 ergs/cm.^{2} from the withdrawal contact angle of 78°. The immersed stearic acid monolayer appears to be more hydrophobic than the paraffin surface, used in this study (W_{SLV} = 54 ergs/cm.^{2}), probably the result of hydrophilic impurities present at the paraffin surface or the diffusion and penetration of water molecules into the paraffin surface. In any event, the un-ionized stearic acid molecules appear to be predominantly oriented with their hydrocarbon tails toward the subsolution.

The lower withdrawal contact angles on polytetrafluoroethylene than on paraffin shown in Table XV are understandable if the vertical dipole moment of the COOH group of the un-ionized stearic acid molecule is directed with the negative end away from the hydrocarbon chain. In this orientation, a repulsive force exists between the dipole moments of the COOH groups and the dipole moments of the CF_2 groups on the polytetrafluoroethylene surface. As a result, less un-ionized stearic acid molecules reorient because of the larger enthalpy increase arising from such a change in orientation on polytetrafluoroethylene.

Table XV shows that the withdrawal contact angle on polytetrafluoroethylene is greater than that on paraffin. One possible explanation is that the surface micelles are not completely reoriented on paraffin, but there is a greater reorientation of the surface micelles on polytetrafluoroethylene. This result is not fully understood. The bilayer deposition studies on polytetrafluoroethylene need further work.

The withdrawal contact angle results indicate that in the immersed monolayers on paraffin the un-ionized stearic acid molecules are oriented with their hydrocarbon tails toward the subsolution; although the calcium stearate surface micelles also reorient, overturning of the surface micelles does not appear to be complete.

In addition, polar groups in the substrate surface appear to influence the extent of molecular overturning.

TRANSFER RATIO AND WITHDRAWAL CONTACT ANGLE BEHAVIOR IN MULTILAYER DEPOSITION

The local transfer ratio of the second layer, ρ_2, is unity below pH 6.8 and, as shown in Fig. 34, decreases with increasing subsolution pH, i.e., the amount of transferred film decreases. The composition of the deposited monolayer may remain the same as that of the original Ca-H-St monolayer, or the composition may change due to a preferential transfer of components of the Ca-H-St monolayer. It is generally assumed that the composition of multilayers is equivalent to the composition of the monolayers from which they are built. However, several workers (27, 124) have questioned the validity of this assumption.

An increase in the surface viscosity might be expected to lead to a decrease in the amount of transferred film. In addition, the withdrawal contact angle which determines the orientation of the monolayer molecules to the solid surface may be expected to influence the probability of interaction. Thus, an increase in the withdrawal contact angle may also reduce the transfer ratio as suggested by Goranson and Zisman (18).

Although the general increase in the surface viscosity shown in Fig. 21 approximately parallels the decrease in the local transfer ratio, the surface viscosity decrease at pH > 8.0 does not correspond to an increase in the transfer ratio. Furthermore, the behavior of the θ_2-pH curve shown in Fig. 38 clearly indicates that the withdrawal contact angle is not the major factor in the transfer ratio decrease. For instance, the transfer ratio is unity at the largest contact angle; and when the withdrawal contact angle decreases between pH 4.2 and 6.4, the transfer ratio remains unity. In addition, when the withdrawal contact angle

decreases above pH 8.0, the transfer ratio decreases instead of increases. However, in the pH range 6.8 to 8.0 where the transfer ratio is decreasing, the withdrawal contact angle does increase. These results indicate that another or additional mechanism is responsible for the decreased amount of transferring film, at least above pH 8.0, if not also between pH 6.8 and 8.0.

The behavior of ρ_2, decreasing at about pH 6.8 and the change in the rate of decrease at about pH 8.0, corresponds to similar changes in the molecular properties of the Ca-H-St monolayer. Thus, the decrease in the transfer ratio is attributed to the partial transfer of the calcium stearate surface micelles. The surface micelles being aggregates of about 100-150 molecules have a very low mobility and are less likely to adsorb than the stearic acid or calcium distearate molecules. Thus, fractionation of the molecular species of the Ca-H-St monolayer is suggested to occur during multilayer deposition along with a concomitant decrease in the metal ion content of the multilayer. However, direct evidence of fractionation effects was not obtained, is beyond the scope of this present investigation, and would be very difficult to quantitatively measure.

The immersed monolayer is nonuniform and contains aqueous pores above pH 8.0. It is assumed that the monolayer molecules do not adsorb on the aqueous pores during the withdrawal operation. In addition, less deposition should occur because the concentration of calcium stearate surface micelles increases with subsolution pH. However, examination of the transfer ratio-pH curve indicates that more film deposits above pH 8.0 during the first withdrawal operation than can be explained when the combined effects of the increasing concentrations of surface micelles and aqueous pores are considered. Consequently, this increased deposition is ascribed to the combined effects of the decreased surface viscosity and withdrawal contact angle above pH 8.0 which increase the mobility and probability of interaction of

the surface micelles at the three-phase line interface, respectively. The transfer ratio appears to be influenced by four factors: surface micelles, aqueous pores, surface viscosity, and withdrawal contact angle.

The withdrawal transfer ratio decreases with increasing number of deposited layers above pH 6.8 as shown by Fig. 34 and Table VIII. The larger decrease in the withdrawal transfer ratio, of the fourth layer, ρ_4, corresponds to an increase in the withdrawal contact angle of the fourth layer, θ_4, between pH 6.8 and 8.0 as shown in Table XIII. However, above pH 8.0 θ_4 is lower than θ_2, and the larger decrease in ρ_4 now corresponds to a smaller withdrawal contact angle. The monolayer properties are assumed not to change during multilayer deposition. This apparent contradiction between the transfer ratio of the fourth layer and the contact angle behavior can be understood if aqueous pores form in the top layer of the immersed multilayer whenever the withdrawal transfer ratio is less than unity, in addition to those already existing in the nonuniform Ca-H-St monolayers above pH 8.0.

The formation of these aqueous pores is believed to occur as follows: The third layer deposits with a transfer ratio of unity onto the second layer whose transfer ratio is less than unity, i.e., it contains holes in its structure. The molecules of the multilayer are known to be in a most dynamic state and continuously exchange places (160). During the immersion time, some of the molecules of the third layer migrate to fill or partially fill the existing holes in the underlying layers; and, as a result, aqueous pores are created in the immersed third layer with a concomitant decrease in γ_{SL} which tends to cause the contact angle to decrease. During deposition of the fourth and sixth layers, the monolayer is assumed not to deposit on the aqueous pores and to continue depositing on the monolayer molecules of the third and fifth layers with the same withdrawal transfer

ratio as that of the second layer. This tacitly implies that the third and fifth layer have the same molecular orientation and composition as the first layer and that the withdrawal contact angle does not change. Using the above model, withdrawal contact angles were calculated for two modes of molecular migration of the immersed monolayer, complete and partial (60%) filling of the holes available in the underlying layers. The molecules are assumed, for simplicity, not to migrate into the holes present in the nonuniform Ca-H-St monolayers. Table XVIII shows the calculated values compared with the measured withdrawal transfer ratios at pH 8.3. The results indicate that molecular migration into the underlying holes is incomplete; a 60% filling of the holes gives good agreement with the measured transfer ratios.

TABLE XVIII

COMPARISON OF THE MEASURED AND CALCULATED LOCAL TRANSFER RATIOS OF Ca-H-St MULTILAYER DEPOSITION AT pH 8.3[a]

	Local Transfer Ratio		
		Calculated[b]	
	Film Balance Measurements	Complete Migration[c]	Partial Migration[d]
ρ_2	0.86	0.86	0.86
ρ_4	0.78	0.74	0.79
ρ_6	0.72	0.52	0.68

[a] $\underline{\Pi}$ = 31 dynes/cm.; $\underline{T}$ = 20.3°C.

[b] Assuming monolayer deposits with a transfer ratio equal to ρ_2 and does not deposit on the aqueous pores created by the two modes of migration.

[c] Complete filling of the holes available in the underlying layers.

[d] Partial (60%) filling.

The withdrawal contact angle behavior of the first several layers in multilayer deposition is shown in Table XIV. The results of Table XIV show that the withdrawal contact angle increases only very slightly at pH 6.8. However, the withdrawal contact angle at pH > 8 decreases slightly and then gradually increases above the initial value with increasing number of deposited layers. These results markedly differ from Goranson and Zisman's results (18) which showed that the withdrawal contact angle increased to 90° after three withdrawals at pH 8.9 and five withdrawals at pH 6.8. Goranson and Zisman attributed this contact angle increase to the mechanism of positive ion adsorption. Goranson and Zisman showed that excess divalent metal ions become trapped in the multilayer during the withdrawal operation. The excess positive charge of the multilayer repels the positive ions adsorbed on the carboxyl groups of the monolayer; and, as a result, the withdrawal contact angle increases with increasing number of layers. Positive ion adsorption is reduced under the present experimental conditions, apparently as a result of the slower withdrawal speed which minimizes trapped calcium ions.

The increase in θ_4 between pH 5.7 and 7.8 observed in Table XIII arises as a result of greater reorientation of the immersed molecules or positive ion adsorption. However, the result that θ_2 and θ_4 are equal at pH 3.2 rules out further reorientation of the un-ionized stearic acid molecules and further supports their complete reorientation on paraffin. As before, it is energetically unfavorable for the calcium distearate molecules to overturn. Thus, it appears that positive ion adsorption is responsible for the increase in the withdrawal contact angle.

Aqueous pores which are formed in the immersed monolayer oppose the effect of positive ion adsorption. Table XIII shows the increase in θ_4 between pH 5.7 and 7.8. However, Table XIII also shows that the increase in θ_4 at pH $\geq$ 6.5 is less than the increase in θ_4 at pH $\leq$ 6.0. This reduction in the increase of θ_4

is attributed to the formation of aqueous pores. The aqueous pores appear to begin forming at about pH 6.4. The withdrawal transfer ratio then appears to begin decreasing at about pH 6.4, the pH at which surface micelles begin forming. The decrease in the transfer ratio is detected at pH 6.8 instead of at pH 6.4 by the film balance measurements due to its insensitivity to detect small changes in the transfer ratio. The withdrawal contact angle measurements are very sensitive to slight changes at the solid/liquid interface.

The decrease in θ_4 above pH 8.0 (Table XIII) is then due to the combined effects of aqueous pores in the third layer arising from those occurring in the nonuniform Ca-H-St monolayer and from molecular migration during immersion. The combined two sources of aqueous pores offset the effect of positive ion adsorption. However, positive ion adsorption eventually manifests itself with increasing number of layers as shown in Table XIV.

The reason that the immersion transfer ratios are unity is not fully understood although deposition is believed to occur by an adsorption process. Before the mechanism can be understood more fully, a technique must be developed for measuring the immersion contact angles.

SURFACE MICELLE FORMATION

In 1949 Debye (161) developed a theory of ionic micelle stability in terms of a balance between a positive free energy due to electrostatic repulsion between the charged head-groups on the micelle surface and a negative free energy of bringing the hydrocarbon tails together. This concept was used as the starting point for examining the contributions to surface micelle formation.

The free energy of surface micelle formation is considered to be the sum of a negative term arising from the cohesive forces of attraction between the

hydrocarbon chains and several positive terms including those due to the electrostatic repulsion between the head-groups and the entropy loss on association. The electrostatic free energy of the monolayer increases as the concentration of stearate anions increases in the film. Above a critical calcium ion concentration in the film, the free energy of the system is reduced by the association of calcium distearate molecules into calcium stearate surface micelles. The electrostatic free energy is suggested to decrease during surface micellization by the staggering of the stearate anions and the penetration of the calcium ions into the plane of the head-groups. (A schematic representation of the proposed structure of the calcium stearate surface micelles is presented in Fig. 60.) A negative entropy contribution arises from the association of the anions and water molecules into the coordination complex in which each Ca^{2+} forms four metal-ligand bonds with the carboxylate anions. These positive free energy contributions are offset by the negative enthalpy contribution arising from the tighter packing of the hydrocarbon chains. The attractive energy of hydrocarbon chains is extremely sensitive to the distance between the aliphatic chains. According to Salem (74), the total dispersion energy is inversely proportional to the fifth power of the intermolecular distance.

In addition, a solvent effect is postulated to also influence surface micelle stability. Poland and Scheraga (162) postulated that there must be an increased structuring of the water with accompanying negative changes in the enthalpy and entropy when the charged head-groups enter a micelle. The withdrawal contact angle behavior previously presented is interpreted, in part, by a highly ordered vicinal water structure being associated with the surface micelles. However, the relative changes in the enthalpy and entropy arising from the change in the water structure during surface micelle formation is unknown.

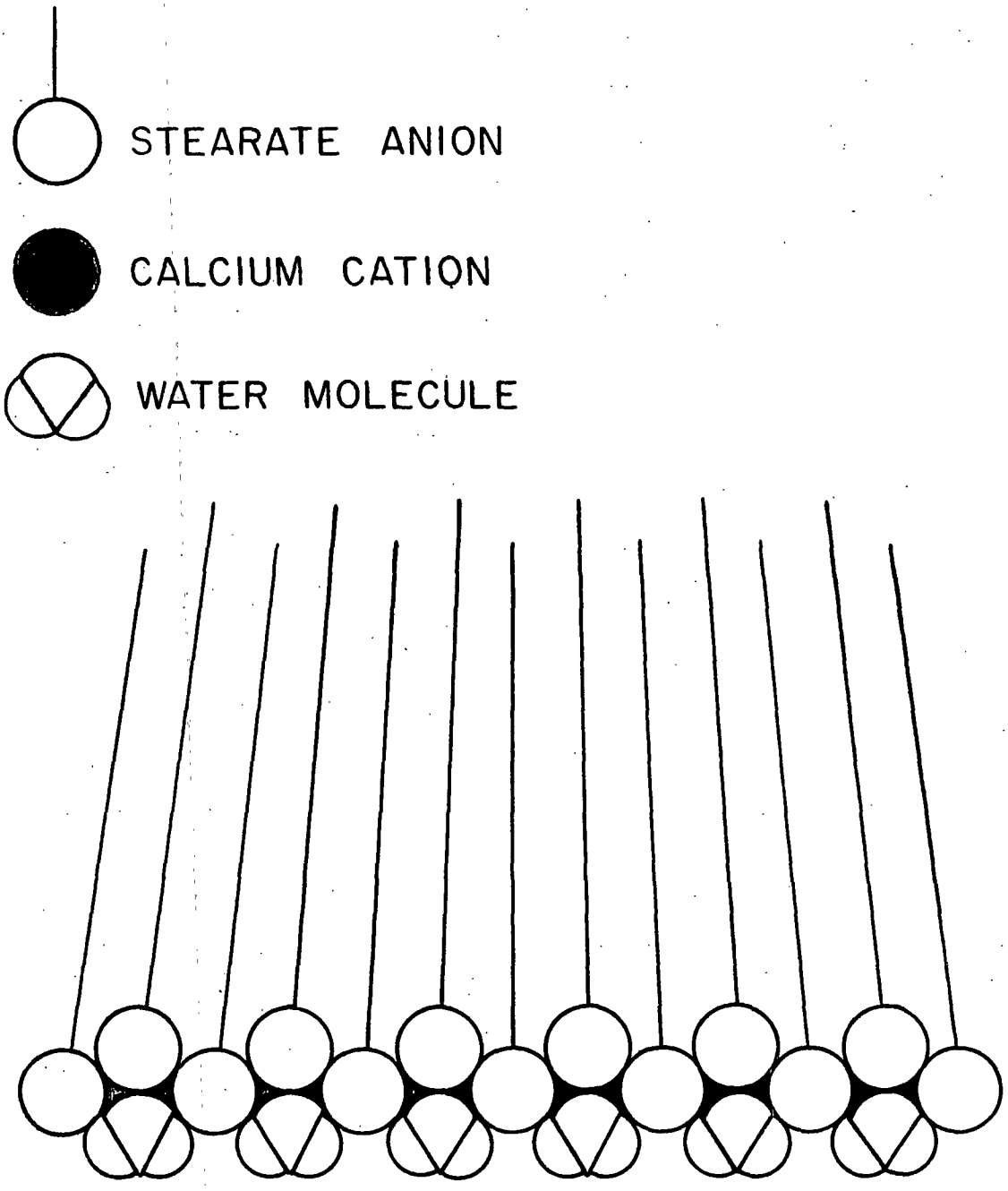

Figure 60. Schematic Representation of the Proposed Lattice Structure of the Calcium Stearate Surface Micelles

Although the monolayer model represents full-size surface micelles abruptly forming at pH 6.4, premicellar surface associations may also occur in a similar manner as for micellization in bulk systems (160).

The idea of two-dimensional molecular clusters of molecules or surface micelles was proposed by Langmuir (163) in 1933 to explain the properties of un-ionized myristic acid monolayers in the intermediate state. However, an alternative explanation for the intermediate state has been proposed (164). Epstein (165) on the basis of electron micrographs of multilayers advanced the hypothesis that the molecules in monolayers were arranged in clusters of about 100 A. in diameter. However, Epstein stated that although the interpretation of the electron diffraction patterns of barium stearate multilayers appears to require micellar structures, the existence of micelles is not necessary for the interpretation of stearic acid multilayer diffraction patterns. Bull (166) showed experimental evidence for surface micelle formation during the compression of a gaseous film of charged sodium dodecyl sulfate. The average surface micelle was supposed to contain four molecules. Chattoraj and Chatterjee (167) also presented evidence that long-chain quaternary ammonium ions upon compression aggregate into surface micelles having an aggregation number of about 19.

Surface micelle formation may also occur in the alkali metal stearate monolayers. Goddard, et al. (79) have postulated that the change of slope in the ΔV-pH curve on 0.01M NaCl subsolutions at about pH 9 is due to the dissociation of an acid-soap complex. The composition of the monolayer on 0.1M NaCl subsolutions at pH 9 is about 60 mole percent stearate (103). In addition, the fatty acid monolayers on pH 9.0-9.5 KOH subsolutions are extremely rigid (47). The striking parallels between the alkali metal and alkaline earth stearate monolayers strongly suggests that sodium stearate molecules associate into sodium stearate surface micelles above pH 9.

In a concluding comment, it is significant to note that Ohki and Aono (168) from a theoretical analysis concluded that changes in the net charge of lipid polar groups give rise to structural changes in the lipid bilayer. The present study demonstrates that when the Ca-H-St monolayer becomes sufficiently ionized, the calcium distearate molecules undergo a structural rearrangement into calcium stearate surface micelles. Structural change and molecular function in biological membranes with calcium ions may be closely related to the structural change of the lipid monolayers considered to be the "fundamental structure" of many natural membranes.

CONCLUSIONS

This investigation supports the hypothesis that a structural change occurs in condensed monolayers as ionized molecules associate into two-dimensional or surface micelles when a critical metal ion concentration in the film is exceeded. The orientation of surface micelles of fatty acid calcium salts and un-ionized fatty acid molecules in condensed monolayers at a nonpolar solid/liquid interface is contrary to conventional views of molecular orientation at interfaces. The polar groups of the surface micelles and the fatty acid molecules appear to be oriented away from the subsolution. In addition, this structural change within the monolayer also influences Langmuir-Blodgett multilayer deposition such that there is a difference in the amount of film depositing during the immersion and withdrawal operations when surface micelles are present in the monolayer.

Large characteristic changes occurred in the monolayer properties of condensed Ca-H-St monolayers at pH 6.4 and 8.0. A surface micelle transformation model explains the behavior of the condensed Ca-H-St monolayer over the pH range 2-9. The monolayer consisted of un-ionized stearic acid molecules in the pH range 2.0-4.2. The monolayer then behaved as a mixture of stearic acid and calcium distearate molecules with increasing subsolution pH. But upon exceeding a critical degree of dissociation of the film molecules occurring at about pH 6.4, some of the calcium distearate molecules associated into calcium stearate surface micelles. The monolayer became nonuniform above pH 8.0 as the surface micelles aggregated into large clusters of micelles and a gaseous monolayer was interspersed within the holes existing in the monolayer structure.

Electron micrographs of deposited monolayers and multilayers indicated that the average diameter of the surface micelles was approximately 50-60 A. The

critical degree of dissociation appeared to be about 60% stearate from an analysis of the existing chemical composition curves for Ca-H-St monolayers.

Caution must be exercised in determining the transfer ratio during multilayer deposition. Film balance measurements must be corrected for monolayer collapse which simultaneously occurs during the deposition process. Film balance measurements, by themselves, provide an apparent transfer ratio because it is uncertain whether the monolayer is completely and uniformly deposited on the solid substrate. Radioactivity measurements on deposited multilayers are a necessary complement to the film balance measurements. However, ascertainment that the counting rates represent homogeneous deposition is necessary. Autoradiographs of the deposited bilayers provide the additional information necessary to determine the local transfer ratios.

Multilayer deposition was observed to proceed by an adsorption mechanism at the three-phase line interface when the local transfer ratio was differentiated from the apparent value of the transfer ratio. During the initial stages of Ca-H-St multilayer deposition on paraffin, the local transfer ratio of the first and all subsequent layers deposited during the immersion operations was unity. The local transfer ratios of the withdrawal operations were also unity below pH 6.8. However, the local withdrawal transfer ratio of the second layer decreased with increasing subsolution pH above pH 6.8, becoming 0.86 at pH 9.0. With increasing number of layers, the withdrawal transfer ratios above pH 6.8 became progressively smaller.

The Ca-H-St monolayers deposited during the withdrawal operation contain voids or "holes" whenever the local transfer ratio is less than unity and the monolayer is nonuniform. During the subsequent immersion operation, the molecules

of the depositing layer migrate and partially fill the holes present in the underlying layers. As a result, aqueous pores exist within the surface of the immersed multilayer.

The decrease in the local withdrawal transfer ratio above pH 6.8 is attributed, in part, to the incomplete transfer of calcium stearate surface micelles due to their intrinsic low mobility. Thus, fractionation of the monolayer components occur during multilayer deposition with a consequential change in the composition of the multilayer. The decrease in the local withdrawal transfer ratio with increasing number of layers is ascribed to the monolayer not depositing on the created aqueous pores. In addition, the withdrawal transfer ratio is influenced by the surface viscosity and the withdrawal contact angle, but to a lesser extent, at least in the initial stages of multilayer deposition before positive ion adsorption becomes a dominant mechanism.

The changes in the withdrawal contact angle are determined primarily by changes in the solid/liquid interfacial free energy. This interfacial free energy change is due to changes in the orientation of the molecules and the proportion of aqueous pores comprising the immersed monolayer.

Although the polar groups of the calcium distearate molecules were oriented toward the subsolution, the orientation of the un-ionized stearic acid molecules and calcium stearate surface micelles was unexpected. The stearic acid molecules reoriented such that their hydrocarbon tails faced the subsolution. Although the surface micelles also overturned, reorientation did not appear to be complete. In addition, polar groups in the solid substrate surface influence the extent of reorientation.

The driving force for reorientation was attributed to changes in the vicinal water structure. A case is presented which supports the view that the water structure below the head-groups of un-ionized stearic acid monolayers and calcium stearate surface micelles is more highly structured than the water at a hydrocarbon/water interface.

The decrease in film area with compression time which occurred simultaneously during multilayer deposition was due to a slow monolayer collapse process. The formation of bulk phases at the liquid/air interface was demonstrated by electron microscopy. The nature, size, and distribution of the bulk phases is different for stearic acid and calcium stearate monolayers. Although monolayer collapse was observed to be bimolecular in nature, large crystals of stearic acid up to about 3 μm. in diameter and 0.2 μm. in height were formed while only bimolecular platelets up to about 1 μm. in diameter were formed in the calcium stearate monolayer.

There was a difference in the stability of inactive and C^{14}-labeled Ca-H-St monolayers at the liquid/air interface. The radioactive monolayer was more stable below pH 5.0 where the molecules are primarily un-ionized stearic acid; however, the inactive monolayer became more stable above pH 7.8 where the monolayer consists predominantly of calcium stearate surface micelles.

GLOSSARY

Ca-H-St = stearic acid-calcium stearate

Ca^{2+} = calcium divalent ion

ESP = equilibrium spreading pressure

G-M = Geiger-Muller

mD = milliDebye

mM = millimole

NBS = National Bureau of Standards

NRL = Naval Research Laboratory

SEM = scanning electron microscopy

TEM = transmission electron microscopy

TFE = polytetrafluoroethylene

A = area per molecule, $A.^2$

A_{31} = average molecular area at a surface pressure of 31 dynes/cm., $A.^2$/molecule

A_m = area of the monolayer "depositing" on a solid slide, $cm.^2$

A_s = geometric area of the solid slide, $cm.^2$

A_t = total area, $cm.^2$

a = slit width, cm.

B = barrier distance, cm.

C = area occupied by the Teflon end loops, $cm.^2$

c = empirical constant in Joly's equation, $cm.^{-1}$

D = time interval of the slide movement, sec.

E = time interval of uniform deposition, sec.

F = time interval of the initial deposition, sec.

g = gravitational constant

Π = surface or film pressure, dynes/cm.

Π_{31} = surface pressure of 31 dynes/cm.

Π-A = surface pressure-area

$\Delta\Pi$ = surface pressure differential, g./sec.^{2}

L = effective length of the float, cm.

ℓ = slit length, cm.

ℓ_c = lever arm for the calibration weights, cm.

ℓ_f = lever arm for the float, cm.

N_1 = counting rate due to the first layer in a bilayer

N_2 = counting rate due to the second layer in a bilayer

n_o = bulk viscosity of the subsolution, g./cm.-sec.

n_s = surface viscosity, surface poise

Q = flow rate of monolayer through slit, cm.^{2}/sec.

ΔS = entropy change, e.u.

T = temperature

V = potential of the film-covered surface, mv.

V_o = potential of the clean subsolution surface, mv.

ΔV = surface potential, mv.

W = length of the subsolution surface, cm.

W^d_{SLO} = dispersion force contribution to the work of adhesion of the liquid to a film-free solid, erg/cm.^{2}

W_{SLV} = "practical" work of adhesion of a liquid to a solid in equilibrium with the saturated vapor pressure of the liquid, erg/cm.^{2}

w = calibration weight, g.

α = mole fraction of the calcium distearate molecules

β = mole fraction of the calcium stearate surface micelles

γ_c = critical surface tension of a solid, dynes/cm.

γ^d_L = dispersion force contribution to the specific surface free energy of the liquid, erg/cm.^{2}

γ_{LV} = specific surface free energy of the liquid/vapor interface, erg/cm.^{2}

γ_S^d = dispersion force contribution to the specific surface free energy of the solid, erg/cm.^{2}

γ_{SL} = specific surface free energy of the solid/liquid interface, erg/cm.^{2}

γ_{SV} = specific surface free energy of the solid/vapor interface, erg/cm.^{2}

θ = contact angle developed between the multilayer and the film-covered subsolution, degrees

μ_1 = surface dipole moment of the un-ionized stearic acid molecules, mD

μ_2 = surface dipole moment of the calcium distearate molecules, mD

μ_3 = surface dipole moment of the calcium stearate surface micelles, mD

μ_ℓ = apparent surface dipole moment, mD

ρ = transfer ratio

ψ_o = electrostatic potential in the plane of the charged head-groups in the monolayer, mv.

SUGGESTIONS FOR FUTURE RESEARCH

Many exciting and pertinent studies involving the formation and mobility of two-dimensional micelles are suggested by this investigation. Several of these studies are briefly mentioned.

The thermodynamic properties of surface micellization should be evaluated. The hydrocarbon and polar group contributions to the energy and entropy of micelle formation can be separated and evaluated following the analysis of Gershfeld and Pagano (152). The effects of temperature and chain length should be investigated. The stearate concentration at which surface micelle formation begins should be further investigated, both experimentally and theoretically.

The techniques for determining the chemical composition of monolayers should be reevaluated. Comparison of the results on Ca-H-St monolayers over the pH range 2-9 would be invaluable. The question of chemical fractionation arising from the surface micelles can be evaluated with multiple internal reflectance spectroscopy by determining the carboxyl content as a function of the number of deposited layers.

Because of its implications toward calcium transport in biological membranes, the monolayer properties arising from the interaction of calcium and acidic phospholipids should be determined and evaluated in order to ascertain whether two-dimensional micelles occur in the phospholipid systems. The orientation of the molecules at the solid/liquid interface should be determined in a similar manner as in this study.

The influence of other low-energy solids, e.g., polyethylene, polystyrene, polymethyl methacrylate, and nylon, on the deposition behavior of Ca-H-St monolayers should be studied. The different molecular groups may influence the amount

of film transferred and the extent of molecular overturning at the solid/liquid interface.

A transmission electron diffraction study of Ca-H-St monolayers on a nitrocellulose substrate would be of interest. Changes in the crystallinity and lateral spacing of the hydrocarbon chains as a function of pH can be followed by this technique.

The difference in the behavior of inactive and radioactive stearic acid monolayers at the liquid/air interface demands further investigation. The surface viscosity should be measured as a function of the activity of the stearic acid monolayer. The location of the labeled group should also be studied.

ACKNOWLEDGMENTS

The author would like to especially express his appreciation to Mr. John W. Swanson, Chairman of the Thesis Advisory Committee, for his continual support and interest during this study. Thanks are also due Dr. Rajai H. Atalla and Mr. Carl V. Piper for serving on this Committee.

The author is deeply indebted to the following individuals: Mrs. Hilkka M. Kaustinen for the electron micrographs, Mr. Fred R. Sweeney and Mr. Donald E. Beyer for the high-quality photographic work, Mr. Keith W. Hardacker for designing and building the electrical systems for the apparatus used in this study, Mr. Marvin C. Filz, Jr. and Paul F. Van Rossum for constructing much of the apparatus, and Mr. LeRoy G. Borchardt for the gas chromatographic analysis of the fatty acids.

LITERATURE CITED

1. Problem solving in the use of additives. Am. Paper Ind. 50, no. 11:18(1968).

2. Swanson, J. W., and Cordingly, R. H., Tappi 39:684-90(1956).

3. Langmuir, I., Trans. Faraday Soc. 15:62-74(1920).

4. Blodgett, K. B., J. Am. Chem. Soc. 56:495(1934); 57:1007-22(1935).

5. Langmuir, I., Proc. Roy. Soc. (London) A170:1-39(1939).

6. Schulman, J. H., Ann. Rept. Chem. Soc. 36:94-115(1939).

7. Adam, N. K. The physics and chemistry of surfaces. 3rd ed. p. 414-17. London, Oxford University Press, 1941.

8. Harkins, W. D. The physical chemistry of surface films. p. 185-92. New York, Reinhold Publishing Corp., 1952.

9. Bull, H. B. Physical biochemistry. 2nd. ed. p. 235-8. New York, John Wiley & Sons, Inc., 1951.

10. Adamson, A. W. Physical chemistry of surfaces. 2nd ed. p. 195-6. New York, Interscience Publishers, 1967.

11. Gaines, G. L., Jr. Insoluble monolayers at liquid-gas interfaces. p. 326-46. New York, Interscience Publishers, 1966.

12. Bikerman, J. J., Proc. Roy. Soc. (London) A170:130-45(1939).

13. Langmuir, I., Schaefer, V. J., and Sobotka, H., J. Am. Chem. Soc. 59:1751-9 (1937).

14. Stenhagen, E., Trans. Faraday Soc. 34:1328-37(1938).

15. Schaefer, V. J., J. Phys. Chem. 45:681-701(1942).

16. Bateman, J. B., and Covington, E. J., J. Colloid Sci. 16:531-48(1961).

17. Rose, G. D., and Quinn, J. A., J. Colloid Interface Sci. 27:193-207(1968).

18. Goranson, R. W., and Zisman, W. A., J. Chem. Phys. 7:492-505(1939).

19. Blodgett, K. B., and Langmuir, I., Phys. Rev. 51:964-82(1937).

20. Clark, G. L., Sterrett, R. R., and Leppla, P. W., J. Am. Chem. Soc. 57:330-1 (1935).

21. Holley, C., and Bernstein, S., Phys. Rev. 49:403(1936).

22. Holley, C., and Bernstein, S., Phys. Rev. 52:525(1937).

23. Bernstein, S., J. Am. Chem. Soc. 60:1511(1938).

24. Ehlert, R. C., J. Colloid Sci. 20:387-90(1965).

25. Mertens, F. P., and Plumb, R. C., J. Phys. Chem. 67:908-10(1963).

26. Handy, R. M., and Scala, L. C., J. Electrochem. Soc. 113:109-16(1966).

27. Stephens, J. F., J. Colloid Interface Sci. 38:557-66(1972).

28. Gustafsson, C., Tammela, V., and Lindh, T., Paper and Timber (Finland) 36:269-74(1954).

29. Zisman, W. A., Adv. Chem. Ser. 87:1-9(1968).

30. Robbins, M. L., and LaMer, V. K., J. Colloid Sci. 15:123-54(1960).

31. Gaines, G. L., Jr., J. Colloid Sci. 15:321-39(1960).

32. Schenkel, J. H., and Kitchener, J. A., Nature 182:131(1958).

33. Gaines, G. L., Jr., J. Phys. Chem. 63:1322-4(1959).

34. Langmuir, I., and Schaefer, V. J., J. Am. Chem. Soc. 59:2400-14(1937).

35. Major, E. H., Jr. The reaction between tetrahydroabietic acid monolayers and aluminum ions. I. The influence of oxalate. Doctor's Dissertation. Appleton, Wis., The Institute of Paper Chemistry, 1969. 108 p.

36. Bergeron, J. A., and Gaines, G. L., Jr., J. Colloid Interface Sci. 23:292-4 (1967).

37. Goddard, E. D., and Ackilli, J. A., J. Colloid Sci. 18:585-95(1963).

38. Dreher, K. D., and Sears, D. F., Trans. Faraday Soc. 62:741-9(1966).

39. Luner, P., and Kempf, U., Tappi 53:2069-76(1970).

40. Washburn, E. R., and Wakeham, H. R. R., J. Am. Chem. Soc. 60:1294-6(1938).

41. Meyers, R. J., and Harkins, W. D., J. Chem. Phys. 5:601-3(1937).

42. Trurnit, H. J., and Lauer, W. E., Rev. Sci. Instr. 30:975-81(1959).

43. Schulman, J. H., and Teorell, T., Trans. Faraday Soc. 34:1337-42(1938).

44. Harkins, W. D., and Kirkwood, J. G., J. Chem. Phys. 6:53, 298(1938).

45. Joly, M., Kolloid-Z. 89:26-35(1939).

46. Crisp, D. J., Trans. Faraday Soc. 42:619-35(1946).

47. Jarvis, N. L., J. Phys. Chem. 69:1789-97(1965).

48. McIntyre, D. E. A study of dynamic wettability on a hydrophobic surface. Doctor's Dissertation. Appleton, Wis., The Institute of Paper Chemistry, 1969. 159 p.

49. Adam, N. K., Adv. Chem. Ser. 43:52-6(1964).

50. Fox, H. W., and Zisman, W. A., J. Colloid Sci. 5:514-31(1950).

51. Fox, H. W., and Zisman, W. A., J. Colloid Sci. 7:109-21(1952).

52. Hall, C. E. Introduction to electron microscopy. p. 313-15. New York, McGraw-Hill Book Company, Inc., 1953.

53. Overman, R. T., and Clark, H. M. Radioisotope techniques. p. 114-19. New York, McGraw-Hill Book Company, Inc., 1960.

54. Yaffe, L., and Justus, K. M., J. Chem. Soc. 1949:s341-51.

55. Spink, J. A., J. Colloid Interface Sci. 23:9-26(1967).

56. Dunning, C. E. An examination of longleaf pine cell-wall morphology by electron microscopy of single fibers. Doctor's Dissertation. Appleton, Wis., The Institute of Paper Chemistry, 1968. 409 p.

57. Ref. (7), p. 46-55.

58. Ref. (11), p. 186-8.

59. Nutting, G. C., and Harkins, W. D., J. Am. Chem. Soc. 61:1180-7(1939).

60. Ref. (8), p. 151-2.

61. Sasaki, T., and Matuura, R., Bull. Chem. Soc. Japan 24:274-8(1951).

62. Spink, J. A., and Sanders, J. V., Trans. Faraday Soc. 51:1154-65(1955).

63. Matsubara, A., Matuura, R., and Kimizuka, H., Bull. Chem. Soc. Japan 38:369-73(1965).

64. Deamer, D. W., and Cornwell, D. G., Biochim. Biophys. Acta 116:555-62(1966).

65. Deamer, D. W., Meek, D. W., and Cornwell, D. G., J. Lipid Research 8:255-63 (1967).

66. Spink, J. A., J. Colloid Sci. 18:512-25(1963).

67. Harkins, W. D., and Anderson, T. F., J. Am. Chem. Soc. 59:2189-97(1937).

68. Rogeness, G., and Abood, L. G., Arch. Biochem. Biophys. 106:483-8(1964).

69. Ref. (8), p. 153.

70. Kavanau, J. L. Structure and function in biological membranes. p. 139. San Francisco, Holden-Day, Inc., 1965.

71. Shah, D. O., J. Colloid Interface Sci. 32:577-83(1970).

72. Ref. (11), p. 221.

73. Ryan, J. P., and Shepard, J. W., J. Phys. Chem. 59:1181-2(1955).

74. Salem, L., J. Chem. Phys. 37:2100-13(1962).

75. Wolstenholme, G. A., and Schulman, J. H., Trans. Faraday Soc. 46:475-87(1950).

76. Durham, K., J. Appl. Chem. 5:686-92(1955).

77. Ref. (11), p. 91-6.

78. Sanders, J. V., and Spink, J. A., Nature 175:644-5(1955).

79. Goddard, E. D., Smith, S. R., and Kao, O., J. Colloid Interface Sci. 21:320-30(1966).

80. Ref. (11), p. 73.

81. Harkins, W. D., and Fischer, E. K., J. Chem. Phys. 1:852-62(1933).

82. Bouhet, C., Ann. de Physique 15:5-130(1931).

83. Zocher, H., and Stiebel, F., A. Physik. Chem. (Leipzig) A147:401-35(1930).

84. Sheppard, E., Bronson, R. P., and Tcheurekdjian, N., J. Colloid Sci. 19:833-7(1964).

85. Ries, H. E., Jr., and Kimball, W. A., J. Phys. Chem. 59:94-5(1955); Proc. Intern. Congr. Surface Activity, 2nd London 1:75-84(1957); Nature 181:901(1958).

86. Sheppard, E., Bronson, R. P., and Tcheurekdjian, N., J. Colloid Sci. 20:755-65(1965).

87. Cook, H. D., and Ries, H. E., Jr., J. Phys. Chem. 60:1533-6(1956).

88. Addink, N. W. H., J. Chem. Phys. 2:574-7(1934).

89. Blank, M., and Britten, J. S., J. Colloid Sci. 20:789-800(1965).

90. Sebba, F., and Briscoe, H. V. A., J. Chem. Soc. 1940:106-14.

91. Langmuir, I., and Schaefer, V. J., J. Franklin Inst. 235:119-62(1943).

92. Archer, R. J., and LaMer, V. K., J. Phys. Chem. 59:200-8(1955).

93. Zisman, W. A., Adv. Chem. Ser. 43:1-51(1964).

94. Bernett, M. K., and Zisman, W. A., J. Phys. Chem. 67:1534-40(1963).

95. Smith, J. W. Electric dipole moments. p. 119-25. London, Butterworths Scientific Publications, 1955.

96. Davies, J. T., and Rideal, E. K. Interfacial phenomena. p. 235-7. New York, Academic Press, 1961.

97. Ref. (53), p. 405.

98. Kakihara, Y., Himmelblau, D. M., and Schechter, R. S., J. Colloid Interface Sci. 30:200-10(1969).

99. Larsson, K., Lundquist, M., Stallberg-Stenhagen, S., and Stenhagen, E., J. Colloid Interface Sci. 29:268-78(1969).

100. Miller, J. R., and Berger, J. E., J. Phys. Chem. 70:3070-5(1966).

101. Smith, T., J. Colloid Interface Sci. 25:443-61(1967).

102. Bagg, J., Abramson, M. B., Fichman, M., Haber, J. D., and Gregor, H. P., J. Am. Chem. Soc. 86:2759-63(1964).

103. Bagg, J., Haber, M. D., and Gregor, H. P., J. Colloid Interface Sci. 22:138-43(1966).

104. Ref. (11), p. 147.

105. Cary, A., and Rideal, E. K., Proc. Roy. Soc. (London) A109:318-30(1925).

106. Clark, G. L., and Leppla, P. W., J. Am. Chem. Soc. 58:2199-201(1936).

107. Yiannos, P. N. Molecular reorientation of some fatty acids when in contact with water. Doctor's Dissertation. Appleton, Wis., The Institute of Paper Chemistry, 1960. 115 p.

108. Johnson, R. E., Jr., and Dettre, R. H., Adv. Chem. Ser. 43:112-35(1964).

109. Ref. (52), p. 335.

110. Echlin, P., and Hyde, P. J. W. The rationale and mode of application of thin films to non-conducting materials. In Johari and Corvin's Scanning electron microscopy/1972. p. 138-46. Chicago, IIT Research Institute, 1972.

111. Beischer, D. E., Science 115:682-4(1952).

112. Gregg, S. J., and Widdowson, E. E., Nature 144:666-7(1939).

113. Roberts, R. W., and Gaines, G. L., Jr., Trans. Nat. Vacuum Symp. 9:515-18(1962).

114. Gaines, G. L., Jr., and Roberts, R. W., Nature 197:787(1963).

115. Spink, J. A., J. Colloid Interface Sci. 24:61-70(1967).

116. Ref. (52), p. 329-31.

117. Hanna, R. B., J. Polymer Sci., Part C, 36:409-13(1971).

118. Shanes, A. M., and Gershfeld, N. L., J. Gen. Physiol. 44:345-63(1960).

119. Kimizuka, H., and Koketsu, K., Nature 196:995-6(1962).

120. Webb, J., and Danielli, J. F., Nature 146:197-8(1940).

121. Adam, H. K., and Zull, J. E., J. Colloid Interface Sci. 34:272-7(1970).

122. Hauser, H., and Dawson, R. M. C., European J. Biochem. 1:61-9(1967).

123. Ellis, J. W., and Pauley, J. L., J. Colloid Sci. 19:755-64(1964).

124. Sobotka, H., Demeny, M., and Chanley, J. D., J. Colloid Sci. 13:565-8(1958).

125. Langmuir, I., and Schaefer, V. J., J. Am. Chem. Soc. 58:284-7(1936).

126. Havinga, E., Rec. Trav. Chim. Pays-Bas 71:72-9(1952).

127. Schulman, J. H., and Hughes, A. H., Proc. Roy. Soc. (London) A138:430-50 (1932).

128. Davies, J. T., Proc. Roy. Soc. (London) A208:224-47(1951).

129. Shah, D. O., and Schulman, J. H., J. Lipid Research 6:341-9(1965).

130. Stanley, E., Nature 175:165(1955).

131. Ablett, R., Phil. Mag. 46:244-56(1923).

132. Yarnold, G. D., and Mason, B. J., Proc. Phys. Soc. B62:125-8(1949).

133. Rose, W., and Heins, R. W., J. Colloid Sci. 17:39-48(1962).

134. Elliott, G. E. P., and Riddiford, A. C., J. Colloid Interface Sci. 23:389-98 (1967).

135. Young, T., Phil. Trans. Roy. Soc. (London) 16:65(1805); Ref. (95).

136. Bernett, M. K., and Zisman, W. A., J. Phys. Chem. 63:1241-6(1959).

137. Bernett, M. K., and Zisman, W. A., J. Phys. Chem. 63:1911-6(1959).

138. Ray, B. R., Anderson, J. R., and Scholz, J. J., J. Phys. Chem. 62:1220-7(1958).

139. Luner, P., and Sandell, M., J. Polymer Sci., Part C, 28:115-42(1969).

140. Shafrin, E. G., and Zisman, W. A., J. Phys. Chem. 64:519-24(1960).

141. Jura, G., and Harkins, W. D., J. Colloid Sci. 1:137-40(1946).

142. Ref. (70), p. 9.

143. Blank, M., and Britten, J. S. Physical principles in monolayer and membrane permeation. In Snell's Physical principles of biological membranes. p. 143-63. Gordon and Breach, Science Publishers, Inc., 1969.

144. Wark, I. W., and Cox, A. B., Am. Inst. Mining Met. Engrs., Tech. Publ. No. 461, 1932. 48 p.

145. Levine, O., and Zisman, W. A., J. Phys. Chem. 61:1188-96(1957).

146. Padday, J. F., Soc. Chem. Ind. (London) Monograph 25:234-50(1967).

147. Seimiya, T., Saito, S., and Sasaki, T., J. Colloid Interface Sci. 30:153-8 (1969).

148. Frank, H. S., and Evans, M. W., J. Chem. Phys. 13:507-32(1945).

149. Ref. (96), p. 369.

150. Mukerjee, P., Adv. Colloid Interface Sci. 1:241-75(1967).

151. Ref. (70), p. 324.

152. Gershfeld, N. L., and Pagano, R. E., J. Phys. Chem. 76:1231-7(1972).

153. Ref. (70), p. 92.

154. Ref. (70), p. 199.

155. Dupre, A. Theorie mechanique de la chaleur. Paris, Gauthier-Villars, 1869. 369 p.; Ref. (95).

156. Ray, B. R., and Bartell, F. E., J. Colloid Sci. 8:214-23(1953).

157. Padday, J. F., Proc. Intern. Congr. Surface Activity, 3rd Cologne 2:457-63 (1960).

158. Phillips, M. C., and Riddiford, A. C., J. Colloid Interface Sci. 22:149-57 (1966).

159. Fowkes, F. M., Adv. Chem. Ser. 43:99-111(1964).

160. Sobotka, H., J. Colloid Sci. 11:435-44(1956).

161. Debye, P., Ann. New York Acad. Sci. 51:575-92(1949).

162. Poland, D. C., and Scheraga, H. A., J. Colloid Interface Sci. 21:273-83(1966).

163. Langmuir, I., J. Chem. Phys. 1:756-76(1933).

164. Harkins, W. D., and Boyd, E., J. Phys. Chem. 45:20-43(1941).

165. Epstein, H. T., J. Phys. Colloid Chem. 54:1053-69(1950).

166. Ref. (9), p. 230.

167. Chattoraj, D. K., and Chatterjee, A. K., J. Colloid Interface Sci. 21:159-69 (1966).

168. Ohki, S., and Aono, O., J. Colloid Interface Sci. 32:270-81(1970).

APPENDIX I

MATERIALS

STEARIC ACID PURITY

It is imperative that the materials used in surface-chemical studies be of extremely high purity, and they must be characterized with respect to chemical composition. Radioactive materials are notorious for containing appreciable chemical impurities although they are of high radiochemical purity. Consequently, three small trial samples (< 100 μc.) of stearic-1-C^{14} acid were obtained from different suppliers.

A sample of high-purity stearic acid from Fluka A.G. and the three radioactive samples were converted to their methyl esters by the method supplied with Diazald (Aldrich Chemical Co.). The methyl esters were subjected to gas chromatographic analysis with an Aerograph 1520-1B chromatograph under the following conditions: 1 μl. injections of cyclohexane solutions of the esters; injection temperature at 190°C.; detection temperature at 235°C.; column temperature isothermal at 170°C. for 15 minutes, then programmed for a 2°C. rise per minute to 220°C.; flow rate at 30 ml./min. for the helium carrier gas; H_2 flame detector; and 8% EGSS-X (Applied Science) on Gas Chrom Q 100/120, 6 feet x 1/8 inch, stainless steel column. The chemical composition was determined from the percentage of total peak area for each peak. The results are presented in Table XIX.

Surface pressure-area isotherms of the stearic acids were also obtained in a further assessment of their purity. The results shown in Fig. 61 clearly indicate the desirability of this surface-chemical technique. Because the stearic-1-C^{14} acid monolayers were spread directly from the vial solutions, their molecular area was not accurately known. For comparative purposes, the surface pressure-area

TABLE XIX

GAS CHROMATOGRAPHIC PURITY OF THE STEARIC ACIDS

Supplier	Specific Activity, mc./mM	Solvent[a]	Radio-chemical Purity, %	Purity by Gas Chromatography Saturated Fatty Acids, %					
				C_{14}	C_{16}	C_{17}	C_{18}	C_{20}	C_{22}
Fluka A.G.	Inactive	n-Hexane	--	--	0.2	--	99.6	--	0.2
Dhom Products, Ltd.	58	Benzene	99+	--	--	--	99.5	0.2	0.3
Sample X	54	n-Hexane	98+				>99.5[b]		
Sample Y	55.5	Benzene	99+	5.9	2.5	0.2	91.4	--	--

[a] Used as received except for the inactive stearic acid which was dissolved in n-hexane.

[b] Sensitivity of instrument was set too low to determine the contribution of the other fatty acids more accurately than that given.

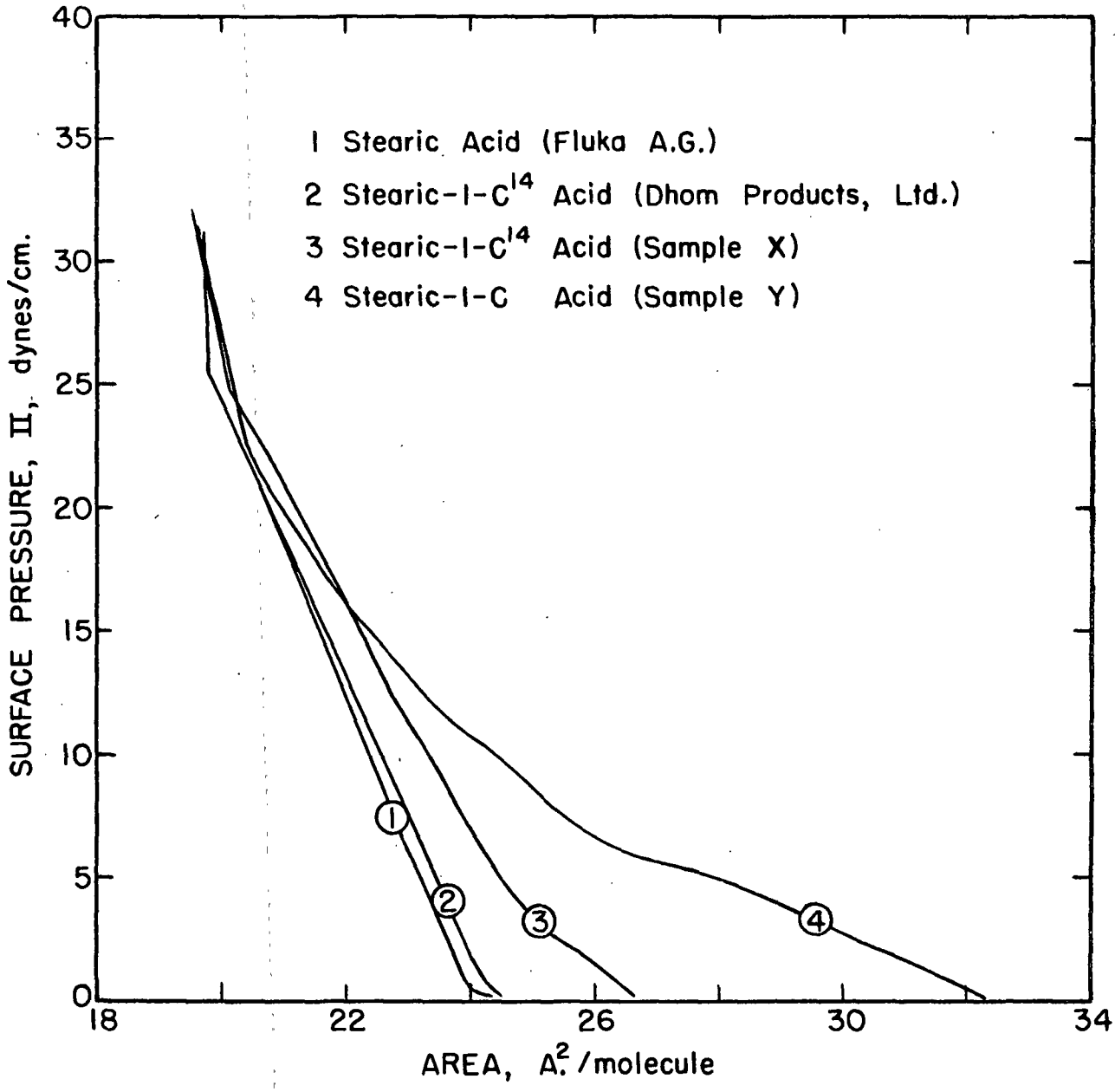

Figure 61. The Surface Pressure-Area Isotherms of Stearic Acid Monolayers on pH 2.00 Subsolutions (Corrected to Have the Same Area at 30 Dynes/cm. as the Inactive Stearic Acid). Compression Rate = 1 A.^{2}/Molecule/Min.; $\underline{T}$ = 20.7°C.

isotherms of the stearic-1-C^{14} acids were corrected to have the same molecular area at 30 dynes/cm. as the inactive stearic acid. Although Sample X is supposed to have a chemical purity of > 99.5%, the deviation of the surface pressure-area isotherm from the other "pure" stearic acids implies that lower homologues of the saturated fatty acid series make a substantial contribution to the observed behavior when present even in very small amounts.

SURFACE-ACTIVE IMPURITIES IN HEXANE

The hexane was tested for surface-active impurities by delivering 15.0 ml. to a clean pH 2.00 subsolution surface. After evaporation of the solvent, a detectable surface pressure was developed on compression. The surface pressure was measured as a function of the area occupied by the nonvolatile surface-active contamination. The results are shown in Fig. 62.

The area per milliliter of purified n-hexane at a surface pressure of 1 dyne/cm. is 1.93 $cm.^2/ml$. The area occupied by a monolayer consisting of 1 g. of stearic acid at a surface pressure of 1 dyne/cm. is 5.08×10^6 $cm.^2/g$. The amount of nonvolatile impurity, reported as stearic acid, per milliliter of hexane is $1.93/5.08 \times 10^6 = 3.80 \times 10^{-7}$ g./ml. This represents the error in the concentration of the spreading solution due to impurities. An error in the area/molecule of stearic acid at $\underline{II}$ = 1 dyne/cm. of +0.03% or approximately +0.01 $A.^2$ results from using a $5 \times 10^{-3}\underline{M}$ spreading solution. This error represents the maximum possible error due to impurities in n-hexane because the exerted surface pressure arises from all the surface-active contaminants in the spreading solvent and subsolution.

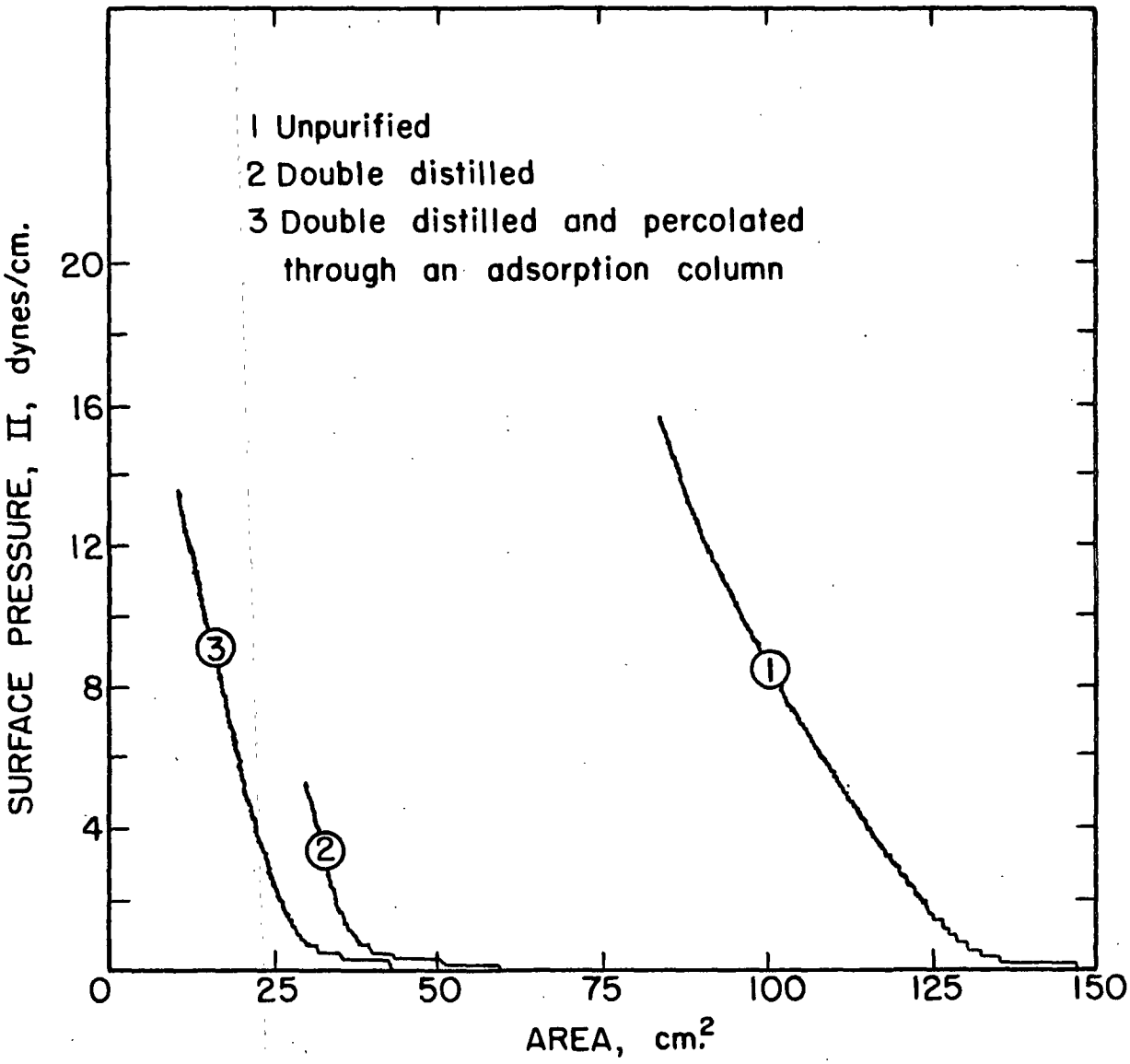

Figure 62. The Surface Pressure-Area Isotherms for Nonvolatile Impurities in n-Hexane Obtained by Allowing 15.0 ml. to Evaporate from a pH 2.00 Subsolution. $\underline{T}$ = 20.2°C.

PARAFFIN

Sun Oil paraffin wax number 5512 (melting range 63-69°C.) was obtained for this investigation. The paraffin was purified to remove possible surface-active impurities. Portions of the paraffin were melted and passed through a 500-mm. Liebig condenser packed with activated silica gel. The condenser jacket was heated with steam, and the silica gel was renewed after 1200 ml. of molten paraffin were processed. The first 300-ml. portion was discarded, and the remainder of the paraffin was collected.

The purified paraffin was tested for surface-active impurities by dropping small pieces of it on the surface of distilled water sprinkled with ignited talc. No spreading was observed.

APPENDIX II

EXPERIMENTAL PROCEDURES

SUBSOLUTION TEMPERATURE MEASUREMENT

A thermistor (Fenwal GB31P2, Framingham, Mass.) was selected to measure the subsolution temperature. The temperature measuring system using the thermistor as one arm of a Wheatstone bridge circuit was designed to be sensitive to ±0.01°C. The glass probe thermistor was mounted in 5-mm. O.D. glass tubing with paraffin wax. The glass tubing was mounted in a Teflon holder attached to an extension arm which was mounted on a vertical Rapid Advance Unislide assembly.

The thermistor calibration was performed both in water and air. For these calibrations, the thermistor was placed in a specially designed brass chamber containing water or air. The container was suspended in a constant temperature water bath. The thermistor was calibrated over the temperature range of 18.0 to 25.5°C. The 95% confidence limits on the temperature obtained from an average of four repeat determinations of the scale reading of the thermistor bridge circuit was ±0.01°C. Because the temperature of the bath was only accurately known to ±0.02°C. and was maintained within ±0.01°C., the estimated error was ±0.04°C. for the determined temperature.

The temperature of the bulk subsolution was measured by immersing the thermistor 7 mm. below the water surface. The initial bulk temperature of the substrate dropped about 1°C. during an experimental run although the temperature was constant to within ±0.1°C. during the actual II-A isotherm determination. The temperature over the dipping well was about 0.2°C. higher than that of the subsolution behind the float. When a monolayer was spread on the subsolution, the temperature over the dipping well appeared to be slightly higher (< 0.1°C.) than

if a monolayer were not present, apparently due to the inhibition of the evaporation rate by the monolayer. It appeared that the temperature of the subsolution was maintained within ±0.3°C. of the measured temperature.

SURFACE VISCOSITY CALCULATIONS

The computer program shown in Table XX was used to calculate the surface viscosity from Joly's equation (45). In addition, the surface viscosities determined from the equations of Meyers and Harkins (41) and Harkins and Kirkwood (44) were also calculated. A subroutine in the program calculated the bulk viscosity of the subsolution, $\underline{n}_o$, from the subsolution temperature. The input data of the program are L1, identification; DP, pressure differential; A, slit width; CA, monolayer area through slit; T, time interval for monolayer area; L, slit length; CNO, $\underline{cn}_o$ interpolated value; CT, temperature; and PI, 3.14159.

PARAFFIN SURFACE PREPARATION

The paraffin-coated microscope slides were formed by dipping and withdrawing the slide three times from molten paraffin. The procedure for preparing the paraffin surfaces was as follows:

1. The microscope slide was cleaned by
   a. abrading with 180 grit Carbimet silicon carbide paper (Buehler Ltd.),
   b. washing in soap and water, rinsing, and drying,
   c. dipping in warm chromic-sulfuric acid solution,
   d. rinsing copiously with distilled water, drying in a grease-free oven, and then cooling in a desiccator.

2. The purified paraffin was melted very slowly in a clean 250-ml. beaker on a hot plate slightly above the melting point temperature of the

TABLE XX

COMPUTER PROGRAM FOR CALCULATING SURFACE VISCOSITY

```
C
C      SEARCH FOR THE VALUE OF 'NS' WHICH SOLVES JOLY'S EQUATION
C
       DIMENSION X(200),Y(200)
       DOUBLE PRECISION DP,A,CA,T,L,CNO,NO,PI,Q,R1,R2,QP,A2,NS,DIV,MULT
       DOUBLE PRECISION CT,NO1,L1
     1 READ(5,9001) L1,DP,A,CA,T,L,CNO,CT,PI
       WRITE(6,9003) L1
 9003 FORMAT('1  SAMPLE IDENTIFICATION =',A5///)
       Q = CA/T
       A3 = A**3
       NO1 = 1301./(998.333+ 8.1855*(CT-20.) + .00585*(CT-20.)**2)
       NO1 = EXP(2.30258509*(NO1 - 3.30103))
       NO = .010019 + (NO1 - .010050)
       WRITE(6,9002) DP,A,Q,L,A3
       R1 = (DP*A**3)/(12.*Q*L)
       R2 = (DP*A**3)/(12.*Q*L) - (A*NO)/PI
     5 TRM1 = DP/(L*CNO)
       WRITE(6,9002) Q,R1,R2
       N = 0
       A2 = A/2.
       DIV = 2.
       MULT = 2.
       ISIG = 1
       NS = (R1 - R2)/R1*(R1 - R2)
     6 QP = TRM1*(A-2.*DSQRT(NS/CNO)*DTANH(DSQRT(CNO/NS)*A2))
       N = N + 1
       WRITE(6,8001) N,Q,NS,QP
 8001 FORMAT(I4,3D15.6)
       IF(N - 200) 100,100,101
  100 X(N) = NS
       Y(N) = QP
  101 IF(DABS(QP - Q) - .000001) 10,10,7
    7 IF(QP - Q) 9,8,8
    8 NS = NS + (NS/DIV)
       IF(ISIG) 81,81,6
   81 DIV = DIV*2.
       ISIG = 1
       GO TO 6
    9 NS = NS - (NS/DIV)
       IF(ISIG) 6,6,91
   91 DIV = DIV*2.
       ISIG = -1
       GO TO 6
   10 WRITE(6,9002) DP,CNO,CT,NO1,NO,Q,NS
       XMIN = X(1)
       XMAX = X(1)
       YMIN = Y(1)
       YMAX = Y(1)
       DO 11 I = 2,N
       XMIN = AMIN1(XMIN,X(I))
       XMAX = AMAX1(XMAX,X(I))
       YMIN = AMIN1(YMIN,Y(I))
   11 YMAX = AMAX1(YMAX,Y(I))
 9001 FORMAT(A5,F5.0,7F10.0)
C      CALL PLOT (X,Y,N,XMIN,XMAX,YMIN,YMAX,1,0)
 9002 FORMAT('0',7D15.8)
       GO TO 1
       END
```

paraffin. At the end of four hours, the temperature of the paraffin was 77-78°C.

3. The microscope slide was dipped into the molten paraffin. When the paraffin completely wetted the glass slide, the slide was withdrawn.

4. The paraffin-coated slide was held in a vertical position until the paraffin solidified. The slide was gently "fanned" in the air for thirty seconds to cool the paraffin.

5. The excess build-up of paraffin at the bottom of the slide was melted by touching the slide bottom to a heated, clean aluminum weighing dish on another hot plate.

6. Step (4) was repeated.

7. The second layer of paraffin was deposited by dipping and withdrawing the slide from the molten paraffin. The entire sequence required one to two seconds.

8. Steps (4), (5), and (6) were repeated.

9. The third layer of paraffin was deposited as in Step (7).

10. Steps (4), (5), and (6) were repeated.

Generally, it was necessary to produce a number of surfaces at one time to ensure having a sufficient number of slides available for multilayer deposition. Only the highest quality paraffin-coated slides were selected because dust particles occasionally contaminated the surfaces. The paraffin slides were stored in a grease-free desiccator and used within 24 hours.

OPERATING POTENTIAL SELECTION FOR G-M COUNTER

For a given radioactive source, the counting rate of a G-M tube varies with the applied potential. An operating potential is selected on the plateau of the curve where the counting rate is relatively insensitive to voltage change. A 0.165 μc. C^{14}-source (New England Nuclear Corp.) was placed under the G-M tube, and a counting rate versus applied voltage curve was obtained. The characteristic curve for the G-M tube (Nuclear Chicago Model 108, Serial No. 1466) is shown in Fig. 63.

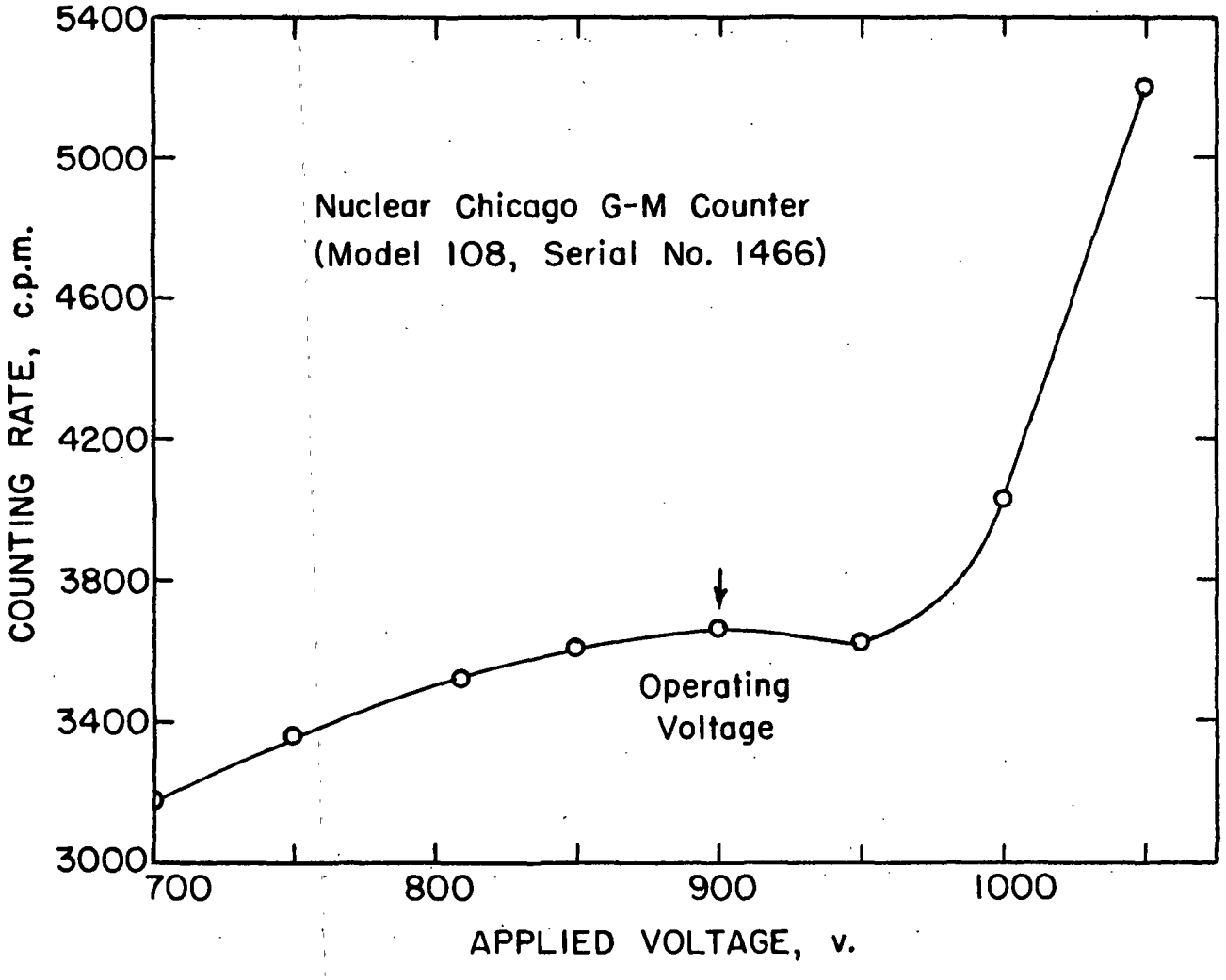

Figure 63. Characteristic Curve for the G-M Tube

SELECTION OF OPTIMUM COUNTING DISTANCE

The counting efficiency of a G-M tube is very sensitive to the sample geometry, i.e., the sample arrangement on the mounting plate as well as the distance of the sample from the sensitive volume of the counter. A C^{14}-labeled bilayer on paraffin was placed under the G-M tube, and the net counting rate was determined as a function of the distance between the brass mask of the G-M tube and the paraffin surface. The results are shown in Fig. 64. The counting rate is essentially insensitive to minor distance changes below a separation of 1 mm.

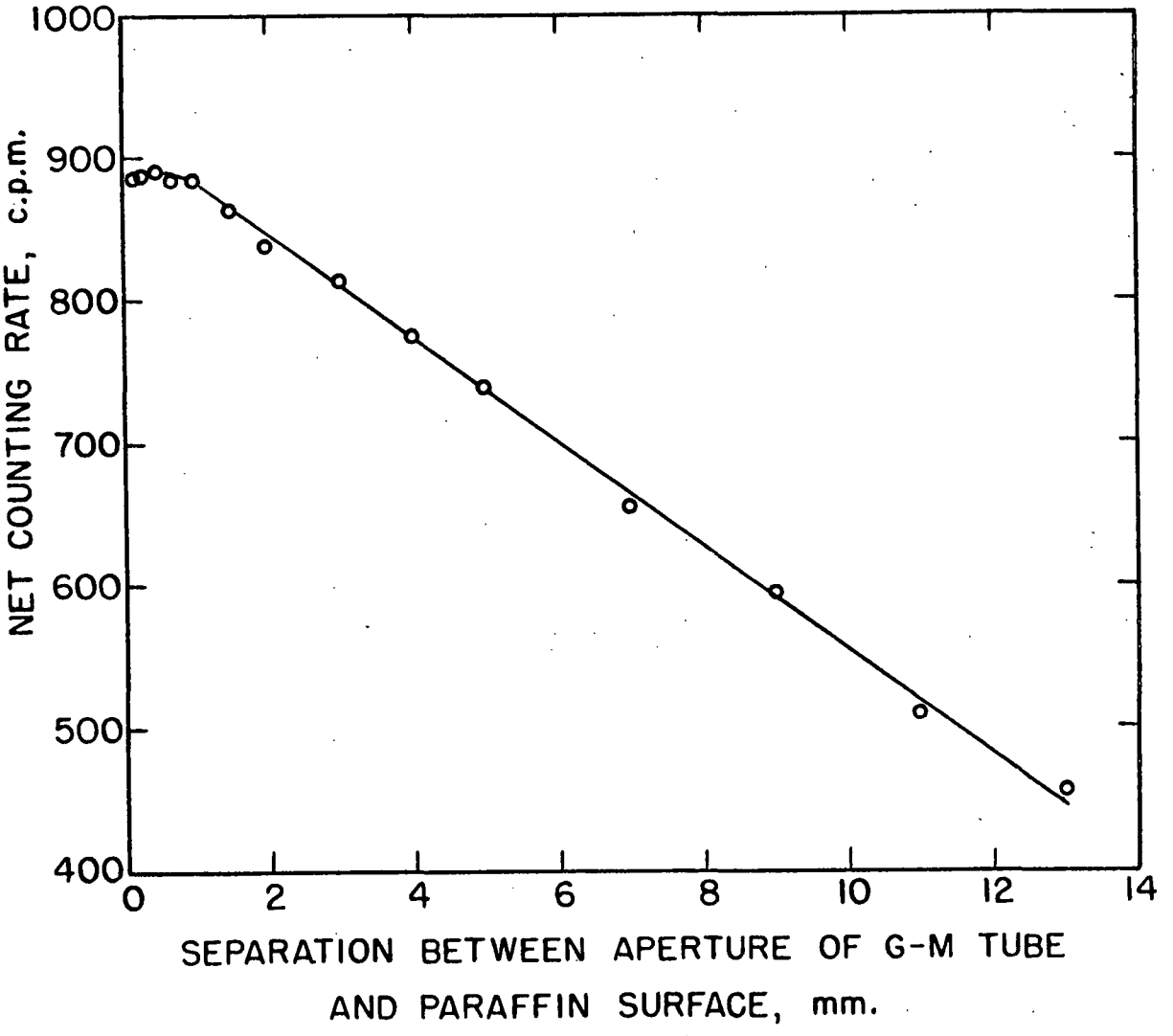

Figure 64. Determination of the Optimum Height of the Counter Aperture Above a Ca-H-St Bilayer Deposited on Paraffin at 31 Dynes/cm. pH = 5.9; $\underline{T}$ = 20.5°C.

TANGENTOMETER ERROR ESTIMATE

The accuracy of the contact angle tangentometer was determined by measuring constructed contact angles from 10 to 120 degrees. Angles were geometrically constructed by making plane right triangles having the approximate angles with a T-square, compass, and triangle. The geometric contact angles were determined by measuring the length of the hypotenuse and the side opposite the angle of the right triangle. A series of eight measurements were made with the tangentometer on each of these constructed contact angles.

The average contact angles determined with the tangentometer agreed very well with the geometric values. However, the results which are shown in Table XXI indicate that the agreement was slightly better for contact angles above 40°. The average 95% confidence limits of the average contact angles was ±0.18 degree.

TABLE XXI

SUMMARY OF MEASUREMENTS WITH THE CONTACT ANGLE TANGENTOMETER ON CONSTRUCTED CONTACT ANGLES

Nominal Contact Angle, °	Constructed[a] Contact Angle, °	Average Contact[b] Angle Measured with Tangentometer, °
10	7.38 ± 1.50[c]	8.53 ± 0.16[c]
20	18.59 ± 0.56	18.96 ± 0.30
30	29.41 ± 0.42	30.06 ± 0.21
40	38.66 ± 0.19	39.08 ± 0.23
50	48.29 ± 0.14	48.61 ± 0.17
60	59.00 ± 0.13	59.06 ± 0.14
70	70.14 ± 0.04	70.20 ± 0.21
80	79.38 ± 0.04	79.21 ± 0.13
90	90.11 ± 0.04	90.08 ± 0.17
100	100.62 ± 0.04	100.79 ± 0.13
110	109.86 ± 0.04	109.80 ± 0.21
120	121.00 ± 0.13	120.94 ± 0.14

[a] Average of six measurements.

[b] Average of eight measurements to the nearest tenth degree.

[c] 95% Confidence limits.

PHOTOGRAPHIC ENLARGER ALIGNMENT

The alignment of the enlarger was checked to determine whether the contact angles were distorted in the photographic enlargement process. This was accomplished by geometrically constructing contact angles on acetate film, enlarging the image onto Ortho film, and measuring the angles with the tangentometer. The results are given in Table XXII. The enlarger system was adequately aligned as shown by the good agreement between the contact angles.

TABLE XXII

ALIGNMENT VERIFICATION OF PHOTOGRAPHIC ENLARGER WITH ACETATE FILM

Method of Measurement	Contact Angle of Gage Line, ° Right	 Left
Construction[a]	44.32 ± 0.17[c]	45.57 ± 0.14[c]
Tangentometer[b]	44.86 ± 0.18	46.33 ± 0.09

[a] Average of six measurements.

[b] Average of nine measurements, three from each of three negatives.

[c] 95% Confidence limits.

CAMERA AND SLIDE ASSEMBLY ALIGNMENT

The alignment of the camera and slide assembly was verified by photographing a standard angle on the slide and measuring the angle with a tangentometer. Brass 45° gage blocks were machined and mounted onto 2 by 3-inch glass microscope slides. The slides were then inserted in the Teflon holder, aligned over the dipping well, and photographed. The angles of the gage blocks were measured with the machinist's precision level protractor, and the photographed contact angles were measured with

the tangentometer. The results are presented in Table XXIII. The good agreement between the two contact angles confirmed that the photographic system was adequately aligned.

TABLE XXIII

CONTACT ANGLE MEASUREMENTS OF 45° GAGE BLOCKS MOUNTED ONTO GLASS SLIDES

Gage Block Width, in.	Method of Measurement	Contact Angle of Gage Block, °: Right	Left
1/4	Bevel protractor[a]	44.82 ± 0.09[c]	44.62 ± 0.13[c]
	Tangentometer[b]	45.64 ± 0.09	45.18 ± 0.11
1	Bevel protractor	44.93 ± 0.12	44.88 ± 0.17
	Tangentometer	44.49 ± 0.14	45.03 ± 0.08

[a]Average of six measurements.

[b]Average of nine measurements, three from each of three negatives.

[c]95% Confidence limits.

APPENDIX III

EXPERIMENTAL DATA

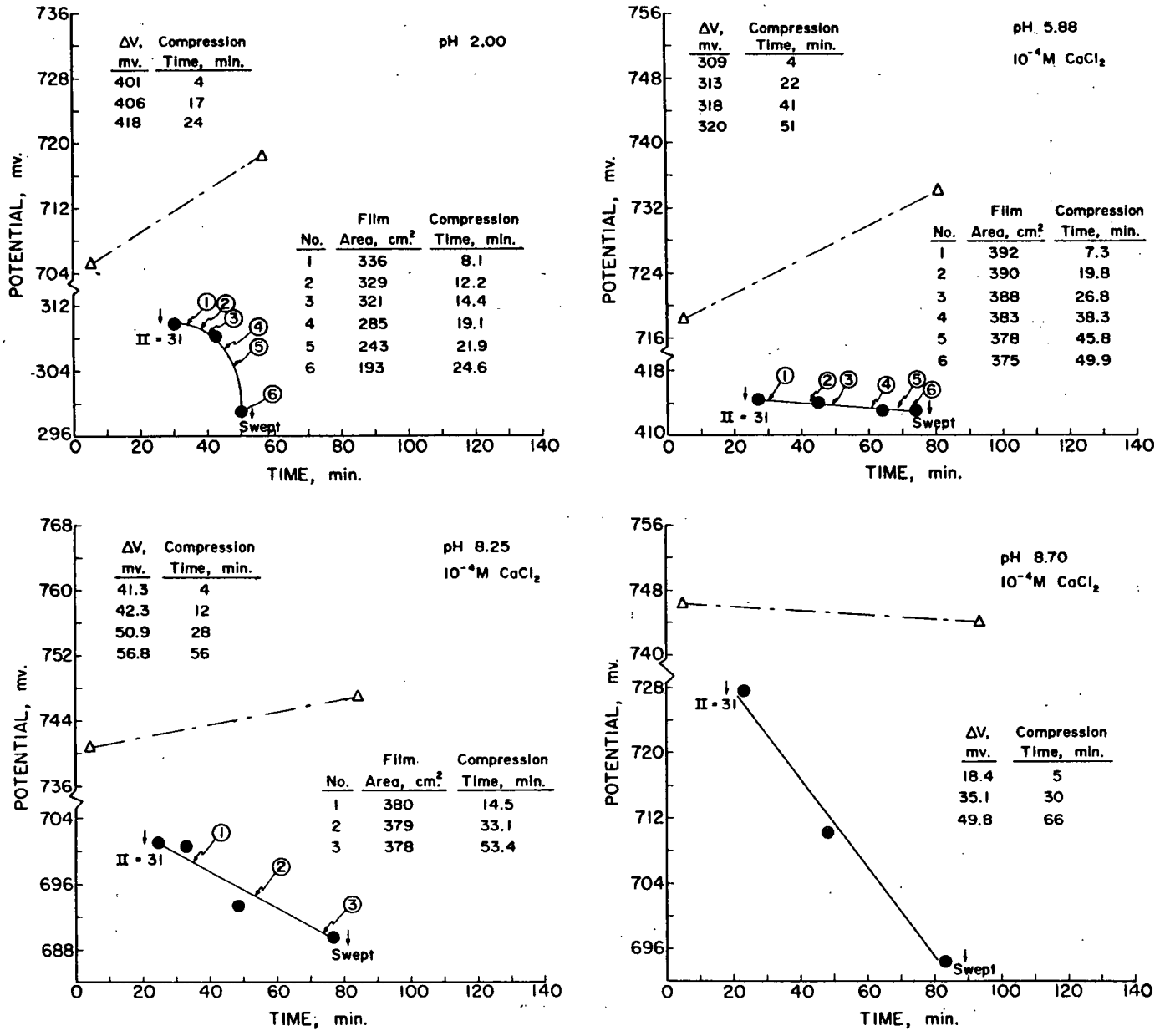

Figure 65. Variation of the Potential of a Clean (Δ) and Stearic Acid Film-Covered (0) Subsolution Surface with Time. II = 31 Dynes/cm.; T = 20.6°C.

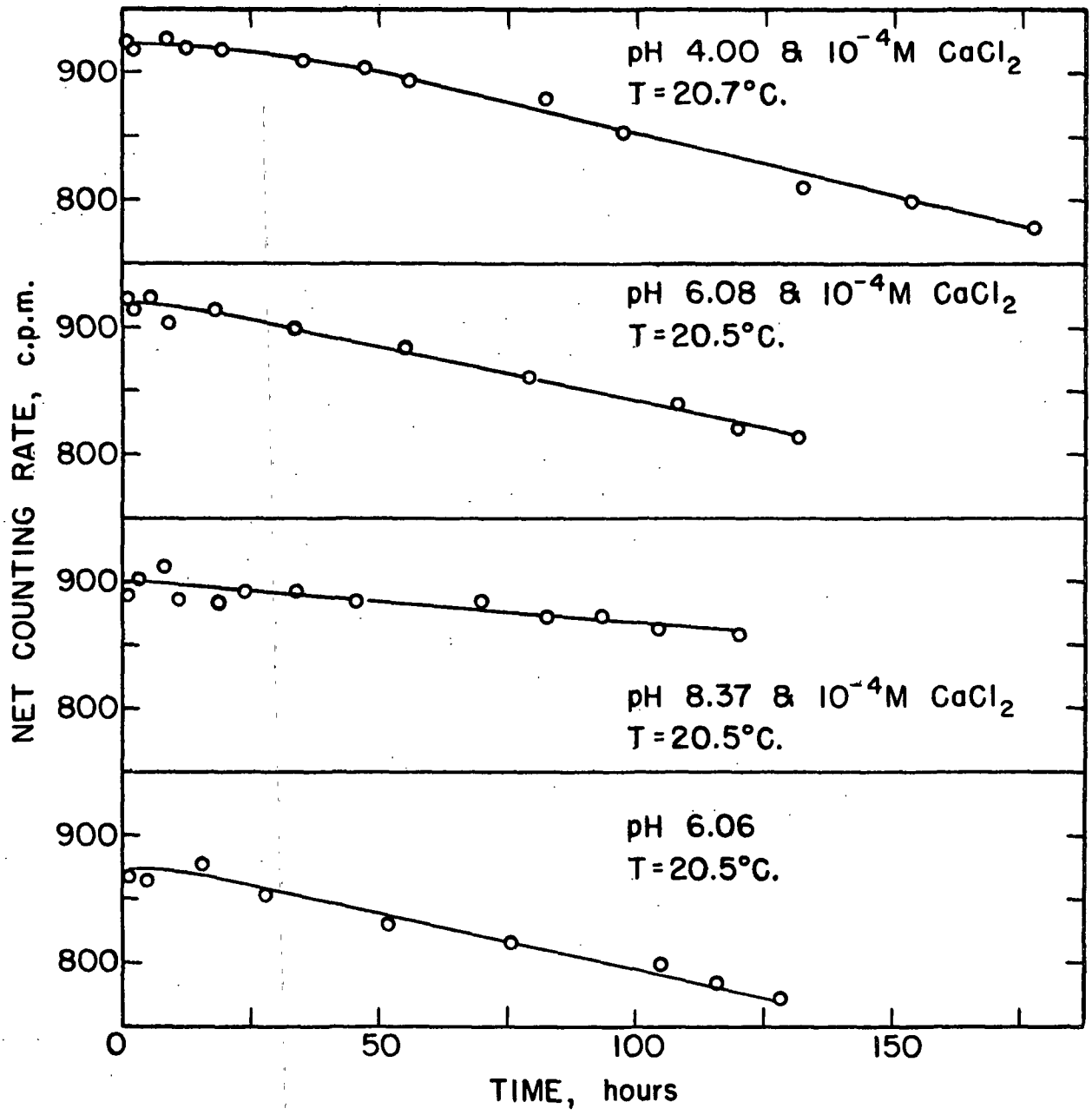

Figure 66. Stability of Bilayers Deposited on Paraffin at 31 Dynes/cm. Upon Exposure to Dry Air at Room Temperature

TABLE XXIV

SURFACE VISCOSITY DATA FOR STEARIC ACID MONOLAYERS ON pH 2.00 SUBSOLUTIONS

	$\Delta\Pi$, dynes/cm.	Slit Width, cm.	Film Area, $cm.^2$	Time, sec.	Slit Length, cm.	Temp., °C.	Surface Viscosity $\times 10^{-4}$, g./sec. Meyers and Harkins	Surface Viscosity $\times 10^{-4}$, g./sec. Joly
Subsolution A								
Stearic acid	30.59	0.0508	7.716	28.25	2.564	20.27	4.77	4.15
Stearic acid (C^{14})	30.81	0.0508	6.601	26.17	2.564	20.21	5.20	4.58
Stearic acid (C^{14})	30.29	0.0508	6.619	25.23	2.564	20.32	4.92	4.30
Subsolution B								
Stearic acid	30.55	0.0508	6.166	27.69	2.564	20.24	5.85	5.22
Stearic acid (C^{14})	30.71	0.0508	6.604	30.68	2.564	20.04	6.08	5.46

TABLE XXV

SURFACE VISCOSITY DATA FOR Ca-H-St MONOLAYERS

pH	$\Delta\Pi$, dynes/cm.	Slit Width, cm.	Film Area, $cm.^2$	Time, sec.	Slit Length, cm.	Temp., °C.	Surface Viscosity, g./sec. Meyers and Harkins	Surface Viscosity, g./sec. Joly
2.00	30.76	0.0508	6.283	29.53	2.564	20.15	6.16×10^{-4}	5.54×10^{-4}
3.16	30.70	0.0508	6.547	24.48	2.564	20.38	4.89	4.27
4.00	30.30	0.0508	6.573	27.50	2.564	19.92	5.40	4.78
4.40	30.31	0.0508	6.720	26.80	2.564	20.15	5.11	4.49
5.04	30.72	0.0508	5.305	22.45	2.564	20.24	5.54	4.92
5.19	31.19	0.0508	6.720	27.95	2.564	20.36	5.53	4.91
5.46	30.74	0.0508	6.720	29.15	2.564	20.39	5.68	5.06
5.74	31.05	0.0508	6.720	38.50	2.564	20.36	7.58	6.96
5.98	30.74	0.0508	5.376	34.05	2.564	20.34	8.30	7.67
6.12	30.91	0.0508	5.376	42.07	2.564	20.38	1.03×10^{-3}	9.68
6.26	30.79	0.0813	6.720	28.70	2.532	20.34	2.32	2.18×10^{-3}
6.39	30.34	0.0813	6.720	32.23	2.532	20.36	2.57	2.43
6.62	31.00	0.0813	6.720	76.40	2.532	20.25	6.23	6.09
6.79	30.55	0.0813	2.016	48.21	2.532	20.10	1.29×10^{-2}	1.28×10^{-2}
7.03	30.90	0.1588	6.720	25.39	2.545	20.25	1.53	1.49
7.35	30.79	0.1588	6.720	66.30	2.545	20.33	3.98	3.94
7.66	30.79	0.1588	5.376	60.52	2.545	20.27	4.54	4.50
7.88	30.95	0.1588	5.376	65.78	2.545	20.16	4.96	4.92
8.04	30.70	0.1588	5.376	65.33	2.545	20.36	4.89	4.85
8.20	30.48	0.1588	4.032	46.69	2.545	20.40	4.62	4.58
8.23	30.79	0.1588	5.376	61.40	2.545	20.20	4.61	4.57
8.27	30.95	0.1588	5.376	61.88	2.545	20.39	4.67	4.63
8.56	31.00	0.1588	5.376	60.48	2.545	20.20	4.57	4.53
8.59	30.74	0.1588	5.376	62.46	2.545	20.27	4.68	4.64
8.95	31.24	0.1588	4.032	45.23	2.545	20.38	4.59	4.55
9.00	30.74	0.1588	4.032	45.25	2.545	20.30	4.52	4.48

APPENDIX IV

ELECTRON MICROSCOPY

TABLE XXVI

PLATE NUMBERS OF THE ELECTRON MICROGRAPHS

Figure 14.	9311 AF, 9315 AF
Figure 15.	6350 AF, 6350 AF
Figure 31.	9824 AF, 9286 AF
	9287 AF, 9288 AF
Figure 32.	9617 AF, 9434 AF
Figure 36.	9281 AF, 9400 AF
	9589 AF
Figure 42.	9315 AF, 9526 AF
	9253 AF
Figure 43.	9334 AF, 9336 AF
	9359 AF
Figure 44.	9665 AF, 9640 AF
	9403 AF, 9528 AF
	9334 AF, 9559 AF
	9590 AF, 9405 AF
Figure 45.	9405 AF, 9405 F
Figure 47.	9886 AF, 9839 AF
Figure 48.	9246 AF, 9271 AF
Figure 49.	9405 AF, 9908 AF
	9836 AF, 9607 AF
Figure 50.	9594 AF, 9591 AF
Figure 51.	9887 AF, 9888 AF
Figure 52.	9822 AF, 9667 AF
	9601 AF
Figure 54.	9613 AF, 9678 AF
	9683 AF, 9671 AF
Figure 67.	9265 AF, 9266 AF
Figure 68.	9429 AF, 9430 AF
Figure 69.	9470 AF, 9472 AF
Figure 70.	9617 AF, 9434 AF
Figure 71.	9840 AF, 9841 AF
Figure 72.	9246 AF, 9271 AF
	9267 AF
Figure 73.	9846 AF, 9845 AF
Figure 74.	9847 AF, 9842 AF

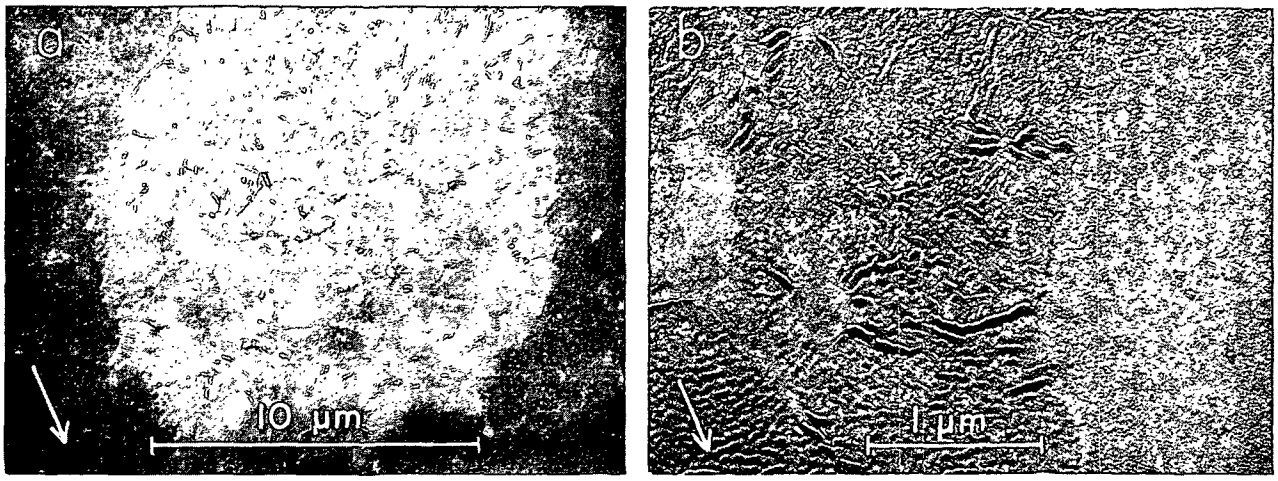

Figure 67. Electron Micrographs of Pd Preshadowed Replicas of (a) Collapsed Regions of a 10% Collapsed C^{14}-Labeled Ca-H-St Monolayer Deposited on Collodion at pH 8.8 and 31 Dynes/cm. (4330X); and (b) Same as (a) Except Greater Magnification (23,100X)

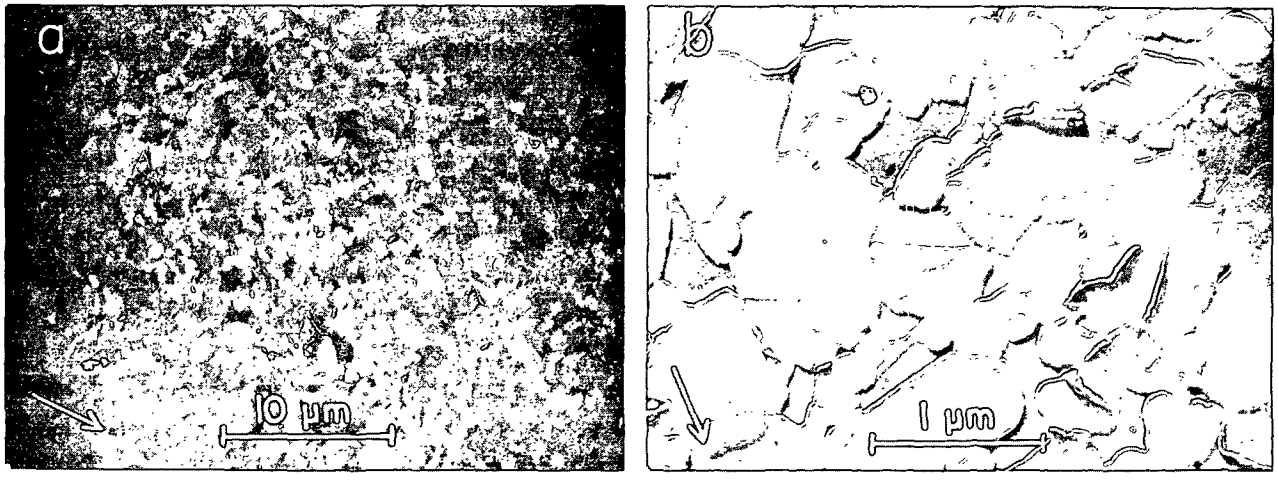

Figure 68. Electron Micrographs of Pt Preshadowed Replicas of (a) Collapsed Regions of a 10% Collapsed C^{14}-Labeled Ca-H-St Monolayer Deposited on Collodion at pH 8.3 and 31 Dynes/cm. (2200X); and (b) Same as (a) Except Greater Magnification (23,100X)

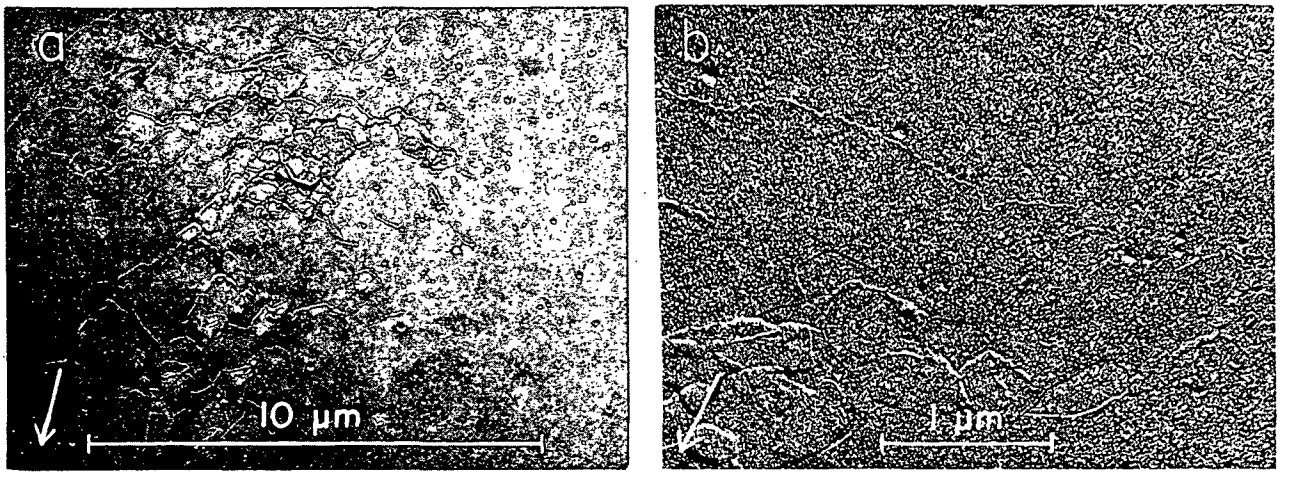

Figure 69. Electron Micrographs of Pd Preshadowed Replicas of (a) Collapsed Regions of a 0.5% Collapsed C^{14}-Labeled Ca-H-St Monolayer Deposited on Collodion at pH 8.8 and 31 Dynes/cm. (6100X); and (b) Same as (a) Except Greater Magnification (22,000X)

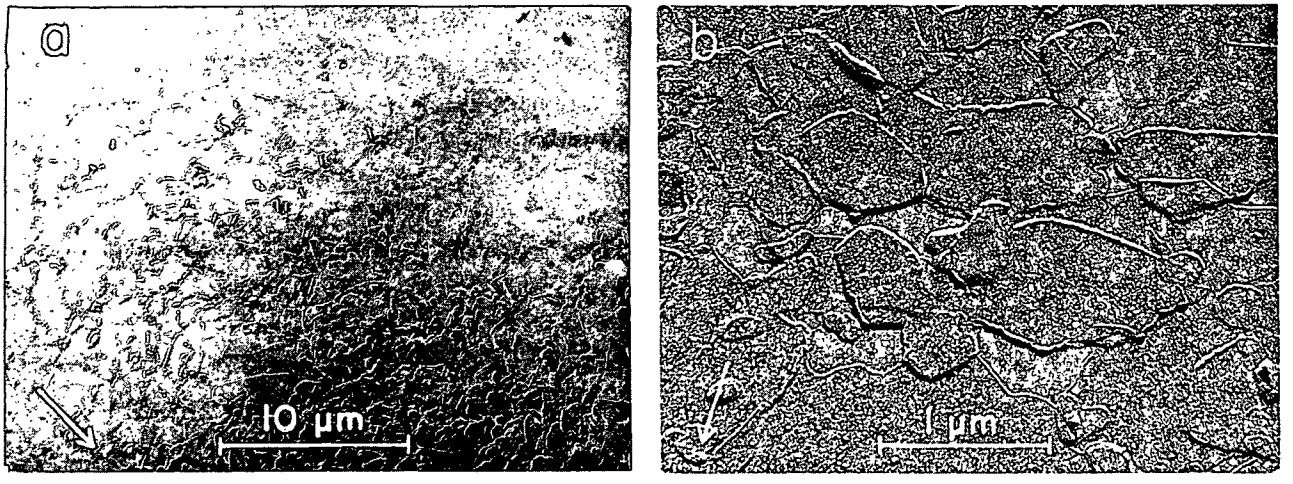

Figure 70. Electron Micrographs of Pd Preshadowed Replicas of (a) Collapsed Regions of a 10% Collapsed C^{14}-Labeled Ca-H-St Monolayer Deposited on Mica at pH 8.3 and 31 Dynes/cm. (2480X); and (b) Same as (a) Except Greater Magnification (22,000X)

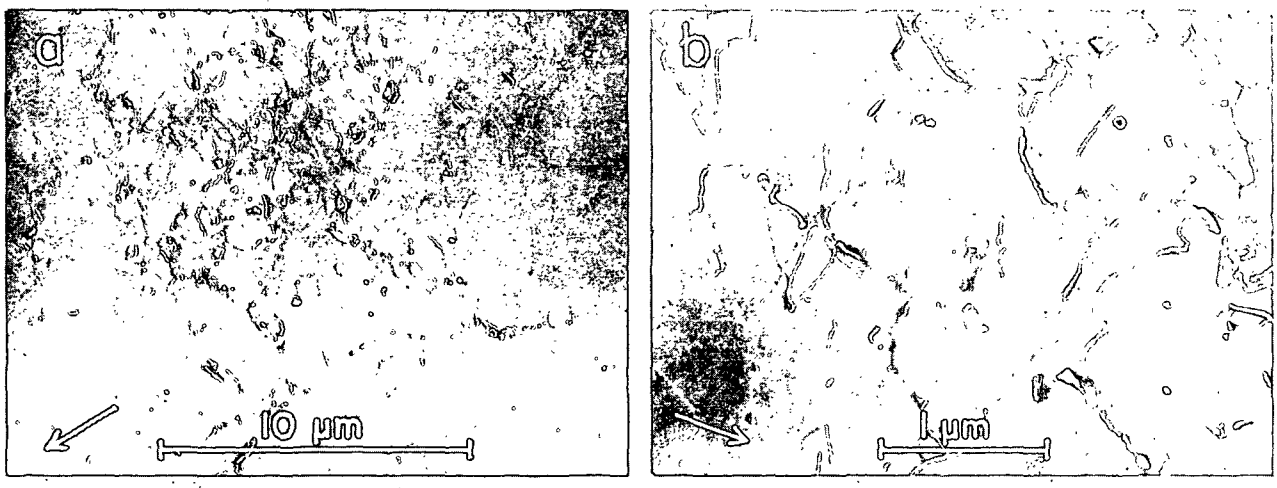

Figure 71. Electron Micrographs of Pt Preshadowed Replicas of (a) Collapsed Regions of a 10% Collapsed C^{14}-Labeled Ca-H-St Monolayer Deposited on Mica at pH 8.3 and 31 Dynes/cm. (4130X); and (b) Same as (a) Except Greater Magnification (21,800X)

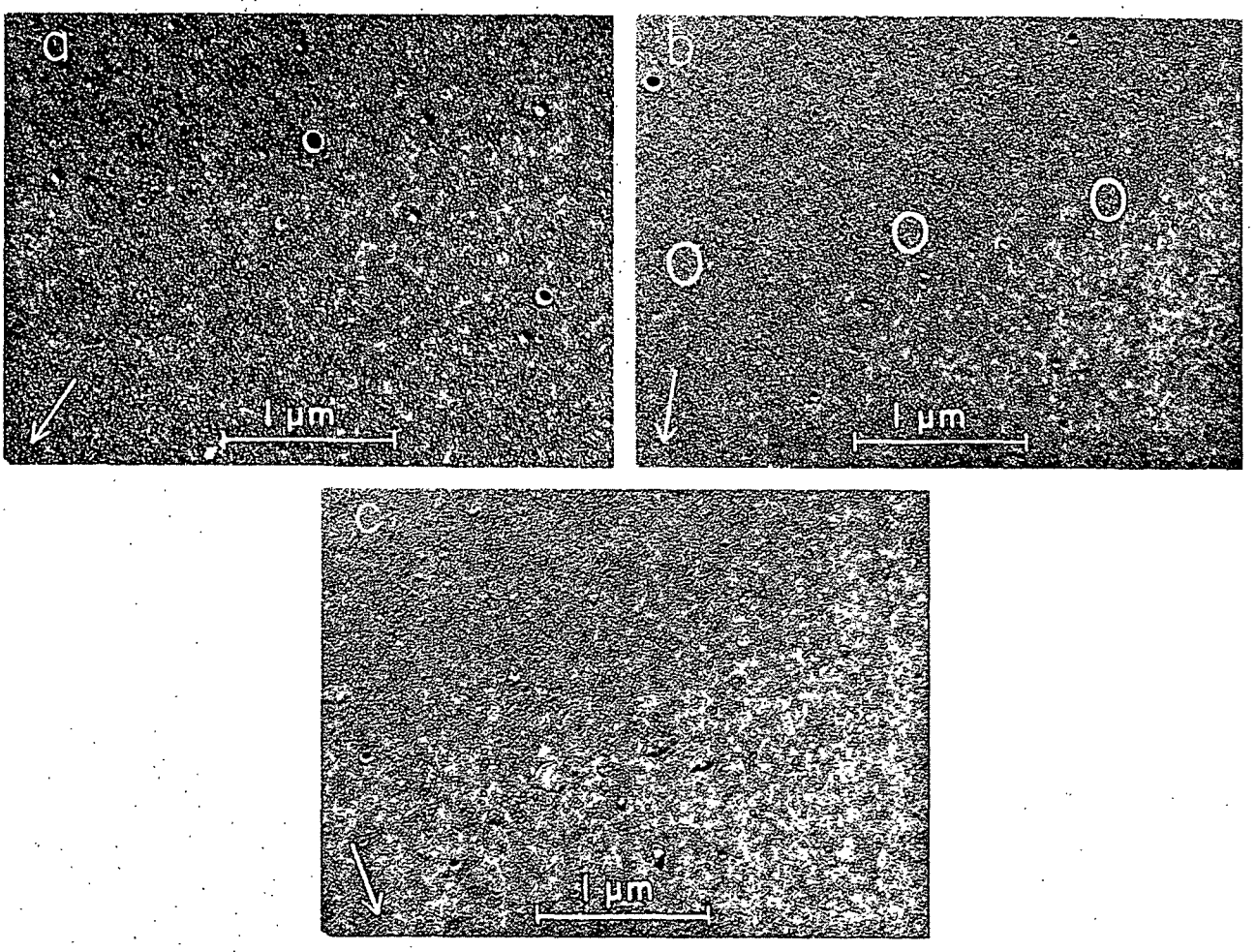

Figure 72. Electron Micrographs of Pd Preshadowed Replicas of (a) Blank Showing the Collodion Substrate with no Film (23,100X); (b) 0.5% Collapsed C^{14}-Labeled Ca-H-St Monolayer Deposited on Collodion at pH 8.8 and 31 Dynes/cm. (23,100X); and (c) 10% Collapsed C^{14}-Labeled Ca-H-St Monolayer Deposited on Collodion at 31 Dynes/cm. and pH 8.8 (23,100X)

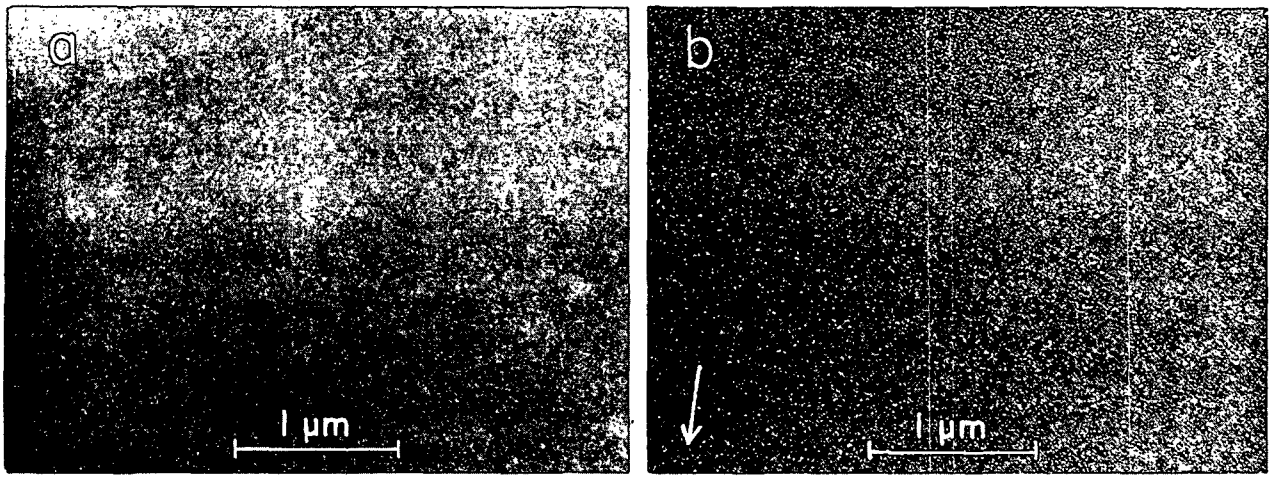

Figure 73. Electron Micrographs of Pd Preshadowed Replicas of (a) Blank Showing the Mica Substrate with no Film (21,800X); and (b) 10% Collapsed C^{14}-Labeled Ca-H-St Monolayer Deposited on Mica at pH 8.3 and 31 Dynes/cm. (21,800X)

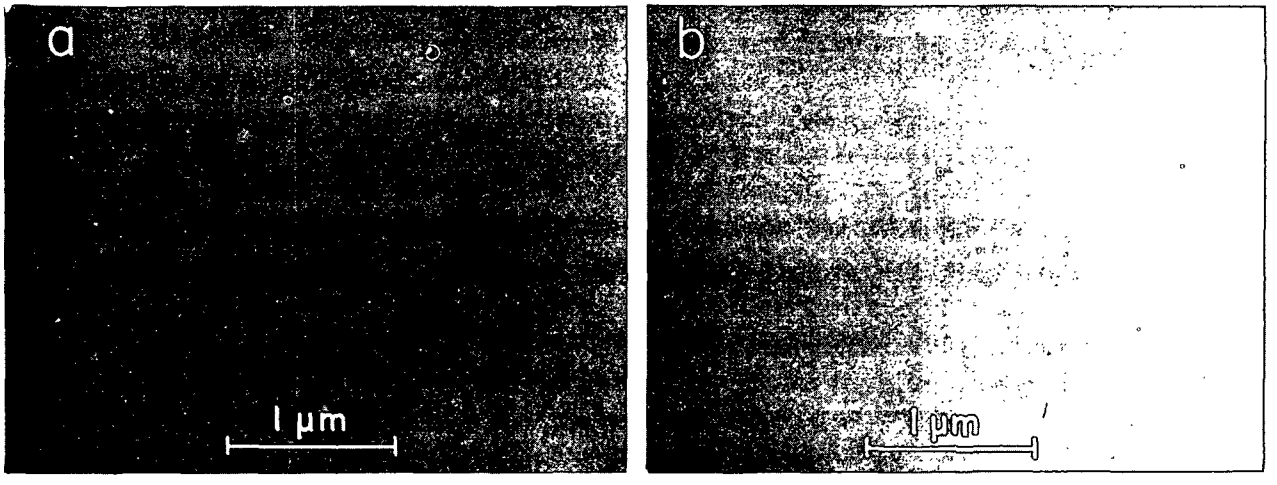

Figure 74. Electron Micrographs of Pt Preshadowed Replicas of (a) Blank Showing the Mica Substrate with no Film (21,800X); and (b) 10% Collapsed C^{14}-Labeled Ca-H-St Monolayer Deposited on Mica at pH 8.3 and 31 Dynes/cm. (21,800X)